Placement of Fluid Viscous Dampers to Reduce Total-Building Seismic Damage

Giuseppe Marcantonio Del Gobbo

St John's College
Department of Engineering Science
University of Oxford

A thesis submitted for the degree of
Doctor of Philosophy

Michaelmas 2017

Placement of Fluid Viscous Dampers to Reduce Total-Building Seismic Damage

Giuseppe Marcantonio Del Gobbo

St John's College
University of Oxford

A thesis submitted for the degree of
Doctor of Philosophy

Michaelmas 2017

Abstract

Nonstructural damage has been found to critically influence economic losses and building downtime following earthquakes. Attaining a target level of seismic performance mandates the harmonisation of structural and nonstructural performance. Retrofitting buildings with fluid viscous dampers (FVDs) can improve interstorey drifts and floor accelerations, parameters which characterise seismic demands. The distribution of dampers within a building and the amount of supplemental damping are critical decisions. Many placement methods have been proposed, however no conclusive optimal method has been identified. The objectives of the thesis included benchmarking the performance of code-compliant buildings, investigating the optimal amount of damping, and comparing major damper placement methods.

The seismic performance of Eurocode-compliant concentric braced frame buildings was benchmarked. Structures were modelled in OpenSees and the FEMA P-58 procedure was used to assess seismic performance in repair costs, a comprehensive measure of total-building performance. Buildings may be demolished following an ultimate limit state earthquake due to high repair costs. Storeys satisfying the Eurocode drift limit for nonstructural protection nevertheless experienced drift- and acceleration-sensitive damage. Most damage was attributed to nonstructural systems. Acceleration-sensitive damage is of comparable or greater consequence than drift-sensitive damage. These findings should be more appropriately reflected in structural design procedures.

The optimal amount of damping to minimise repair costs was identified as 30-40%, larger than previously suggested levels based on structural parameters. Six damper placement methods were evaluated using linear FVDs. No method produced optimal results for both drifts and accelerations. Iterative methods that purport to optimise performance did not achieve that objective: local rather than global parameters are considered, and optimising for a single parameter may worsen another that impacts damage. The storey shear strain energy method and uniform damping produced repair costs more favourable than, or equal to, the other placement methods. Damper placement optimisation may be successful for high-rise or irregular structures.

Dedicated to:

Miei nonni — per il loro coraggio e sacrifici

Assuntina — my favourite sister

Gabby — my partner

Mom and papà — for everything

Acknowledgements

Professor Martin Williams and Professor Tony Blakeborough, for their guidance and supervision

Robin, for the lunch breaks and commiseration

St John's College, for the conference funding, academic grants and accommodation

The Clarendon Fund and the Natural Sciences and Engineering Research Council of Canada, for funding my Oxford experience

McMaster professors, including Dr. Samir Chidiac, Dr. John Wilson, Dr. Michael Tait and Dr. David Potter, for their mentorship and instruction during my undergraduate degree (and the reference letters!)

Contents

List of Figures

List of Tables

List of Abbreviations

16S 16-storey standard design

4D four-storey drift design

4S four-storey standard design

8D eight-storey drift design

8S eight-storey standard design

CBF concentric braced frame

EDP engineering demand parameter

ESEM efficient storey shear strain energy method

FSDA fully stressed design algorithm

FVD fluid viscous damper

IDR interstorey drift ratio

MARE mean absolute relative error

MSE mean squared error

PACT performance assessment calculation tool

PED passive energy dissipation

PFA peak absolute floor acceleration

PFV peak absolute floor velocity

PGA peak ground acceleration

RC reinforced concrete

RE relative error

SEM storey shear strain energy method

SLS serviceability limit state

SSSA simplified sequential search algorithm

ULS ultimate limit state

List of Symbols

C_{total} total viscous damper coefficient added to the structure

D drift design buildings

E_D energy dissipated by all dampers in a structure

$E_{k,o}$ maximum kinetic energy of a system

E standard designs retrofitted with fluid viscous dampers. Coefficients calculated using the energy method

K_j stiffness of storey j

M_n^p modal mass participation of each mode n

R standard designs retrofitted with fluid viscous dampers. Coefficients calculated using the modified energy method

S standard design buildings

T_1 fundamental period of vibration

W_B energy dissipated by the hysteretic behaviour of brace members

W_D energy dissipated by the fluid viscous dampers

W_R energy dissipated by Rayleigh damping

W_{eq} work done by the earthquake ground motion

Ω overstrength of brace diagonal

β standard deviation of natural logarithm values

$\mathbf{\Phi}$ matrix of eigen vectors

δ_u logarithmic decrement

$\dot{u}_{ri}$ relative velocity of the damper i ends

η damping correction factor

γ_j simplified sequential search algorithm location index of storey j

$\mathbf{A}$ system matrix

$\mathbf{C}$ damping matrix

$\mathbf{K}^*$ global system matrix

$\mathbf{K}$ stiffness matrix

$\mathbf{M}$ mass matrix

μ mean

ω_D damped fundamental frequency of vibration

ω_n undamped fundamental frequency of vibration

ϕ mode shape

σ standard deviation

ζ_d supplemental damping ratio

ζ total damping ratio

c_i viscous damping coefficient of damper i

f_i force output of a linear fluid viscous damper i

pi_j^k fully stressed design algorithm performance index of storey j at iteration k

s_i complex eigen value of pair i

x_m median

Chapter 1

Introduction: Motivation for Research

1.1 Overview of Chapter

Earthquakes such as the 2010 Canterbury earthquake and the 2010 Chile earthquake have demonstrated that buildings which experience minimal structural damage may still incur extensive damage to nonstructural systems (Dhakal 2010; Miranda *et al.* 2012). Nonstructural systems refer to building contents, architectural components, and mechanical, electrical and plumbing systems. Nonstructural damage has been found to critically influence economic losses and building downtime following earthquakes. Since key stakeholders such as building and business owners are fundamentally interested in economic loss and downtime, investigating building performance in terms of these factors should be a top priority for engineers after life-safety is ensured. This thesis examines the use of fluid viscous dampers (FVDs), a type of energy dissipation device, to improve the nonstructural and structural seismic performance of buildings.

Nonstructural systems are introduced and briefly described in Section 1.2. The significance of nonstructural seismic performance is examined in Section 1.3. Section 1.4 identifies several notable shortcomings of the conventional seismic design philosophy with regards to nonstructural seismic performance. Research needs on the topic of improving nonstructural performance using FVDs are detailed in Section 1.5. Section 1.6 outlines the thesis and provides an overview of each chapter.

1.2 Introduction to Nonstructural Systems

Nonstructural systems encompass all objects and components in a building that are not part of the load-bearing system. There are three major categories of nonstructural systems:

1. Building contents (furniture, office equipment, items on shelves)
2. Architectural components (cladding, ceilings, partitions)
3. Mechanical, electrical and plumbing systems (ductwork, transformers, piping)

Figure 1.1 displays some typical nonstructural systems. It can be observed that there are a wide variety of nonstructural components and that these components are distributed throughout the entire structure.

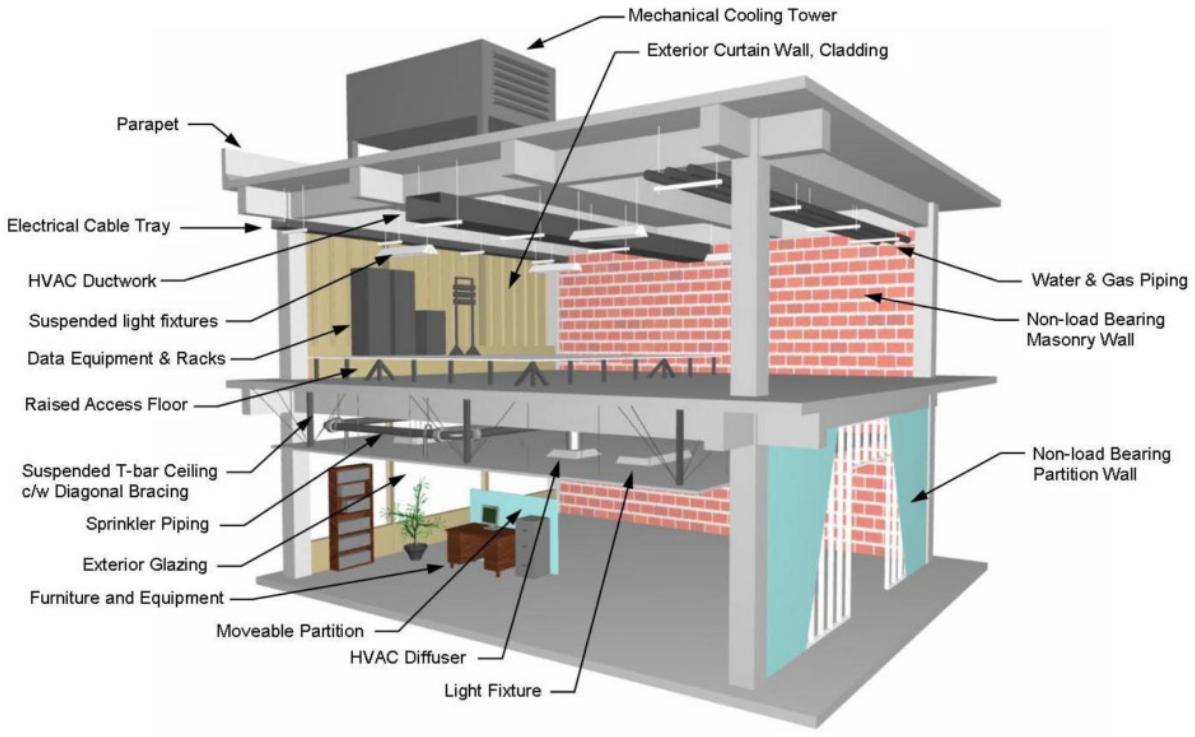

Figure 1.1: Examples of nonstructural systems (Wang 2008)

Earthquakes commonly initiate nonstructural damage in several ways. Inertial forces from ground motions can cause nonstructural components to rock, slide or overturn, and sustain damage in the process. It is possible for internal components to be damaged by inertial forces without any visible movement during intense shaking. As nonstructural

systems move separately from one another, they can also strike other nonstructural components or the structure itself. Two examples of nonstructural components that are particularly susceptible to this mode of damage are suspended ceilings and sprinkler pipes. Building displacements and interstorey drifts are another source of damage. Displacements affect components that are rigidly attached to the structure such as partition walls (FEMA 2012a). Nonstructural components are typically classified as acceleration-sensitive (e.g. piping systems and bookshelves) or drift-sensitive (e.g. cladding) based on the means of incurring damage (Wieser *et al.* 2012).

It has been observed that even the nonstructural systems of essential facilities, which are subject to more stringent design procedures than normal structures, can experience extensive damage during earthquakes. Villaverde (1997) recognised in a comprehensive review of nonstructural systems that extensive research must be conducted with respect to improving nonstructural seismic performance. The significance of nonstructural seismic performance is therefore examined.

1.3 Significance of Nonstructural Seismic Performance

Nonstructural seismic performance has a significant impact on the overall seismic performance of a building. Nonstructural seismic performance is important due to the impact on property loss, building functionality and life safety.

Figure 1.2 illustrates that nonstructural components and contents represent the majority of investment in buildings (Taghavi and Miranda 2003). As nonstructural systems are susceptible to damage at levels of deformation or acceleration much smaller than structural systems, the likelihood of property loss is increased (Taghavi and Miranda 2003). Several publications (Retamales *et al.* 2008; Taghavi and Miranda 2003; Astrella and Whittaker 2005) have recognised that nonstructural systems compose a large portion of the potential economic losses from earthquakes.

Nonstructural systems are essential to building operations (Astrella and Whittaker 2005). Damage to nonstructural components can result in lengthy disruptions to building

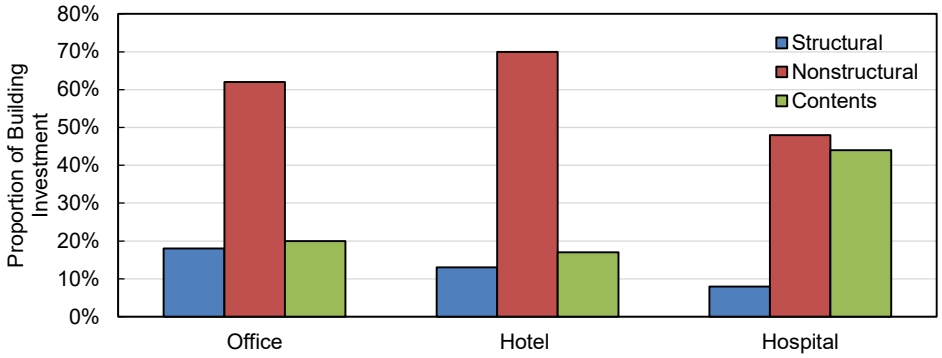

Figure 1.2: Distribution of building investment (Taghavi and Miranda 2003)

service. For example, two major airports and several hospitals lost functionality exclusively due to nonstructural system failures following the 2010 Chile earthquake (Miranda *et al.* 2012). Ramifications include business interruptions and a decrease in the quality of life for those in the affected areas (Almufti 2014; Gould and Griffin 2003; Chaudhuri and Hutchinson 2005).

Falling nonstructural components or debris have the proven potential to injure or kill individuals (McKevitt *et al.* 1995; Taly 1988; Elsesser 1984). Debris can also block building egress, preventing building occupants from evacuating or rescue personnel from entering (FEMA 2012a). Damage to the fire sprinkler system can also compromise safety should a fire occur following an earthquake (FEMA 2012a).

Nonstructural seismic performance is critically important due to the impact on property loss, building functionality and life safety. Poor nonstructural performance can lower the performance level of the complete building system regardless of structural performance. The performance of nonstructural systems in structures designed using the conventional seismic design philosophy is therefore of considerable interest.

1.4 Problem Definition: Conventional Seismic Design

Seismic design aims to provide structures with the ability to perform favourably when experiencing earthquake effects. The conventional seismic design philosophy typically calls for three levels of seismic performance (Booth and Key 2006):

1. Withstand minor earthquakes without sustaining damage

2. Withstand moderate earthquakes without structural damage while expecting some nonstructural damage

3. Withstand major earthquakes without collapse while accepting structural and nonstructural damage

Typically only the major earthquake is explicitly defined as the design load in conventional seismic design. During these earthquakes, conventional design relies on the structure having sufficient ductility capacity in order to undergo substantial inelastic deformations (Christopoulos and Filiatrault 2006). These large inelastic deformations are concentrated in members of the lateral force resisting system specifically designed to dissipate seismic energy in a controlled manner. Although the inelastic deformations cause irreparable damage in the structural members, life safety is ensured. This is referred to as the concept of ductility balance (Towashiraporn *et al.* 2002).

This traditional design approach was called into question in the 1990s after major seismic events such as the 1994 Northridge earthquake in the USA and the 1995 Kobe earthquake in Japan caused tremendous property losses. The limitations of this methodology were further revealed when earthquakes of more probable occurrence levels caused more damage than anticipated (Christopoulos and Filiatrault 2006; Booth and Key 2006). By current standards, the designs could be considered successful since the design goal of preventing life-threatening hazards was achieved. However, structural damage was often so extensive that repairs were not economically feasible and building demolition was required (Vargas and Bruneau 2006).

The limitations of the conventional design approach are apparent. Building owners are acknowledging the consequences of "successful" seismic design on their operations and are calling for improved performance. These demands have led to the concept of performance-based earthquake engineering. This alternative design philosophy specifies multiple performance objectives corresponding to different seismic intensities. The performance targeted at each seismic level is based on the importance of the structure being designed

(Christopoulos and Filiatrault 2006). The performance of the structure at each identified seismic hazard level is examined. This concept is illustrated in Figure 1.3. The concept of limit states in conventional seismic design can be considered a simple form of performance-based design, however only a single performance level of life safety is considered.

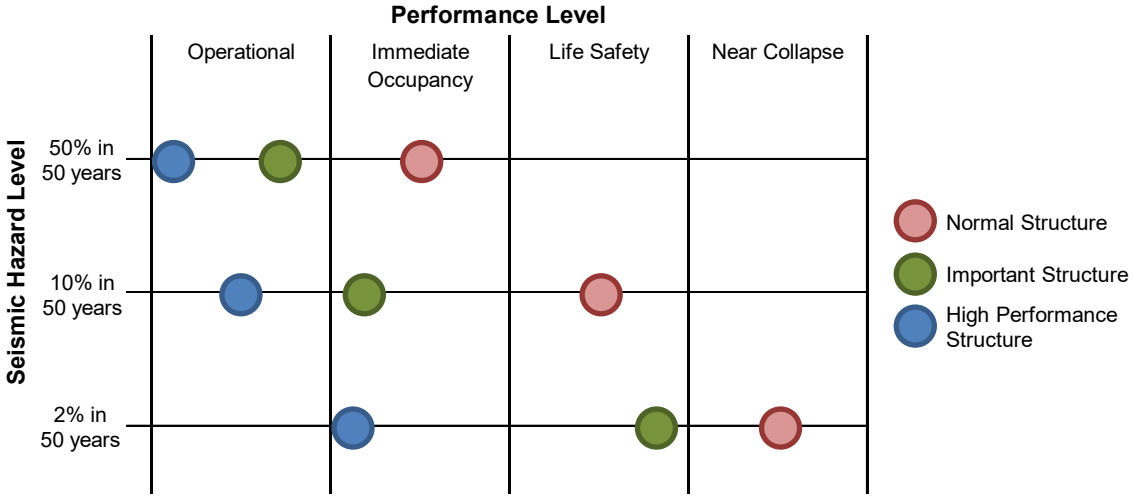

Figure 1.3: Performance-based design (Christopoulos and Filiatrault 2006)

Despite the improvements in seismic design, experts have suggested that modern building standards still do not accomplish resilience: "the ability of an organization or community to recover quickly after an earthquake" (Almufti 2014). Attaining a target level of seismic performance mandates the harmonisation of structural and nonstructural performance levels. Buildings designed to modern standards have incurred crippling nonstructural damage during moderate earthquakes, resulting in major economic losses and downtime. This suggests that research is needed to improve conventional seismic performance. One such design alternative is the use of FVDs.

1.5 Research Needs: Fluid Viscous Dampers

It has been established that the conventional seismic design philosophy permits undesirable levels of nonstructural damage. For example, conventional seismic design limits interstorey drift ratios (IDRs) but does not control floor accelerations. However, several major non-structural systems are acceleration-sensitive (Achour *et al.* 2011). Design procedures which enhance total-building seismic performance are needed. Seismic analysis of nonstructural

systems involves additional complexities due to the large variety of configurations and components (Retamales *et al.* 2008). As a result, research on nonstructural systems has been limited in comparison to primary structural systems (Filiatrault *et al.* 2001b).

The objective of supplemental damping is to dissipate a portion of the seismic energy introduced into a structure, thereby lessening structural response during earthquakes. Supplemental damping devices can substantially reduce drifts and improve the seismic performance of buildings (Christopoulos and Filiatrault 2006). Of these supplemental damping devices, FVDs are the most promising for nonstructural applications as the devices can uniquely improve both interstorey drifts and floor accelerations (Pavlou and Constantinou 2006). Despite this potential, research on FVD applications for enhancing the nonstructural performance of buildings has been limited. Previous research focuses on evaluating structural parameters. There have been minimal attempts to maximise nonstructural performance in terms of both the amount of damping and the damper distribution within a structure. There is a need to clarify what seismic performance improvements can and cannot be achieved using FVDs. These research needs serve as the motivation for this thesis.

1.6 Thesis Outline

The motivation for research on total-building seismic performance has been established. This thesis examines the structural and nonstructural seismic performance of modern code-compliant structures. The capability of FVDs to improve the seismic performance of standard designs is investigated.

1.6.1 Chapter 2 Overview

Literature Review and Research Objectives

This chapter comprises a critical review of literature on the topics of nonstructural seismic performance and the use of FVDs to improve total-building performance. The objectives of this chapter are to assess relevant literature, identify gaps in current knowledge

and define research objectives for the thesis, situating these objectives within the current body of research.

1.6.2 Chapter 3 Overview

Seismic Evaluation Method and Building Design

The aim of this chapter is to introduce the seismic performance evaluation method used in this thesis. This includes the creation of several code-compliant building designs that adhere to different Eurocode 8 (CEN 2013) performance limits. The building designs and the seismic performance assessment method established in this chapter are needed in order to benchmark the seismic performance of conventional and FVD retrofitted buildings.

1.6.3 Chapter 4 Overview

Seismic Performance Benchmark of Code-Compliant Buildings

Attaining a target level of seismic performance mandates the harmonisation of structural and nonstructural performance. An improved understanding of the expected overall seismic performance of code-compliant buildings is needed. This chapter benchmarks the seismic performance of conventional multi-storey buildings designed for seismic regions. The applicability of the Eurocode 8 (CEN 2013) performance limits are assessed. The results of the seismic performance assessment provide a benchmark on which to evaluate alternative building designs.

1.6.4 Chapter 5 Overview

Damping and Repair Costs

Retrofitting buildings with supplemental damping devices can substantially reduce drifts and improve the seismic performance of buildings. FVDs were identified as the most promising of these devices for nonstructural considerations as they can improve both drifts and floor accelerations. This chapter investigates the application of FVDs to minimise structural and nonstructural damage. The damping ratio calculated using a popular energy method is compared to the achieved level of damping. A modification to

the frequently used formula is proposed to improve the accuracy of the energy method. The improved energy formula can be used to rapidly select linear damper coefficients to achieve a desired level of damping. The optimal amount of damping to minimise repair costs is investigated. The results of this study will provide insight when selecting levels of damping for structural design and retrofit.

1.6.5 Chapter 6 Overview

Improving Seismic Performance: Damper Retrofit or Drift Design?

Designing buildings to reach strict IDR limits in adherence to Eurocode 8 (CEN 2013) and retrofitting buildings with FVDs are two methods with the same aim: to improve the seismic performance of standard buildings. This chapter investigates and compares the resulting performance of both methods. The performance assessment of the FVD retrofitted and drift design structures demonstrate the advantages and limitations of using FVDs to improve total-building seismic performance.

1.6.6 Chapter 7 Overview

Optimal Damper Placement

Seismic performance improvements were realised in the previous chapters using uniform damper placement. A large number of damper placement methods that claim to improve performance have been proposed in literature. The distribution of dampers within a building is a critical decision, as damper placement affects structural response and the required damper investment. However, only limited comparisons of damper placement methods have been conducted. The objective of this chapter is to compare the effectiveness of different damper placement methods considering structural and nonstructural performance. The investigated set of methods was selected based on prevalence in literature and level of practicality. The results of this chapter provide recommendations on the optimal damper placement method for improving total-building seismic performance.

1.6.7 Chapter 8 Overview

Conclusions and Future Work

This chapter summarises the findings of this thesis in relation to the research objectives established following the literature review. Areas for future research are also identified.

Chapter 2

Literature Review and Research Objectives

2.1 Overview of Chapter

This chapter comprises a critical review of literature on the topics of nonstructural seismic performance and the use of fluid viscous dampers (FVDs) to improve total-building performance. The objectives of this chapter are to assess relevant literature, identify gaps in current knowledge, and situate the research objectives of this thesis within the current body of work. Section 2.2 examines literature on the seismic performance of nonstructural systems. This review encompasses observations from earthquakes, existing regulations, and damage mitigation strategies. Previous research on assessing the seismic performance of structures is examined in Section 2.3. The concepts of fragility functions and building loss estimation are considered. Section 2.4 explores supplemental damping and passive energy dissipation (PED). Several categories of PED devices are reviewed along with seismic applications of PED considering nonstructural systems. Section 2.5 surveys literature on the placement of FVDs. Research on damper placement methods and the comparison of placement methods is assessed. Pertinent gaps in research are identified and the research objectives of the thesis are established in Section 2.6.

2.2 Nonstructural Seismic Performance

2.2.1 Observed Performance During Earthquakes

In areas where the primary structural system is subject to deficiencies, nonstructural damage can be considered of secondary importance due to the likelihood of structural collapse and fatalities. In countries with developed and enforced seismic codes, a considerable amount of economic loss can be attributed to poor nonstructural performance. Buildings that experience minimal to no structural damage frequently have been observed to sustain extensive damage to their nonstructural systems. This nonstructural damage can require lengthy repair and prevent an immediate return to building occupancy despite the adequate performance of the structural components. There have been numerous reports produced by the earthquake engineering community describing the extensive damage and failure of nonstructural systems experienced during earthquakes. One such document produced by Fierro *et al.* (2011) states that nonstructural damage accounted for billions of dollars of losses in 2010 alone. Damage and loss of building function have followed even moderate intensity earthquakes (Tajirian 2009).

Nonstructural damage from the 1994 Northridge earthquake in the USA was observed in commercial, institutional and industrial structures. Only $1.1 billion of the $6.3 billion earthquake losses was attributed to structural damage (Kircher 2003). Numerous structures that resisted the earthquake with little or no structural damage experienced extensive nonstructural damage (McKevitt *et al.* 1995). Examples include extended building closure due to failure of suspended ceiling systems, and damage to heating, ventilation, and air conditioning (HVAC) equipment. Essential facilities such as hospitals were forced to close due to poor nonstructural seismic performance (McKevitt *et al.* 1995). At least five deaths and thousands of injuries were caused by poor nonstructural performance; structural collapse caused 20 deaths (McKevitt *et al.* 1995).

The 1995 Kobe earthquake in Japan was responsible for considerable structural and nonstructural damage. Disruptions of elevator and escalator services were commonplace (Filiatrault *et al.* 2001b). Ductwork, ceiling, and piping systems collapsed. Fire sprinkler

systems failed and caused water damage (Filiatrault *et al.* 2001b). The cost of repairs to nonstructural systems was determined to be equal to the cost of structural damage (Gioncu and Mazzolani 2011).

Following the 2001 Nisqually earthquake in the USA, a reconnaissance team found that a large gap existed between structural and nonstructural performance (Filiatrault *et al.* 2001a). Suspended ceiling systems were responsible for much of the disruption. Wall, cladding, and window systems all exhibited poor performance. Building content damage extended downtime. The rupture of gas lines and flooding from broken water pipes necessitated the evacuation of several structures (Filiatrault *et al.* 2001a).

The 2010 Canterbury (Darfield) earthquake in New Zealand reasserted the vulnerability of nonstructural systems. Multiple commercial facilities that resisted the earthquake with only minor structural damage incurred lengthy downtime due to poor nonstructural performance (Kam *et al.* 2010). Dhakal (2010) noted the trend; "although noticeable structural damage occurred only in a small proportion of the building stock, damage to nonstructural components and contents was apparent in almost all buildings in this event". Widespread damage to suspended ceiling systems, facades, and partition walls was responsible for a major portion of the $4 billion economic losses.

Damage to ceilings, fire sprinkler systems, HVAC equipment, and partition walls was common following the 2010 Chile earthquake (Miranda *et al.* 2012). Minimal structural damage was observed, while nonstructural damage resulted in major disruptions and economic losses (Miranda *et al.* 2012; Saatcioglu *et al.* 2013). Industrial facilities suffered extensive nonstructural damage (Tremblay *et al.* 2013). Two major airports and several hospitals lost functionality exclusively due to the failure of nonstructural systems (Miranda *et al.* 2012).

The 2011 Christchurch earthquake in New Zealand reaffirmed the vulnerability of nonstructural systems. A study inspecting 217 multi-storey buildings found that 74% of the inspected buildings suffered partition damage and 39% of the inspected glazed facades presented a falling hazard (Baird *et al.* 2014). The poor performance of nonstuc-

tural systems during this and previous earthquakes warrants further study on current nonstructural regulations.

2.2.2 Survey of Existing Regulations

Examining structural engineering provisions for nonstructural seismic performance has been the subject of significant research in the 2010s. Current structural codes use simplified analysis methods to calculate the acceleration and deflection demands on nonstructural systems (Sullivan *et al.* 2013). The nonstructural requirements are founded on engineering judgement, rather than on verified empirical or analytical tests (Retamales *et al.* 2008; Filiatrault and Sullivan 2014). Simplified methods are necessary in order to facilitate the efficient and safe design of structures by professional engineers. However, nonstructural damage as a result of earthquakes in the 1990s to 2010s has exposed a gap between the desired and actual performance of these components.

Kam and Pampanin (2012) underlined the large discrepancy between societal expectations and the reality of current seismic performance. The paper demonstrated that nonstructural regulations are unsatisfactory and called for urgent changes in engineering policy. Villaverde (1997) also concluded that building code requirements were inadequate, while recognising the difficultly in creating methods practical enough to be used in design by practising engineers but accurate enough to give meaningful design parameters.

Seismic regulations regarding nonstructural systems in building codes generally only give attention to the attachment of the nonstructural component to the main structural system (Wolff and Constantinou 2004). Although this addresses occupant life safety, it is insufficient to protect the nonstructural component itself. Common engineering practice is to design the stiffness of the lateral force resisting system to achieve deflection limits mandated by building codes. The resulting building accelerations are used to calculate equivalent static forces. The static forces are then used for the design of the nonstructural anchorage (Sullivan *et al.* 2013).

European requirements regarding nonstructural seismic performance can be found in Eurocode 8: Part 1 (CEN 2013). The standard seeks to minimise nonstructural

damage by specifying interstorey drift ratio (IDR) limits dependent on the classification of nonstructural components in the building as either brittle, ductile, or isolated. The most strict interstorey drift limits are 0.5% during the serviceability limit state (SLS) and 1.0% during the ultimate limit state (ULS). This procedure is limited as direction is not provided on how to classify a nonstructural component. Furthermore, a component can still be damaged by deflections regardless of its ductile behaviour (Soós and Vigh 2012). Equivalent static forces are specified considering acceleration, however a study of two reinforced concrete (RC) buildings (Sullivan *et al.* 2013) found that prescribed acceleration demands were inaccurate.

Seismic design procedures for nonstructural systems in the USA are provided in the ASCE/SEI 7-10 standard (American Society of Civil Engineers 2013). Equivalent static design forces and relative displacement demands are prescribed. Non-critical nonstructural systems installed in regular structures are expected to resist minor earthquakes without affecting functionality, resist moderate earthquakes with some functionality impairment, and resist the design earthquake with a loss of functionality but a protection of life safety. More stringent regulations and seismic qualifications exist for certain nonstructural components installed in critical facilities such as healthcare centres. Filiatrault and Sullivan (2014) presented a survey of regulations and specifications for nonstructural seismic design in the USA. The interstorey drift limits are less strict than those prescribed by Eurocode 8, with an allowable ULS interstorey drift limit of 2% (American Society of Civil Engineers 2013).

Sullivan *et al.* (2013) noted that the standards in the USA, Europe and New Zealand all have different methods to calculate acceleration requirements for nonstructural components. It was suggested that the three code approaches are "approximate" and must become more accurate.

2.2.3 Damage Mitigation Strategies

Several damage mitigation strategies have been developed to improve the seismic performance of nonstructural systems. Strategies have been developed for individual components

as well as for total-building considerations. There has been limited research regarding the application of PED devices for nonstructural purposes; this area is thoroughly examined in Section 2.4.3.

2.2.3.1 Strategies for Individual Components

Seismic restraint, also referred to as anchorage, is one of the most common damage mitigation strategies for nonstructural systems. Seismic restraint involves bolting, bracing or strapping nonstructural components to the main structural system. The goals of anchorage are position retention and life safety. A case study on the design and cost of anchoring equipment (Comerio *et al.* 2001) featured nonstructural components ranging from bench top items to large tanks. Observations following earthquakes as well as experimental studies have confirmed that anchorage can improve seismic performance when adequate strength is provided (McKevitt *et al.* 1995; Tian *et al.* 2013).

Disadvantages of seismic restraint have been cited as loss of convenience or mobility, loss of manufacturer warranty on the nonstructural component, and the potential for seismic damage caused by the connection (Comerio and Holmes 2003). Anchors must be properly designed and detailed in order to be effective. Investigations after the 2010 Chile earthquake found multiple instances of failure due to inadequate strength or poor connections (Tremblay *et al.* 2013). Poorly designed restraints can even decrease performance by introducing torsional effects (Dhakal 2010). Anchorage can also be detrimental to acceleration-sensitive nonstructural systems. Konstantinidis and Makris (2005) conducted shake table experiments on laboratory content. It was found that anchored equipment can experience peak accelerations up to seven times greater than that of free-standing equipment.

Mounting individual components on isolation systems is another method that seeks to improve nonstructural seismic performance. This approach has been used for critical equipment and is more expensive than the relatively simple process of providing rigid anchorage. A two part parametric study on isolation and restraint for mechanical equipment was completed by Fathali and Filiatrault (2007a; 2007b). Computer floor

isolation is commonly used in Japan. Many data centres with computer floor isolation experienced uninterrupted service during the 1995 Kobe earthquake (Tajirian 2009). Research from Wanitkorkul and Filiatrault (2008) found that generic nonstructural components mounted on isolation systems exhibited performance superior to that of the rigidly restrained equivalents.

There have been observed cases of vibration systems failing and damaging nonstructural components during earthquakes (Lloyd 2003). It has been shown that computer server isolation systems can cause large acceleration spikes during major earthquakes if the maximum displacement capacity of the isolation system is reached (Tajirian 2009). Equipment isolation may not be economically feasible for large numbers of nonstructural systems. This method is also not practically applicable for several types of nonstructural systems. Further limitations are similar to those for anchorage, such as a loss of component mobility.

In addition to damage mitigation strategies for individual components, total-building strategies have also been implemented. It should be noted that the use of both approaches is not mutually exclusive.

2.2.3.2 Strategies for Total-Building Performance

Base isolation is a leading method to improve the seismic performance of buildings. Multiple analytical and experimental investigations have concluded that base isolation minimises drift and acceleration demands on nonstructural systems (Astrella and Whittaker 2005; Wolff and Constantinou 2004; Fan and Ahmadi 1992; Morgan and Mahin 2011). Although base isolation is effective, it is also a costly option and may be impractical for retrofitting existing structures (Tajirian 2009). This is reflected in the population of existing base isolated structures, the majority of which are historical structures, hospitals and museums (Wolff and Constantinou 2004).

Resilience-based design is a concept where total-building performance is considered in the design phase. This strategy can encompass several previously mentioned methods. A major development in this area is the Resilience-based Earthquake Design Initiative

(REDi) (Almufti and Willford 2013). The REDi system is a holistic design approach that aims to achieve beyond-code structural performance. Several performance states based on building functionality are considered (Almufti and Willford 2013). This methodology for building design places emphasis on nonstructural performance and demonstrates that the importance of nonstructural systems is being recognised by major industry organisations.

Figure 2.1 presents the expected resilience of a structure designed to the three REDi targets as well as to code standards. A REDi case study was conducted in which a 42-storey RC building was designed to modern performance-based USA standards (Almufti 2014). It was estimated that $47 million and two years of repairs would be required to achieve functional recovery after a major earthquake. The majority of losses resulted from poor nonstructural seismic performance. In comparison, designing the building with REDi standards reduced expected losses to $5.8 million. Functional recovery was estimated to be reached after one month. There is an anticipated 2-5% cost premium over conventional designs. The REDi case study demonstrates the advantages of considering nonstructural performance in the structural design phase.

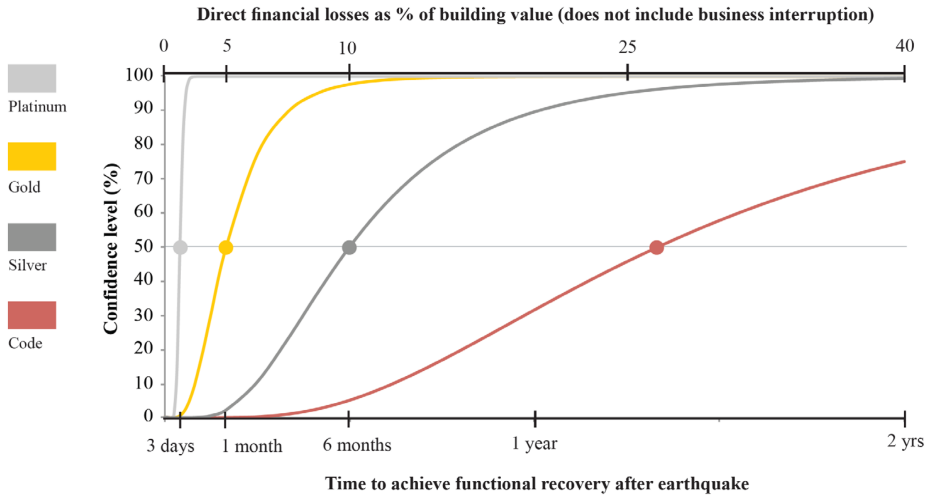

Figure 2.1: REDi resilience objectives (Almufti 2014)

2.3 Seismic Performance Assessment

Code-compliant structures have been shown to generally exhibit poor nonstructural performance. A seismic performance assessment procedure that includes nonstructural

systems is required to evaluate total-building performance.

2.3.1 Fragility Functions

Filiatrault *et al.* (2001b) stated that systematic research associating records of nonstructural damage with detailed structural analysis only commenced after the 1989 Loma Prieta and 1994 Northridge earthquakes. Interstorey drift and peak floor acceleration are the engineering demand parameters (EDPs) most widely used to characterise seismic demands on nonstructural systems. Taghavi and Miranda (2003) developed a database on nonstructural seismic performance and established maximum IDR and peak floor acceleration as the EDPs best correlated to damage. Maximum IDR and peak floor acceleration have been used as EDPs in multiple studies (Puthanpurayil and Reynolds 2008; Bruno and Valente 2002; Hunt and Stojadinovic 2010).

Nonstructural seismic research has moved towards evaluating EDP values from structural analysis and using these results in combination with fragility functions to determine expected damage. Fragility functions represent the relationship between an EDP and the probability of experiencing damage. They are constructed by observing earthquake-induced damage, experimental testing, or analytical simulations (Taghavi and Miranda 2003). The FEMA P-58 project (FEMA 2012b) included the creation of a database of fragility functions for nonstructural systems including wall partitions, ceilings, lighting, piping, and heavy equipment. Figure 2.2 shows fragility functions created by Porter and Kiremidjian (2001) for a partition wall with two damage states. The functions are based on experimental results.

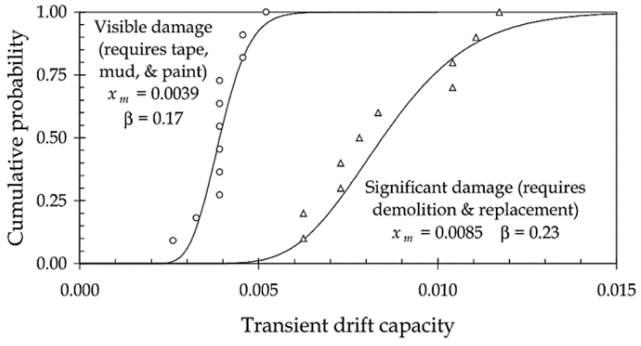

Figure 2.2: Partition wall fragility functions, x_m = median, β = logarithmic standard deviation (Porter and Kiremidjian 2001)

Fragility functions are a powerful tool to determine expected damage to both structural and nonstructural systems. However, the damage is expressed in terms of defined damage states. Building loss estimation is a procedure that builds on this tool to express damage in terms of a universal measure: monetary cost.

2.3.2 Building Loss Estimation

One of the first building-specific loss estimation methods, referred to as assembly-based vulnerability, was proposed by Porter and Kiremidjian (2001). In this method, the entire building is considered as a collection of individual components. Fragility functions are used to determine the expected damage to individual components, while unit cost functions determine the corresponding repair costs. The total building repair cost can be calculated from the sum of the individual component damages. This enables the seismic performance of a structure to be measured in repair costs rather than a set of structural parameters or discrete performance levels. This is a major advantage of the procedure, as repair costs clearly communicate seismic performance and are useful for decision making.

The assembly-based vulnerability concept was integrated into the FEMA P-58 performance assessment procedure (FEMA 2012b). The procedure requires the creation of a building performance model. This model is a collection of data representing the building assets at risk during an earthquake, including both structural and nonstructural systems. Fragility functions and consequence functions are provided for the building assets. The performance assessment calculation tool (PACT) performs the FEMA P-58 probabilistic calculations and accumulation of losses using a Monte Carlo procedure.

Previous studies comparing seismic performance or optimal designs often evaluate IDRs and floor accelerations (Lavan and Dargush 2009). As these structural parameters typically are competing objectives, complexities arise in the assessments. The selected optimal design will be dependent on the relative weighting placed on each parameter. Assumptions and limitations are introduced when determining appropriate weights to represent the seismic performance. By using repair costs, these ambiguities are avoided.

Using interstorey drift to compare the performance of different structural systems also presents further limitations. Peak drifts may not provide an appropriate comparison, as different structural systems initiate damage at different IDR levels (Terzic *et al.* 2014). The use of repair costs explicitly takes different damage initiation thresholds into account.

Many studies use a damage index to represent seismic performance (Motahari *et al.* 2007; Mahjoubi and Maleki 2015). The damage indices are influenced by several major assumptions. Repair costs again present an advantage, as the assumptions and approximations needed to create and use the indices are avoided.

The FEMA P-58 procedure (FEMA 2012b) has been used to conduct comparative studies. Mayes *et al.* (2013) used the FEMA P-58 procedure to evaluate six alternative structural systems, including a FVD design, for a three-storey office and lab building. Terzic *et al.* (2014) conducted a life-cycle cost analysis of five structural designs for a three-storey office building. A structure with FVD was included. Jarrett *et al.* (2015) presented two new structural systems and compared the seismic performance to traditional systems using FEMA P-58. Four-, nine- and 18-storey structures were considered.

Repair costs clearly communicate seismic performance and are useful for decision making. The FEMA P-58 procedure can be used to evaluate the effectiveness of PED systems in improving total-building seismic performance.

2.4 Passive Energy Dissipation Systems

2.4.1 Supplemental Damping

The concept of supplemental damping has been the subject of extensive research. Several comprehensive reviews have been published (Christopoulos and Filiatrault 2006; Soong and Dargush 1997; Constantinou *et al.* 1998; Hanson and Soong 2001). The objective of supplemental damping is to dissipate a portion of the seismic energy introduced into a structure, thereby lessening structural response during earthquakes (Christopoulos and Filiatrault 2006). Primary structural members are protected by concentrating inelastic deformations and the corresponding damage into supplemental damping devices, referred to as dampers. Dampers may be advantageously replaced after a seismic event as they are

not part of the load-bearing structural system (Towashiraporn *et al.* 2002). Supplemental damping devices have gained acceptance throughout the world and are available in a range of forms (Christopoulos and Filiatrault 2006). Dampers can be categorised as active, semi-active, and passive.

Active dampers monitor the state of the structure using an electronic system, process the data through a control system, and use an actuating system to apply internal forces to improve the state of the structure (Christopoulos and Filiatrault 2006). Active dampers require an external power source to function. Concerns of power interruptions as well as instability of the control algorithm during major earthquakes has limited the use of these dampers for seismic control (Connor 2003). Semi-active dampers do not utilise a global structural monitoring system and cannot add energy to the structure. Only local device properties are modified by the control system, reducing the amount of external power needed to nominal levels and removing instability concerns (Soong and Dargush 1997). Passive dampers do not utilise external inputs and have device properties that remain unaltered during the seismic response of the structure (Christopoulos and Filiatrault 2006). Thorough research has proven PED to be an effective, resilient and economical seismic control solution (Christopoulos and Filiatrault 2006; Ahmadizadeh 2007). Passive dampers have substantially outnumbered the implementation of active and semi-active dampers. The remaining literature review focuses on PED solutions due to these advantages.

2.4.2 Types of Passive Dampers

Numerous types of passive dampers have been researched. Symans *et al.* (2008) presented a summary of PED principles, passive damper mathematical modelling, and the advantages and disadvantages of several passive dampers. The two most prevalent categories of passive dampers are hysteretic and viscoelastic. A third category of dampers, motion-activated devices (e.g. tuned-mass dampers), are mainly utilised for wind considerations rather than seismic performance enhancements (Hanson and Soong 2001). Figure 2.3 displays idealised force-displacement (hysteresis) functions for several common types of dampers. PED has developed into a workable technology and passive dampers are now installed

in buildings throughout the world (Constantinou *et al.* 1998; Towashiraporn *et al.* 2002; Crosby *et al.* 1994; Astrella and Whittaker 2005; Soong and Spencer Jr 2002).

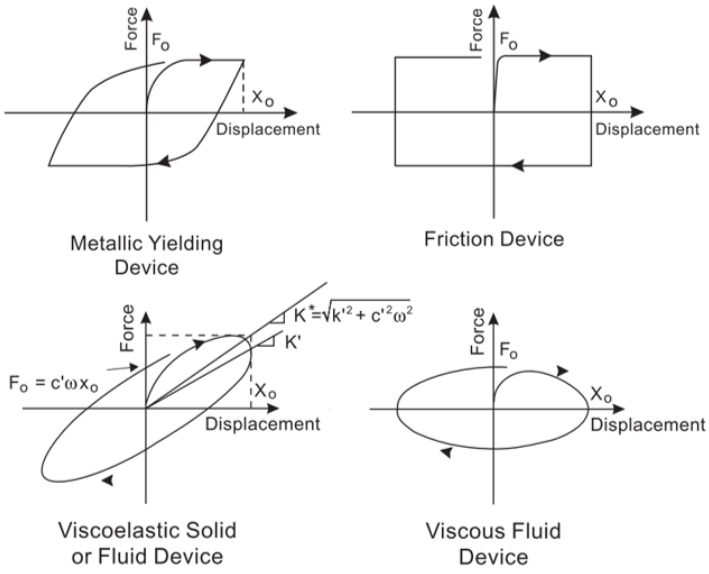

Figure 2.3: Idealised force-displacement functions of passive dampers (Constantinou *et al.* 1998)

Hysteretic dampers dissipate energy when the device attachment points undergo relative displacements. Peak forces generated by hysteretic dampers occur concurrently with the maximum internal forces in structural members (Christopoulos and Filiatrault 2006). These displacement-dependent devices include metallic yielding dampers and friction dampers. Metallic yielding dampers utilise the inelastic deformation of metals to provide energy absorbing capability (Craig *et al.* 2002). Other materials have also been explored such as shape-memory alloys (Soong and Spencer Jr 2002). Friction dampers dissipate seismic energy through friction at the interface of two sliding solid elements (Symans *et al.* 2008).

Unlike hysteretic dampers, the energy dissipation of viscoelastic dampers is influenced by the relative velocities of the connected points. The use of viscoelastic dampers for seismic applications is relatively new compared to the use of hysteretic dampers (Craig *et al.* 2002). This category of passive damper includes FVDs and viscoelastic dampers. Viscoelastic dampers dissipate energy through the shear deformation of viscoelastic material (Soong and Spencer Jr 2002). These dampers are typically mounted in the structure within bracing elements (Symans *et al.* 2008). A FVD consists of a piston filled

with a silicone compound or similar fluid. As the piston moves, fluid passes through small orifices around and through the piston head. The resulting differential of high upstream pressure and minimal downstream pressure produces a large force resisting the motion of the damper (Lee and Taylor 2001). FVDs are robust and have no practical limit on expected life (Lee and Taylor 2001). A conventional FVD is shown in Figure 2.4. Both linear and nonlinear FVDs have been studied (Lin and Chopra 2003).

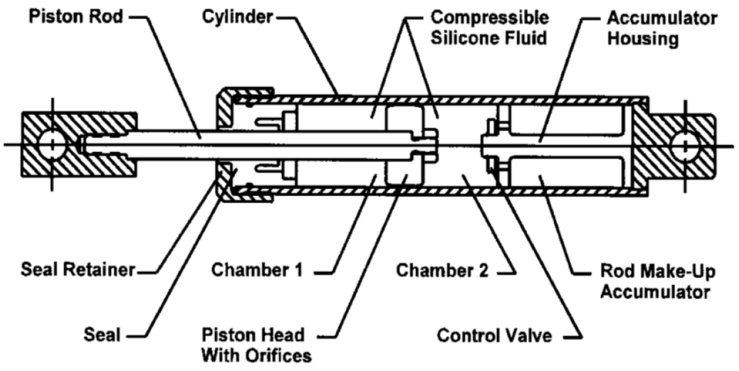

Figure 2.4: Conventional fluid viscous damper (Lee and Taylor 2001)

A range of PED devices, including FVDs, have been introduced. Of the numerous dampers, the type(s) most suited to improving nonstructural seismic performance should be identified.

2.4.3 Use of Passive Dampers to Improve Seismic Performance

Analytical research has demonstrated that PED is an excellent strategy for the seismic rehabilitation of low- (Craig *et al.* 2002), mid- (Vulcano and Mazza 2000) and high-rise structures (Kasai *et al.* 1998). There is also extensive experimental evidence (Kasai *et al.* 2010; Antonucci *et al.* 2004) supporting the use of PED to reduce lateral deformations and inelastic demands on primary structural members. Passive dampers appear to be promising for nonstructural applications, however, this concept must be examined further. Both IDRs and floor accelerations are relevant for nonstructural seismic performance and must be addressed for a PED system to be successful.

Examining nonstructural EDPs rules out metallic yielding dampers, one of the most popular dampers. Metallic yielding dampers effectively limit interstorey drifts, mitigating damage to deformation-sensitive nonstructural systems. However, the added lateral

stiffness reduces the period of the structure and accordingly increases floor accelerations (Vargas and Bruneau 2007). This is detrimental to the seismic fragility of building contents and nonstructural components that are sensitive to acceleration. Several studies have recognised that equipping structures with hysteretic dampers can decrease nonstructural seismic performance (Vargas and Bruneau 2006; Pavlou and Constantinou 2006; Wanitkorkul and Filiatrault 2008; Mayes *et al.* 2004).

An investigation of FVDs suggests that these dampers may be the most promising with regards to nonstructural considerations. Dicleli and Mehta (2007) performed nonlinear time history analyses of single- and multi-storey concentric braced frame (CBF) structures simulating moderate and large intensity earthquakes. It was noted that FVDs can moderate both base shear force and deflections, as the maximum velocity-dependent damper force is out-of-phase with the peak structural deflections. Christopoulos and Filiatrault (2006) also identified this advantage, stating that structural elements experience lower design forces as peak internal seismic forces are out-of-phase with the maximum damper forces. However, this out-of-phase behaviour is influenced by the damper non-linearity as shown in Figure 2.5. Multiple retrofit strategies were assessed by Astrella and Whittaker (2005). Of the models without base isolation, the smallest drift and acceleration demands on nonstructural components were generated in the FVD retrofit system. A case study by Tajirian (2009) investigated options for seismically protecting computers in a database centre including base isolation, metallic dampers, FVDs, computer floor isolation and anchorage. It was concluded that FVDs minimised floor accelerations and drifts while remaining cost-effective.

Pavlou and Constantinou (2006) directed one of the first studies to investigate explicitly the impact of passive dampers on nonstructural seismic performance. Three-storey steel frames with several types of dampers were modelled. Nonlinear response history analyses with several sets of ground motions were performed. FVDs considerably decreased peak floor accelerations and peak floor velocities.

Wanitkorkul and Filiatrault (2008) also researched the application of dampers to improve nonstructural seismic performance. Viscous and hysteretic dampers were used to

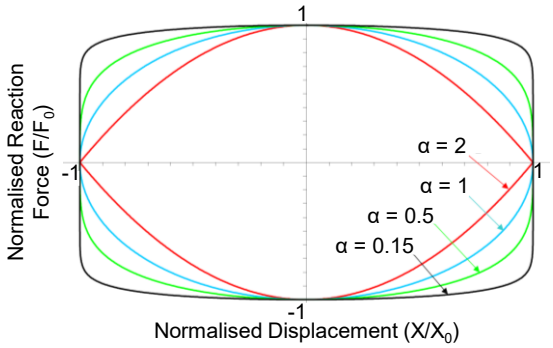

Figure 2.5: Force and displacement relationship for fluid viscous dampers considering different velocity coefficients (α) (Antonucci *et al.* 2004)

retrofit a four-storey steel structure containing generic rigidly anchored and isolated non-structural components. Fragility functions for nonstructural components were constructed using incremental dynamic analysis. FVDs improved seismic performance, indicated by a shift of the fragility functions to the right as shown in Figure 2.6.

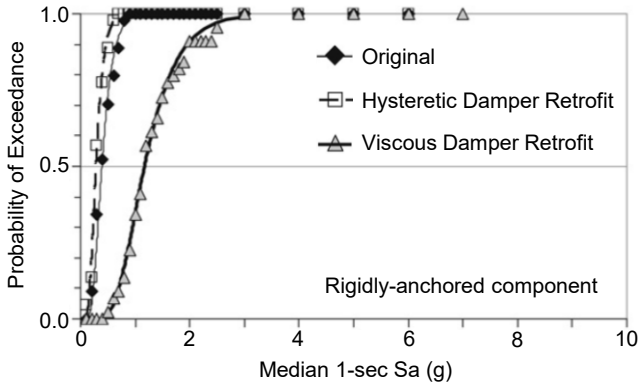

Figure 2.6: Nonstructural fragility functions for functional damage, S_a = spectral acceleration (Wanitkorkul and Filiatrault 2008)

The literature suggests that FVDs are the most promising type of damper for non-structural considerations. Further research is needed on the optimal amount of damping for nonstructural seismic performance. Christopoulos and Filiatrault (2006) stated that a maximum total damping of 35% in the first mode can reasonably be achieved with FVDs. Occhiuzzi (2009) found a maximum of 20% to 25% total damping in the first mode to be ideal. Additional damping increased acceleration and produced reductions in IDR that were deemed negligible by the author. However, solely the author's judgement was used to determine that the IDR reductions were negligible. Studies have not evaluated the optimal amount of damping in terms repair costs, a more appropriate measure of total-building

seismic performance as reviewed in Section 2.3.2. In addition to the amount of damping, another major design decision is the placement of dampers within the building.

2.5 Placement of Fluid Viscous Dampers Within a Building

The distribution of dampers within a building is a critical decision, as damper placement affects structural response and the required damper investment. Despite this, building codes do not prescribe a damper placement method. Many damper placement techniques have been proposed in literature (Whittle *et al.* 2012). Research on damper placement has focused on finding an optimal vertical distribution of dampers within a structure.

In addition to producing an efficient damper distribution, it is desirable that placement methods are practical enough to be used routinely by practising engineers. The scope of this thesis excludes placement methods that require extensive problem-specific tailoring or rely on complex tools and techniques not familiar to practising engineers. These characteristics inhibit the common uptake of a method in practice, as the method cannot be easily incorporated into the design process. One such method is the algorithm for minimum transfer functions proposed by Takewaki (1997), which is commonly referenced in research.

2.5.1 Placement Methods Proposed in Literature

Damper placement methods were reviewed and a set for further study was identified based on prevalence in literature and level of practicality. A review of these selected damper placement methods, as well as the simple placement methods of uniform and stiffness proportional damping, follows.

2.5.1.1 Uniform Damping

Uniform damping evenly distributes the total viscous damping coefficient between each storey. This simple technique is one of the most commonly used placement methods in research and often serves as a benchmark (Lopez Garcia and Soong 2002; Pavlou and

Constantinou 2006; Hwang *et al.* 2013; Palermo *et al.* 2013; Landi *et al.* 2015; Dall'Asta *et al.* 2016). The damping coefficient at storey j (c_j) is calculated using the equation

$$c_j = \frac{C_{total}}{n}, \tag{2.1}$$

where C_{total} is the total viscous damper coefficient added to the structure and n is the number of storeys. The main advantage of uniform damping is its simplicity. However, no attempt is made to optimise damper placement.

2.5.1.2 Stiffness Proportional Damping

Stiffness proportional damping is a second simple placement method widely used in research (Whittle *et al.* 2012; Landi *et al.* 2015; Gidaris and Taflanidis 2015). Stiffness proportional damping distributes the dampers in proportion to the relative storey stiffness. This placement method often results in damper coefficients concentrated in the lower storeys, with reduced coefficients in the upper storeys compared to uniform damping. The method is presented by the equation

$$c_j = \frac{K_j}{\sum_i K_i} C_{total}, \tag{2.2}$$

where K_j is the stiffness of storey j and i is each storey.

2.5.1.3 Simplified Sequential Search Algorithm

The simplified sequential search algorithm (SSSA) aims to be a practical placement method while being more efficient than simple placement methods (Lopez-Garcia 2001). The method seeks to place dampers sequentially where their effect will be maximised. It is assumed that the optimal storey to place a damper in is the one which undergoes a maximum structural response during the ground motion. The optimal location indices are calculated using

$$\gamma_j = \alpha_1 \delta_j + \alpha_2 \dot{\delta}_j, \tag{2.3}$$

where γ_j is the location index of storey j, δ_j is the interstorey drift, $\dot{\delta}_j$ is the interstorey velocity, and α_1 and α_2 are constants defined according to the energy dissipation characteristics of the dampers under investigation (Lopez-Garcia 2001).

The response of the bare frame to a ground motion record is determined through a time history analysis. The first damper is placed at the storey with the greatest location index. The damper properties are incorporated into the model and the process is repeated until all dampers have been placed. As linear FVDs are velocity-dependent dampers, the location indices are given by peak interstorey velocity ($\alpha_1 = 0$ and $\alpha_2 = 1$).

Lopez Garcia (2001) introduced the SSSA and investigated the case of linear FVDs. The effectiveness of the SSSA was compared to two advanced placement methods that require increased analytical effort. Comparable seismic performance, measured by IDRs, was achieved. The study was limited to linear-elastic buildings, one building per advanced method, shear building models rather than realistic structural configurations, four ground motion records, and small damping ratios.

The SSSA was further investigated for linear FVDs by Lopez Garcia and Soong (2002). Greater levels of supplemental damping and several numbers of storeys were considered. It was concluded that the SSSA is more effective for low-rise buildings. Limitations of the study include the use of linear-elastic buildings and simplified shear building models.

One limitation of the SSSA is that the optimal damper distribution is dependent on the ground motion record used in the method. If multiple ground motion records are used, the resulting damper distributions can differ for each record (Lopez Garcia and Soong 2002). The SSSA requires engineering judgement to select a final damper distribution. Another limitation of the SSSA is that the required C_{total} is estimated assuming a linear first mode shape. This assumption is inaccurate for many buildings such as high-rise structures. It implies that damper placement does not effect the damping ratio for a given C_{total}. A third limitation of the SSSA is the assumption that the optimal damper location is the storey which experiences a peak structural response during the ground motion. This assumption has not been completely justified. A major limitation of the method is that it requires iteration, introducing a major resource demand (time and computational). Hwang *et al.* (2013) illustrated an additional limitation of the SSSA. In several case studies, it was found that the SSSA clustered dampers in a small number of storeys. Damper forces would therefore be concentrated in these storeys during an

earthquake. This concentration could cause capacity problems in structural members adjacent to the dampers.

2.5.1.4 Fully Stressed Design Algorithm

Another notable damper placement method was proposed by Levy and Lavan (2006), referred to as the fully stressed design algorithm (FSDA) in this thesis. The method is an analysis and redesign iterative procedure familiar to design engineers. The FSDA seeks to minimise the total added damping coefficient subject to a constraint on the upper bound of a performance index. The method uses the recurrence relationship

$$c_j^{k+1} = c_j^k \left(pi_j^k\right)^{\frac{1}{q}}, \tag{2.4}$$

where c_j^k is the damping coefficient of the jth-storey at iteration k, pi_j^k is the performance index, and q is a convergence parameter with a suggested value of 0.5 for linear problems (Levy and Lavan 2006). The maximum interstorey drift normalised by the allowable interstorey drift (d_a) is the performance index for 2D linear models: $pi_j = \frac{d_j}{d_a}$, where $d_j = \max_t \left(\text{drift}_j(t)\right)$.

The analysis and redesign procedure is conducted for one ground motion record until the desired performance is achieved. The new design is then evaluated using the remaining ground motion records in the suite of interest. If the performance index is exceeded, the ground motion record producing the greatest value is added to the analysis and redesign ensemble. The procedure is repeated until the desired performance is achieved for the entire ground motion suite (Levy and Lavan 2006). The FSDA was compared to a formal optimisation technique by Levy and Lavan (2006) with good results, however the study was limited to shear frames.

It is possible that the FSDA will lead to unrealistically large values of added damping, as was the case in a second Levy and Lavan study (2009) in which the added damping was 53.6%. Lavan and Levy (2009) addressed this limitation by modifying the recurrence relationship of Eq. 2.4. The modified equation is

$$c_j^{k+1} = c_j^k \left(pi_j^k\right)^{\frac{1}{q}} \frac{C_{total}}{\sum_i c_i^k \left(pi_i^k\right)^{\frac{1}{q}}}. \tag{2.5}$$

For 2D linear problems, the modified algorithm minimises the maximum mean squared interstorey drift given a constrained amount of total added damping.

A major limitation of the FSDA is the use of interstorey drift as the performance index. Acceleration-sensitive nonstructural systems are ignored and repair costs are not considered. The procedure can also be time consuming and computationally intensive, as many iterations may need to be performed.

2.5.1.5 Storey Shear Strain Energy Method

Hwang *et al.* (2013) proposed a damper placement method referred to as the storey shear strain energy method (SEM). The method distributes the damping coefficient in a structure in proportion to the storey shear strain energy corresponding to the first mode of vibration. The damping coefficient at storey j is calculating using

$$c_j = \frac{S_j \phi_{rj}}{\sum_i S_i \phi_{ri}} C_{total}, \tag{2.6}$$

where ϕ_{rj} is the relative modal displacement of storey j and S_j is a storey parameter proportional to the shear force of storey j. The storey parameter $S_j = \sum_{i=j}^{roof} m_i \phi_i$, where m_i is the mass of the ith storey and ϕ_i is the modal displacement. A shear building and elastic structural response are assumed in this method to estimate C_{total}. An advantage of this approach is that iteration is not required. A limitation of the method is the assumption that the optimal damper location is related to the storey shear strain energy, an assumption that has not been completely justified.

2.5.1.6 Efficient Storey Shear Strain Energy Method

Hwang *et al.* (2013) modified the SEM with the aim of using FVDs more efficiently. The introduced approach, referred to as the efficient storey shear strain energy method (ESEM), places dampers only in the storeys with a shear strain energy greater than the average storey shear strain energy. This condition is represented as

$$S_j \phi_{rj} > \frac{1}{n} \sum_{i=1}^{n} S_i \phi_{ri}, \tag{2.7}$$

where j is the storey of interest and n is the number of storeys. The damping coefficient is distributed to the "efficient" storeys using

$$c_j = \frac{S_j \phi_{rj}}{\sum_{z=1}^{k} S_z \phi_{rz}} C_{total}, \tag{2.8}$$

where k is the number of storeys whose shear strain energy is greater than the average storey shear strain energy and z refers to all storeys meeting that condition.

An advantage of the ESEM is that iteration is not required. A limitation of the ESEM is the assumption that the optimal damper location is related to the storey shear strain energy, as is the case for the SEM.

2.5.2 Comparison of Placement Methods

A prevalent area of research is the creation of damper placement methods that optimise some measure of seismic performance. In the majority of damper placement studies, a new method is proposed and compared to a small number of existing methods. While a large number of FVD placement methods have been proposed, only limited comparisons of methods have been conducted.

2.5.2.1 Cimellaro and Retamales (2007)

Cimellaro and Retamales (2007) explored the softening and damping design concept. The algorithm proposed by Takewaki (1997), the SSSA and an optimal control theory method were modified to include storey softening. Two shear building models were used to evaluate the methods using peak IDRs and peak absolute floor accelerations from time history analyses. It was concluded that no specific damper distribution method can improve the IDR and acceleration optimally. As all methods produced similar structural responses, it was recommended to adopt methods based on the ease of implementation. Limitations of the study include the use of shear building models, the use of only the ULS earthquake hazard level, and the omission of repair costs when evaluating seismic performance. It was not stated if the time history analysis was linear or nonlinear. In addition, actual damping ratios were not calculated. The use of modified placement methods limits the relevance of the study to cases incorporating softening.

2.5.2.2 Whittle *et al.* (2012)

Whittle *et al.* (2012) recognised the need for a comprehensive comparison of FVD placement methods. Uniform damping, stiffness proportional damping, the SSSA, the Takewaki algorithm and the FSDA were applied using linear FVDs. A regular and an irregular moment resisting steel frame designed in accordance with the Eurocode standards (CEN 2010c) were retrofitted. C_{total} was constrained to the same value for all placement methods, with a target supplemental damping ratio of 32% for the regular structure and 35% for the irregular structure. A maximum IDR of 1% was targeted for the ULS. According to Eurocode 8 (CEN 2013), this limit corresponds to an approximate performance level of immediate occupancy for the SLS and life safety for the ULS. A ground motion suite of 20 records was used. Nonlinear time history analyses of lumped plasticity models resulted in comparable peak IDRs and floor accelerations for all placement methods. The FSDA was recommended by the authors, however it was recognised that the performance advantages were marginal.

On reviewing the time history analysis results from Whittle *et al.* (2012), it can be seen that selecting an optimal placement method using EDPs is inconclusive. Global optimal performance cannot be identified, as there are variations between storeys and between structural parameters. This demonstrates an advantage of using expected economic losses to measure seismic performance.

Whittle *et al.* (2012) did not attempt to determine the optimal amount of damping to maximise seismic performance. The SLS performance was not evaluated. Lumped rather than distributed plasticity models were used. The C_{total} value was equal for all placement methods, however the added damping ratio is affected by damper placement. The actual damping ratios differed between placement methods, ranging from 32% to 48% for the regular structure and 35% to 49% for the irregular structure. These damping ratios were calculated using the energy method, therefore they are approximate rather than exact values.

2.5.2.3 Hwang *et al.* (2013)

Hwang *et al.* (2013) compared several placement methods for linear FVDs. Uniform damping, storey shear proportional damping, the SSSA, the SEM and the ESEM were implemented. The authors proposed using the ratio of maximum damper force and damper coefficient at each storey to measure the efficiency of the placement methods. A 10-storey regular structure, a 10-storey structure with soft-storeys, and a 12-storey building with a setback designed to the Taiwan building code were studied.

Hwang *et al.* (2013) used an approximate formula to calculate the C_{total} value corresponding to a desired supplemental damping ratio of 10% based on a shear building assumption. The actual damping ratios, which differed from the desired ratios, were determined using free vibration. The target damping ratio was not based on seismic performance levels. It was recognised that using the same C_{total} for all placement methods does not necessarily allow for an adequate comparison, as specifying the C_{total} value does not result in the same damping ratio for different damper distributions. Constraining the damping ratio or the C_{total} value can influence the determined "optimal" method.

The IDR results from time history analyses were inconclusive, as there was no global optimal performance when considering all storeys. This demonstrates the advantage of using repair costs to evaluate and compare the seismic performance of damper placement methods. The time history results of the SSSA were of particular interest. The algorithm concentrated dampers in a small number of storeys. As a result, the IDR control of the SSSA was the most favourable out of all considered methods at the storeys with dampers and the worst at the remaining storeys. This is of concern, as drift-sensitive nonstructural systems on the floors without dampers may be heavily damaged during an earthquake.

The analysis conducted by Hwang *et al.* (2013) was limited to elastic planar models. Only two ground motion records that were arbitrarily scaled were considered. Floor accelerations were not evaluated. Another limitation is the use of a single level of damping that was not related to any performance targets.

2.5.2.4 Landi *et al.* (2015)

Landi *et al.* (2015) compared the effectiveness of several damper placement methods for the seismic retrofit of multi-storey RC frames. Simple methods (uniform, mass proportional, stiffness proportional, shear storey proportional and IDR proportional damping), the SEM, the ESEM, and the SSSA were evaluated. Nonlinear FVD were used to produce 10% and 20% supplemental damping in three regular and two irregular RC plane frames. Nonlinear time history analyses with plastic hinges were performed using seven ULS ground motion records. Damper forces, IDRs and floor accelerations were recorded.

Landi *et al.* (2015) found that the IDR profiles were comparable for all placement methods. However, the ESEM and the SSSA did not provide displacement control at the storeys without dampers. Peak floor accelerations were greatly reduced for all retrofitted structures, although it was noted that the efficient storey energy method provided less reduction.

As in the Hwang *et al.* study (2013), consistency between the damping coefficient distribution and the damper force distribution was used as a measure of damper placement efficiency. Using this measure, uniform damping was determined to be inefficient while the energy methods were the most efficient. The ESEM also produced the lowest values of maximum damper forces, a parameter related to damper cost. Landi *et al.* (2015) recommended the energy methods as they "provided good results in terms of reduction in cost, efficiency of the distribution and simplicity of application, compared to other effective, but more complex methods".

The Landi *et al.* study (2015) evaluated the seismic performance of the structures only at the ULS. A limited set of seven ground motion records was used. Lumped rather than distributed plasticity models were used. Repair costs were not considered. The study did not investigate the optimal amount of damping to improve seismic performance or confirm the actual damping ratios of the FVD retrofitted structures.

Reviewing the literature on damper placement and the comparison of competing methods has identified several gaps in the current state of research knowledge. These

limitations, along with those identified throughout the literature review, should be examined further.

2.6 Literature Gaps and Research Objectives

A critical review of literature on the topics of nonstructural seismic performance and the use of FVDs to improve total-building performance was presented. This section provides a summary of the literature gaps and defines research objectives for the thesis. By identifying gaps in current knowledge, the research objectives can be situated within the current body of literature.

Nonstructural systems are essential to building operations and comprise the majority of building investment. Earthquakes in the 1990s to 2010s revealed that conventional seismic design philosophy permits undesirable levels of nonstructural damage. Nonstructural provisions in the major building codes have proven to be inadequate, while anchorage and equipment isolation have limitations. Achieving a desired seismic performance requires the coordination of structural and nonstructural performance. An improved understanding of the total-building seismic performance of conventional code-compliant structures is therefore needed.

A large amount of research evaluating the seismic performance of buildings centres on structural parameters such as IDR and floor acceleration. Complexities arise as these parameters are often competing objectives, while limitations are introduced when determining appropriate parameter weights to represent the overall performance. Other studies use damage indices that are influenced by several assumptions to represent seismic performance. Economic losses are a more appropriate measure of total-building seismic performance and avoids these limitations.

Objective 1: Benchmark the total-building seismic performance of code-compliant buildings designed for seismic regions in terms of repair costs

Supplemental damping devices can substantially reduce drifts and improve the seismic performance of buildings. FVDs have been identified as the most promising of these

devices for nonstructural considerations as they can improve both interstorey drifts and floor accelerations. Despite having the potential to be effective and economically viable solutions, research focusing on FVD applications for nonstructural enhancement has been limited. The majority of research on the use of FVDs to improve seismic performance evaluates structural parameters rather than repair costs. Research is needed on the optimal amount of damping for total-building seismic performance. Previous studies on FVD retrofits have not calculated overall damping ratios, or have provided estimates based on simplifying assumptions. There is also a need to clarify what seismic performance improvements can and cannot be achieved using FVDs.

Objective 2: Investigate the optimal amount of damping for structural and nonstructural seismic performance considering expected repair costs

Objective 3: Evaluate the energy method frequently used to approximate the supplemental damping ratio produced by FVDs

Objective 4: Identify the advantages and limitations of using FVDs to improve seismic performance

The distribution of dampers within a building is a critical decision, as damper placement affects structural response and the required damper investment. Despite this, building codes do not prescribe a damper placement method. While a large number of FVD placement methods have been developed, many require complex tools that limit their uptake by practising structural engineers. The SSSA, the FSDA, the SEM and the ESEM were found to be practical methods, in addition to the simple methods of uniform and stiffness proportional damping. Existing placement methods seek to optimise structural parameters or derived indices rather than earthquake repair costs. Studies evaluating individual placement methods were shown to have several limitations.

Many damper placement techniques have been proposed in literature, however only limited comparisons of techniques have been conducted. There is a need to evaluate and compare the effectiveness of several major placement methods considering structural and

nonstructural performance. Comprehensive assessments for FVD placement optimisation using the FEMA P-58 procedure have not been completed. Research comparing FVD placement methods evaluate structural parameters rather than repair costs. A conclusive optimal placement technique is often not identified due to performance variations between storeys and between structural parameters. Other common limitations include the use of shear building models, the use of a limited set of ground motions, the selection of only a small number of different placement techniques, and the omission of SLS performance.

Objective 5: Evaluate and compare the effectiveness of several major damper placement methods considering structural and nonstructural economic losses, using realistic building models, large ground motion suites and multiple earthquake intensities

The following chapters of this thesis work towards addressing the research objectives defined in this section. The objectives represent a significant opportunity for research contributions to the fields of structural and earthquake engineering.

Chapter 3

Seismic Evaluation Method and Building Design

3.1 Overview of Chapter

A clear understanding of the seismic performance of conventional structures is first needed in order to measure the change in performance obtained from the use of fluid viscous dampers (FVDs). This performance evaluation will serve as a benchmark when evaluating building designs that incorporate FVDs. Details of the conventional performance can also be used when developing retrofit strategies, as areas in need of improvement can be identified. The aim of this chapter is to introduce the seismic performance evaluation method used in the thesis. This includes the creation of several code-compliant building designs.

A set of benchmark building designs were created to represent conventional multi-storey structures in seismic regions. Descriptions of the buildings are provided in Section 3.2. The design procedure is outlined in Section 3.3. The buildings were modelled in the finite element program OpenSees (McKenna 2017). Section 3.4 provides information on the nonlinear finite element models and modal properties of the structures. The creation of ground motion suites for each building is detailed in Section 3.5. Section 3.6 describes the FEMA P-58 (FEMA 2012b) building performance models created to represent structural and nonstructural fragilities. Key points of the chapter are summarised in Section 3.7.

3.2 Description of Benchmark Buildings

The benchmark buildings should be representative of structures designed to modern codes for regions with significant seismic hazards. The intent is for the benchmark buildings to be generic designs with commonplace features. Multi-storey office buildings have been selected as the building type of interest.

The Eurocode standards (CEN 2010c) were selected for the design of the structures. The scope of the investigation is limited to steel concentric braced frame (CBF) buildings. Braced steel frames are a common design type and can also be used to accommodate dampers (Chen and Mahin 2012). Four-, eight- and 16-storey structures were chosen to cover a range of building heights. The storey height is 3.5 m, resulting in building heights of 14 m, 28 m and 56 m for the four-, eight- and 16-storey buildings respectively.

Eurocode 8 (CEN 2013) defines two fundamental requirements. The no-collapse requirement, referred to as the ultimate limit state (ULS) in this thesis, has a 10% probability of exceedance in 50 years. Structures are designed to withstand the ULS design seismic action while retaining structural integrity after the earthquake. The damage limitation requirement, or the serviceability limit state (SLS) in this thesis, has a 10% probability of exceedance in 10 years. Damage at the SLS should be limited to a point that does not compromise building serviceability.

Eurocode 8 Cl 4.4.3 (CEN 2013) specifies damage limitation requirements as interstorey drift limits based on the composition of nonstructural systems in the building. The maximum allowable serviceability drift is 1% for buildings with nonstructural components "fixed in a way so as not to interfere with structural deformations", 0.75% for buildings having ductile nonstructural components, and 0.5% for brittle nonstructural components. Designs respecting the largest drift limit of 1% meet standard code-compliant performance, while designs achieving the most stringent drift limit of 0.5% should minimise nonstructural damage. Serviceability limits considering brittle nonstructural components are therefore expected to be met at 0.5% drift according to the Eurocode methodology.

Two levels of seismic performance were chosen when creating the building designs. One set of buildings was designed to meet the 0.5% drift criterion during the SLS, meeting

the most stringent drift requirements of Eurocode-compliant structures. These designs are referred to as the four-storey standard design (4S), the eight-storey standard design (8S) and the 16-storey standard design (16S).

There is a growing interest in performance-based design and achieving resiliency during structural design. Current code provisions impose stringent drift limits with the objective of reducing damage. A second set of buildings was designed to achieve beyond-code performance, while still applying the Eurocode approach. The second set of buildings were designed to meet the 0.5% drift criterion during the ULS, representing beyond-code performance. These designs are referred to as the four-storey drift design (4D) and the eight-storey drift design (8D). The advanced drift criterion was unable to be met feasibly for the 16-storey building; brace sections could not be selected to meet the ULS drift limit and the Eurocode steel design requirements without placing them in an impractical number of bays. Elevation views of the benchmark structures are shown in Figure 3.1. Further information on the design criteria is provided in Section 3.3.3.

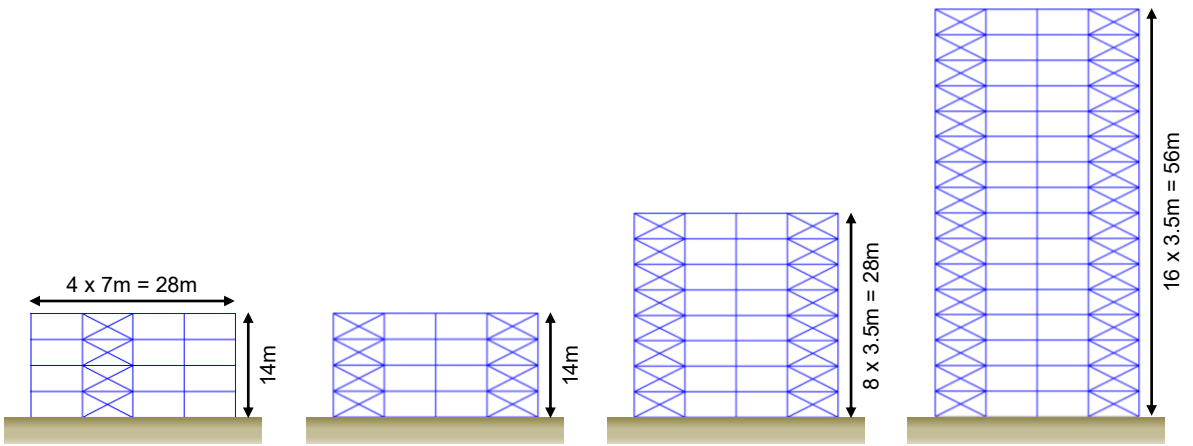

(a) 4S **(b)** 4D **(c)** 8S and 8D **(d)** 16S

Figure 3.1: Elevation view of the office buildings

The steel frame for each building is composed of three 7 m bays in the North-South (N-S) direction and four 7 m bays in the East-West (E-W) direction. The lateral load resisting system consists of CBFs located around the perimeter of the structure. The brace members are pinned at both ends. Buildings 4D, 8S, 8D and 16S have the same plan, with four braced bays in each direction for a total of eight braced bays per storey.

Building 4S has two braced bays per storey in each direction, as the drift limit was able to be met with a smaller number of braced bays. Plan views of the benchmark structures are shown in Figure 3.2 with the braced bay locations indicated.

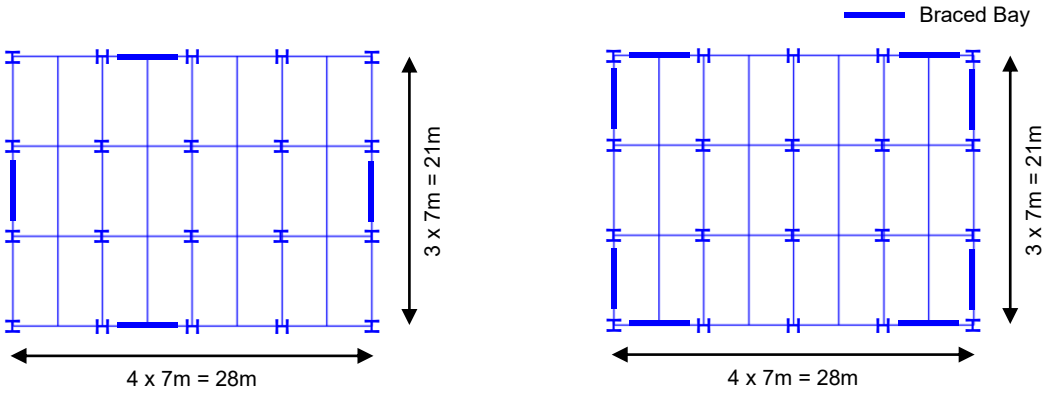

(a) 4S layout **(b)** All other layouts

Figure 3.2: Plan view of the office buildings

Gravity loads are supported by Precast Concrete Hollowcore slabs (Flood Precast n.d.) that span uni-directionally between the N-S aligned beams. It is assumed that there is no composite behaviour between the slab and beams. The slabs are assumed to provide a rigid horizontal diaphragm at each floor level.

Pinned beam-to-column connections and pinned beam-to-beam connections are used. The columns are continuous over several storeys. Column splices are located at mid-storey height and assumed to be rigid. Studies by Elghazouli (2010) have found that continuous columns improve the seismic behaviour of CBF structures by promoting a favourable ductility distribution over the building height. Columns are pinned at the base level, located on the ground floor. A basement was not considered.

The buildings are characteristic of structures designed for regions with significant seismic hazards. A peak ground acceleration (PGA) of 0.306 g was selected for the building site. This level of ground acceleration represents a region where the seismic load is likely to govern structural design. The selected PGA is bounded by the two strongest seismic zones in Greece, zones II (PGA of 0.24 g) and III (PGA of 0.36 g), as well as the two strongest seismic zones in Turkey, zones II (PGA of 0.3 g) and I (PGA of 0.4 g) (Solomos

et al. 2008). Establishing the desired properties of the benchmark buildings, including the design PGA, allows for the building designs to be created.

3.3 Design Procedure

3.3.1 Calculation of Loads

The office buildings are designed to resist dead, imposed (live), snow, wind and seismic loads. Eurocode 0 (CEN 2010c) specifies load combinations, Eurocode 1 (CEN 2010a) details load actions, and Eurocode 8 (CEN 2013) stipulates seismic provisions. Eurocode 3 (CEN 2010b) is the standard for the design of steel structures.

Dead loads considered in the design include the self-weight of structural members and allowances for nonstructural components such as cladding, suspended ceilings, floor finishes, and mechanical, electrical and plumbing systems (DL = $4.47\,\mathrm{kN/m^2}$). Stairs and elevator shafts were excluded to simplify the design. The imposed loads (IL = $3.2\,\mathrm{kN/m^2}$) correspond to office use (Category B1) and the intermediate partition load value (CEN 2010a). Snow loads and wind loads were considered, however they did not govern the structural design. Second order P-delta effects, including equivalent horizontal forces, were accounted for according to Eurocode 3 (CEN 2010b). Both the ULS and the SLS were considered.

The Type One horizontal elastic response spectrum corresponding to a site with earthquakes greater than magnitude 5.5 was used (CEN 2013). Medium sand (ground class C) was assumed for the building site (CEN 2013). A behaviour factor (q) of four was selected, corresponding to a ductility class medium frame with concentric diagonal bracings (CEN 2013). The behaviour factor accounts for the energy dissipation capacity of a structure through ductile response. To avoid explicit inelastic analysis during design, the behaviour factor is used to reduce the elastic response spectrum. An elastic analysis can then be conducted using the resulting design spectrum. The design spectrum for elastic analysis is given in Figure 3.3 along with the elastic response spectrum, showing the significant reduction caused by the behaviour factor.

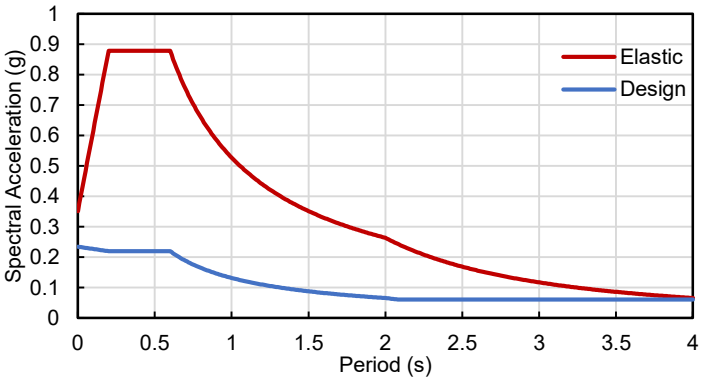

Figure 3.3: Design spectrum used in elastic analysis

Eurocode 8 Cl 4.2.3 (CEN 2013) allows the use of planar models and linear-elastic analysis using the lateral force method if the criteria for regularity in plan and elevation are met. The benchmark structures satisfied the regularity conditions. As a result, 2D models in the program OpenSees (McKenna 2017) were used to determine the response of the structures. The four- and eight-storey structures were designed using the lateral force method. The seismic base shear force was distributed by approximating the fundamental mode shape as horizontal displacements increasing linearly along the building height in accordance with Eurocode 8 Cl 4.3.3.2.3 (CEN 2013). The lateral force equation is

$$F_j = F_b \frac{z_j m_j}{\sum_i z_i m_i}, \tag{3.1}$$

where F_j is the horizontal force acting on storey j, F_b is the seismic base shear, and z_j refers to the height of mass m_j above the ground.

The 16-storey structure did not meet the Eurocode 8 Cl 4.3.3.2.1 requirement that the fundamental period (T_1) be $\leq 2.0\,\text{s}$. As a result, modal response spectrum analysis rather than the lateral force method was used to determine the appropriate seismic loads. The analysis was conducted in SAP2000 (Computers and Structures Inc. 2013). All modes with a significant effect on the global response were taken into account as prescribed in Eurocode 8 Cl 4.3.3.3.1 (CEN 2013). Accidental torsion was captured using the amplification factor (δ) according to Eurocode 8 Cl 4.3.3.2.4 (CEN 2013). Seismic action effects are multiplied by the amplification factor calculated as

$$\delta = 1 + 1.2\frac{x}{L_e}, \tag{3.2}$$

where x is the distance of the considered element to the building centre of mass in the direction perpendicular to the seismic action, and L_e is the distance between the two outermost lateral load resisting elements.

Second-order effects of the seismic design action were considered through the use of the interstorey drift sensitivity coefficient (θ) from Eurocode 8 Cl 4.4.2.2 (CEN 2013). The coefficient is calculated using

$$\theta = \frac{P_{tot} d_r}{V_{tot} h}, \tag{3.3}$$

where P_{tot} is the total gravity load at and above the storey of interest, d_r is the design interstorey drift, V_{tot} is the total seismic storey shear and h is the storey height. If $\theta < 0.1$ the second order effects can be ignored, while if $0.1 < \theta \leq 0.2$ the seismic action effects are amplified by $1/(1-\theta)$. Eurocode 8 applies a limit of 0.3 to θ.

Corner columns of the structures with braced corner bays are affected by earthquakes in both horizontal directions. The horizontal components of seismic action were combined using Eurocode 8 Cl 4.3.3.5.1 (CEN 2013).

3.3.2 Member Requirements

The dissipative zones of CBF structures should be located in the braces in accordance with Eurocode 8 Cl 6.3.1 (CEN 2013). CBFs are designed so that the braces undergo inelastic deformations before the columns and beams. Class one braces were used, meeting the requirements of Eurocode 8 Cl 6.5.3 (CEN 2013) for the medium ductility class and a behaviour factor of four. This ensures sufficient local ductility of brace members to reduce susceptibility to low cycle fatigue failures.

To design the diagonal brace sections, it was assumed that the braces do not carry gravity loads. Only tension diagonals were taken into account during the elastic analysis. These assumptions are in accordance with Eurocode 8 Cl 6.7.2 (CEN 2013). Slenderness requirements for cross braces are provided in Eurocode 8 Cl 6.7.3 (CEN 2013), where the non-dimensional slenderness ($\bar{\lambda}$) should be between 1.3 and 2.0. The lower limit is provided to avoid overloading the columns prior to brace buckling, while the upper limit is provided to ensure adequate behaviour under cyclic loading.

It is known that CBF structures are prone to form soft-storey mechanisms (Tremblay 2003; Ji *et al.* 2009; Elghazouli 2010; Merczel *et al.* 2013; Banihashemi *et al.* 2015). Ductility demands tend to concentrate in an individual storey once brace yielding occurs at the storey. Eurocode 8 seeks to mitigate this mechanism by balancing the overstrength of braces over the building height. Eurocode 8 Cl 6.7.4 (CEN 2013) requires that the maximum overstrength (Ω) of an individual brace not differ from the minimum value by more than 25%. The aim is to promote the simultaneous yield of braces at every storey. The overstrength equation is

$$\Omega_i = \frac{N_{Rd,i}}{N_{Ed,i}}, \tag{3.4}$$

where Ω_i is overstrength of diagonal i, $N_{Rd,i}$ is the design resistance of diagonal i, and $N_{Ed,i}$ is the design value of the axial force.

The design seismic axial forces of beams and columns are amplified to account for brace overstrength. Eurocode 8 Cl 6.7.4 specifies the required buckling resistance as

$$N_{Rd}(M_{Ed}) \geq N_{Ed,G} + 1.1\gamma_{ov}\Omega_{min}N_{Ed,E}, \tag{3.5}$$

where $N_{Rd}(M_{Ed})$ is the design buckling resistance considering the seismic design bending moment M_{Ed}, $N_{Ed,G}$ is the axial force due to gravity loads included in the seismic design combination, $N_{Ed,E}$ is the axial force due to the design seismic action, γ_{ov} is an overstrength factor, and Ω_{min} is the minimum value of Ω_i for all braces in the structure. The objective of this requirement is to ensure satisfactory capacity of the non-dissipative members until brace yield.

Once the design forces were obtained using the combinations of Eurocode 0 (CEN 2010c), the columns and beams were verified according to the provisions of Eurocode 3 (CEN 2010b). Both structural element types were restricted to class one or class two sections. The beams were assumed to have lateral torsional restraint provided by the slabs. The beam sections were evaluated for shear, bending, and serviceability vertical deflections. The columns were verified for compression, bending, bending and axial force, buckling in compression, lateral torsional buckling, and buckling in bending and axial compression.

3.3.3 Damage Limitation

The Eurocode 8 provisions for damage limitation are provided in Cl 4.4.3 (CEN 2013). It stipulates that damage limitation is achieved for an earthquake with a larger probability of occurrence than the design earthquake if given drift limits are respected. These limits are based on the composition of the nonstructural systems in the building. The drift limits and the corresponding nonstructural system information are reproduced below, where d_r is the design interstorey drift, h is the storey height and v is a reduction factor based on the lower return period of the damage limitation earthquake:

(a) "for buildings having non-structural elements of brittle materials attached to the structure": $d_r v \leq 0.005h$

(b) "for buildings having ductile non-structural elements": $d_r v \leq 0.0075h$

(c) "for buildings having non-structural elements fixed in a way so as not to interfere with structural deformations, or without non-structural elements": $d_r v \leq 0.01h$

A reduction factor of $v = 0.5$ is recommended for Importance Class II (ordinary buildings) and was used in this project (CEN 2013). It should be noted that the design seismic displacements are calculated by multiplying the displacements from the linear analysis by the behaviour factor as stipulated in Eurocode 8 Cl 4.3.4 (CEN 2013).

3.3.4 Final Design

The structural system is composed of standard UK structural steel sections: UK beam (UKB), UK column (UKC), and structural hollow (SHS) sections. The beams are Grade S275 and the columns and bracing are Grade S355 with a nominal yield stress of 355 MPa (Tata Steel Europe Limited 2014). The local axes of each perimeter column were aligned so that strong axis bending occurs in the direction of the braced bays. The corner columns are exceptions. In this case, the strong axis was aligned in the building's smaller horizontal direction (N-S).

Visual Basic for Applications (VBA) in Microsoft Excel was used to perform the initial building design. 2D models were created in OpenSees to apply the seismic lateral load.

It was discovered that the 16-storey structure (16S) had a fundamental period greater than two seconds. This necessitated the use of modal response spectrum analysis. A 2D SAP2000 model was created to determine the appropriate seismic loads for 16S. Once all loads were determined, the VBA code was used to iterate the design of steel sections.

Once the loading and member capacities converged, the number of selected member sizes was limited to produce feasible construction designs. The four-storey structures have a single column section size throughout the building height. The column sections of the eight- and 16-storey buildings were allowed to change at the splice locations to minimise steel section sizes. Corner columns in the buildings with braced corner bays have unique sections due to the combination of seismic action in both horizontal directions.

During the design of the eight- and 16-storey standard buildings, it was found that respecting the brace uniformity condition led to excessive overdesign of brace members. Elghazouli (2010) observed that respecting the overstrength uniformity requirement can cause practical difficulties in the selection of brace sizes. This problem was noted by Brandonisio *et al.* (2012) and Merczel *et al.* (2016), who also found that the overstrength uniformity requirement led to impractical and inefficient designs.

Studies by Elghazouli (2010) have shown that column continuity along the building height can compensate for the increase in potential for a soft-storey due to relaxing the overstrength continuity requirement. Other studies (Tremblay 2003; MacRae *et al.* 2004; Ji *et al.* 2009) also found that continuous columns decrease the possibility of large drift concentrations in CBF structures. In order to produce feasible designs that satisfied the brace slenderness requirements and did not have excessive brace overstrength ratios, braces on the top two storeys of the eight- and 16-storey standard buildings were excluded from the uniformity condition. The building designs have continuous columns, which supports this decision.

Despite excluding the braces in the two upper storeys from the uniformity condition, the selection of many brace sections was still governed by uniformity. The resulting structural designs successfully met the standard drift requirements.

The advanced drift building designs were created by modifying the standard designs. The design of these buildings was governed by ULS deflections. Larger brace sections were used to increase lateral stiffness. This led to lower deflections, however it also decreased the fundamental period of the buildings. This led to an increase in the lateral force, which then increased deflections. The process was iterated until the design and deflections converged. In order to meet the advanced drift requirements, the number of braced bays in the four-storey drift design was doubled with respect to the standard four-storey design. The eight-storey drift design excluded the braces in the two upper storeys from the uniformity condition.

The final beam member sections are presented in Table 3.1 for all buildings. The final brace and column sections are provided in Table 3.2 – 3.6. The brace overstrength factors are also provided. Interior columns refer to the inner gravity columns and exterior columns refer to the perimeter columns. Only the smaller section size is provided in the tables for the storeys in which a column section change occurs.

Table 3.1: Beam member sizing

Level	**E-W Direction (UKB)**	**N-S Direction (UKB)**
Floors	406x178x85	305x165x54
Roof	356x171x57	254x146x37

Table 3.2: Column and brace information of building 4S

Storey	**Column (UKC)**		**Brace (SHS)**	**Ω**
	Interior	Exterior		
4	203x203x71	254x254x167	140x140x5	1.42
3	203x203x71	254x254x167	140x140x8	1.18
2	203x203x71	254x254x167	140x140x12.5	1.22
1	203x203x71	254x254x167	140x140x12.5	1.11

Table 3.3: Column and brace information of building 8S

Storey	**Column (UKC)**			**Brace (SHS)**	**Ω**
	Interior	Exterior	Corner		
8	152x152x44	152x152x51	203x203x71	140x140x5	4.08
7	152x152x44	152x152x51	203x203x71	140x140x5	1.80
6	203x203x71	203x203x100	254x254x132	140x140x5	1.24
5	203x203x71	203x203x100	254x254x132	140x140x6.3	1.18
4	203x203x113	254x254x167	305x305x198	140x140x6.3	1.05
3	203x203x113	254x254x167	305x305x198	140x140x8	1.13
2	254x254x132	305x305x240	305x305x283	140x140x8	1.09
1	254x254x132	305x305x240	305x305x283	140x140x8	1.04

Table 3.4: Column and brace information of building 16S

Storey	**Column (UKC)**			**Brace (SHS)**	**Ω**
	Interior	Exterior	Corner		
16	152x152x44	203x203x71	203x203x71	140x140x5	4.39
15	152x152x44	203x203x71	203x203x71	140x140x5	2.36
14	203x203x71	203x203x100	203x203x100	140x140x5	1.76
13	203x203x71	203x203x100	203x203x100	140x140x5	1.54
12	203x203x100	254x254x132	254x254x167	140x140x6.3	1.66
11	203x203x100	254x254x132	254x254x167	140x140x6.3	1.55
10	254x254x132	305x305x198	305x305x198	140x140x6.3	1.47
9	254x254x132	305x305x198	305x305x198	140x140x8	1.64
8	254x254x167	305x305x240	305x305x240	140x140x8	1.56
7	254x254x167	305x305x240	305x305x240	140x140x8	1.50
6	305x305x198	305x305x283	356x406x287	140x140x10	1.64
5	305x305x198	305x305x283	356x406x287	140x140x10	1.58
4	305x305x198	305x406x340	356x406x393	140x140x10	1.53
3	305x305x198	305x406x340	356x406x393	140x140x12.5	1.68
2	305x305x240	356x406x393	356x406x467	140x140x12.5	1.66
1	305x305x240	356x406x393	356x406x467	140x140x12.5	1.57

Table 3.5: Column and brace information of building 4D

Storey	**Column (UKC)**			**Brace (SHS)**	**Ω**
	Interior	Exterior	Corner		
4	203x203x71	254x254x167	305x305x198	140x140x5	2.49
3	203x203x71	254x254x167	305x305x198	140x140x8	2.02
2	203x203x71	254x254x167	305x305x198	140x140x12.5	2.13
1	203x203x71	254x254x167	305x305x198	140x140x12.5	1.93

Table 3.6: Column and brace information of building 8D

Storey	**Column (UKC)**			**Brace (SHS)**	**Ω**
	Interior	Exterior	Corner		
8	152x152x44	203x203x60	203x203x100	140x140x12.5	7.39
7	152x152x44	203x203x60	203x203x100	140x140x12.5	3.30
6	203x203x71	254x254x167	305x305x198	160x160x14.2	2.86
5	203x203x71	254x254x167	305x305x198	180x180x14.2	2.59
4	203x203x113	305x305x283	356x406x340	180x180x14.2	2.46
3	203x203x113	305x305x283	356x406x340	180x180x14.2	2.46
2	254x254x132	356x406x393	356x406x551	180x180x14.2	2.35
1	254x254x132	356x406x393	356x406x551	180x180x14.2	2.23

3.4 OpenSees Models for Nonlinear Analysis

Finite element models enable nonlinear time history analysis to be conducted. The OpenSees program was selected to model the buildings, as it allows the user to manipulate modelling assumptions. The software also contains a wide variety of material models and analysis algorithms. OpenSees has been used in numerous research projects and its benefits are discussed in several earthquake engineering publications (Comerio 2005; Tian *et al.* 2013; Wieser *et al.* 2012).

3.4.1 Model Features

OpenSees was used to generate 2D models of the structural systems. Structural members are represented by line beam-column elements spanning between two nodes. Centreline dimensions were used to define the nodes. Three degrees-of-freedom (DoF) were defined per node. Seismic masses due to gravity loads and member self-weight were lumped at nodes using tributary areas.

Connections were defined as perfectly pinned or perfectly rigid. Pins were modelled using truss elements, or by creating a duplicate slave node and using the *equalDOF* command to constrain the x and y DoF. Rigid diaphragm constraints in the x direction were imposed on all nodes of each floor using rigid truss elements.

The pinned beams were modelled using truss elements (*trussSection*). Distributed plasticity force-based beam-column elements were used to model columns with the OpenSees

default Gauss-Lobatto integration (*forceBeamColumn*). This element type is frequently used in OpenSees seismic analysis (Uriz and Mahin 2008; Kostic and Filippou 2012). Integration points are located at the ends and along the length of the element. Five integration points were used for the columns. Fibre cross-sections are located at each integration point. The fibre cross-sections are composed of several fibres, each of which is assigned a uniaxial stress-strain relationship. A bilinear stress strain relationship was assumed for the columns and beams, assigned using the *Steel01* material in OpenSees. The force-based member representation is shown in Figure 3.4.

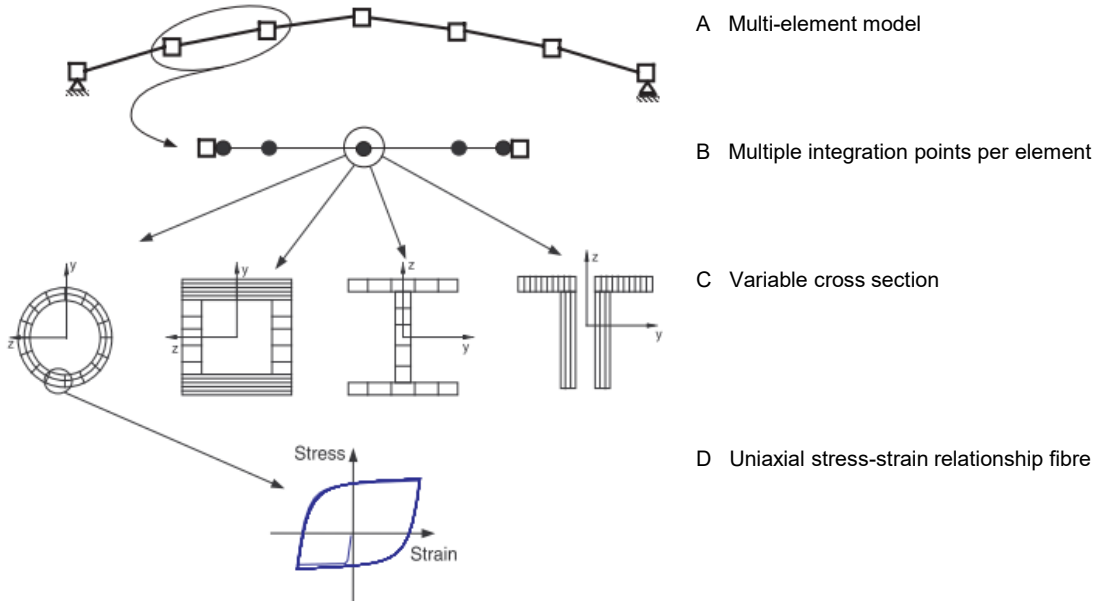

Figure 3.4: OpenSees element representation (Uriz and Mahin 2008)

Kostic and Filippou (2012) investigated the number of fibre sections required for accurate and efficient representation of the local response of cross-sections. Four fibres in each flange and four fibres in the web was recommended for steel wide-flange sections under combined axial and bending loading. It was noted that between 24 to 40 fibres may be required for sections with significant weak axis bending.

A study was conducted to verify an efficient fibre section representation for nonlinear dynamic analysis. A cantilever column with a constant axial load was subjected to displacement controlled cyclic loading. Fibre cross-sections of 12, 40 and 48 fibres were examined. The "exact" solution was modelled by 288 fibres, as was done in the study by Kostic and Filippou (2012). It was determined that 12 fibres were satisfactory for

major axis bending, while minor bending requires 40 fibres to achieve a balance between accuracy and computational resources. The bending moment and curvature relationship for weak axis bending of a sample column is shown in Figure 3.5.

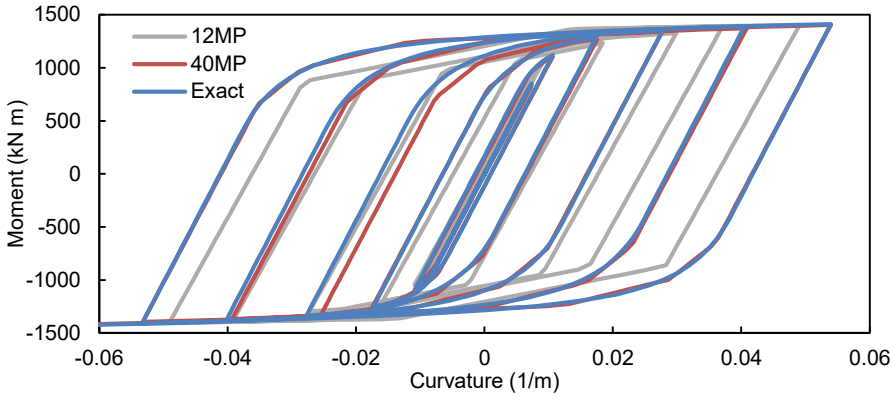

Figure 3.5: Bending moment-curvature relationship from fibre study for weak axis bending

A leaning column was employed to account for P-Delta effects from vertical loads acting on gravity columns in the tributary plan area. Leaning columns have been used to reduce problems to 2D in several studies (Goulet *et al.* 2007; Uriz and Mahin 2008; Chen and Mahin 2012; Jarrett *et al.* 2015). The leaning column is pinned at the base, continuous over the building height, and constrained to have the same lateral displacements at each floor level as the floor diaphragms in the seismic frame. Section properties of the leaning column were determined from the summation of the area and flexural stiffness of each gravity column in the tributary area. The beam-column elements were assigned the P-Delta geometric transformation in OpenSees (*geomTransf PDelta*). Vertical loads equal to the summation of the loads on the tributary gravity columns were applied to the leaning column.

Gravity loads during time history analysis were considered as point loads assigned to nodes. Appropriate tributary areas were used the define the point loads. Seismic loads were applied as an acceleration time series at the base of the structure.

3.4.2 Brace Modelling

The global response of CBF structures is controlled by brace behaviour. It is therefore important to accurately capture the hysteretic behaviour of the brace members. Extensive

experimental studies on the inelastic response of brace members have been conducted since the 1980s (Black *et al.* 1980; Uriz and Mahin 2008). A survey of past experimental research highlighted that the complex nonlinear behaviour of brace members depends on numerous parameters (Tremblay 2002). As a result, a wide range of analytical models have been developed to simulate this behaviour.

Models developed to simulate brace behaviour can be classified as phenomenological, physical-theory, and 3D finite element. The strengths and limitations of each approach have been discussed in several papers (Jin and El-Tawil 2003; Uriz and Mahin 2008; Uriz *et al.* 2008; Wijesundara *et al.* 2014; Karamanci and Lignos 2014; Hsiao *et al.* 2012). Phenomenological models use a truss element with an assigned hysteretic behaviour to reproduce a brace response. This approach requires calibration against available brace response data using numerous empirical parameters for each individual specimen. 3D finite element models are the most rigorous and accurate approach. These models are not commonly used in large structural engineering studies due to the computation expense and complexity (Hsiao *et al.* 2012).

Physical-theory models have been shown to be practical to implement for efficient structural analysis (Uriz and Mahin 2008). The physical-theory approach uses a beam-column element and considers the interaction between bending and axial force. Many proposed physical-theory models use a plastic hinge at the brace midlength, however these models require empirical parameters and produce results of mixed accuracy (Jin and El-Tawil 2003; Uriz *et al.* 2008).

Uriz *et al.* (2008) proposed a physical-theory model using a distributed plasticity element. Comparisons of the axial force-displacement relationship of the model to experimental results verified that an accurate representation of the hysteretic behaviour of compact brace sections is achieved. This method has been frequently used to model brace members in seismic studies since its introduction (Erduran *et al.* 2012; Goggins and Salawdeh 2013; Salawdeh and Goggins 2013; McCrum and Broderick 2013; Wijesundara *et al.* 2014; Karamanci and Lignos 2014; D'Aniello *et al.* 2015; Cutfield and Ryan 2016).

The Uriz method was chosen to model brace members in this thesis. The method is unable to capture the effects of local buckling and low cyclic fatigue, however, studies have shown that the effect of local buckling on the overall behaviour of braces with compact sections is insignificant (Uriz *et al.* 2008; Wijesundara *et al.* 2014). All brace sections selected in the building designs of this project are compact according to Eurocode 3 (CEN 2010b), so it was assumed that local buckling would be minimal. Low cyclic fatigue was determined to be out of scope, as parameters calibrated with test data must be used (Uriz and Mahin 2008; Salawdeh and Goggins 2013).

It has been shown that connection detailing influences the overall response of braces (Hsiao *et al.* 2012). Pin end connections were selected for this project to keep the building design as general as possible, however buildings with specified connection details could be considered.

The Uriz brace model can be implemented in OpenSees (Uriz *et al.* 2008). The model uses force-based beam-column elements with distributed plasticity (*element forceBeamColumn*). Large displacement geometry is accounted for during the transformation from the element reference system to the global reference system using the co-rotational formulation (*geomTransf Corotational*). The Menegotto-Pinto material is used (*uniaxialMaterial steel02*) for the fibre cross-section. At least two elements must be used to represent a single brace member and a node must be placed at the brace midspan. An initial camber at the brace midpoint is introduced to induce axial buckling. Uriz (2008) recommended the following selections for the model parameters: two beam-column elements, three integration points, an initial camber of 0.05% to 0.1% of the brace length, and 10-15 fibre layers across the cross-section depth with five layers in the tension and compression edges.

There have been a wide variety of proposals in literature for the number of elements and integration points required to model a single brace member (McCrum and Broderick 2013; Salawdeh and Goggins 2013; Karamanci and Lignos 2014; D'Aniello *et al.* 2015). Parametric studies were conducted and it was found that the hysteretic behaviour was relatively insensitive to the number of integration points and beam-column elements

beyond the values recommended by Uriz (2008). As a result, each brace is modelled using two elements and three integration points in this project.

The initial imperfection value was found to have a noticeable effect on the initial buckling capacity. This finding agrees with results from D'Aniello *et al.* (2015). However, the study by D'Aniello *et al.* (2015) also determined that the hysteretic area representing the dissipated energy varied by less than 5%. Wijesundara *et al.* (2014) also determined that the selected initial camber has an insignificant influence on buckling loads at subsequent cycles and on overall post-buckling response. As simple pin end connections are used in this thesis and brace connection details are unknown, the initial buckling load is not of particular concern. Accuracy in the total dissipated energy is desired and can be achieved using any reasonably small imperfection. An initial imperfection of 0.1% at the midspan was therefore selected.

All brace sections in this project are SHS. Five fibre layers across the depth of each flange and five fibre layers along the web were used. Two layers were used in the widths. The fibre cross-sections are modelled to capture the brace hysteretic characteristics about the weak axis, which is in the direction of the imperfection. Figure 3.6 displays the cross-section representation. The Menegotto-Pinto material is used with the relevant yield strength and initial elastic tangent. The strain-hardening ratio was set to 0.3% as in the work done by Uriz (2008). The Menegotto-Pinto material parameters that control the transition from elastic to plastic branches were found to have a minimal influence on the brace behaviour when within reasonable values. If further refinement is desired, Karamanci and Lignos (2014) calibrated the Menegotto-Pinto parameters with sets of experimental data.

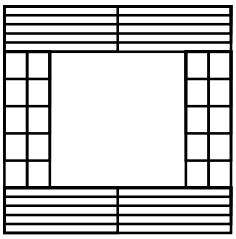

Figure 3.6: Fibre cross-section of the SHS brace members

It was discovered during validation tests that some brace members would exhibit erroneous behaviour during cyclic loading. A brace member would buckle as expected for several cycles, but could then experience yielding in compression. A sample of this behaviour is shown in Figure 3.7. It was discovered that the brace imperfection can straighten to a camber of zero following tension loading. Once the camber was numerically zero, buckling would not occur. To solve this problem, a fictitious force was applied at each brace midspan which developed 5% of the member yield moment.

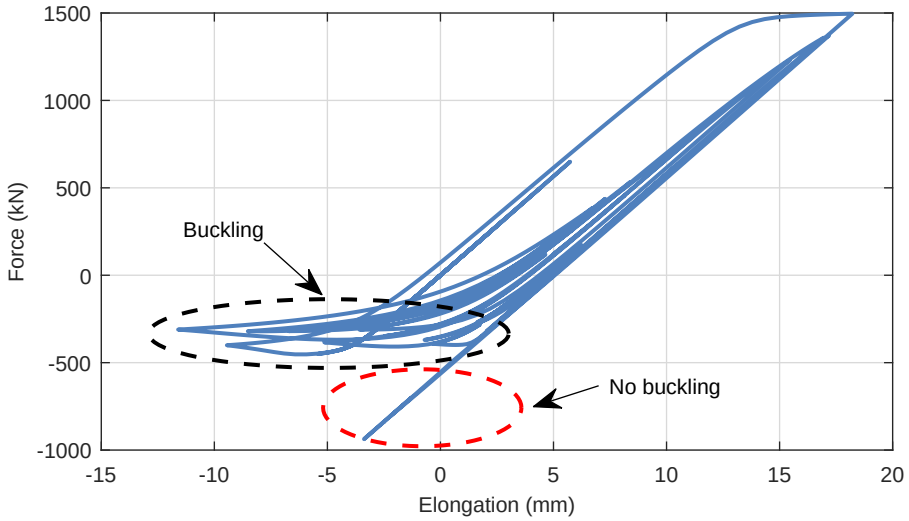

Figure 3.7: Brace force-elongation relationship with erroneous buckling behaviour

The final analytical model to be used in this project was verified using cyclic loading experimental data from Black *et al.* (1980). The results of a validation test are shown in Figure 3.8. The hysteretic behaviour is captured with acceptable accuracy in both the compression and tension regions. The brace behaviour will control the lateral response of the CBF structures, including the modal properties.

3.4.3 Modal Analysis

Modal analysis of the building designs was conducted in OpenSees. Modal properties were used to perform modal response spectrum analysis, calculate inherent damping parameters, and scale ground motion records for time history analysis. Modal analysis was also used to verify the OpenSees model of the 16-storey building. It was found that the periods and mode shapes calculated in OpenSees were nearly identical to those from

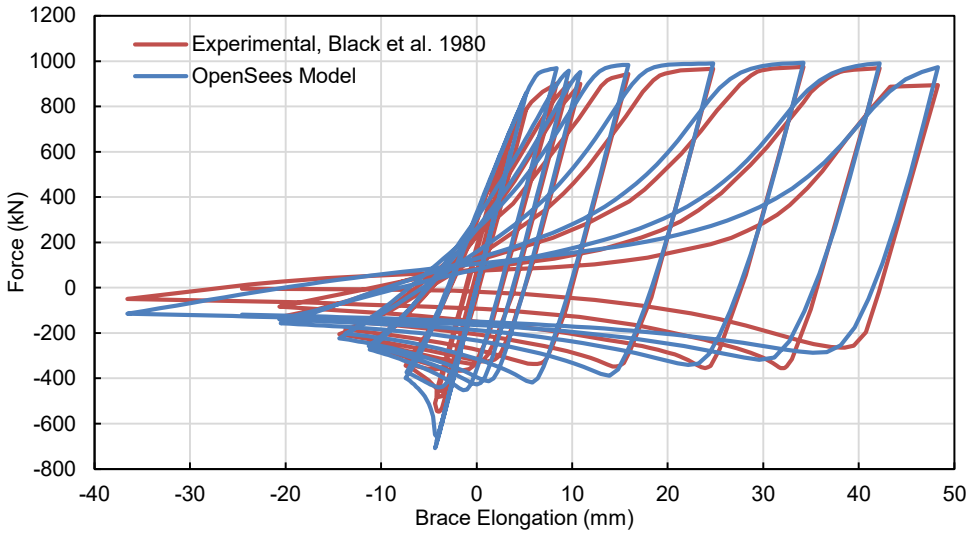

Figure 3.8: Comparison of experimental and analytical brace hysteretic behaviour

SAP2000. The periods of the first three modes of vibration for each building are provided in Table 3.7. The mode shapes for the corresponding modes are displayed in Figure 3.9 – 3.13.

Table 3.7: Periods of the benchmark buildings

Mode	4S	8S	16S	4D	8D
1	0.52 s	0.97 s	2.34 s	0.37 s	0.67 s
2	0.20 s	0.32 s	0.67 s	0.14 s	0.22 s
3	0.12 s	0.18 s	0.35 s	0.09 s	0.12 s

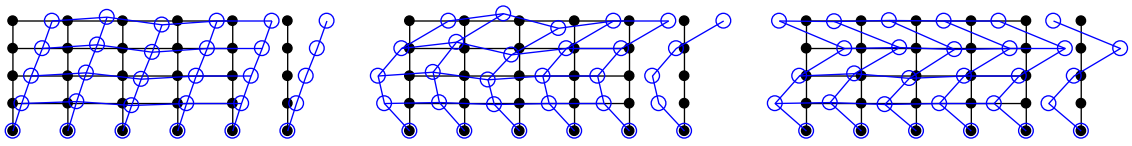

(a) Mode 1 **(b)** Mode 2 **(c)** Mode 3

Figure 3.9: Mode shapes of the 4S model

All modes that contribute significantly to the global response of a structure must be considered when conducting modal response spectrum analysis or assigning inherent damping. Eurocode 8 Cl 4.3.3.3.1 (CEN 2013) considers these significant modes to be captured if the cumulative effective modal mass is at least 90% of the total building mass (M_{total}), and if all modes with an effective modal mass greater than 5% of M_{total} are included. The effective modal mass of a mode is defined such that the base shear

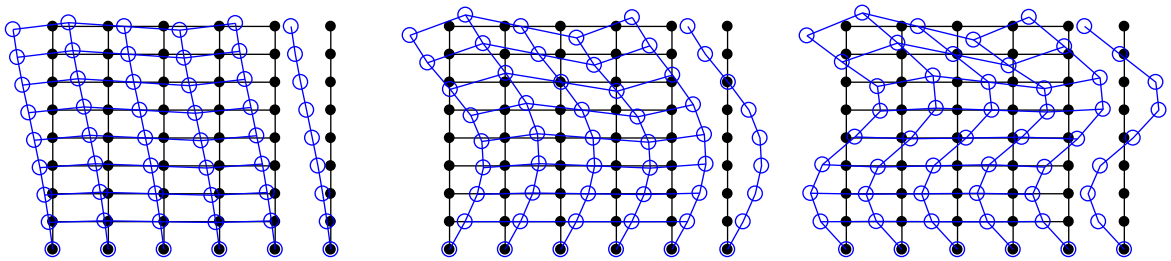

(a) Mode 1 **(b)** Mode 2 **(c)** Mode 3

Figure 3.10: Mode shapes of the 8S model

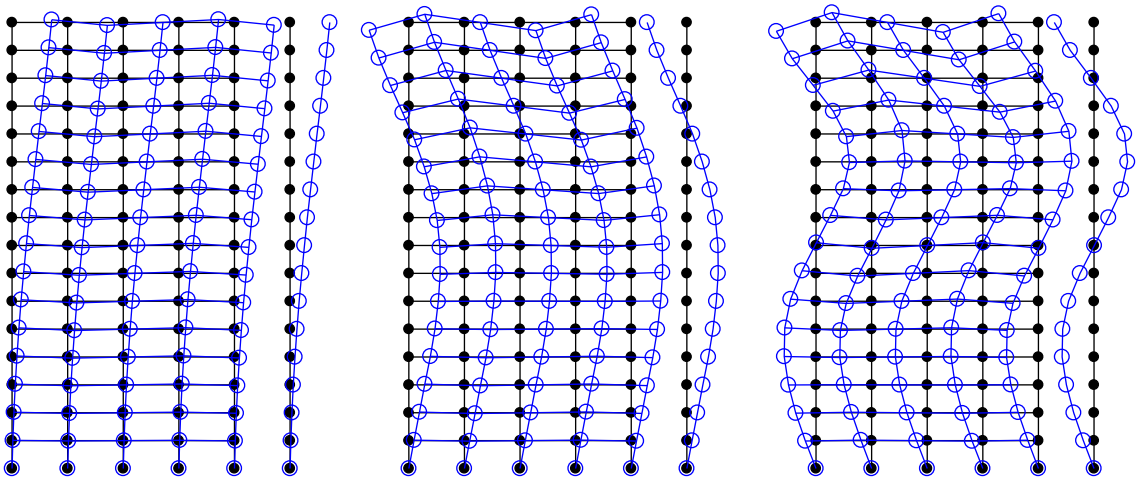

(a) Mode 1 **(b)** Mode 2 **(c)** Mode 3

Figure 3.11: Mode shapes of the 16S model

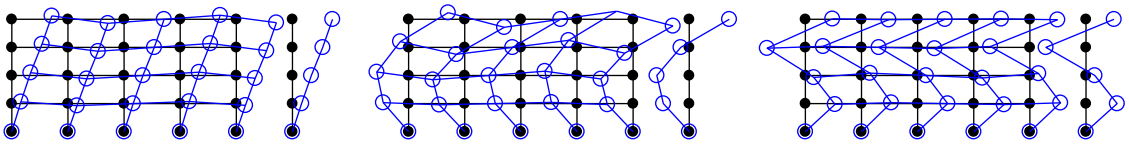

(a) Mode 1 **(b)** Mode 2 **(c)** Mode 3

Figure 3.12: Mode shapes of the 4D model

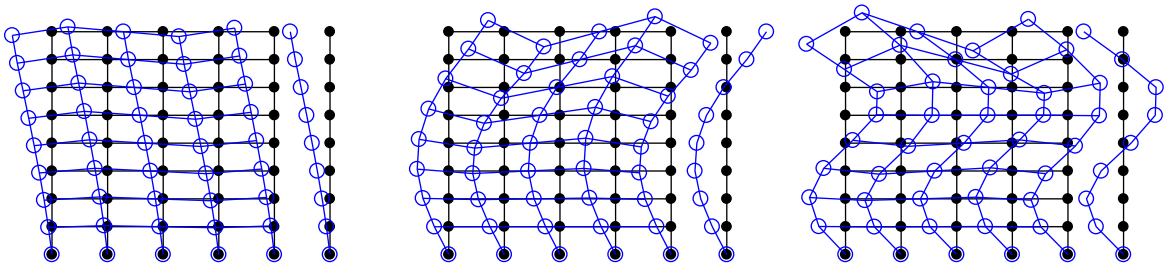

(a) Mode 1 **(b)** Mode 2 **(c)** Mode 3

Figure 3.13: Mode shapes of the 8D model

force experienced by the mode during an earthquake is equal to the effective modal mass multiplied by the spectral acceleration at the mode's period of vibration. The effective modal mass M_n^* of mode n is calculated by

$$M_n^* = \frac{\left(\boldsymbol{\phi}^T \mathbf{M} \mathbf{i_v}\right)^2}{\boldsymbol{\phi}^T \mathbf{M} \boldsymbol{\phi}}, \tag{3.6}$$

where $\boldsymbol{\phi}$ is the mode shape, $\mathbf{M}$ is the mass matrix and $\mathbf{i_v}$ is the influence vector. The modal mass participation of each mode (M_n^p) can be calculated using

$$M_n^p = \frac{M_n^*}{M_{total}}. \tag{3.7}$$

The modal mass participation factors are summarised in Table 3.8 for all buildings. The first two to three modes will control the global response of each structure. These modes must be considered when assigning inherent damping to the structural models.

Table 3.8: Modal mass participation factors of the benchmark buildings

Mode	**4S**	**8S**	**16S**	**4D**	**8D**
1	80.7%	75.0%	65.2%	80.7%	74.2%
2	14.8%	17.4%	21.2%	14.8%	18.1%
3	3.2%	4.2%	6.3%	3.1%	4.5%
Cumulative	98.7%	96.6%	92.6%	98.6%	96.8%

3.4.4 Inherent Damping and Integration Method

Inherent damping was assumed to be 5% in the first mode. Although lower values are often used, the value of 5% damping was selected to match the default for the Eurocode 8 horizontal response spectrum (CEN 2013). It is consistent with several previous studies (Merczel *et al.* 2016; Whittle *et al.* 2012) as well as a report on modelling assumptions for seismic analysis (ATC 2010).

Mass and stiffness proportional Rayleigh damping was used to model the inherent damping. The selection of initial or tangent stiffness will influence analysis results, as significant nonlinear behaviour can be expected from CBF structures during major earthquakes.

Initial stiffness proportional Rayleigh damping is commonly used. However, it has been shown to generate artificial damping in yielding structures (Charney 2008). D'Aniello *et al.* (2013) investigated the influence of modelling assumptions on the seismic response of CBFs. Initial stiffness produced large artificial damping and greatly underestimated displacements when inelastic structural behaviour was observed. In comparison, tangent stiffness provided a close match to the experimental results. Karamanci and Lignos (2014) also found that tangent stiffness produced more realistic responses than initial stiffness for CBFs. As a result of these findings, tangent stiffness was selected. The effect of initial or tangent stiffness on estimated earthquake repair costs will be measured in later chapters.

The Rayleigh coefficients can be determined by specifying damping ratios for two modes. Damping ratios should be specified for the first and last mode that contribute significantly to the structural response (Chopra 2012). The first and third modes were used to determine the Rayleigh damping coefficients (modal properties reviewed in Section 3.4.3). The first periods were elongated to mitigate the generation of artificial damping due to inelastic structural behaviour as recommended by Charney (2008). The elongated periods were calculated by using the Eurocode 8 assumption of tension-only bracing (CEN 2013).

The Newmark integration method was used to solve the dynamic response of the structures (*integrator Newmark 0.5 0.25*). The Newmark parameters were chosen to implement the average acceleration method. The Krylov-Newton algorithm (*algorithm KrylovNewton*) was used to iterate until convergence was achieved (PEER 2017). The minimum value between the time-step of the ground motion record and 0.01 s was selected as the analysis time-step for each record considered. Free vibration equal to four cycles of T_1 were added to the end of the records.

Extensive verification of the OpenSees models was performed. Member forces, node displacements and modal properties were confirmed by comparing the results to those from SAP2000, hand calculations, and the finite element program Plane Frame (Chidiac 2013). Both static and dynamic loadings were used to verify the OpenSees model.

3.5 Ground Motion Scaling and Selection

Suites of ground motion records were compiled to represent the ULS and the SLS earthquake intensities. The ULS earthquake has a 10% probability of exceedance in 50 years. Structures are designed to withstand the ULS seismic action without collapse. The SLS earthquake has a 10% probability of exceedance in 10 years. Damage at the SLS should be limited to a point which does not compromise building serviceability (CEN 2013). Nonlinear time history analyses of the structural models can be performed using these ground motions. Records were obtained from the PEER ground motion database (PEER 2013).

The Eurocode 8 response spectrum was used as the target to scale and select relevant ground motions. A factor of 0.5 was used to define the SLS spectrum. ULS ground motions were constrained to have a magnitude greater than 5.5 to match the Eurocode Type One spectrum. Ground motions for the ULS and the SLS were limited to those with an average shear wave velocity appropriate for ground type C (CEN 2013). A maximum of one record was selected per historical earthquake.

The ground motions were selected and scaled following the Eurocode 8 requirements for recorded accelerograms and nonlinear time history analysis. The mean ground motion suite spectrum must be $\geq 90\%$ of the Eurocode response spectrum in the range of $0.2T_1$ to $2T_1$ (CEN 2013). This condition was generally met as a result of the scaling procedure used. The average of the response quantities can be used as the design value if at least seven nonlinear time history analyses are conducted, otherwise the most unfavourable values from the analyses should be used. A minimum of three records must be analysed (CEN 2013). It is difficult to perform robust analysis with such a small number of ground motions. The number of records required to achieve representative results is liable to be substantially more than the mean of seven records or the maximum of three records as suggested by the Eurocode. For this reason, 25 ground motions were selected for each suite. Separate suites were created for the ULS and SLS.

A linear scale factor was applied to each examined record to minimise the mean squared error (MSE) between the ground motion spectrum and the target Eurocode spectrum

over the period range of $0.2T_1$ to $2T_1$. The scale factor was restricted to the range of 0.5-2. This limit was chosen to prevent excessive ground motion scaling, while more stringent limits did not allow for enough records to be selected. The MSE was calculated using

$$\text{MSE} = \sum_i \left(\ln \frac{SA^{target}(T_i)}{f \times SA^{record}(T_i)} \right)^2, \tag{3.8}$$

where T_i is a period within the range of interest, $SA^{target}(T_i)$ and $SA^{record}(T_i)$ are the spectral accelerations at period T_i of the target and record response spectra respectively, and f is the scale factor applied to the record response spectrum (PEER 2013).

As the ground motions were scaled considering the T_1 value, separate ground motion suites were created for each building. For each limit state, 25 ground motions with the smallest MSE were selected. This resulted in 50 records per benchmark building and a total of 250 records overall. The properties of the ground motion suites are listed in Table A.1 – A.10 in Appendix A. Figure 3.14 – 3.18 compare the mean ground motion suite and the Eurocode 8 elastic response spectra for all buildings and limit states. The period range of interest has been indicated in each figure, as well as the spectra with the largest and smallest MSE.

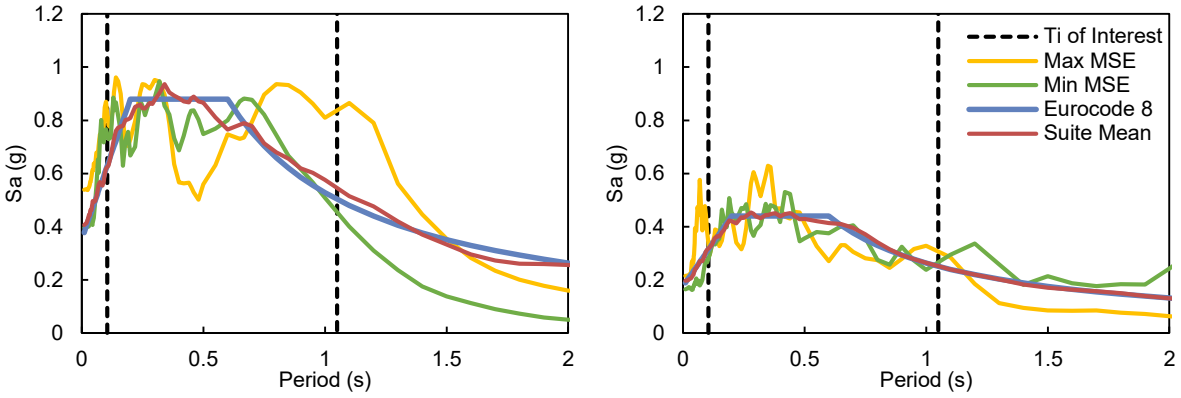

(a) ULS comparison **(b)** SLS comparison

Figure 3.14: Comparison of the 4S ground motion suite and Eurocode 8 spectra

The ground motion suites will allow nonlinear time history analyses to be conducted. The structural response from each analysis is used in the FEMA P-58 seismic performance assessment procedure (FEMA 2012b).

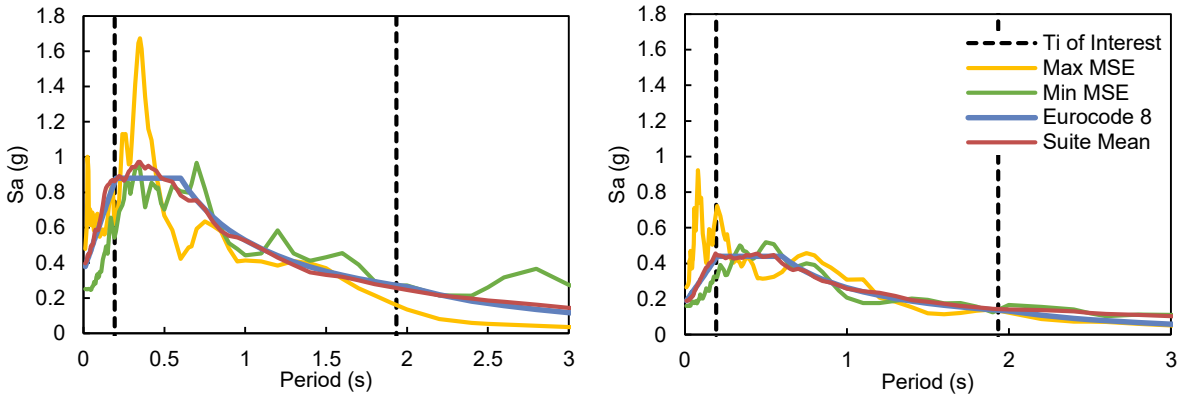

(a) ULS comparison **(b)** SLS comparison

Figure 3.15: Comparison of the 8S ground motion suite and Eurocode 8 spectra

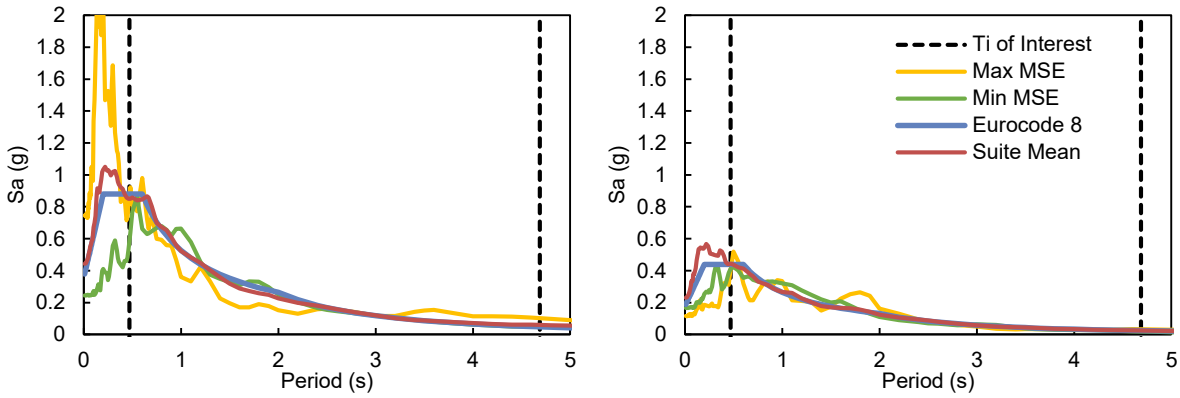

(a) ULS Comparison **(b)** SLS comparison

Figure 3.16: Comparison of the 16S ground motion suite and Eurocode 8 spectra

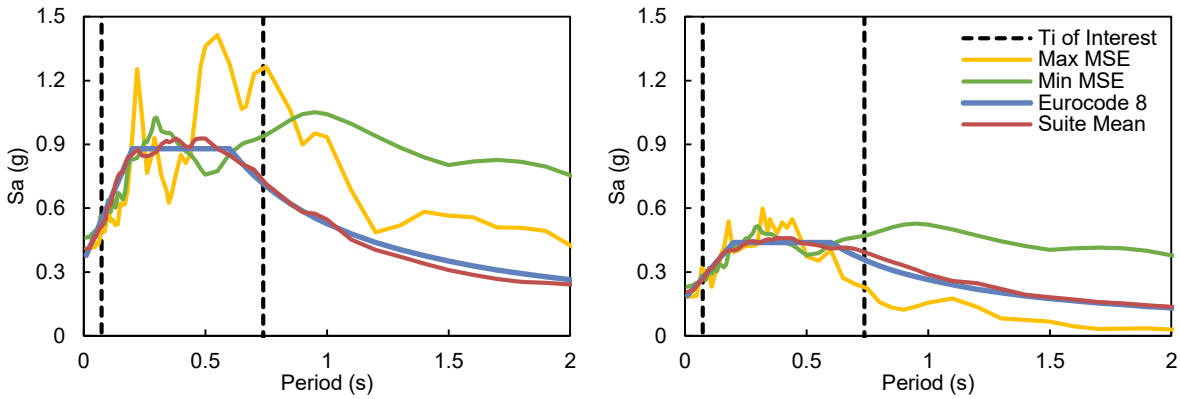

(a) ULS comparison **(b)** SLS comparison

Figure 3.17: Comparison of the 4D ground motion suite and Eurocode 8 spectra

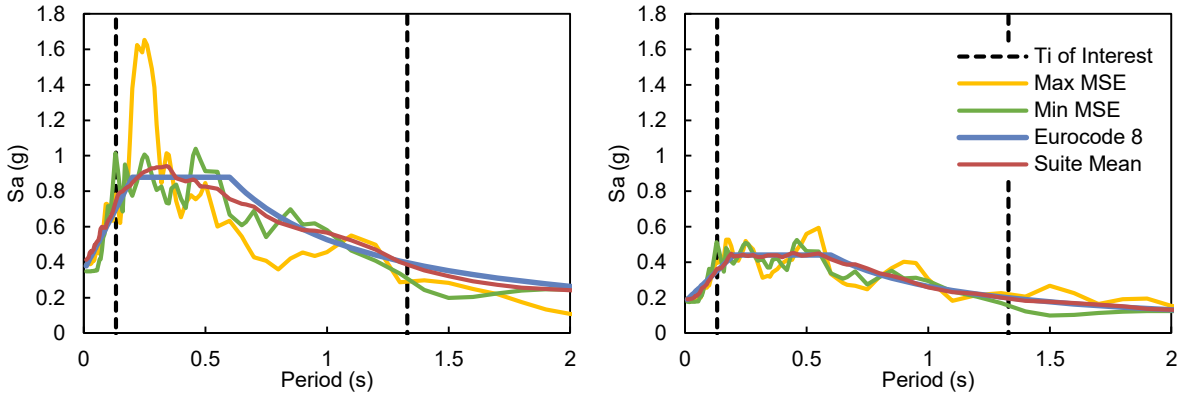

(a) ULS comparison **(b)** SLS comparison

Figure 3.18: Comparison of the 8D ground motion suite and Eurocode 8 spectra

3.6 FEMA P-58 Building Performance Model

The FEMA P-58 intensity-based nonlinear performance assessment procedure (FEMA 2012b) is used in this thesis to evaluate the seismic performance of buildings. The procedure is a methodology for assessing the seismic performance of individual buildings through probabilistic loss calculations. It has been implemented in an electronic tool referred to as the performance assessment calculation tool (PACT). Structural analysis results and a Building Performance Model are PACT inputs, and the output is a measure of seismic performance. The definition of component quantities, fragility functions and cost functions are the major contributions of FEMA P-58.

3.6.1 FEMA P-58 Procedure

The Building Performance Model is a collection of data representing the building assets at risk during an earthquake. Each type of building component is associated with fragility functions and repair cost functions. Fragility functions indicate the probability of exceeding a damage state at a given engineering demand parameter (EDP) value. Repair cost functions indicate the economic losses for each damage state. Peak structural response parameters from time history analyses of a structure are used in combination with fragility functions to determine probable damage states for the building components. Corresponding repair costs are calculated using the repair cost functions. Building

downtime and occupant casualties were out of the thesis scope, as methods for estimating these consequences were considered too inaccurate.

Both structural and nonstructural systems can be included in the Building Performance Model. Components that are not vulnerable to damage are deemed rugged and are not included. The selection of rugged components was compiled by FEMA P-58 based on post-earthquake observations and laboratory experiments.

The EDPs used to characterise demands on structural and nonstructural systems in FEMA P-58 are absolute floor acceleration, absolute floor velocity, and interstorey drift. Peak values of the EDPs at each floor or storey are used. Fragility functions are typically represented by log-normal cumulative distribution functions. Multiple fragility functions corresponding to different damage states can be defined for a component. A sample fragility function set with three damage states is shown in Figure 3.19 for a gypsum wall partition with metal studs.

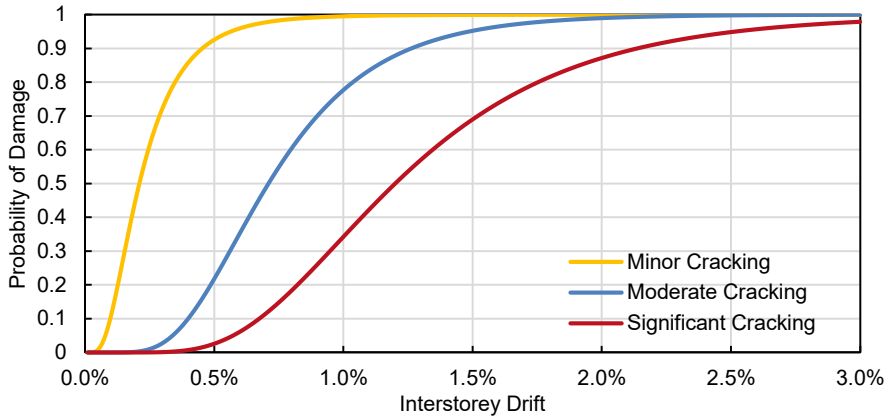

Figure 3.19: Fragility functions for a gypsum wall partition with metal studs from FEMA P-58 (2012b)

Monte Carlo analysis is used to determine probable distributions of losses. FEMA P-58 enables the seismic performance of a structure to be measured in repair costs rather than a set of structural parameters. This is a major advantage of the procedure, as repair costs clearly communicate seismic performance and are useful for decision making.

3.6.2 Implementation of FEMA P-58

The results of seismic performance assessments in this thesis are expressed by repair costs in 2011 US dollars. These are direct repair costs and do not include indirect costs due to building downtime as well as flooding due to piping failure. Although these indirect costs are substantial, they are difficult to calculate accurately for a general building and were deemed out of scope.

Structural component fragility groups and the quantities of each were determined based on the structural design. For column splices of two different sections, the section with the greater self-weight was used to determine the appropriate fragility group.

Nonstructural fragility groups and quantities were obtained using the Normative Quantity Estimation Tool (FEMA 2012b). The Normative Quantity Estimation Tool is an Excel tool that provides typical nonstructural quantities based on occupancy type and floor area. The default nonstructural component types and median component quantities for a commercial office building were considered with some modifications (noted below and in Section 3.6.3.1). As specified in Volume 2 of the FEMA P-58 documentation (FEMA 2012d), median drifts of the damage states for curtain wall systems were adjusted based on the actual panel height.

A seismic design category of D was selected for nonstructural components when available. This design category represents stringent seismic considerations and is grouped together with D, E and F (essential facilities) within FEMA P-58 (2012b). Robust equipment anchorage was assumed for HVAC components when available. These conservative assumptions represent buildings with stringent seismic design and will avoid the overestimation of repair costs.

Repair cost functions indicate the economic losses for each damage state. The default cost functions were used when available.

Several parameters must be assigned in PACT. The suggested height factors were used to reflect cost increases due to loss of repair works efficiency on upper levels. A hazmat factor of 1 was selected to represent a modern building without hazardous materials. The recommended occupancy factor for commercial office buildings of 1.2 was used to reflect

the increased cost of working around ongoing building operations. The non-directional conversion factor, which estimates the non-directional value of an EDP as a factor of the maximum value of either horizontal direction, was set to 1.3. This reflects the Eurocode 8 combination of horizontal seismic actions. The total loss threshold is a limit on the repair costs at which a building will be replaced rather than repaired. A value of 1.0 was used so that assessment information will be obtained for every realization.

Monte Carlo analyses is conducted using 1000 realizations per limit state. To perform the analyses, a modelling dispersion parameter is specified in PACT. This parameter is a function of the construction quality and the quality of the analytical model. Average values were assumed, producing a modelling dispersion of 0.3536. Prior to conducting the Monte Carlo analysis in PACT, several modifications to the FEMA P-58 procedure were appropriate for this thesis.

3.6.3 Modification of FEMA P-58

3.6.3.1 Nonstructural Quantities

Quantity distribution parameters were assigned a value of zero for all nonstructural fragility groups. As a result, each performance analysis of a given building used the same quantity of nonstructural components. The default quantities of suspended ceiling components and roof tile components were replaced by the actual plan area of the structures being considered. The default quantities of cladding were also replaced to reflect the actual perimeter and storey height values.

3.6.3.2 Brace Fragility

Cutfield *et al.* (2016) found that damage to CBFs contributed significantly to the FEMA P-58 losses even during minor loading when the structural model did not predict damage to the brace or gusset plate. As a result, brace fragility functions in the paper were overridden to negligible values when the model determined that brace or gusset stresses were not within 2% of the yield stress.

This observed erroneous brace damage was confirmed by studies conducted in this thesis. There are three fragility functions for CBFs in FEMA P-58. Damage state one is of particular concern. The description for damage state one is:

> Buckling of the brace has begun but does not exceed the depth of the brace. Initial yielding of the gusset has begun. Residual deformation of the brace has occurred but is barely noticeable to the naked eye and does not exceed half the brace depth. Residual drift is slight (FEMA 2012b).

The repair procedures for damage state one are for aesthetic reasons, described in PACT as follows:

> Brace damage is largely aesthetic. Heat straightening may be desirable but replacement would be for aesthetic reasons (FEMA 2012b).

From the Consequence Estimation Tool (FEMA 2012b), it is revealed that approximately 85% of the damage state one repair costs are due to temporary access to the member (removing and replacing partition walls, MEP modifications, etc.) rather than the frame repair itself. It is reasonable to assume that this aesthetic repair procedure is unlikely to take place. The FEMA P-58 background documentation on CBFs recognises that the provided fragility functions must be used with caution as they are strongly influenced by factors such as brace cross-section, brace slenderness, connection detailing, and frame design (Roeder *et al.* 2009). As a result, it was decided to evaluate damage state one further using the OpenSees models.

Pushover analyses of single CBFs were performed in OpenSees. Each CBF was pushed to an interstorey drift ratio (IDR) beyond the median drift value for damage state one. This was done in two separate analyses, one to produce brace tension and one to produce brace compression. The brace force and the displacement of the brace midpoint were monitored. This pushover analysis was conducted for each brace section used in the benchmark designs. The results for the SHS 180x180x14.2 section are shown in Figure 3.20 and 3.21, where Figure 3.20 is the brace force-frame drift relationship and Figure 3.21 is the displacement of the brace midpoint. It can be seen that the brace behaves in a

linear elastic manner in tension. In compression some slight stiffness loss occurs due to the onset of brace buckling, however this behaviour is elastic. There are no residual forces or residual brace deformation. As a result, the fragility function representing damage state one was removed.

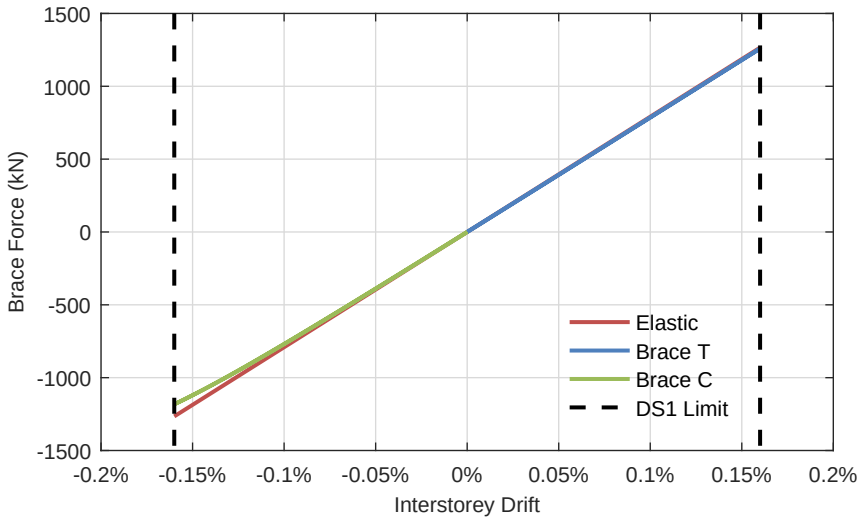

Figure 3.20: Force-drift relationship of an OpenSees brace and damage state one limit

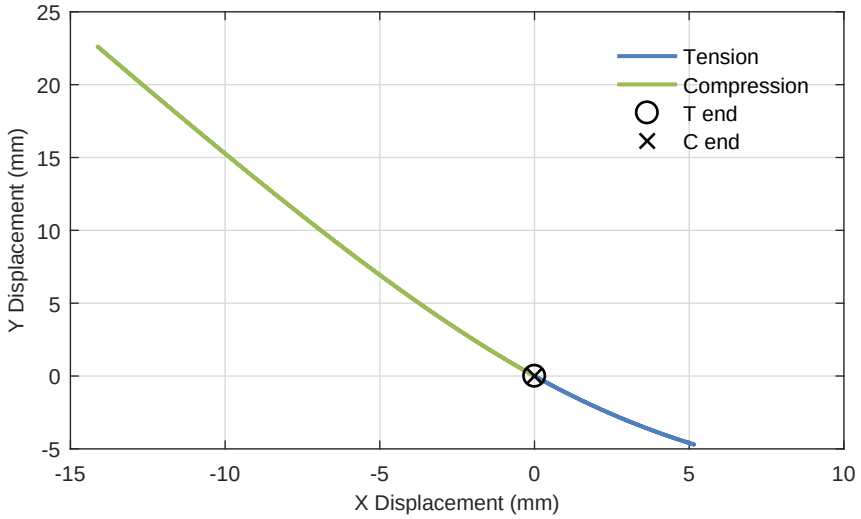

Figure 3.21: Midpoint deflection of an OpenSees brace during a pushover analysis test considering damage state one

3.6.3.3 Replacement Costs

Replacement costs are not provided by PACT for work stations, desktop electronics, bookcases and filing cabinets. The replacement cost for desktop electronics was assumed

to be \$1800 per unit based on the estimate from Cutfield *et al.* (2016). The unit costs for work stations, bookcases, and filing cabinets were taken as the median costs from a 2011 office furniture price list (National Office Furniture 2011). Work stations were set to \$105 per unit (5% of purchase cost as recommended by FEMA P-58), bookcases to \$1350 per unit, and filing cabinets to \$2375 per unit. FEMA P-58 specifies that repair costs include the removal of damaged components, and the transportation and installation of new components. The extra costs are difficult to estimate accurately and were not considered. This simplification was accepted as the repair costs are consistent amongst the considered buildings and will allow for comparisons. It is a conservative assumption that will prevent the overestimation of costs.

3.6.4 Summary of Fragility Information

Table 3.9 provides a summary of the critical fragility information selected for use in the thesis, where PFA is peak absolute floor acceleration, x_m is the median EDP value, and β is the logarithmic standard deviation of the EDP values. The fragility information is available from FEMA P-58 (FEMA 2012b). Full fragility information used in the project is provided in Appendix B.

3.7 Summary of Methods and Conclusions

This chapter presented the seismic performance assessment procedure employed in the thesis. Five conventional building designs were created in accordance with the Eurocode. Standard and advanced drift performance levels were considered. The structures were modelled in the finite element program OpenSees. The Uriz physical-theory brace model was used (Uriz *et al.* 2008). It was discovered that some brace members could experience yielding in compression during cyclic loading due to brace straightening. A fictitious force was applied at the midspan to enable brace buckling.

FEMA P-58 Building Performance Models (FEMA 2012b) were created to represent structural and nonstructural systems. Anchorage and seismic design category assumptions were made to represent buildings with stringent seismic design and avoid the overestimation

Table 3.9: Summary of critical structural and nonstructural system fragility information. x_m = median, β = logarithmic standard deviation

System	**EDP**	**Damage State**	$\boldsymbol{x_m}$	$\boldsymbol{\beta}$
Concentric braced frame	IDR	Buckling and yielding	0.01	0.3
		Fracture or local buckling	0.0178	0.3
Glass curtain wall	IDR	Glass cracking	0.01097	0.45
		Glass falls from frame	0.01254	0.45
Gypsum wall partition with metal studs	IDR	Minor cracking	0.0021	0.6
		Moderate cracking or crushing	0.0071	0.45
		Significant cracking or crushing	0.012	0.45
Suspended ceiling, vertical and lateral support	PFA	Minor tile dislodgement	0.35g	0.4
		Moderate tile dislodgement and grid damage	0.55g	0.4
		Total ceiling collapse	0.8g	0.4
Air handling unit	PFA	Equipment does not function	0.25g	0.4
Desktop electronics	PFA	Falls, does not function	0.4g	0.5

of repair costs. Damage state one of the brace fragility set was shown to be for aesthetic concerns and was removed following an OpenSees pushover study.

The conventional designs and the seismic performance assessment method established in this chapter are needed in order to benchmark the seismic performance of modern multi-storey buildings. Chapter 4 will conduct the seismic performance benchmark, investigating the expected nonstructural and structural damage in repair costs. This performance evaluation will serve as a benchmark when evaluating FVD retrofitted designs.

Chapter 4

Seismic Performance Benchmark of Code-Compliant Buildings

4.1 Overview of Chapter

Damage to nonstructural systems during earthquakes in the 1990s to 2010s resulted in costly repairs and extended building downtime. Attaining a target level of seismic performance mandates the harmonisation of structural and nonstructural performance levels. An improved understanding of the expected overall seismic performance of code-compliant buildings is therefore needed. This chapter investigates the seismic performance of conventional multi-storey buildings designed for seismic regions. A benchmark of this performance will be used to measure the effectiveness of fluid viscous damper (FVD) retrofits in the following chapters.

Eurocode 8 (CEN 2013) prescribes interstorey drift limits with the aim of controlling nonstructural damage. This chapter assesses the seismic performance of Eurocode-compliant concentric braced frame (CBF) buildings designed to meet different drift limits. Previous research on Eurocode CBF buildings has focused on structural performance. The determination of total-building seismic performance considering nonstructural systems has not been evaluated in detail. In addition, the applicability of the Eurocode 8 drift limits for nonstructural damage remains uncertain.

Previous studies comparing seismic performance consider structural parameters such as interstorey drifts and floor accelerations (Lavan and Dargush 2009; Terzic *et al.* 2014). Complexities arise as these parameters are often competing objectives. Limitations are

introduced when determining appropriate parameter weights to represent performance. Other studies use damage indices that are influenced by several assumptions to represent performance (Motahari *et al.* 2007; Mahjoubi and Maleki 2015). The use of repair costs is a more appropriate measure of total-building seismic performance and avoids these limitations. The breakdown of total repair costs by engineering demand parameter (EDP) and by fragility group is novel.

Nonlinear time history analyses of the case study buildings were conducted in OpenSees (McKenna 2017). The analysis implementation and results are examined in Section 4.2. Section 4.3 provides estimations of the building values. These values are useful when examining the expected repair costs. Repair costs including structural and nonstructural damage were determined using the FEMA P-58 performance assessment procedure in Section 4.4. Section 4.5 assesses the effectiveness of the Eurocode nonstructural provisions. Section 4.6 reviews the results of a sensitivity study on the FEMA P-58 repair costs with regards to various assumptions. The main conclusions of the chapter are reviewed in Section 4.7.

4.2 Nonlinear Time History Analysis

Nonlinear time history analysis of the benchmark buildings was conducted using the ground motion suites compiled in Section 3.5. The ultimate limit state (ULS) and the serviceability limit state (SLS) were considered. The set of buildings designed to represent the maximum performance of Eurocode-compliant structures are referred to as the four-storey standard design (4S), the eight-storey standard design (8S) and the 16-storey standard design (16S). The second set of buildings representing beyond-code performance are referred to as the four-storey drift design (4D) and the eight-storey drift design (8D). Descriptions of building design and OpenSees modelling were detailed in Section 3.3 and Section 3.4, respectively.

4.2.1 OpenSees Implementation

The ground motion records were input into OpenSees as a time series object (*timeSeries Path*), which represents the relationship between the load factor and time as a series of discrete points. Each record was applied to the models as a uniform excitation acting in the global x direction (*pattern UniformExcitation*).

Structural response parameters used to characterise demands on structural and non-structural systems are absolute floor acceleration, absolute floor velocity and interstorey drift ratio (IDR). These EDPs are recorded during the time history analyses. Absolute acceleration and velocity were obtained using the node recorder with the time series option enabled (*recorder Node ... -timeSeries*). Floor displacements were obtained using the node recorder (*recorder Node*). Floor displacements were used to calculate IDRs with the equation

$$\text{IDR} = \frac{\Delta u_i}{h_i} = \frac{u_i - u_{i-1}}{h_i}, \tag{4.1}$$

where u_i and u_{i-1} refer to the horizontal displacements of consecutive floors and h_i corresponds to the storey height. The peak EDPs were retained from each time history analysis to be input in the FEMA P-58 Building Performance Models.

4.2.2 Engineering Demand Parameters

The peak EDP results from the time history analyses are shown in Figure 4.1 and 4.2 for the ULS and the SLS. These plots include the mean (μ) values as well as values one standard deviation (σ) from the mean. The mean velocity values are given in Table 4.1 as they did not vary substantially over the building height.

Table 4.1: Mean of the peak floor velocities

Building	ULS Mean	SLS Mean
4S	3.78 m/s	1.86 m/s
8S	3.78 m/s	1.82 m/s
16S	4.30 m/s	2.26 m/s
4D	3.87 m/s	1.99 m/s
8D	3.89 m/s	1.76 m/s

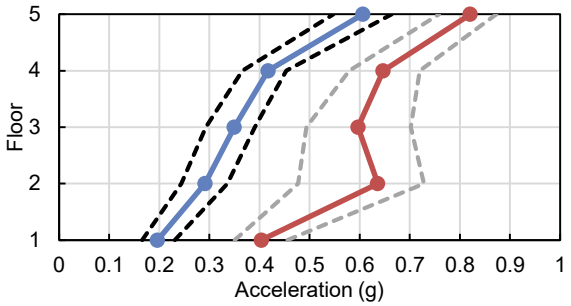

(a) Peak absolute floor accelerations of 4S

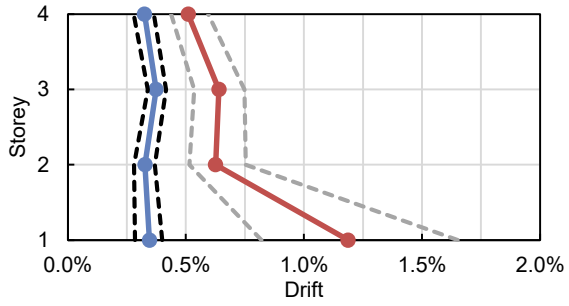

(b) Peak interstorey drifts of 4S

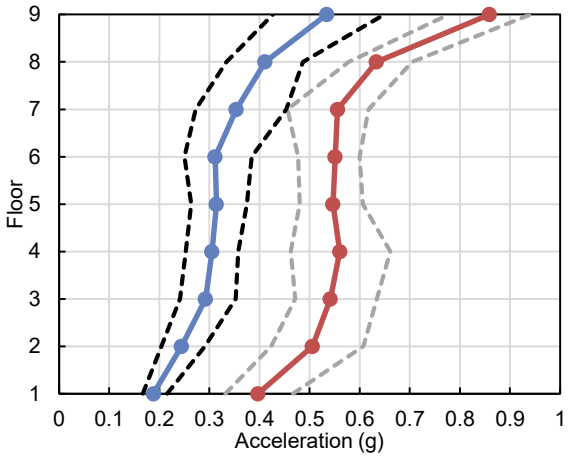

(c) Peak absolute floor accelerations of 8S

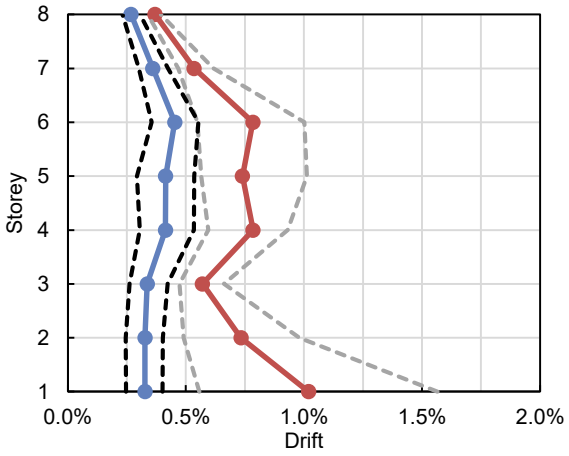

(d) Peak interstorey drifts of 8S

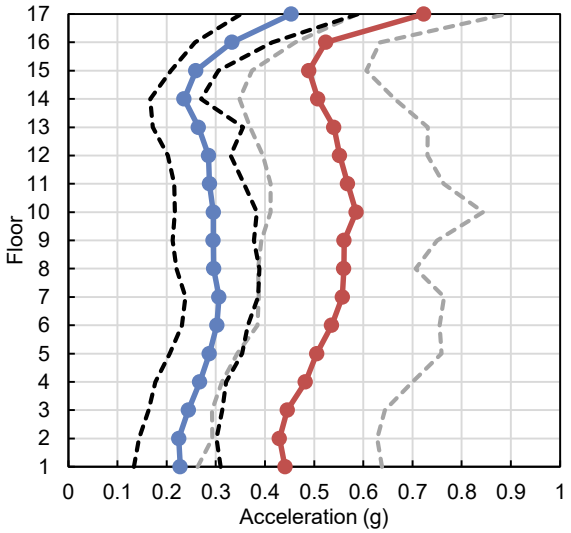

(e) Peak absolute floor accelerations of 16S

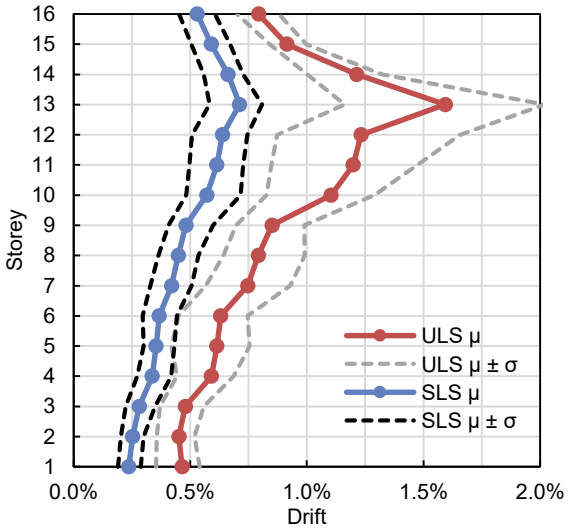

(f) Peak interstorey drifts of 16S

Figure 4.1: Peak structural response parameters of the standard buildings from the nonlinear time history analyses, mean (μ) and one standard deviation (σ) range

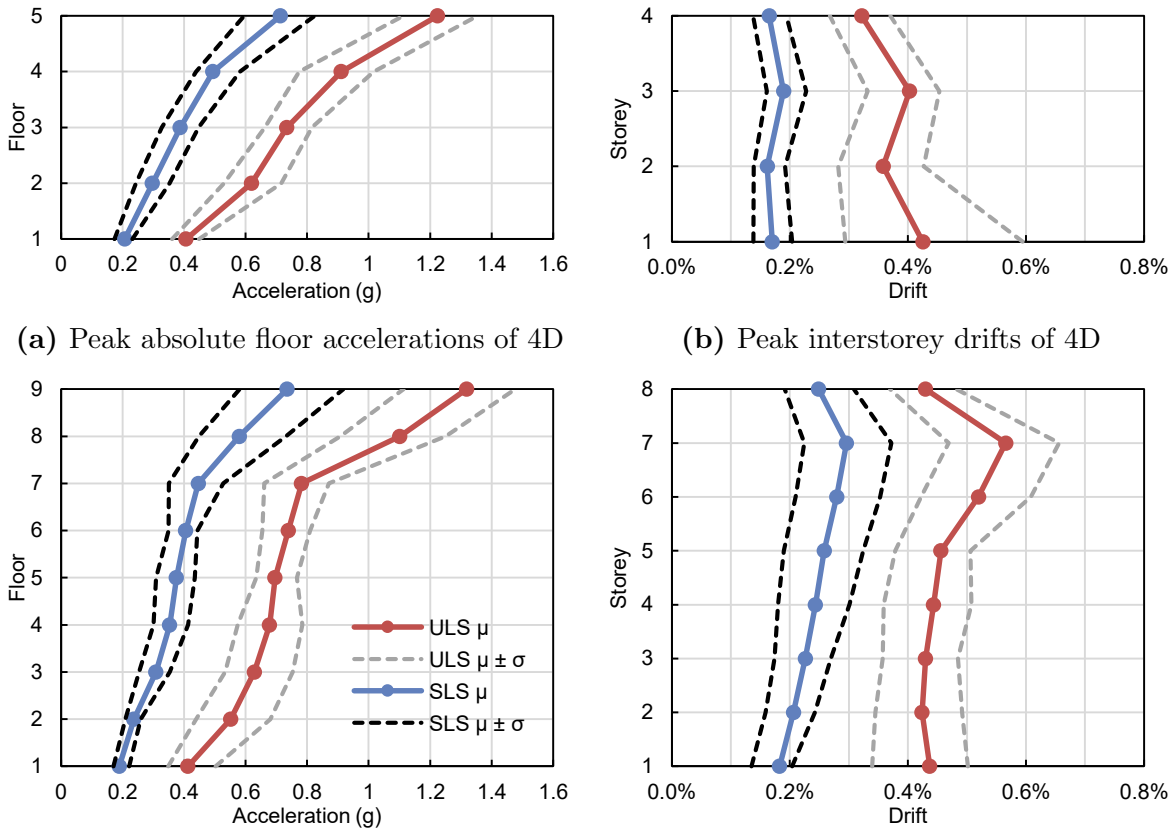

(a) Peak absolute floor accelerations of 4D

(b) Peak interstorey drifts of 4D

(c) Peak absolute floor accelerations of 8D

(d) Peak interstorey drifts of 8D

Figure 4.2: Peak structural response parameters of the drift design buildings from the nonlinear time history analyses, mean (μ) and one standard deviation (σ) range

The standard and drift buildings were designed to achieve serviceability following the SLS and the ULS, respectively. Considering the mean performance, it can be seen in Figure 4.1 that structures 4S and 8S are within the design SLS drift limit of 0.5%. Structure 16S exceeds this drift limit in the upper storeys. The target ULS drift limit of 1% is met for 8S, slightly exceeded by the first storey of 4S, and exceeded by the upper storeys of 16S. Figure 4.2 displays that the drift designs meet the target 0.5% limit for the ULS, excluding the seventh storey of 8D. According to the Eurocode provisions (discussed in Section 3.3.3), serviceability is therefore predicted for 4D and 8D following the ULS, and 4S and 8S following the SLS. An important result is that the drifts do not exceed 2-3%, the approximate magnitude for the development of a localised plastic collapse mechanism (Banihashemi *et al.* 2015; Merczel *et al.* 2013).

Figure 4.1 reveals that the standard designs exhibit an even distribution of storey demands over the building height for the SLS. This desirable behaviour is not achieved

during the ULS. A concentration of drift occurs in the first storey of 4S. This also occurs for 8S, although in a less pronounced manner. Storey 13 of 16S undergoes significant drift compared to the other storeys, with a value of approximately 1.5%. In comparison, the drift designs in Figure 4.2 avoid the concentration of drifts in individual storeys during both the SLS and the ULS.

The ULS EDP results have a greater spread than the SLS results. This result is influenced by the variance of the ground motion suites. The ULS ground motion suites have a greater average mean squared error (MSE) than the SLS suites with respect to the target Eurocode spectrum, as can be seen in Table 4.2.

Table 4.2: Average mean squared error (MSE) of the ground motion suites with respect to the target Eurocode spectrum

Building	**ULS MSE**	**SLS MSE**
4S	0.0421	0.0297
8S	0.0536	0.0384
16S	0.0754	0.0438
4D	0.0309	0.0218
8D	0.0565	0.0338

The spread of the EDP results also coincides with the significant nonlinear behaviour exhibited by the braces during the larger intensity ULS earthquakes. Figure 4.3 compares typical brace behaviour observed during a ULS analysis and a SLS analysis. The selected brace is located in the eighth storey of building 16S. The same ground motion record of Imperial Valley-02 1940 was used with a ULS scale factor of 1.34 and a SLS scale factor of 0.68. The brace exhibits predominantly elastic behaviour during the SLS with the initiation of minor buckling. The brace experiences considerable nonlinear behaviour during the ULS, as substantial buckling and some yielding takes place.

The EDP results indicate that the drift designs may have advantages over the standard designs. For this reason, it is of interest to directly compare the EDP results of the standard and drift designs.

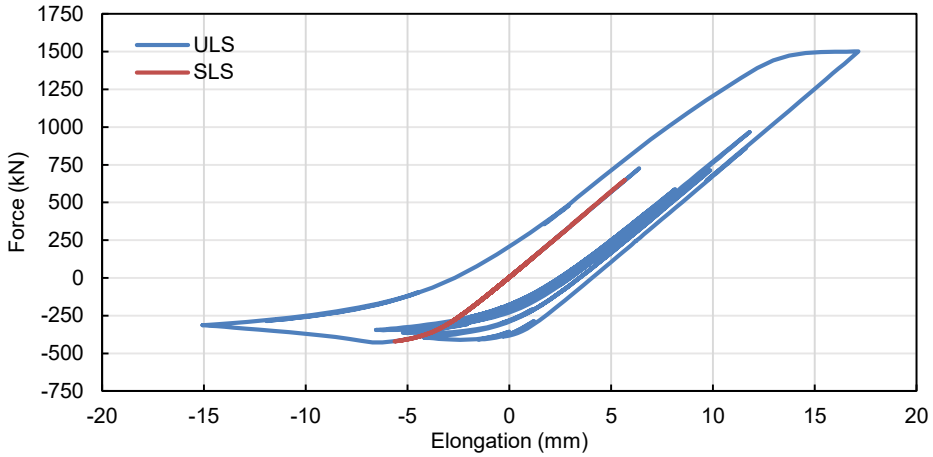

Figure 4.3: Sample brace response during a ULS analysis and a SLS analysis

4.2.3 Comparison of the Standard and Drift Designs

The standard and drift building designs can be compared using the EDP results from the time history analyses. The mean peak EDPs at each building level were examined, and the maximum value for each structure and limit state were identified. A summary of these maximum EDP results is provided by Figure 4.4. The drift designs have a greater maximum acceleration and a lower maximum drift in comparison to the standard designs as anticipated. The relative position of the points are also as expected, trending downwards to the right from the stiffest building (4D) to the most flexible building (16S). The relative positions of 4S and 8S change for the ULS. This is likely due to the initiation of a soft-storey in the first storey of 4S, increasing drifts and decreasing accelerations.

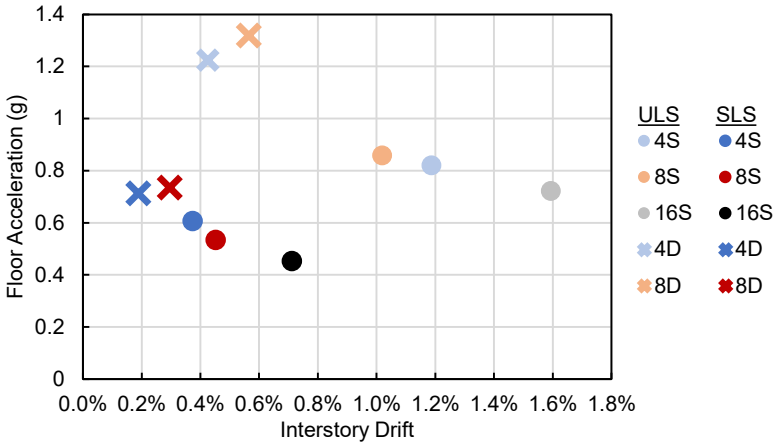

Figure 4.4: Maximum of the mean peak values of acceleration and drift for all buildings

The mean peak EDPs of the drift and standard designs are compared in Figure 4.5, where S refers to the standard designs and D refers to the drift designs. The drift designs exhibit significantly greater accelerations from floors three and up. The greater accelerations can be attributed to two factors: (1) the drift designs are stiffer; (2) it is expected that more nonlinear brace behaviour occurs in the standard designs, therefore providing greater energy dissipation through hysteresis.

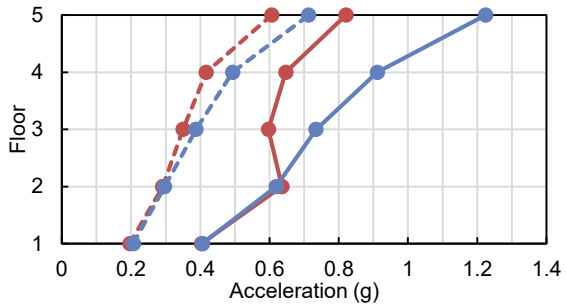

(a) Four-storey peak absolute floor accelerations

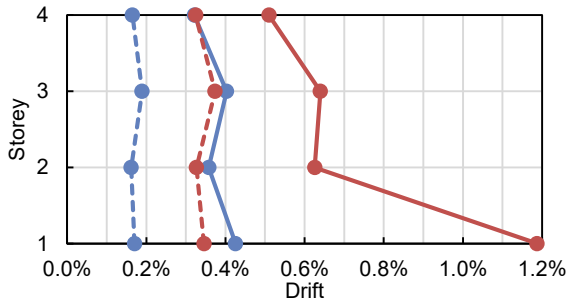

(b) Four-storey peak interstorey drifts

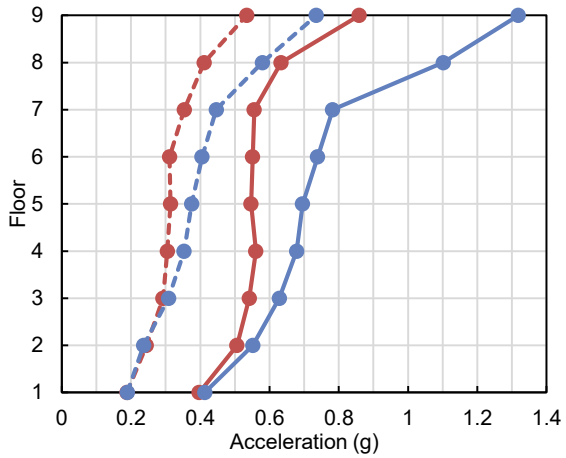

(c) Eight-storey peak absolute floor accelerations

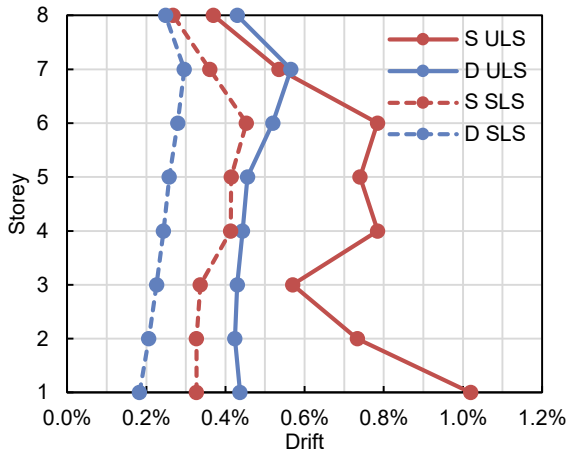

(d) Eight-storey peak interstorey drifts

Figure 4.5: Comparison of mean peak structural response parameters of the standard (S) and drift (D) designs

The drift designs have comparable drift demands at each storey. This is an advantage of the drift designs, as a reduced probability of soft-storey formation during the ULS is shown. The ULS drifts of the drift designs are comparable to the SLS drifts of the standard designs. This was the anticipated result of the design procedure. The FEMA P-58 analysis in Section 4.4 will allow the difference in expected damage due to the trade-off between acceleration and drift to be quantified.

4.2.4 Nonlinear Structural Response

In addition to evaluating peak EDP results, investigating the initiation of nonlinear structural response can also provide insight on the expected seismic performance of buildings. The maximum interstorey drift following a time history analysis was recorded for various scales of the ULS peak ground acceleration (PGA). The acceleration was factored from 0.05 of the actual acceleration to 1, representing the full scale ground motion record, at intervals of 0.05. Examples of typical response are provided in Figure 4.6, which displays the maximum interstorey drifts of each storey with respect to the acceleration scale factor.

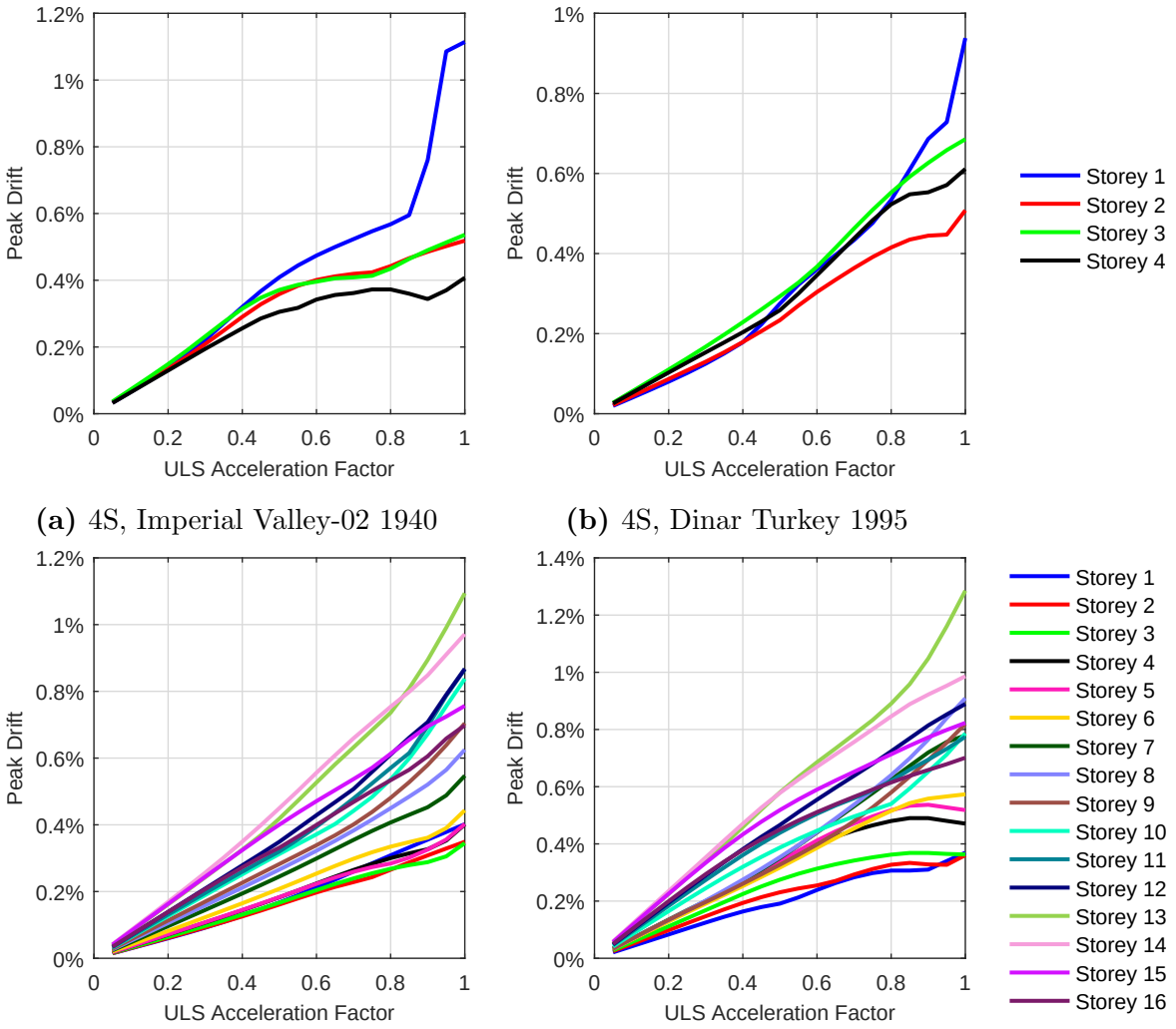

(a) 4S, Imperial Valley-02 1940 **(b)** 4S, Dinar Turkey 1995

(c) 16S, Coalinga-01 1983 **(d)** 16S, Niigata Japan 2004

Figure 4.6: Relationship between the peak interstorey drift per storey and ULS acceleration factor

An acceleration factor of 0.25 corresponds to the design acceleration with a Eurocode behaviour factor of four. It is anticipated that nonlinear structural behaviour will commence at an acceleration factor of approximately 0.25 or greater due to brace overstrength variations (described in Section 3.3.4). Figure 4.6 reveals that notable nonlinear structural response initiates at acceleration factors in the range of 0.25 to 0.5. In Figure 4.6a, the first storey drift deviates substantially from the others at an acceleration factor of approximately 0.85. It is observed that the maximum drift is nearly triple the magnitude of the minimum storey drift. The first storey therefore undergoes larger plastic deformation, resulting in poorly distributed energy dissipation.

The formation of soft-storeys is visualised in Figure 4.7 for two example analyses. The evolution of maximum IDRs over time is displayed with each storey response represented separately. The ground motion record is superimposed to allow the structural response to be related to the ground acceleration. The examples are selected from 4S and 16S, the buildings with the most pronounced drift concentration. For each building, one ground motion analysis is displayed that is representative of typical analysis results. The time window is limited to the first 30 seconds of the analysis where the maximum drift values occur for the selected examples. It can be seen that the concentration of drifts in a select number of storeys occurs after a large spike in ground motion acceleration. The drift of the storey with the largest IDR is several times larger than that of the minimum IDR.

The IDR results of CBFs are controlled by brace behaviour. The nonlinear brace response of interest can be classified as buckling or yielding. Yielding was defined to occur once the recorded brace force reached the calculated yield force in tension. The occurrence of buckling was determined by examining the brace force-elongation relationships for all ground motion analyses. Buckling was defined as the occurrence of inelastic brace behaviour in compression. The percentages of all braces that either yield or buckle considering all ground motion analyses are shown in Table 4.3. It should be recalled that the initial buckling loads of the OpenSees brace models are approximations due to the use of simple pin end connections and an assumed initial imperfection value, as noted in Section 3.4.2.

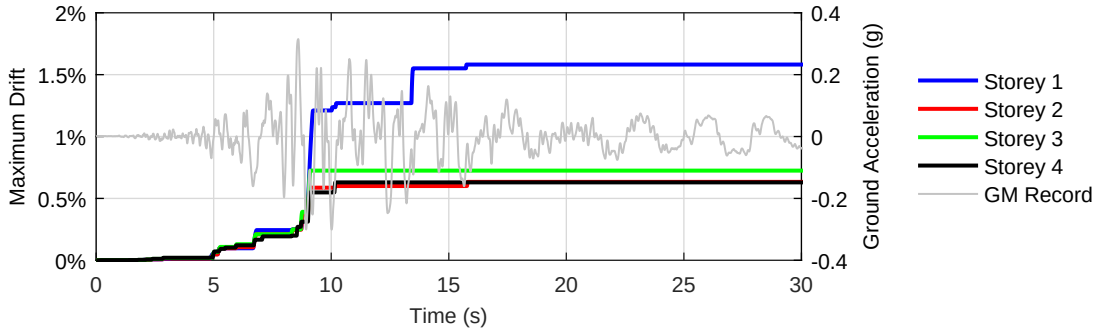

(a) 4S response, Loma Prieta 1989

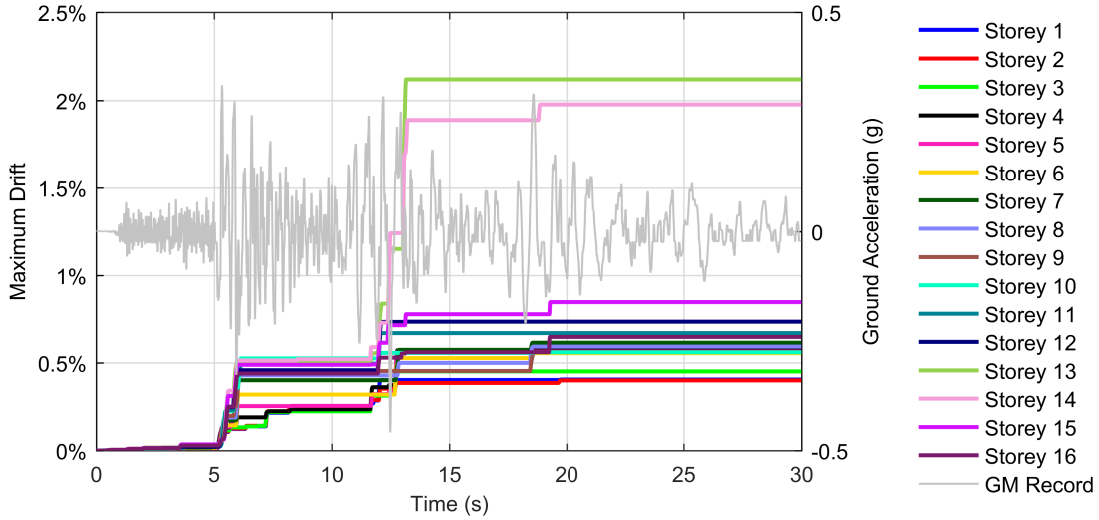

(b) 16S response, Imperial Valley-06 1979

Figure 4.7: Example of typical maximum interstorey drift per storey over time of the 4S and 16S buildings

Negligible yielding occurs during the SLS for all buildings. Eurocode braces are designed as tension-only members and are not expected to yield during the SLS. The 4- and 8-storey standard buildings experience a small amount of SLS buckling ($< 6\%$ of brace members), and the 16-storey standard building experiences more notable SLS buckling (14% of brace members). A significant number of braces yield and buckle during the ULS for the standard buildings. In comparison, the drift designs experience a small amount of ULS brace yielding and buckling. This is due to large brace overstrength in the drift buildings, as drifts rather than forces controlled member design.

A visualisation of the mean brace buckling and brace yielding per storey considering all ground motion analyses is provided in Figure 4.8 and 4.9 for the standard and drift design buildings, respectively. The IDRs from the time history analyses (shown in Figure

Table 4.3: Mean brace buckling and yielding

Condition	**4S**	**8S**	**16S**	**4D**	**8D**
Yield SLS	1%	0%	0%	0%	0%
Buckle SLS	5%	6%	14%	0%	0%
Yield ULS	41%	29%	17%	4%	2%
Buckle ULS	74%	56%	79%	11%	7%

4.1 and 4.2) can be related to the nonlinear brace behaviour. For the standard buildings, the majority of brace yielding and buckling corresponds to the concentration of drifts (4S — storey one, 8S — storeys one and four, 16S — storeys ten to 14). The drift designs do not exhibit this behaviour.

While nonlinear brace behaviour is expected during the ULS for Eurocode-compliant CBFs, columns are designed to remain elastic. The columns were examined during each time-step of the time history analyses for nonlinear behaviour. All column failure conditions were examined using Eurocode 3 as described in Section 3.3, providing a conservative check. According to the Eurocode capacity design procedure, columns are non-dissipative members. Members in non-dissipative zones should withstand the design seismic loading and permit the dissipation of seismic energy in the tension braces (CEN 2013). However, column buckling capacity in axial loading-bending was exceeded during some ULS analyses. Table 4.4 summarises the observed column capacity failures, including the ground motion record number causing the buckling, the buckled column, and the maximum calculated demand/capacity (D/C) ratio.

Table 4.4: Occurrences of column buckling capacity failure with demand/capacity (D/C) ratios

Building	**Record**	**Storey**	**Column**	**D/C Ratio**
4S	11	1	Exterior (2)	1.10
	14	1	Exterior (2)	1.07
16S	1	11	Exterior (4)	1.09
	3	12	Exterior (2)	1.11
	21	13	Exterior (2)	1.07
		13	Corner (5)	1.14
	25	13	Corner (1)	1.09

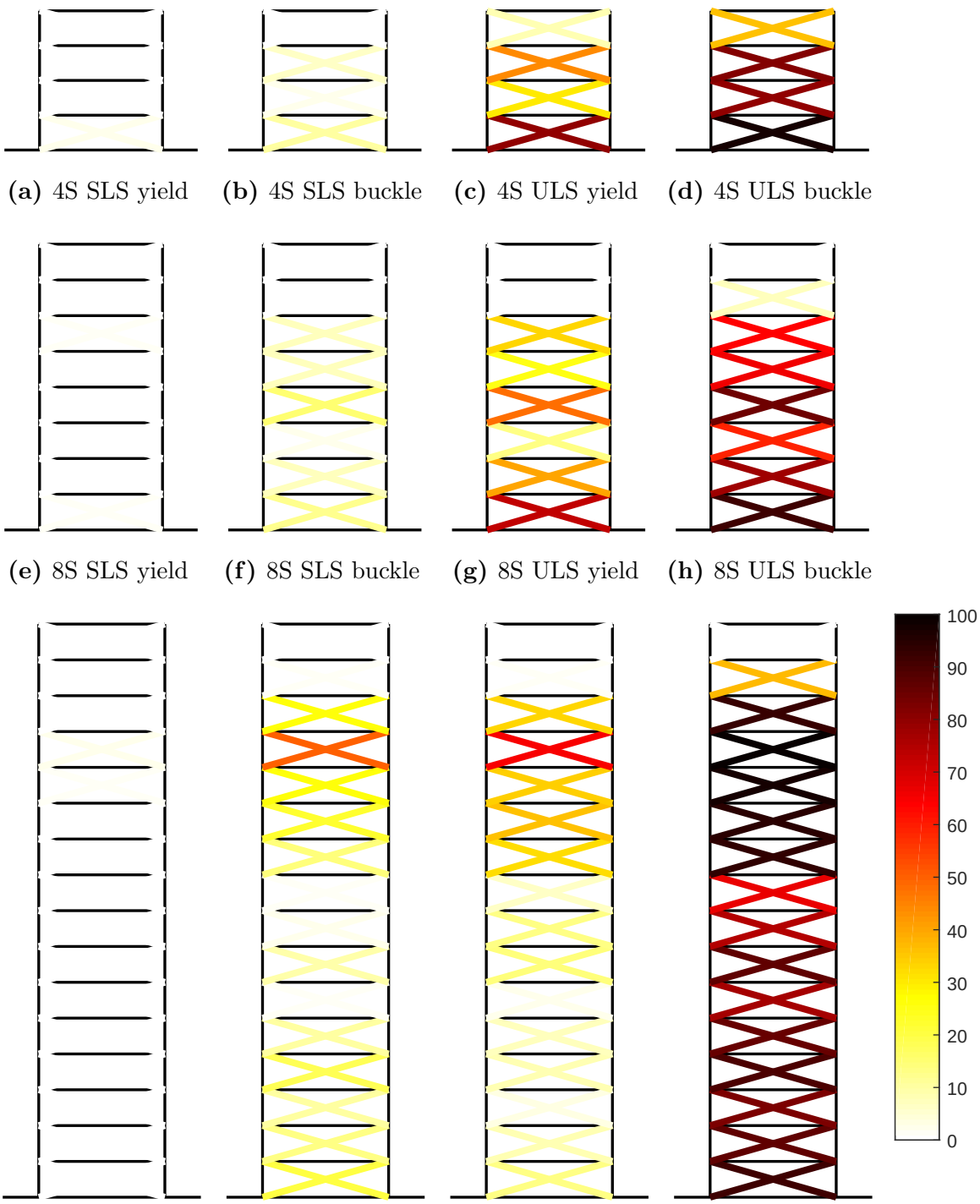

(a) 4S SLS yield **(b)** 4S SLS buckle **(c)** 4S ULS yield **(d)** 4S ULS buckle

(e) 8S SLS yield **(f)** 8S SLS buckle **(g)** 8S ULS yield **(h)** 8S ULS buckle

(i) 16S SLS yield **(j)** 16S SLS buckle **(k)** 16S ULS yield **(l)** 16S ULS buckle

Figure 4.8: Percentage of brace buckling and yielding in the standard buildings

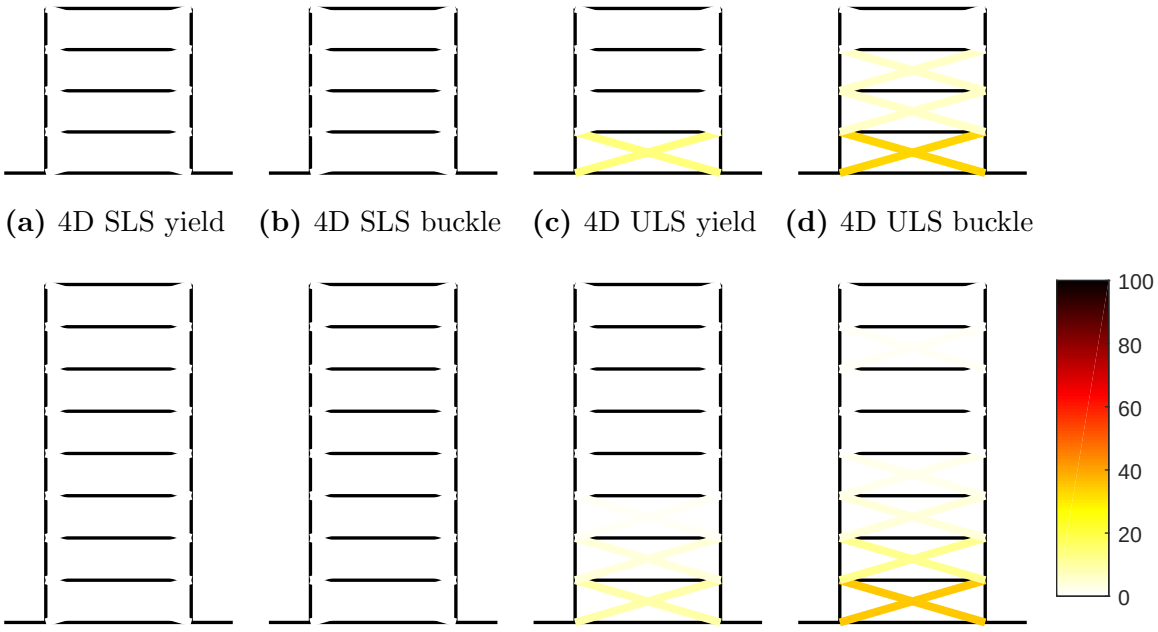

(a) 4D SLS yield **(b)** 4D SLS buckle **(c)** 4D ULS yield **(d)** 4D ULS buckle

(e) 8D SLS yield **(f)** 8D SLS buckle **(g)** 8D ULS yield **(h)** 8D ULS buckle

Figure 4.9: Percentage of brace buckling and yielding in the drift buildings

Section 3.3 describes the Eurocode column design procedure. Linear analysis leads to dominant axial forces in the columns due to brace truss action. The design axial forces of the columns are amplified considering brace overstrength. However, once braces in a storey lose lateral loading capacity due to yielding and buckling, continuous columns experience bending. This internal bending due to brace deterioration is not considered in Eurocode design and can lead to underdesign of column members. Pinned columns would experience a storey mechanism and local collapse.

It was determined that column buckling is not of major concern in this study. A negligible amount of column buckling occurred when considering the 250 analyses. In addition, Eurocode 8 (CEN 2013) stipulates the use of mean load effects when using seven or more time history analyses. All columns are within capacity when considering the mean design forces of all analyses. Material overstrength was also not considered in detail. As a result, the effects of column buckling on structural response were not considered.

Investigating column buckling and other structural responses based on EDPs can provide insight on seismic performance. However, it has been shown that repair costs

are a more comprehensive measure of seismic performance. When examining earthquake repair costs, building values can serve as a useful scale.

4.3 Estimation of Building Value

The RSMeans square foot cost estimator (RSMeans Online 2017) was used to determine values of the benchmark buildings. RSMeans is a leading provider of construction cost data. The building cost estimates include material costs, labour costs and other charges such as contractor fees.

The RSMeans cost estimator calculates building values for a specific region in 2016 US dollars based on the total floor area. The benchmark buildings are likely to have costly nonstructural systems due to the chosen seismic design category. Although RSMeans does not include a premium cost option due to seismic design, the selection of a region with substantial seismic risk should incorporate seismic design costs. As a result, San Diego was selected to produce the building cost estimates. The RSMeans values rounded to the nearest \$100,000 are \$3.8M, \$8.6M and \$18.2M for the four-, eight- and 16-storey buildings, respectively.

Guerrero *et al.* (2017) used the steel weight of a structure to interpolate building cost. The structural cost (C_s) is estimated as \$3/kg of steel. It is assumed that the structural system accounts for 20% of the total cost (C_t), i.e. $C_t = 5C_s$. The approach from Guerrero *et al.* (2017) was used to verify the RSMeans estimates. The results are given in Table 4.5, including the difference between the RSMeans estimate and the steel weight estimate ($\Delta C_t = (C_t - C_{RSMeans}) / C_{RSMeans}$). The estimated costs using the steel weight approach are acceptably similar to the RSMeans costs.

The difference in building cost between the standard and drift designs was accounted for using the steel weight approach. As the nonstructural systems are unchanged for both design methods, the difference in building cost is limited to the structural systems. The cost increase for the drift designs due to the difference in C_s is \$70,000 for 4D and \$440,000 for 8D, rounded to the nearest \$10,000. The standard building values were taken as the RSMeans costs. No conversion was made for 2011 dollar values. This uncertainty is small

Table 4.5: Costs of the benchmark buildings based on steel weight. W_s = steel weight, C_s = structural cost, C_t = total cost

Building	W_s (kg)	C_s	C_t	ΔC_t
4S	224,958	\$0.675M	\$3.374M	-11%
8S	495,632	\$1.487M	\$7.424M	-14%
16S	1,174,210	\$3.523M	\$17.613M	-3%
4D	247,820	\$0.742M	\$3.717M	-3%
8D	643,847	\$1.932M	\$9.658M	13%

in comparison to the overall project assumptions, while only consistent and reasonable values are required for comparisons. The final building costs are provided in Table 4.6. These building values will serve as a scale when investigating the FEMA P-58 repair costs.

Table 4.6: Final costs of the benchmark buildings

Building	Building Cost
4S	\$3.80M
8S	\$8.60M
16S	\$18.2M
4D	\$3.87M
8D	\$9.04M

4.4 FEMA P-58 Analysis

The structural parameter results of the time history analyses were converted to repair costs using the FEMA P-58 procedure (2012b) described in Section 3.6. The evaluation of seismic performance expressed in economic losses allows for in-depth investigation and assessment of total-building performance. Direct repair costs in 2011 US dollars resulting from damage to building assets were calculated, while indirect costs due to building downtime were out of scope.

4.4.1 Total Repair Costs

A Monte Carlo analysis with 1000 realizations for each limit state was performed in the performance assessment calculation tool (PACT), surpassing the minimum number of 500 realizations recommended by the FEMA P-58 methodology (FEMA 2012b). The

total repair costs for the code-compliant building designs subjected to a ULS or SLS earthquake were determined. Cumulative distribution functions of the ULS and the SLS total repair costs normalised by the respective building cost are shown in Figure 4.10. The mean, median and 90th percentile total repair costs are given in Table 4.7 to provide the non-normalised data.

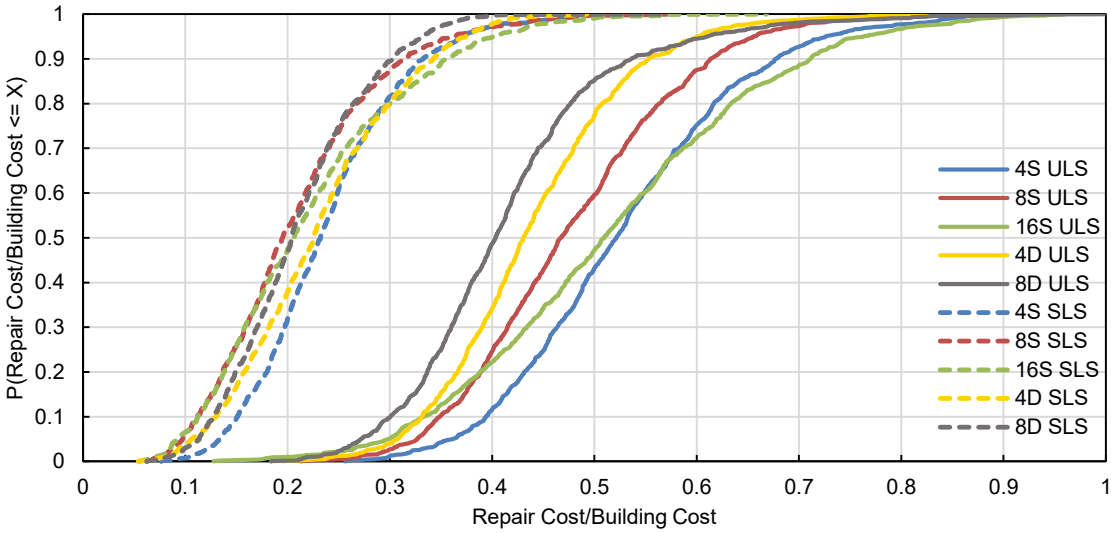

Figure 4.10: Cumulative distribution functions of the ULS and SLS total repair costs normalised by building value for the benchmark buildings

Table 4.7: Total repair costs ($M) of the benchmark buildings for the ULS and SLS

Limit State	Building	Mean	Median	90th Percentile
ULS	4S	2.01	1.98	2.58
	8S	4.11	4.02	5.28
	16S	9.40	9.28	12.95
	4D	1.70	1.67	2.14
	8D	3.75	3.65	4.85
SLS	4S	0.91	0.88	1.26
	8S	1.79	1.68	2.70
	16S	4.03	3.75	6.46
	4D	0.89	0.87	1.33
	8D	1.90	1.85	2.74

The ULS repair costs are greater than the SLS repair costs. This was anticipated due to the difference in earthquake intensity. The spread of the ULS data is also greater, reflecting the results of the time history analyses. The 16-storey ULS repair cost distribution has a noticeably greater dispersion than the four- and eight-storey dispersions. This can be

explained in part by the dispersion of the ULS ground motion suites used to conduct the time history analyses, as the MSE of the 16S ULS ground motion suite is the greatest (refer to Table 4.2).

The SLS cost distributions are comparable among the considered buildings. The median damage ranges from 20% to 23% of the building cost. The SLS repair costs are of particular concern, as damage at this intensity should be limited to a level which does not compromise building serviceability. However, the assessment results indicate that extensive repairs are required. This suggests that modern building standards do not accomplish SLS earthquake resilience: the ability to quickly recover after an earthquake.

Owners often elect to demolish and replace the existing building if repair costs exceed 40% of the building cost (FEMA 2012b). It is recognised that this demolition limit is an approximate guide based on past observations, rather than a rule. The median ULS repairs for all of the buildings are between 41% to 52% of the building cost. The standard designs reach the 40% limit at the 11th and 25th percentiles. The ULS results therefore suggest it is probable that buildings designed to current structural codes (Eurocode) may be demolished and replaced following a ULS earthquake. The implications for a city centre are severe, where it can be expected that many similar buildings will be present.

The effectiveness of the drift design method can be evaluated by comparing the resulting repair cost distributions to those of the standard designs. The total repair cost distributions for standard and drift designs are compared in Figure 4.11.

The drift designs achieve reduced ULS repair costs with respect to the standard designs. There is a median difference of \$320,000 (16%) for the four-storey structure and \$376,000 (9%) for the eight-storey structure. As a point of reference, the increases in building value are \$70,000 for 4D and \$440,000 for 8D. Although the ULS repair costs of the drift designs decrease, the median repairs are still above the 40% building value level (i.e. the FEMA P-58 demolish limit).

In contrast to the ULS results, the SLS repair costs of the drift designs are not improved. The four-storey buildings have similar SLS repair cost distributions, while the

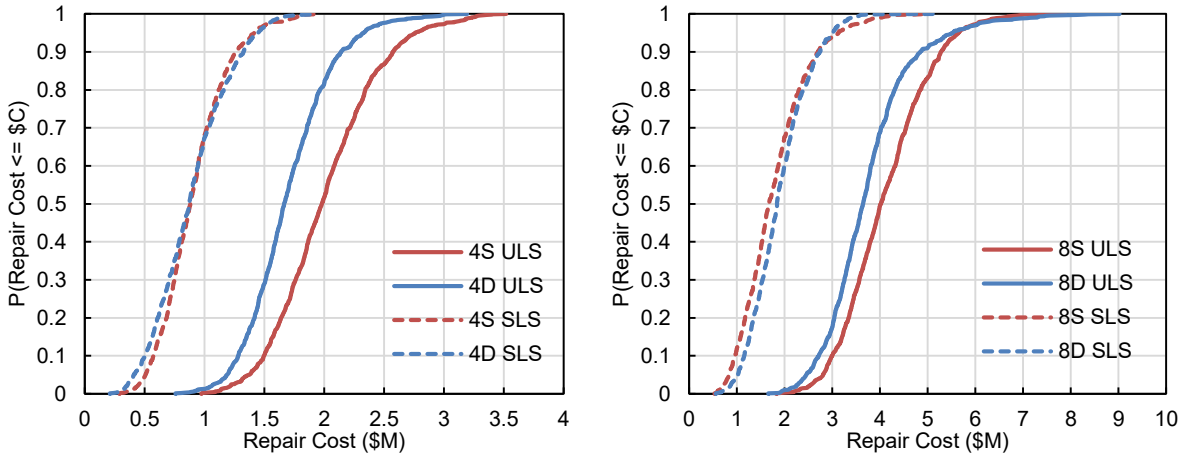

(a) Four-storey standard and drift designs **(b)** Eight-storey standard and drift designs

Figure 4.11: Comparison of total repair cost cumulative distributions for the standard and drift designs

eight-storey drift design has greater repair costs than the standard design. The increase for the eight-storey median damage is $165,000 (4%).

Comparing the standard and drift design repair cost distributions has determined that the drift design method can improve ULS seismic performance. However, the level of improvement is relatively modest. In addition, the SLS performance of the drift designs are comparable or reduced with respect to the standard designs. In order to further understand the seismic performance of code-compliant buildings, repair costs can be examined based on the associated EDP.

4.4.2 Repair Costs and Engineering Demand Parameters

Repair costs from the seismic performance assessments were attributed to the EDPs that generated the damage. The mean repair costs of the benchmark buildings considering the associated EDP are shown in Figure 4.12, normalised by the mean repair cost of the respective building.

The ULS costs are shown in Figure 4.12a. Acceleration-sensitive damage is comparable to drift-sensitive damage for structure 16S. 16S is the most flexible benchmark building and experiences larger drifts. The importance of acceleration-sensitive damage is even more significant for the four- and eight-storey buildings. Acceleration damage is responsible for

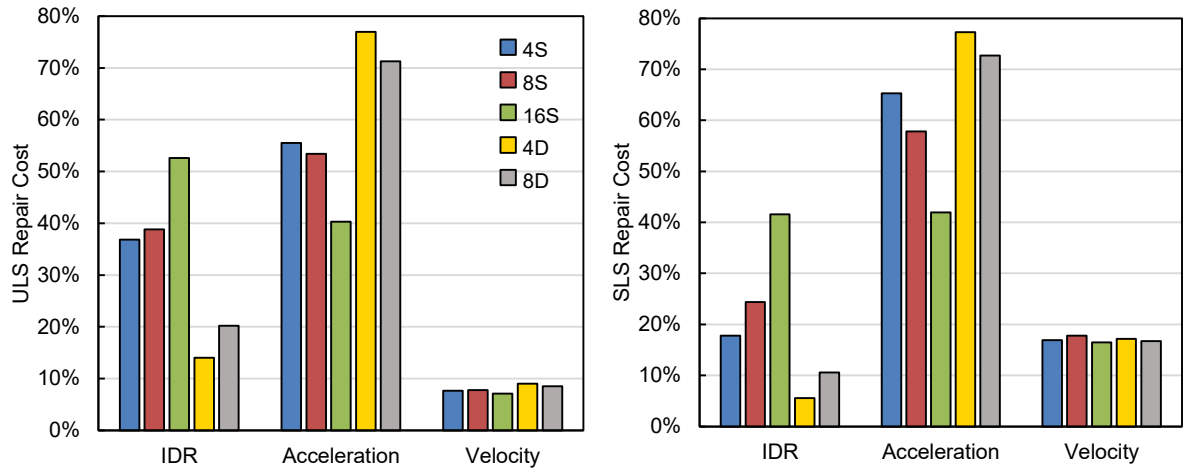

(a) ULS normalised EDP repair costs **(b)** SLS normalised EDP repair costs

Figure 4.12: Mean repair costs of the benchmark buildings grouped by associated EDP and normalised by total repair costs

more than half of the repair costs. Figure 4.12b reveals that the influence of acceleration is even greater for the SLS.

Conventional building codes control drifts but do not place limitations on allowable floor accelerations. Accelerations are typically only taken into account for calculations of anchorage strength. Figure 4.12 reveals that acceleration- and drift-sensitive damage comprise the majority of repair costs for both limit states. The influence of acceleration on seismic performance should be more appropriately reflected in the design procedures of structures.

The drift designs significantly reduce drift damage but increase acceleration damage with respect to the standard buildings. Acceleration-sensitive damage accounts for over 70% of all calculated repair costs. This likely explains why the drift designs (4D and 8D) achieve only modest reductions in total repair costs when compared to the standard designs.

In order to further investigate the relationship between EDPs and repair costs, mean EDP repair costs were organised based on floor level. Mean EDP repair costs associated with building floors are displayed in Figure 4.13 – 4.15, where floor one indicates the ground level.

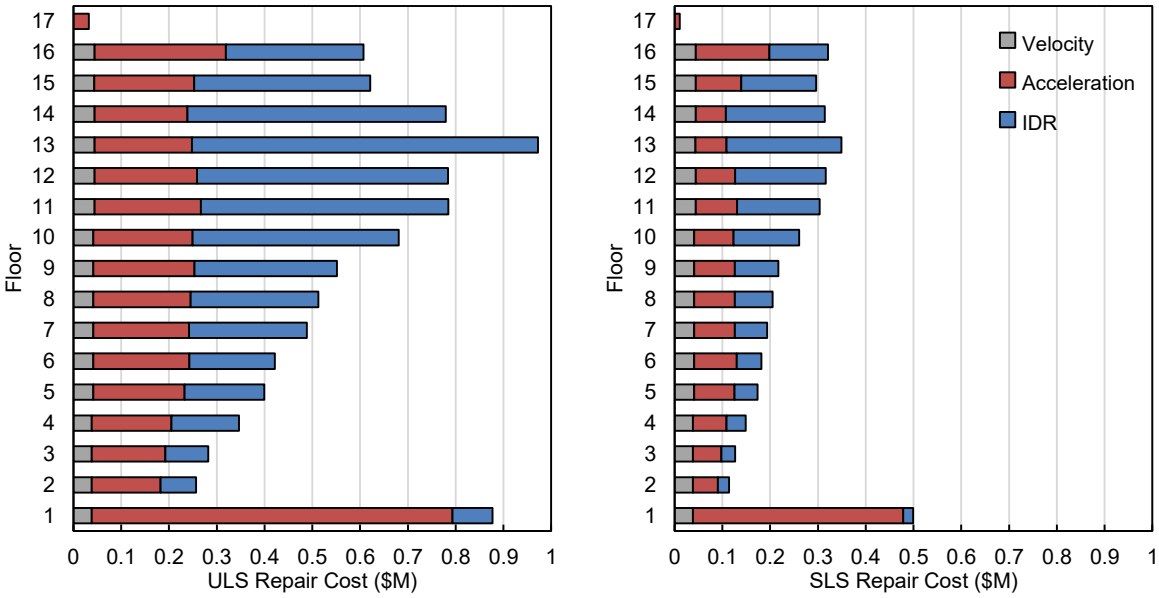

(a) ULS repair costs **(b)** SLS repair costs

Figure 4.13: Mean EDP repair costs for each floor of 16S

The floor costs of the 16-storey building in Figure 4.13 have a similar distribution for both the ULS and the SLS. Large repair costs are indicated on floor one, the majority of which are attributed to acceleration. This is due to a concentration of acceleration-sensitive nonstructural components on the ground floor such as HVAC equipment. Floor 17 exhibits minimal damage as there are few components located on the roof of the building.

The remaining floors (two to 16) are office occupancy and have similar nonstructural and structural quantities. The respective levels of acceleration- and velocity-sensitive repair costs are comparable throughout each floor. This is in accordance with the time history analysis results in which the peak velocities and accelerations were similar for floors two to 16. The difference in repair costs at these floors is predominantly controlled by drift-sensitive costs. The distribution of drift-sensitive costs correlates with the mean IDR results from the time history analyses. For example, floor 13 exhibits the maximum drift repair cost as well as the maximum mean IDR.

The floor repair costs of the four-storey structures are shown in Figure 4.14. This figure provides a comparison of the standard and drift designs. The drift design has reduced drift damage on each floor with respect to the standard design. The greatest difference occurs at the first storey. This is the location of a drift concentration in 4S (previously shown

in Figure 4.1). The drift design experiences greater acceleration damage from floor two onwards. The drift design trade-off of greater IDRs for reduced accelerations is favourable (results in lower costs) for floors one and two. The difference in repair costs for floor three is negligible, while floors four and five produce greater damage in the drift design (drift and acceleration trade-off is unfavourable). The magnitude of these differences are meaningful only for the ULS. The trade-off between acceleration and drift damage clarifies the modest ULS cost reductions achieved by the drift designs with respect to the standard designs.

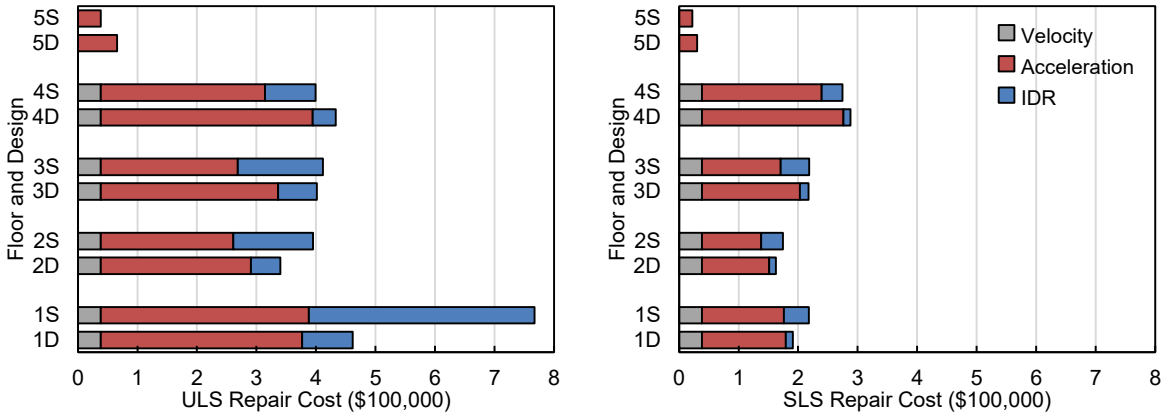

(a) ULS four-storey floor comparison **(b)** SLS four-storey floor comparison

Figure 4.14: Mean EDP repair costs for each floor of the four-storey buildings

The floor repair costs of the eight-storey structures are shown in Figure 4.15. The drift design has greater acceleration damage from floor two onwards with respect to the standard design. This result is consistent with the four-storey findings. The drift design has lower drift damage on each floor excluding floors seven and eight, which underwent larger interstorey drifts in the time history analyses (shown in Figure 4.5). The drift design has smaller repair costs on floors one to six (the drift and acceleration trade-off is favourable) and larger costs on floors seven to nine.

Figure 4.14 and 4.15 display slightly different acceleration costs on the ground floor for the standard and drift designs. Although the ground floor acceleration is equal to the ground motion acceleration, this difference in cost can be attributed to two causes: (1) The mean PGA at a period of 0.01 s is greater for the drift design ground motion suites. For example, 8D has a PGA of 0.413 g and 8S has a PGA of 0.398 g. (2) The difference

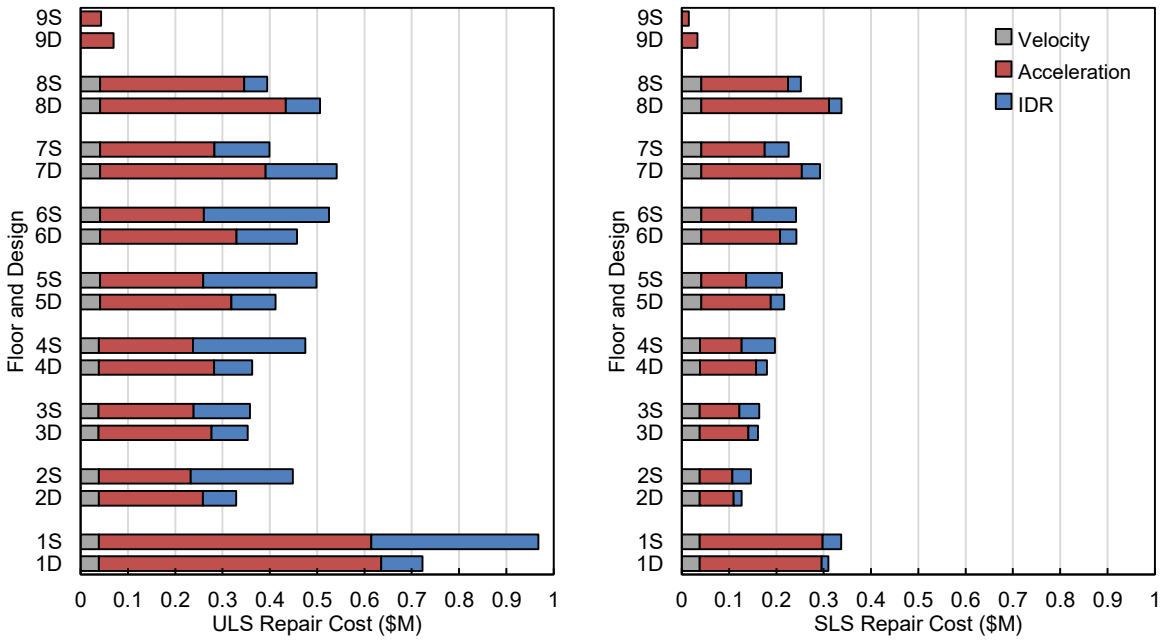

(a) ULS eight-storey floor comparison **(b)** SLS eight-storey floor comparison

Figure 4.15: Mean EDP repair costs for each floor of the eight-storey buildings

is also an artefact of the PACT calculations. The suspended ceilings fragility group is defined to be in the first storey. As such, its costs are attributed to the ground floor. However, the ceilings are suspended from the second floor. As a result, the EDP demands experienced by the ceilings are those of the second floor.

4.4.3 Repair Costs and Fragility Groups

The total repair cost for a building is a sum of the damage experienced by all fragility groups. For each fragility group, the repair cost is a function of the number of components in the group, the replacement cost per component, and the damage state experienced by each component. The mean repair costs of the benchmark buildings were disaggregated by structural and nonstructural fragility groups. This disaggregation is shown for all structures and both limit states in Figure 4.16. The repair costs of each fragility group have been normalised by the total repair cost of the respective building.

Figure 4.16 indicates that negligible repair costs can be attributed to stairs, access flooring, elevators, piping, fire sprinkler systems, and electrical systems. Subsequent seismic performance studies can exclude the fragility groups with negligible repair costs to

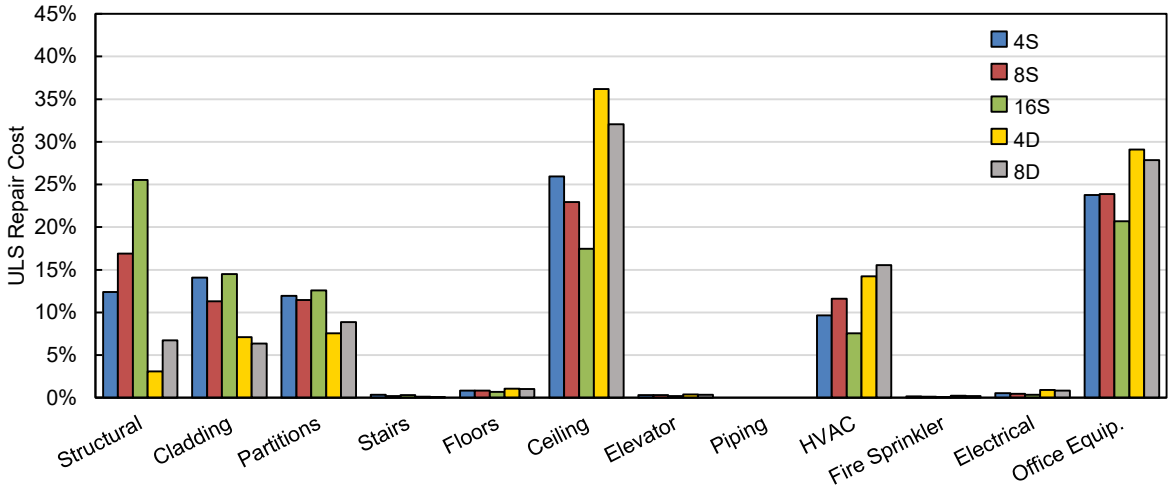

(a) ULS normalised fragility costs

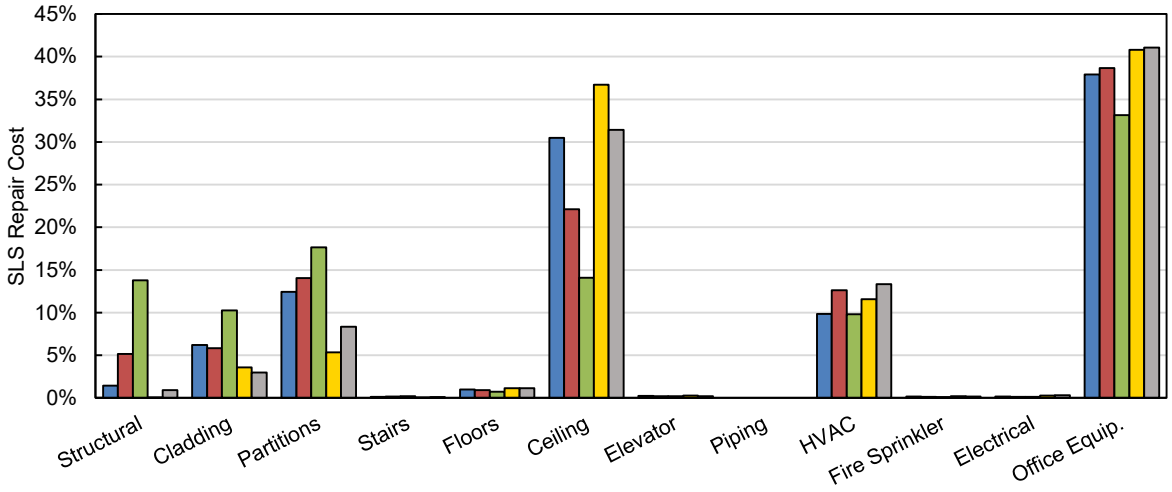

(b) SLS normalised fragility costs

Figure 4.16: Fragility-sorted repair costs of the benchmark buildings normalised by total repair cost

decrease the required computation time. These groups will also be excluded from future figures as the cost contributions are negligible.

Considering the distribution of ULS repair costs, ceilings and office equipment are responsible for the most damage in the four- and eight-storey buildings. These fragility groups are acceleration-sensitive components. The 16-storey building has large repair costs in those fragility groups, but the largest contributor is structural damage. Economic losses associated with cladding, partitions and HVAC fragility groups are comparable to one another.

The distribution of SLS costs remains similar to the ULS distribution with the exception of structural damage. Structural costs significantly decrease to $\leq 5\%$ of the total costs

for the four- and eight-storey buildings. The 16-storey structure experiences a smaller reduction, as the structural damage is approximately 15% of the total costs.

Brace damage is responsible for virtually all of the structural cost. Structural damage is anticipated for the ULS, as conventional seismic design relies on structural members experiencing inelastic deformation. These large inelastic deformations are concentrated in members designed to dissipate seismic energy in a controlled manner. Although the inelastic deformations damage structural members, the life safety of building occupants is ensured during a major earthquake.

Damage to structural members would introduce significant delays to building re-occupancy following an earthquake. Structural damage should therefore be minimised during the SLS. Based on the results shown in Figure 4.16, structural damage would delay building re-occupancy following an SLS event for buildings 8S and 16S.

Nonstructural systems are often omitted or treated in a simplified manner during structural design. However, between 74% to 88% of the ULS repair costs of the standard buildings can be attributed to these systems. This proportion rises to between 86% and 99% for the SLS. These results highlight the importance of considering nonstructural seismic performance when designing for a rapid return to building occupancy. Attaining a target level of seismic performance mandates the harmonisation of structural and nonstructural performance levels.

The drift and standard designs are compared considering fragility groups in Figure 4.17. Repair costs are shown in dollars rather than a normalised measure.

The level of structural damage is successfully reduced by the drift designs. 4D has negligible ULS structural damage and 8D has negligible SLS structural damage. Section 4.4.1 found that the mean ULS repair costs of the drift designs exceed the limit that corresponds to building replacement (40% of building value). Figure 4.17 reveals that the 4D structure sustains only minimal structural damage during the ULS. This demonstrates that the 40% replacement level is not a strict rule, as it is unlikely that the 4D structure would be demolished without sustaining notable structural damage.

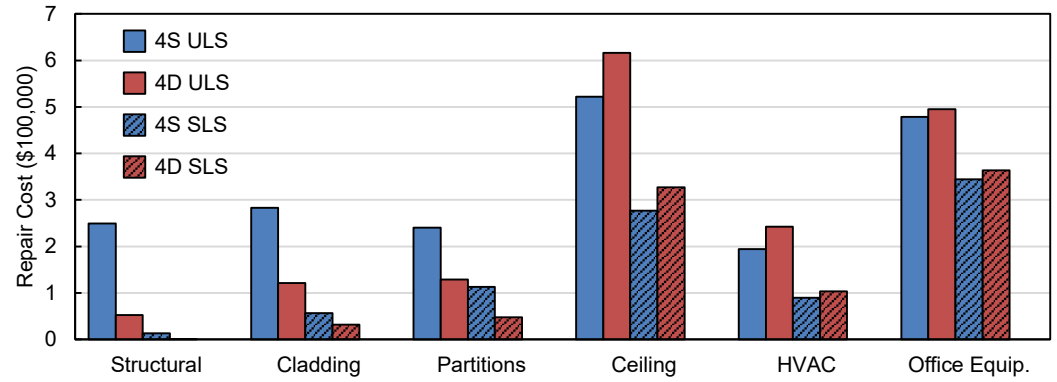

(a) Four-storey standard and drift design fragility costs

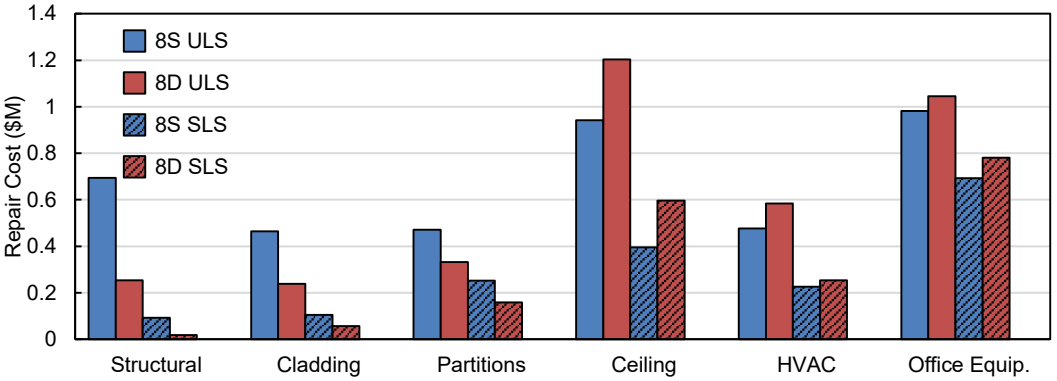

(b) Eight-storey standard and drift design fragility costs

Figure 4.17: Comparison of fragility-sorted repair costs of the standard and drift designs

The FEMA P-58 analysis determined that the majority of repair costs can be attributed to nonstructural systems. This finding encourages further evaluation of the Eurocode nonstructural provisions.

4.5 Evaluation of Eurocode Nonstructural Provisions

The FEMA P-58 analyses of the benchmark buildings revealed that Eurocode-compliant structures exhibit poor nonstructural seismic performance. This prompted further investigation of the Eurocode nonstructural provisions.

4.5.1 Acceleration Demands

It was assumed that anchorage of sufficient strength was provided for all architectural components and MEP systems. These forces are dependent on the absolute accelerations of the building. Eurocode 8 Cl 4.3.5 (CEN 2013) estimates the acceleration demand on

nonstructural systems using the equation

$$S_a = \alpha S \left(\frac{3\,(1 + z/H)}{1 + (1 - T_a/T_1)^2} - 0.5 \right) \geq \alpha S, \tag{4.2}$$

where α is the design ground acceleration on type A ground in units of g, S is the soil factor, z is the height of the nonstructural element above the ground level, H is the total building height, T_a is the natural period of the nonstructural element under consideration, and T_1 is the natural period of the building in the relevant direction of excitation.

By assuming $T_a = 0\,\text{s}$, the estimated acceleration demand could be calculated at each floor using Eq. 4.2. Figure 4.18 compares the floor accelerations estimated using the Eurocode 8 approximation to the ULS values determined from the time history analyses of the five buildings. The Eurocode 8 estimated values provide mixed results. The estimated values deviate from the mean time history analysis results by 2-17%, while the maximum difference is approximately 38%.

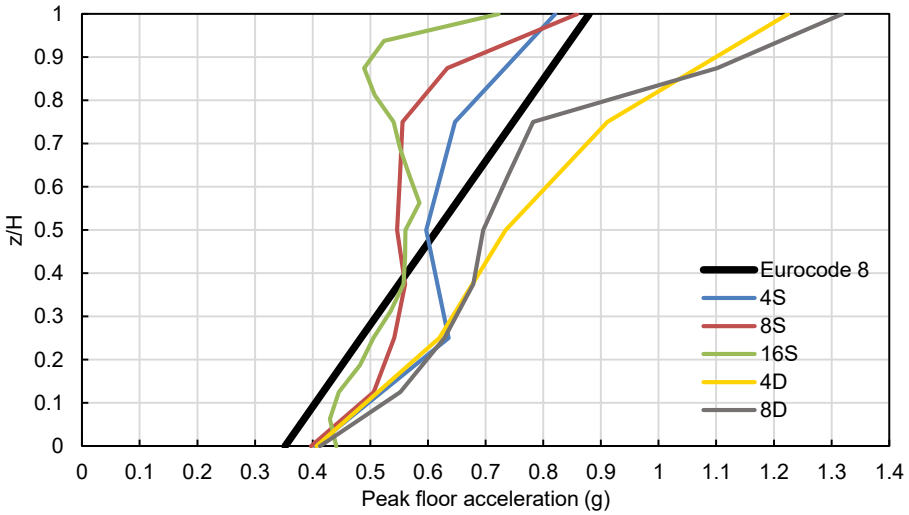

Figure 4.18: Comparison of floor accelerations using the Eurocode 8 approximation and the time history analysis results. z = height of the nonstructural element above the ground level, H = total building height.

4.5.2 Time History Analyses and FEMA P-58 Assessments

The most stringent Eurocode requirement to protect nonstructural systems is a maximum allowable IDR of 0.5% (CEN 2013). The standard buildings were designed to meet the 0.5% drift limit for the SLS, while the drift designs were designed to meet this limit for

the ULS. The standard and drift designs should therefore achieve serviceability at the SLS and the ULS respectively.

Section 4.2 provided IDR results from the time history analyses. According to the Eurocode provisions, nonstructural damage should be minimised at the storeys that satisfy the drift limit. However, the FEMA P-58 analysis determined that storeys with mean drifts within the allowable limit still experienced nonstructural damage.

The success of the drift limit in mitigating drift-sensitive damage was inspected using fragility-sorted repair costs. Figure 4.17 provides fragility-sorted repair costs of the four- and eight-storey designs. The 4S and 8S buildings experience a significant level of partition damage during the SLS. 4D experiences ULS damage to both cladding and partitions, and 8D undergoes cladding, partition and structural damage during the ULS. These results suggest that the Eurocode drift limit is inadequate to prevent damage to drift-sensitive nonstructural systems.

In addition to drift-sensitive damage, acceleration-sensitive nonstructural systems produced extensive repair costs. This EDP is not controlled by the drift requirement and highlights a significant limitation of the Eurocode nonstructural provisions.

It should be noted that the nonstructural systems considered in the benchmark study are of the highest seismic design category. Significant increases in nonstructural repair costs could occur for buildings with nonstructural components of a more vulnerable seismic design category.

4.5.3 Fragility Functions

The Eurocode nonstructural provisions are further examined by considering drift-sensitive fragility functions. Figure 4.19 provides the fragility functions for wall partitions, cladding, and brace systems. The Eurocode target of 0.5% is indicated in the figures.

The Eurocode drift limit successfully reduces the probability of damage to minimal values for cladding as well as to CBFs, but is unsuccessful for the wall partitions. If the 0.5% drift limit is respected, a wall partition is expected to sustain damage. The probability of reaching damage state one and damage state two is 93% and 22%, respectively.

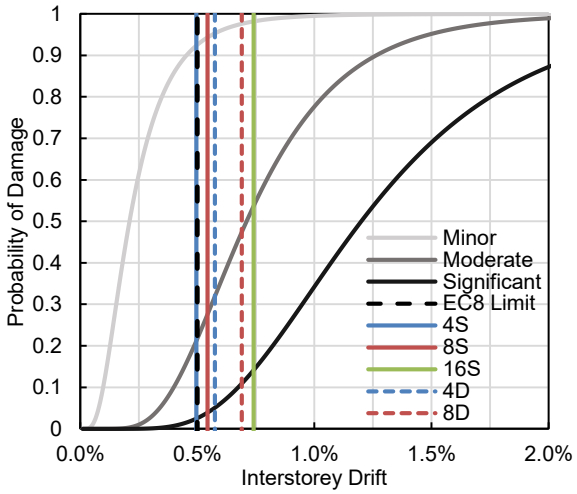

(a) Wall partition fragility functions

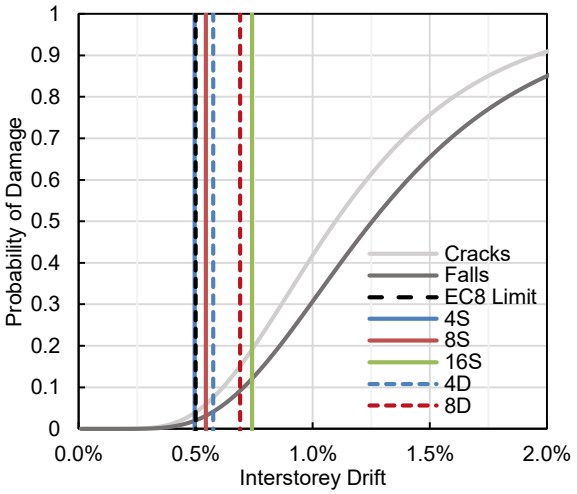

(b) Cladding fragility functions

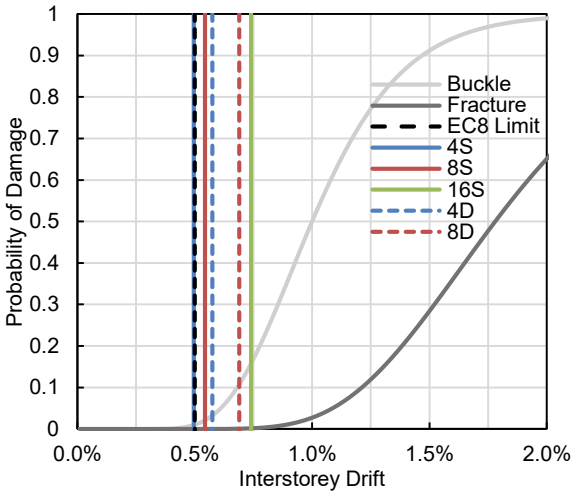

(c) Brace system fragility functions

Figure 4.19: Drift-sensitive fragility functions, Eurocode 8 drift limit and time history analysis results within one standard deviation of the mean ($\mu + \sigma$)

The median IDR of each building is well under the Eurocode limit with regards to the SLS for the standard designs and the ULS for the drift designs. The 4S, 8S and 16S buildings had SLS median drifts of 0.33%, 0.35%, and 0.45% respectively. The 4D and 8D buildings had ULS median drifts of 0.37%, and 0.45% respectively. However, values within one standard deviation of the mean ($\mu + \sigma$) representing the 84th percentile may be beyond the 0.5% limit for the relevant limit state. Figure 4.19 displays the $\mu + \sigma$ building drifts on the drift-sensitive fragility functions. SLS values are provided for the standard designs and ULS values are given for the drift designs.

The IDRs of building 4S are under 0.5%, however the other structures exceed the allowable limit. Damage to wall partitions is more probable, with damage state one nearly

certain, damage state two between 22% and 55%, and damage state three now feasible for 16S and 8D. Damage to cladding and brace systems are also now feasible for 16S and 8D. These results highlight the need for further review of the Eurocode nonstructural provisions.

4.6 Repair Cost Sensitivity Study

It was noted that the repair cost results are subject to change if the FEMA P-58 inputs are modified. For example, the selection of seismic design category affects the vulnerability of the nonstructural systems. This served as motivation for a sensitivity study on the FEMA P-58 repair cost calculations to various assumptions.

4.6.1 Rayleigh Damping

Section 3.4.4 justified the selection of tangent rather than initial stiffness for the calculation of Rayleigh damping. However, initial stiffness proportional Rayleigh damping is still frequently used. This section examines the effect of using initial or tangent stiffness on the determination of repair costs.

Figure 4.20 displays EDPs for two of the benchmark buildings using initial and tangent stiffness proportional Rayleigh damping in the OpenSees models. Mean peak results from the ULS and SLS time history analyses are provided. It can be seen that the use of initial stiffness results in reduced drifts and accelerations. The impact on the ULS accelerations is notable, while all other changes are minor. As discussed in Section 3.4.4, the use of initial stiffness for Rayleigh damping is expected to produce additional energy dissipation with respect to the use of tangent stiffness. This additional damping supports the observations.

The modified time history analysis results were used to conduct FEMA P-58 assessments. A representative selection of the case study buildings was chosen for this sensitivity study. Table 4.8 gives the change in repair costs due to the use of initial stiffness for Rayleigh damping with respect to the use of tangent stiffness. The difference

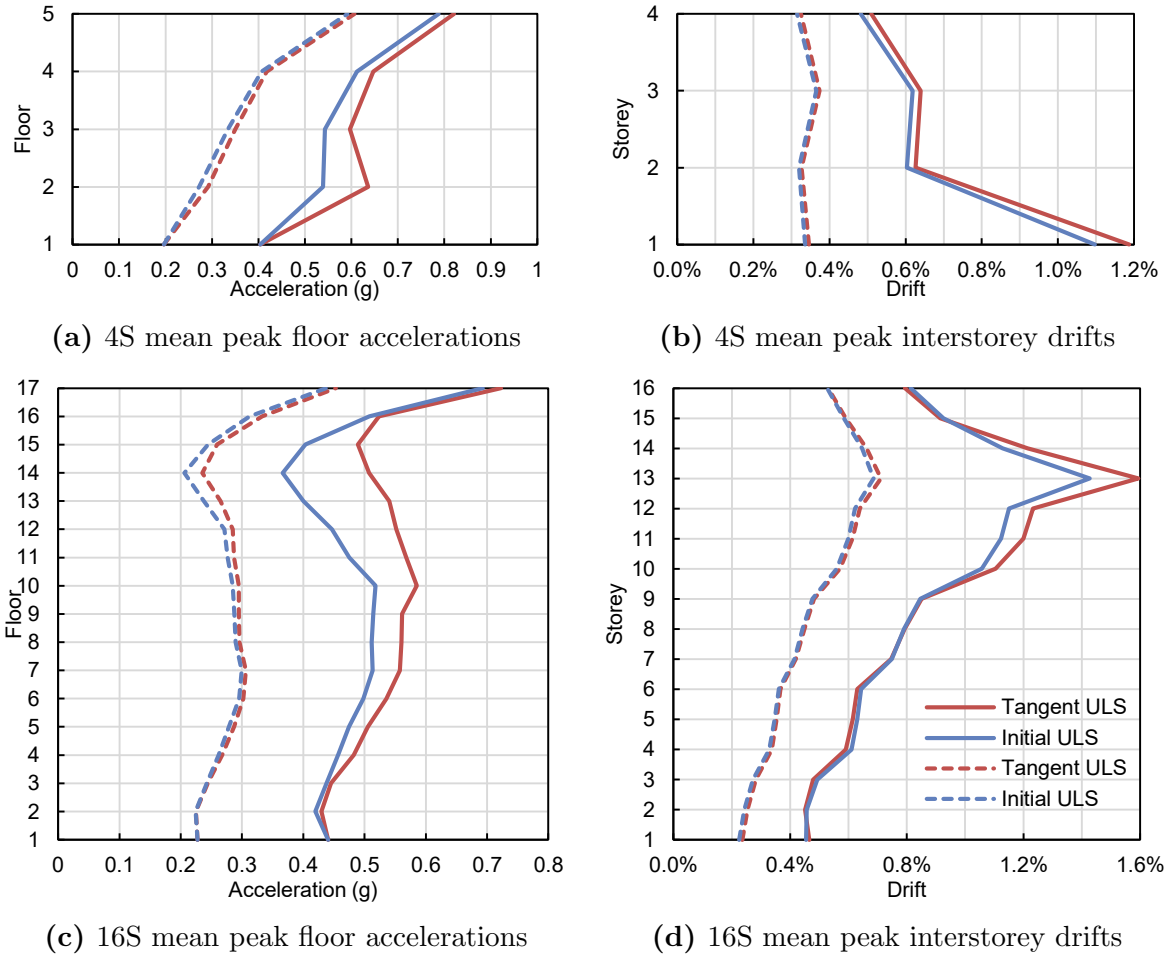

(a) 4S mean peak floor accelerations

(b) 4S mean peak interstorey drifts

(c) 16S mean peak floor accelerations

(d) 16S mean peak interstorey drifts

Figure 4.20: Mean peak EDPs comparing the use of initial and tangent stiffness for Rayleigh damping

in repair costs is normalised by the repair costs associated with tangent stiffness (i.e. $\Delta_C = (C_{new} - C_{original})/C_{original} \times 100\%$).

Repair costs are underestimated as a consequence of using initial stiffness. However, the sensitivity to the use of initial or tangent stiffness is secondary. The difference in repair costs ranges from 1.1% to 6.9%.

The drift design is less sensitive to the selection of initial or tangent stiffness. The drift design structure would remain elastic for larger portions of a time history analysis. It follows that initial and tangent stiffness would remain equal for these extended periods of elastic structural response. The same reasoning holds true for the SLS, where less nonlinear structural response is expected to occur. Figure 4.21 illustrates the magnitude of the difference in repair costs. Repair cost distributions for the largest difference (4S)

Table 4.8: Change in repair costs due to the use of initial stiffness rather than tangent stiffness for Rayleigh damping

Limit State	Building	Mean	Median	90th Percentile
ULS	4S	-6.6%	-6.9%	-6.1%
	16S	-5.3%	-5.4%	-2.5%
	4D	-3.6%	-2.5%	-1.9%
SLS	4S	-3.9%	-3.9%	-2.8%
	16S	-4.0%	-4.3%	-3.9%
	4D	-1.1%	-1.2%	-1.9%

and the second largest difference (16S) are provided. As can be seen, the sensitivity of repair costs is minor even for these maximum cases.

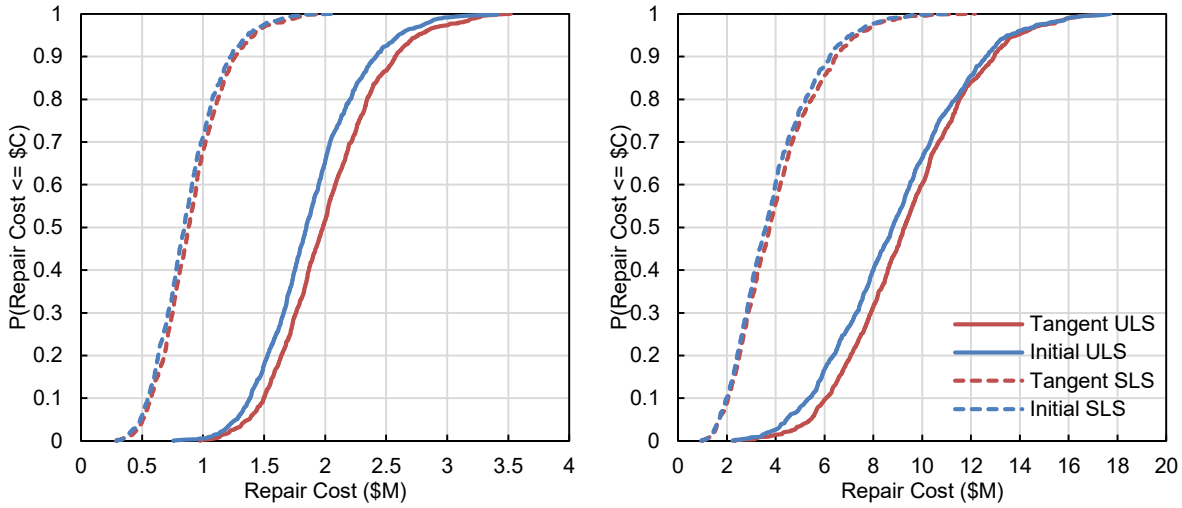

(a) 4S (largest difference) **(b)** 16S (second largest difference)

Figure 4.21: Repair cost distributions considering the use of initial and tangent stiffness proportional Rayleigh damping

4.6.2 Nonstructural Quantities

Section 3.6.2 documented the selection of nonstructural component quantities using the Normative Quantity Estimation Tool (FEMA 2012b). The tool estimates quantities at the 10th, 50th, and 90th percentile levels based on a survey of buildings (FEMA 2012c). Median component quantities were selected for the benchmark buildings in order to represent an average of possible repair costs. The sensitivity of the calculated costs to probable differences in nonstructural component quantities is now examined.

The 90th percentile of office nonstructural quantities was chosen to approximate an upper bound on nonstructural damage for buildings that are densely populated. Appendix B.3 lists the median and 90th percentile nonstructural quantities. A representative selection of the case study buildings was selected for this sensitivity study. FEMA P-58 assessments were conducted applying both sets of quantities. Table 4.9 provides the resulting change in repair costs due to the increased quantities of nonstructural components. The difference in repair costs is normalised by the original (median quantities) repair costs.

Table 4.9: Change in repair costs due to the use of 90th percentile nonstructural quantities rather than median quantities

Limit State	Building	Mean	Median	90th Percentile
ULS	4S	24.7%	25.1%	22.8%
	16S	16.7%	17.2%	12.8%
	4D	29.0%	29.9%	25.1%
SLS	4S	35.4%	34.0%	29.9%
	16S	28.8%	30.1%	21.7%
	4D	36.4%	35.6%	29.9%

Employing increased nonstructural quantities increased repair costs by 16.7% to 36.4%. The cases with a smaller amount of structural damage are more sensitive due to the larger proportion of nonstructural costs. This outcome is valid with regard to the buildings (16S has more structural damage than 4S, which has more structural damage than 4D), as well as for the limit states (the ULS results in more structural damage than the SLS). Figure 4.22 illustrates the influence of nonstructural quantities on the calculated repair costs using the same buildings as in the previous sensitivity study. It can be concluded that repair costs are highly sensitive to nonstructural quantities.

4.6.3 Nonstructural Specifications

A seismic design category of D was selected for nonstructural components as described in Section 3.6.2. This design category represents stringent seismic considerations and is grouped together with D, E and F (essential facilities) within FEMA P-58 (2012b).

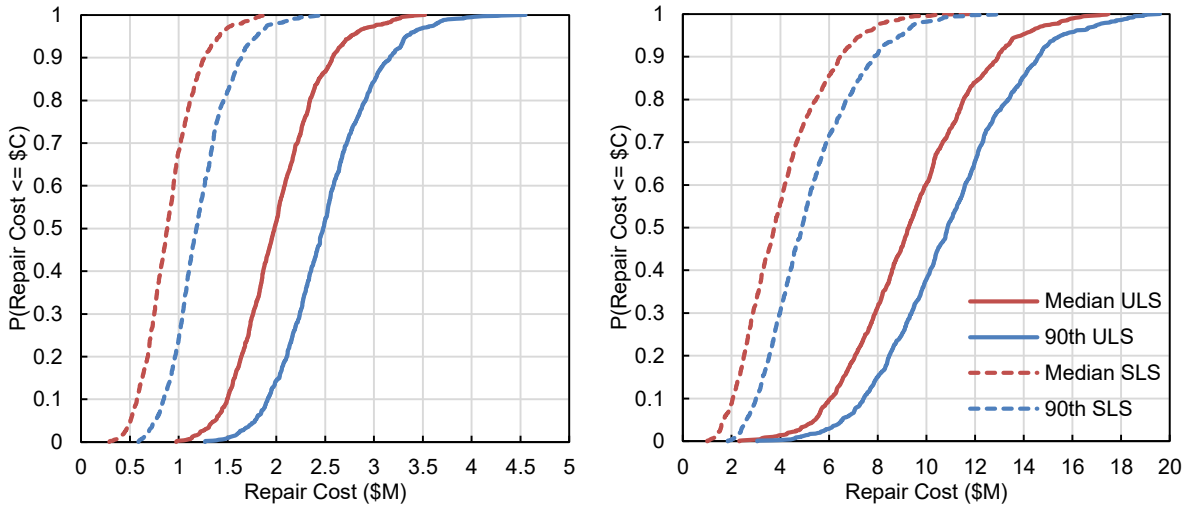

(a) 4S comparison **(b)** 16S comparison

Figure 4.22: Repair cost distributions considering the use of median and 90th percentile nonstructural quantities

The sensitivity of repair costs to the seismic design category of nonstructural systems is investigated.

The advanced nonstructural seismic specifications include techniques such as additional bracing or lateral support for the nonstructural system. Seismic design category A/B was selected in this sensitivity study to represent standard nonstructural components. Appendix B.3 lists the selected nonstructural fragility groups. FEMA P-58 analyses were conducted with the more vulnerable fragility groups. Table 4.10 lists the difference in repair costs normalised by the original (seismic design category D,E and F) repair costs.

Table 4.10: Change in repair costs due to the lower nonstructural seismic design category

Limit State	Building	Mean	Median	90th Percentile
ULS	4S	9.8%	10.2%	7.1%
	16S	8.8%	9.1%	5.5%
	4D	9.5%	10.6%	5.6%
SLS	4S	22.2%	24.1%	18.3%
	16S	14.0%	16.9%	12.1%
	4D	22.8%	25.7%	14.3%

The use of more vulnerable nonstructural systems led to increased repair costs. The sensitivity of the repair costs to the design category is moderate, with increases ranging from 5.5% to 25.7%. As with the nonstructural quantities study, the cases with less

structural damage prove to be more sensitive to the selection of seismic design category. Figure 4.23 illustrates the impact of seismic design category selection on the repair cost distributions. The examined buildings are consistent with those of the previous sensitivity studies. As can be seen, the sensitivity of repair costs is sizeable.

These results demonstrate that advanced nonstructural specifications such as lateral bracing do improve repair costs. However, the repair costs for the buildings with strict nonstructural specifications are still significant. This suggests that advanced nonstructural detailing alone cannot prevent damage. There is a need and opportunity for building-level solutions such as the use of FVDs.

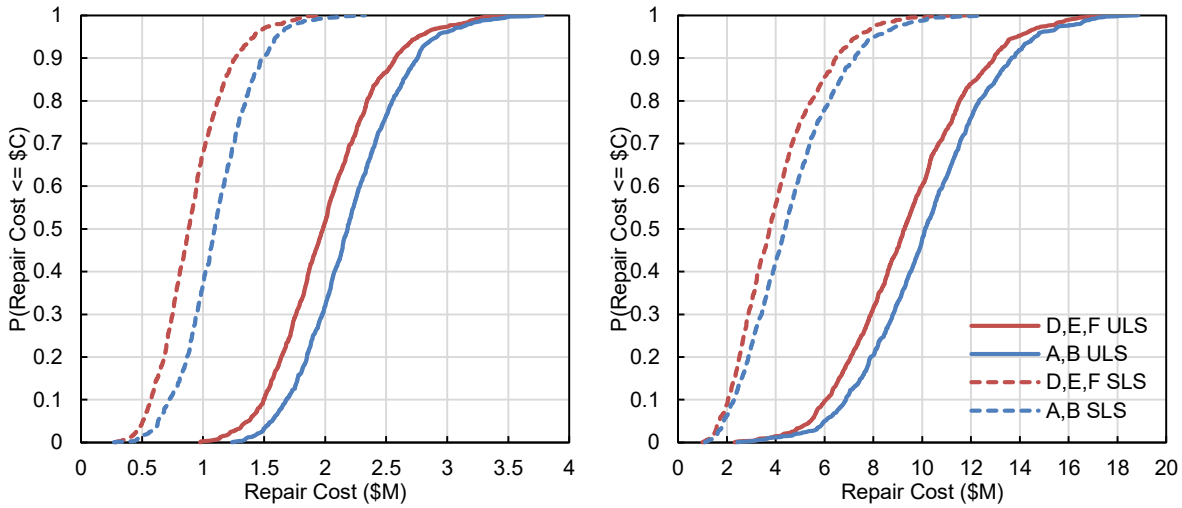

(a) 4S **(b)** 16S

Figure 4.23: Repair cost distributions considering the use of different nonstructural seismic design categories

4.7 Conclusions

This chapter investigated the seismic performance of conventional multi-storey buildings designed for seismic regions in accordance with the Eurocode. Structural response parameters used to characterise demands on structural and nonstructural systems were determined from nonlinear time history analyses. The Eurocode 0.5% drift limit was generally met, predicting ULS serviceability for 4D and 8D, and SLS serviceability for

4S and 8S. The drift designs experienced a greater maximum acceleration and a lower maximum drift in comparison to the standard designs.

A significant number of braces yield and buckle during the ULS for the standard buildings, while the drift designs experienced negligible nonlinear brace behaviour. The standard designs exhibited some drift concentration during the ULS. Column bending due to brace deterioration is not considered in Eurocode design and can lead to underdesign of column members.

The EDP results were translated to repair costs using FEMA P-58. Large repair costs were generated for both limit states. These direct losses would be compounded by indirect costs due to downtime and disruptions. Buildings designed to modern structural standards (Eurocode) may be demolished following a ULS earthquake due to the high repair costs. The implications for a city centre are severe. Substantial repair costs are expected for the SLS scenario and structural damage was predicted for 8S and 16S. These results suggest that modern building standards do not accomplish earthquake resilience: the ability of a community to recover quickly after an earthquake.

Conventional building codes control drifts but do not place limitations on floor accelerations. It was observed that acceleration-sensitive damage is comparable or of greater consequence than drift-sensitive damage. The influence of acceleration on seismic performance should be more appropriately reflected in structural design procedures.

Negligible repair costs were associated with stairs, access flooring, elevators, piping, fire sprinkler systems, and electrical systems. Future seismic performance assessments may exclude these fragility groups to decrease computation effort.

Nonstructural systems are treated in a simplified manner during structural design. However, the majority of repair costs can be attributed to these systems. This highlights the importance of considering nonstructural seismic performance when designing for a rapid return to building occupancy. Attaining a target level of seismic performance mandates the harmonisation of structural and nonstructural performance.

The level of structural damage was reduced by the drift designs. Although the ULS repair costs decreased with respect to the standard designs, the median repair costs were

still above the building replacement limit (40% of building value). However, the building replacement limit is only an approximation; it is unlikely that the 4D building would be demolished without sustaining structural damage. The SLS repair costs of the drift designs were comparable to the standard designs.

Limitations of the Eurocode damage mitigation methodology were exposed as the prescribed interstorey drift limit did not prevent nonstructural damage. Storeys satisfying the limit experienced drift-sensitive nonstructural damage, and extensive acceleration-sensitive nonstructural costs were also produced. The studied nonstructural systems are of the highest seismic design category — significant amplification of repair costs would be expected for more vulnerable systems. These results draw attention to the need for structural design procedures which enhance nonstructural seismic performance. This shift in seismic design philosophy is required to achieve a rapid return to building occupancy after an earthquake.

The sensitivity of FEMA P-58 repair cost calculations was investigated. The sensitivity of repair costs to nonstructural quantities is considerable, as costs significantly rose when using the 90th percentile quantities. The use of more vulnerable nonstructural seismic design categories caused moderate repair cost increases, revealing that advanced nonstructural specifications can improve performance. However, buildings with strict nonstructural specifications still experienced significant damage. This suggests that advanced nonstructural detailing alone cannot prevent damage. There is a need for building-level solutions such as the use of FVDs.

The results of the seismic performance assessment provide a benchmark on which to evaluate alternative building designs. This benchmark is valuable when selecting retrofit alternatives for existing buildings and design options for new structures. FVDs will be incorporated into the structures in the following chapters. The results of the code-compliant seismic performance benchmark will enable the capability of FVDs to be assessed.

Chapter 5

Damping and Repair Costs

5.1 Overview of Chapter

FEMA P-58 analyses in Chapter 4 revealed that Eurocode-compliant structures exhibit poor nonstructural seismic performance. Retrofitting buildings with supplemental damping devices can substantially reduce interstorey drift ratios (IDRs) and improve the seismic performance of buildings. Section 2.4 identified fluid viscous dampers (FVDs) as the most promising of these devices for nonstructural considerations as they can improve both IDRs and floor accelerations. This study investigates the application of FVDs to minimise structural and nonstructural damage during earthquakes.

Despite having the potential to be effective and economically viable solutions, research focusing on FVD applications for reducing nonstructural damage in buildings has been limited. Previous research on the use of FVDs has focused on structural performance, while nonstructural performance is often not considered. Structural parameters such as IDR are often evaluated rather than repair costs. Damping ratios achieved using FVDs are not calculated or are estimated based on simplifying assumptions. There is also a need to clarify what seismic performance improvements can and cannot be achieved through the use of FVDs.

This chapter addresses these research gaps using the seismic performance assessment method described in Chapter 3. The relationship between damping and repair costs considering nonstructural seismic performance is investigated.

The additional methods, modelling and background information necessary for this chapter are provided in Section 5.2. Calculating the level of damping achieved through

the use of FVDs is examined in Section 5.3. A comparison of damping calculated using a popular energy method approximation and the actual level of damping achieved is provided in Section 5.4. This investigation includes the presentation of a modified energy formula to improve the accuracy of the energy method. Section 5.5 investigates the optimal amount of damping to minimise repair costs. Conclusions for the chapter are presented in Section 5.6.

5.2 Methods: Fluid Viscous Dampers

Additional methods, modelling and background information are introduced in this chapter in order to investigate the use of FVDs. This investigation is limited to uniform damper placement. It is recognized that nonlinear FVDs are often used in practice, however this thesis is one of the first studies of its kind. As a result, the scope is limited to linear FVDs.

5.2.1 Required Amount of Damping

Eurocode 8 (CEN 2013) and ASCE 7-10 (American Society of Civil Engineers 2013) determine the total damping ratio (ζ) required to achieve a desired performance level through the use of damping correction factors. The damping correction factor, represented as η in this study, is a ratio of the desired and bare frame performance. The factor is calculated using

$$\eta = \frac{P_{damped}}{P_{bare}}, \tag{5.1}$$

where P refers to some measure of seismic performance. The most commonly used measure of performance is maximum IDR.

The required amount of damping can be determined given the desired damping correction factor. Eurocode 8 Cl. 3.2.2.2 (CEN 2013) provides the relationship

$$\eta = \sqrt{\frac{10}{5+\zeta}} \geq 0.55, \tag{5.2}$$

where the damping ratio is expressed as a percentage. ASCE 7-10 (American Society of Civil Engineers 2013) presents the damping correction factor-damping ratio relationship

in table format (Table 18.6-1). A portion of this information is reproduced in Table 5.1. Values are also provided for the damping correction factor calculated using Eq. 5.2 from Eurocode 8. The ASCE factors are very similar to the Eurocode 8 factors. The main difference between the two methods is the limit of $\eta \geq 0.55$ imposed on the Eurocode 8 equation.

Table 5.1: Damping ratios and corresponding damping correction factors

Total Damping (%)	**ASCE $1/\eta$**	**Eurocode $1/\eta$**
≤ 2	0.8	0.8
5	1.0	1.0
10	1.2	1.2
20	1.5	1.6
30	1.8	-
40	2.1	-

Supplemental damping (ζ_d) is the total damping less the inherent damping. Once the required amount of supplemental damping is calculated, the damper coefficients and the associated damper placement that produce this level of damping can be determined.

5.2.2 Calculation of Damper Coefficients

The force output of a linear FVD is given by

$$f_i = c_i \dot{u}_{ri}, \tag{5.3}$$

where f_i is the force, c_i is the viscous damping coefficient and $\dot{u}_{ri}$ is the extensional velocity of damper i.

Uniform damper placement is used in this chapter, i.e. distributing the total damping coefficient equally to each storey. This simple technique is one of the most commonly used placement methods (Lopez Garcia and Soong 2002; Pavlou and Constantinou 2006; Hwang *et al.* 2013; Palermo *et al.* 2013; Landi *et al.* 2015; Dall'Asta *et al.* 2016). One damper per storey is used in this study.

In order to size and place the dampers, the desired supplemental damping to be introduced by the FVDs must be converted to viscous damping coefficients. The energy

method from Whittaker *et al.* (2003) is frequently used to perform this procedure. The energy method formula for linear FVDs is

$$\zeta_{d,n} = \frac{T_n \sum_j c_j \cos^2 \theta_j \phi_{rj}^2}{4\pi \sum_i m_i \phi_i^2}, \tag{5.4}$$

where $\zeta_{d,n}$ is the supplemental damping ratio in mode n, θ_j is the angle of damper inclination at storey j, ϕ_{rj} is the relative modal displacement, m_i is the mass of storey i and ϕ_i is the modal displacement.

The numerator of Eq. 5.4 is based on the energy dissipated by a linear viscous damper per cycle of motion in the mode of interest. Assume the structure undergoes a harmonic vibration given by

$$\mathbf{u} = u_A \boldsymbol{\phi}_i \sin \frac{2\pi}{T_n} t, \tag{5.5}$$

where u_A is a constant. The vertical displacements are assumed to be insignificant in comparison to the horizontal displacements. The relative horizontal motion experienced by damper j, u_{rj}, can then be presented by

$$u_{rj} = u_A \left(cos\theta_j \phi_{rj}\right) \sin \frac{2\pi}{T_n} t. \tag{5.6}$$

The energy dissipated by damper j, $E_{D,j}$, therefore is defined as

$$E_{D,j} = \int_0^{T_n} f_j \dot{u}_{rj} dt = \frac{2\pi^2}{T_n} u_A^2 c_j \cos^2 \theta_j \phi_{rj}^2. \tag{5.7}$$

The sum of the energy dissipated by all dampers (E_D) is given by

$$E_D = \frac{2\pi^2}{T_n} u_A^2 \sum_j c_j \cos^2 \theta_j \phi_{rj}^2. \tag{5.8}$$

The denominator of Eq. 5.4 is based on the maximum kinetic energy in the frame. During the motion given by Eq. 5.5, the kinetic energy due to mass i (referred to as $E_{k,i}$) is given by

$$E_{k,i} = \frac{1}{2} m_i \dot{u}_i^2 = \frac{2\pi^2}{T_n^2} u_A^2 m_i \phi_i^2 \cos^2 \frac{2\pi}{T_n} t. \tag{5.9}$$

The maximum kinetic energy of the entire structure ($E_{k,o}$) is therefore defined by

$$E_{k,o} = \frac{2\pi^2}{T_n^2} u_A^2 \sum_i m_i \phi_i^2. \tag{5.10}$$

The equivalent viscous damping ratio in mode n is given by Eq. 5.11. This equation was developed for a single-degree-of-freedom (DoF) system by Chopra (2012). Accepting that this procedure can be extended to multi-DoF structures on a mode-by-mode basis with sufficient accuracy (Chopra 2012), the energy method formula can be reproduced.

$$\zeta_{d,n} = \frac{E_D}{4\pi E_{k,o}} \tag{5.11}$$

The energy method formula produces an approximation of the supplemental damping, or an equivalent viscous damping ratio, by assuming vertical motions are insignificant and that the modes can be uncoupled. Given the desired damping ratio and the damper distribution, the damper coefficients can be determined using the energy method. Once the damper coefficients are known, FVDs with appropriate properties can be modelled.

5.2.3 OpenSees Modelling

The OpenSees models of each conventional structure, previously described in Section 3.4, were altered to include FVDs. Dampers are modelled as linear viscous dashpots using the OpenSees element *element twoNodeLink* with the material *uniaxialMaterial Viscous*.

As a sample of the validation performed in this chapter, Figure 5.1 compares the damper member force-elongation record from a time history analysis with the theoretical damper force using Eq. 5.3. A single braced bay was modelled with a linear FVD and subjected to an acceleration time history. The damper member and theoretical damper forces display a good match, even with a larger time-step (dt).

Elevation views of the standard and drift designs with FVDs are show in Figure 5.2. The locations of FVDs are indicated in red. Once FVDs have been modelled in the structure, it should be verified that the target and achieved damping ratio agree.

5.3 Calculation of Achieved Damping

The supplemental damping ratio calculated by the energy method formula is an approximation. Occhiuzzi (2009) noted that only a small number of research papers calculate an estimate of modal damping ratios. The first attempt in this chapter to determine

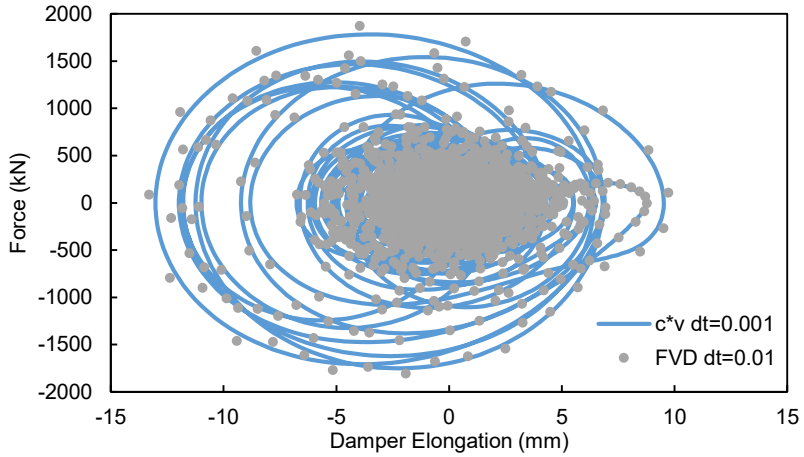

Figure 5.1: Comparison of the damper force-elongation relationship of an OpenSees model and the theoretical result. dt = time-step in seconds

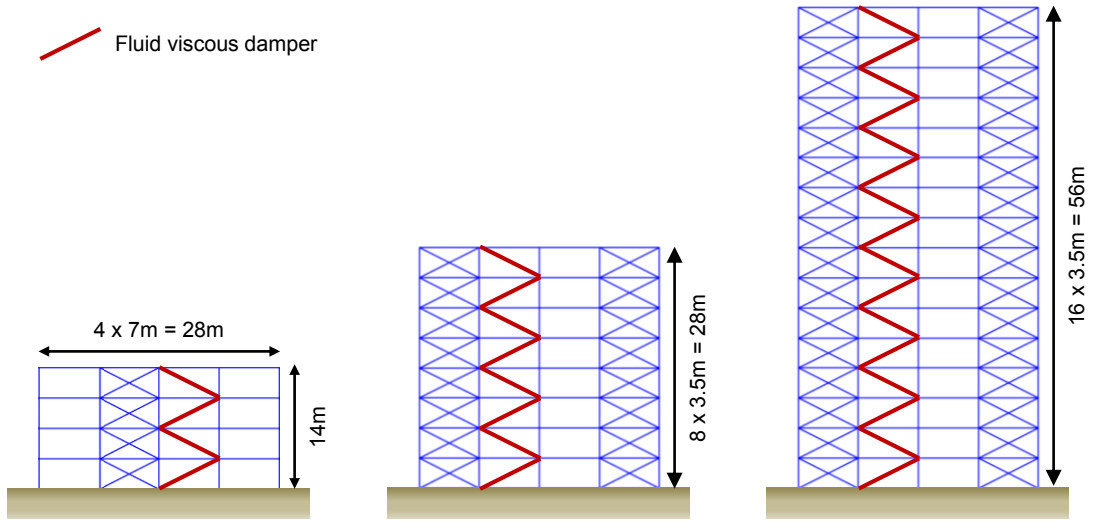

(a) Standard designs with FVDs

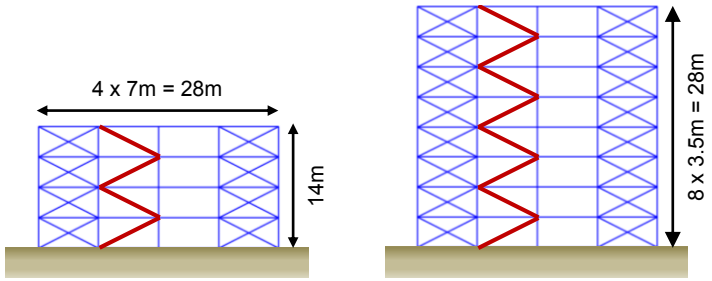

(b) Drift designs with FVDs

Figure 5.2: Elevation views of the office buildings with locations of FVDs

damping ratios of buildings with FVDs used the logarithmic decrement of free vibration. This attempt proved to be unsuccessful due to the coupling of modes. As a result, a general modal analysis considering complex-valued modes was performed.

5.3.1 Logarithmic Decrement of Free Vibration

Damping ratios are often determined by measuring the decay of the response during free vibration. The solution to the equation of motion for an underdamped system undergoing free vibration is given by

$$u(t) = \exp(-\zeta\omega_n t)\left[u(0)\cos\omega_D t + \frac{\dot{u}(0) + \zeta\omega_n u(0)}{\omega_D}\sin\omega_D t\right], \tag{5.12}$$

where ω_n is the undamped fundamental frequency of vibration and ω_D is the fundamental frequency of damped vibration given by $\omega_D = \omega_n\sqrt{1-\zeta^2}$. The ratio of the displacement at time t and at time $t + jT_D$, where T_D is the natural period of damped vibration and j is the number of cycles, reduces to

$$\frac{u(t)}{u(t+jT_D)} = \exp\left(\frac{2\pi j\zeta}{\sqrt{1-\zeta^2}}\right). \tag{5.13}$$

Isolating the damping ratio in Eq. 5.13 leads to

$$\zeta = \frac{\delta_u}{\sqrt{4\pi^2 j^2 + \delta_u^2}}, \tag{5.14}$$

where δ_u is the logarithmic decrement given by $\delta_u = \ln\left(u(t)/u(t+jT_D)\right)$. Eq. 5.14 enables the damping ratio to be calculated using the decay of motion of the system.

The damping ratio realised in the first mode is the most common measure of damping. In order to excite the first mode of the considered structure, an acceleration time history was used to disturb the structure from its static equilibrium position. The structure was then allowed to vibrate without any external excitation. The resulting roof displacement time history during free vibration was used to calculate the achieved damping ratio.

A sine wave with a period equal to T_1 and an amplitude of A was examined. Ten cycles of excitation are followed by free vibration for the equivalent time of ten further cycles. The acceleration input function is provided by

$$a(t) = \begin{cases} A\sin\frac{2\pi}{T_1}t & 0 \le t \le 10T_1 \\ 0 & 10T_1 < t \le 20T_1. \end{cases} \tag{5.15}$$

The discrete Fourier transform of the input function for the four-storey standard design (4S) using an amplitude of 0.03 g was computed using a fast Fourier transform function

algorithm in MATLAB (The MathWorks Inc. 2017) to examine the excited frequencies. The Fourier transform is given in Figure 5.3a, with the frequency of the first and second modes indicated as f_1 and f_2, respectively. It can be seen that the first mode is excited, although other frequencies are also affected.

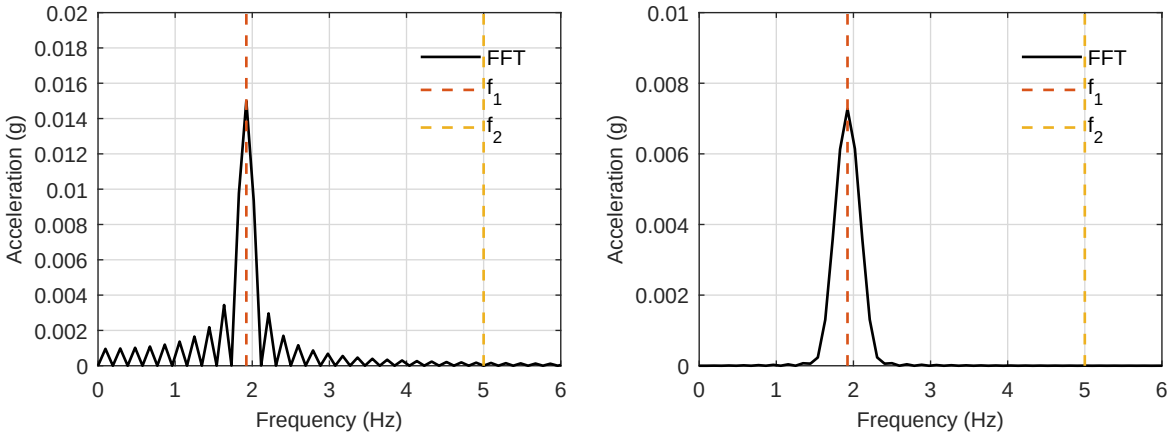

(a) Unfiltered acceleration **(b)** Filtered acceleration

Figure 5.3: Fourier transforms of the unfiltered and filtered acceleration input functions for 4S

The abrupt end of the sine function in the acceleration input represented by Eq. 5.15 produces an impulse-like response in which many frequency components are present. The log decrement theory used in Eq. 5.14 is only valid for a single-frequency vibration. To address this issue, a discrete window function was used to filter the time domain function. The confined Gaussian window function approximation proposed by Starosielec and Hagele (2014) was used. The windowed acceleration input function is the product of the sine acceleration function and the Gaussian window function. The Fourier transform of the corresponding windowed input function is provided in 5.3b. It can be seen that there is a better fit to the frequency of the first mode for the filtered input function than for the unfiltered input function.

The log decrement procedure using the filtered acceleration inputs was verified by examining structures with inherent Rayleigh damping of 5%. An example is provided in Figure 5.4a for building 4S. The initiation of free vibration conditions is indicated by T_{end}. The achieved damping ratio in the first period was calculated to be 4.2%, differing from the target of 5% due to the use of the elongated first period in the calculation of Rayleigh

coefficients (as discussed in Section 3.4.4). The achieved damping ratio was calculated to be 5.0% when the elastic first period was used to determine the Rayleigh coefficients.

Figure 5.4b provides an example of the damping ratio calculation for building 4S with FVDs. A total damping ratio of 15% was targeted, with damper coefficients corresponding to 10% supplemental damping determined using the energy method and uniform damper placement. The amplitude of the acceleration was increased to 0.15 g in order to produce a sufficient number of free vibration cycles for the structure with increased damping. Steel materials were constrained to elastic behaviour. The damping ratio was calculated to be 16.6%, close to the target ratio of the energy method.

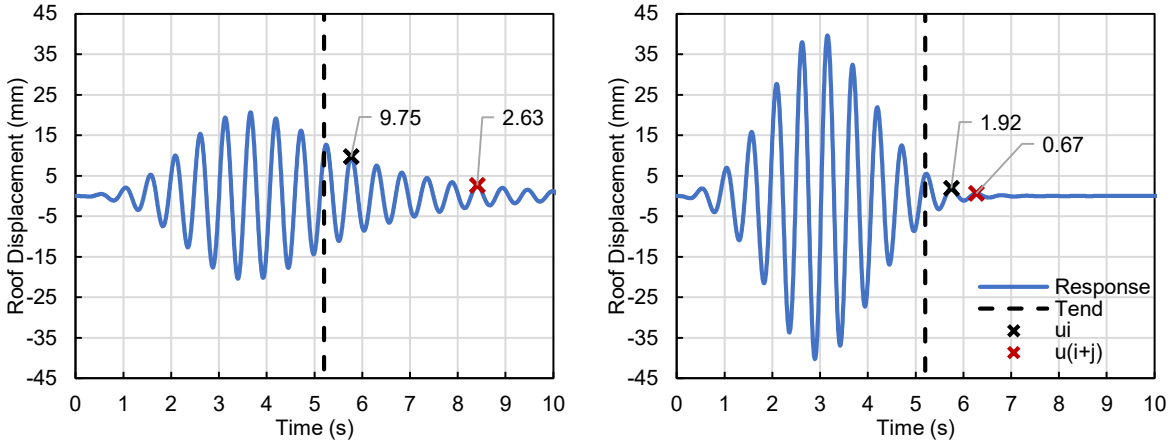

(a) 5% Rayleigh damping **(b)** 15% total damping

Figure 5.4: Calculating the achieved damping ratio using the decay of motion of 4S in OpenSees. Initiation of free vibration conditions = T_{end}, u = roof displacement

Damping ratios for the remainder of the benchmark designs were examined using this procedure. Upon further study, it was found that this method is unsuitable for structures with large amounts of damping using uniform FVD placement when the lateral structural stiffness is not uniform throughout the building height. Erroneous damping ratios were recorded and the period between peaks was found to decrease rather than increase. Results for the 4S and 16-storey standard design (16S) buildings with FVDs are provided in Table 5.2.

The erroneous damping ratio calculations can be attributed to the coupling of modes due to non-classical damping. The logarithmic decrement procedure produced acceptable results for the 4S building due to the design's nearly uniform storey stiffness. As a result

Table 5.2: Damping ratios calculated using the logarithmic decrement

Target Damping	**4S**		**16S**	
	Damping	**T_1 (s)**	**Damping**	**T_1 (s)**
10%	10%	0.53	13%	2.31
15%	16%	0.53	19%	2.18
20%	22%	0.52	19%	2.04
25%	27%	0.52	19%	1.97
30%	31%	0.51	18%	1.92
35%	34%	0.50	17%	1.88
40%	38%	0.49	17%	1.84
45%	41%	0.49	16%	1.83

of this structural property, uniform damping is similar to a classically damped system. Another method must be used to calculate the achieved damping ratios of non-classically damping systems.

5.3.2 General Modal Analysis Considering Complex-Valued Modes

The logarithmic decrement method is unsuccessful when modes are coupled due to non-classical damping. Veletsos and Ventura reviewed modal analysis of non-classically damped linear systems (1986). Viscous damped systems that do not meet the classically damped conditions generally have complex-valued modes. Modal properties can be evaluated by a generalisation of the modal superposition method. Occhiuzzi (2009) applied this method to structural systems with FVDs.

The equation of motion for a system experiencing free vibration is given by

$$\mathbf{M}\ddot{\mathbf{x}} + \mathbf{C}\dot{\mathbf{x}} + \mathbf{K}\mathbf{x} = \mathbf{0}, \tag{5.16}$$

where $\mathbf{M}$, $\mathbf{K}$ and $\mathbf{C}$ are the mass, stiffness, and damping matrix of the system respectively. By defining the state space as

$$\mathbf{z} = \begin{Bmatrix} \mathbf{x} \\ \dot{\mathbf{x}} \end{Bmatrix}, \tag{5.17}$$

the state space representation of the system with n modes of interest can be written as

$$\dot{\mathbf{z}} = \frac{\mathrm{d}}{\mathrm{dt}} \begin{Bmatrix} \mathbf{x} \\ \dot{\mathbf{x}} \end{Bmatrix} = \begin{bmatrix} \mathbf{0} & \mathbf{I} \\ -\mathbf{M}^{-1}\mathbf{K} & -\mathbf{M}^{-1}\mathbf{C} \end{bmatrix} \begin{Bmatrix} \mathbf{x} \\ \dot{\mathbf{x}} \end{Bmatrix} = \mathbf{A}\mathbf{z}, \tag{5.18}$$

where $\mathbf{I}$ is a $n \times n$ identity matrix, $\mathbf{0}$ is a $n \times n$ null matrix, and $\mathbf{A}$ is the system matrix (Occhiuzzi 2009). The eigenvalues ($s_{i,\ldots,2n}$) of system $\mathbf{A}$ are complex conjugate pairs, i.e. $s_{1,2} = -\zeta_1\omega_1 \pm i\omega_1\sqrt{1-\zeta_1^2}$ (Occhiuzzi 2009). For the ith pair, the imaginary part of s_i is the ith damped circular frequency $\omega_{d,i}$ of the system; $\omega_{d,i} = \mathrm{Im}(s_i)$. The damping ratio can be determined from the negative ratio of the real part and modulus; $\zeta_i = -\frac{\mathrm{Re}(s_i)}{|s_i|}$.

The mass, stiffness and damping matrices are required in order to use the general modal analysis method. Although these matrices are not directly available in OpenSees, they can be extracted from the global system matrix ($\mathbf{K}^*$). The global system matrix is a combination of $\mathbf{M}$, $\mathbf{K}$ and $\mathbf{C}$. The OpenSees command *printA* records the current global system matrix. The command can only be issued following an *analyze* command. In order to issue the *printA* command, the system of the structure must be a full general linear system of equations. This condition can be produced through the use of the command *system FullGeneral* when creating the OpenSees model. The system command ensures that no memory space saving techniques are used and a $n \times n$ matrix is produced, where n is the number of DoF.

The global system matrix will be equal to the stiffness matrix if a static analysis is performed, as the force is proportional to the stiffness matrix multiplied by the displacement ($\mathbf{F} = \mathbf{Kx}$). The *printA* command was issued following a static analysis of each model without a load to record the stiffness matrix.

The equation for the global system matrix with the Newmark integration method is

$$\mathbf{K}^*_{t+\Delta t} = \mathbf{K}_t + \frac{\gamma}{\beta\Delta t}\mathbf{C}_t + \frac{1}{\beta\Delta t^2}\mathbf{M}, \tag{5.19}$$

where Δt represents the time-step used in the analysis (PEER 2017). The Newmark integration method was used (*integrator Newmark*) with coefficients $\gamma = 0.5$ and $\beta = 0.25$ corresponding to the average acceleration method.

Rayleigh damping was not assigned to the structural members and FVDs were not included in the structural model, resulting in $\mathbf{C} = \mathbf{0}$. A dynamic analysis of one time-step was conducted. With $\mathbf{K}$ known from the static analysis, $\mathbf{M}$ can be solved. Once this was conducted, Rayleigh damping and FVDs were added to the model. A second transient

analysis was performed, which allowed $\mathbf{C}$ to be determined from the resulting global system matrix.

The mass matrix was found to be singular due to the presence of DoF without rotational mass. In order to use the general modal analysis method, a mass orthonormal set, where $\mathbf{\Phi}^T\mathbf{M}\mathbf{\Phi} = \mathbf{I}$, was approximated using a select number of valid undamped eigen vectors. The eigen vectors with horizontal components and a non-negligible effective modal mass were selected to approximate the matrix of eigen vectors ($\mathbf{\Phi}$).

General modal analysis considering complex-valued modes allows the achieved damping ratios to be calculated for any structure. This approach can be used to verify that the energy method formula produces an achieved damping ratio that is sufficiently close to the target ratio.

5.4 Energy Method and Achieved Damping

5.4.1 Comparison of Target and Achieved Damping

A comparison of the damping ratio targeted by the energy method and the actual ratio achieved has not been previously performed. The target damping ratio from the energy method was evaluated with respect to the achieved damping ratio.

The five benchmark building models were retrofitted with uniformly-distributed FVDs. The damper coefficients were calculated using the energy method formula (Eq. 5.4). A range of 10% to 45% total damping in the first mode was investigated using an interval of 5%. Table 5.3 provides the damper coefficients determined using the energy method.

Table 5.4 compares the actual damping ratios achieved with the target ratios of the energy method. The energy formula underestimates the achieved damping for all cases. It can also be observed that the approximated damping ratio is closer to the target ratio for the shorter buildings. This may be influenced by higher mode effects, which are more pronounced for taller buildings. The four-storey buildings were shown to have a modal mass participation factor (M_n^p) of 80% for the first mode (Section 3.4.3). In comparison, the eight- and 16-storey structures have modal mass participation factors of approximately 75% and 65%, respectively.

Table 5.3: Damper coefficients calculated using the energy method

Target Damping	c_j **(N s/mm)**				
	4S	**8S**	**16S**	**4D**	**8D**
10%	1,566	3,034	3,684	2,229	4,283
15%	3,131	6,069	7,368	4,457	8,566
20%	4,697	9,103	11,052	6,686	12,849
25%	6,262	12,137	14,736	8,914	17,132
30%	7,828	15,172	18,421	11,143	21,416
35%	9,393	18,206	22,105	13,371	25,699
40%	10,959	21,240	25,789	15,600	29,982
45%	12,524	24,275	29,473	17,828	34,265

Table 5.4: Damping ratios achieved using damper coefficients from the energy method

Target	**4S**	**8S**	**16S**	**4D**	**8D**
10%	11%	12%	14%	11%	13%
15%	17%	19%	23%	17%	21%
20%	23%	27%	32%	23%	29%
25%	29%	33%	41%	29%	36%
30%	35%	38%	47%	34%	40%
35%	40%	42%	49%	39%	43%
40%	44%	45%	50%	44%	46%
45%	48%	48%	51%	48%	48%

The damping ratio for structure 16S plateaus at approximately 51%. Damping ratios near this maximum level of damping are reached when the c_j values are greatly decreased. For example, increasing c_j from 18 421 N s/mm to 29 473 N s/mm only increases the damping by 2%, from 49% to 51%. This suggests that there is a limit at which FVDs can no longer increase the total damping. However, this limit occurs at a damping value larger than the 35% suggested by Christopoulos and Filiatrault (2006).

The discrepancy between the target and achieved damping ratio is significant for higher levels of damping, and for the eight- and 16-storey buildings. These results motivated a modification of the energy method to improve its accuracy.

5.4.2 Modification of the Energy Method

The main advantage of the energy method formula is that calculations can be easily and quickly performed. However, the results of Section 5.4.1 demonstrate that the

approximation may only be accurate for low-rise structures. This section modifies the energy formula to decrease the variation between the target and achieved damping ratios, while maintaining the ease-of-use advantage of a single formula.

Recall Eq. 5.11 used by the energy method: $\zeta_{d,n} = E_D/4\pi E_{k,o}$. This common method for defining equivalent viscous damping was developed for a single-DoF system (Chopra 2012). Considering harmonic motion defined as $u = u_o \sin \omega t$ for a single-DoF system, the viscous damper force $f_D = c\dot{u} = cu_o\omega \cos \omega t$. The energy dissipated by viscous damping in one cycle of motion is given by

$$E_D = \int f_D du = \pi c \omega u_o^2. \tag{5.20}$$

The maximum strain energy in the system is $E_{s,o} = \frac{1}{2}ku_o^2$. Expressing Eq. 5.20 in terms of the viscous damping ratio and natural frequency (ω_n), and given that the maximum strain energy is equal to the maximum energy, produces $E_D = 4\pi\zeta\frac{\omega}{\omega_n}E_{k,o}$. Rearranging for the viscous damping ratio produces the equation

$$\zeta = \frac{\omega_n}{\omega}\frac{E_D}{4\pi E_{k,o}}. \tag{5.21}$$

The above analysis is true for a single-DoF system with a theoretical viscous damper. However, the formula is applied to other systems with energy dissipation to produce an equivalent viscous damping ratio. To define an equivalent viscous damping ratio for an actual structure, the energy dissipated in the structure during an experiment is equated to the viscous damping given by Eq. 5.21. It is assumed that the method can be applied on a mode-by-mode basis, and that the experiment producing the force-deformation relationship is conducted at $\omega = \omega_n$. Eq. 5.21 then reduces to Eq. 5.11 used by the energy method: $\zeta_{d,n} = E_D/4\pi E_{k,o}$.

The ω_n/ω term should be considered, as the response of a structure to earthquake-induced ground motions cannot be assumed to occur at $\omega = \omega_n$. It was opted to use the inverse of the modal mass participation factor of each mode as a proxy for the frequency ratio term. This value serves as an approximation for the contribution of each modal response to the total response of the system during an arbitrary motion. The calculation

of the modal mass participation factor does not significantly increase the effort involved in the energy method. Determining this factor only requires the mode shape, the mass matrix, and the influence vector (refer to Eq. 3.7). The mode shape and mass matrix are already required for the energy formula, while determining the influence vector is a relatively simple process. The modified energy formula is

$$\zeta_{d,n} = \frac{T_n \sum_j c_j \cos^2 \theta_j \phi_{rj}^2}{4\pi M_n^p \sum_i m_i \phi_i^2}, \tag{5.22}$$

with all terms previously defined. This equation is limited to the case of linear FVDs.

The modified formula was used to calculate the damper coefficients for all of the building designs and all levels of damping. The non-classical damping method was then used to determine the achieved damping ratios, which are shown in Table 5.5.

Table 5.5: Damping ratios (%) achieved using the original (O) and modified (M) energy formulas

Target	**4S**		**8S**		**16S**		**4D**		**8D**	
	O	**M**	**O**	**M**	**O**	**M**	**O**	**M**	**O**	**M**
10	11	9	12	10	14	10	11	9	13	11
15	17	15	19	16	23	16	17	15	21	17
20	23	20	27	21	32	23	23	20	29	23
25	29	25	33	27	41	29	29	24	36	29
30	35	30	38	31	47	34	34	29	40	34
35	40	34	42	36	49	40	39	34	43	38
40	44	38	45	39	50	44	44	38	46	41
45	48	42	48	42	51	48	48	41	48	43

The accuracy of the original and modified energy formulas was compared using the mean absolute relative error (MARE). The MARE was calculated by the equation

$$\text{MARE} = \frac{1}{n_d} \sum_d \frac{|\zeta_{T,d} - \zeta_{A,d}|}{\zeta_{T,d}}, \tag{5.23}$$

where the target and achieved damping ratio for each level of damping d considered are $\zeta_{T,d}$ and $\zeta_{A,d}$, respectively, and n_d is the number of damping levels considered. The MARE results expressed as a percentage are shown in Table 5.6 for all levels of damping and all buildings.

Table 5.6: Mean absolute relative error of the energy formulas

Formula	**Mean Absolute Relative Error**				
	4S	**8S**	**16S**	**4D**	**8D**
Original	13%	23%	44%	11%	29%
Modified	3%	4%	11%	4%	10%

The modified formula results in a smaller error for all buildings with respect to the original energy formula. In particular, a substantial improvement is realised for the eight- and 16-storey structures. This suggests that the modified energy formula is an improvement on the original formula and should be considered in future studies. These results highlighting the deviation between the target and achieved damping ratio will be taken into account in the following study on the optimal amount of damping.

5.5 Optimal Amount of Damping

The amount of damping in a building significantly influences structural response during an earthquake. Occhiuzzi (2009) concluded that a maximum of 20-25% total damping in the first mode is ideal, as additional damping above this level increased accelerations and further reductions in IDR were judged to be negligible. An investigation was conducted to determine the optimal amount of damping with regards to expected economic losses following ultimate limit state (ULS) and serviceability limit state (SLS) earthquakes.

Each of the five original buildings are included in the study: 4S, the eight-storey standard design (8S), 16S, the four-storey drift design (4D), and the eight-storey drift design (8D). Repair costs are determined for a range of total damping using the performance assessment methods introduced in Chapter 3. The maximum damping ratio considered in the investigation is 45%, beyond the maximum level of 35% considered achievable by Christopoulos and Filiatrault (2006). The damping ratio was increased by 5% for each iteration, covering the range of 5% to 45% total damping in the first mode. FVD damping coefficients were calculated according to the generalised modal method and time history analyses were conducted.

5.5.1 Engineering Demand Parameters

The effect of the amount of damping on the seismic response of a building can be observed by comparing the time history analysis results of the FVD designs. Damper coefficients calculated for each building and each level of damping using the generalised modal method are provided in Table 5.7.

Table 5.7: Damper coefficients considering non-classical damping

Damping	c_j **(N s/mm)**				
	4S	**8S**	**16S**	**4D**	**8D**
10%	1,420	2,350	2,250	2,020	2,855
15%	2,630	4,320	4,220	3,780	5,370
20%	3,870	6,350	6,190	5,570	7,920
25%	5,140	8,450	8,170	7,410	10,570
30%	6,450	10,680	10,170	9,340	13,420
35%	7,885	13,250	12,220	11,410	16,750
40%	9,450	16,450	14,430	13,720	21,430
45%	11,300	20,800	17,070	16,350	28,780

Time history analyses were performed using the retrofitted building models and the ground motion suites previously compiled in Section 3.5. The mean of the peak absolute floor accelerations and IDRs per building level are shown in Figure 5.5 and 5.6 for the standard and drift buildings, respectively. The peak absolute velocity results are omitted. Although the dampers influence relative velocities, the relative values are small compared to the ground velocity and the impact on absolute velocities is modest.

The standard structures exhibit drift concentrations in a single storey during the ULS. This undesirable behaviour occurs in the first storey of 4S and 8S, and in storey 13 of 16S. In comparison, the FVD retrofitted standard buildings exhibit an even distribution of drift demand at each storey. A reduced likelihood of soft-storey formation during ULS is demonstrated even for 10% supplement damping. This is a major improvement in seismic performance provided by the use of FVDs.

Both drifts and accelerations are significantly reduced by the introduction of supplemental damping. It can be observed that interstorey drifts are more sensitive than accelerations to the level of damping. The peak IDRs continue to decrease as the damping

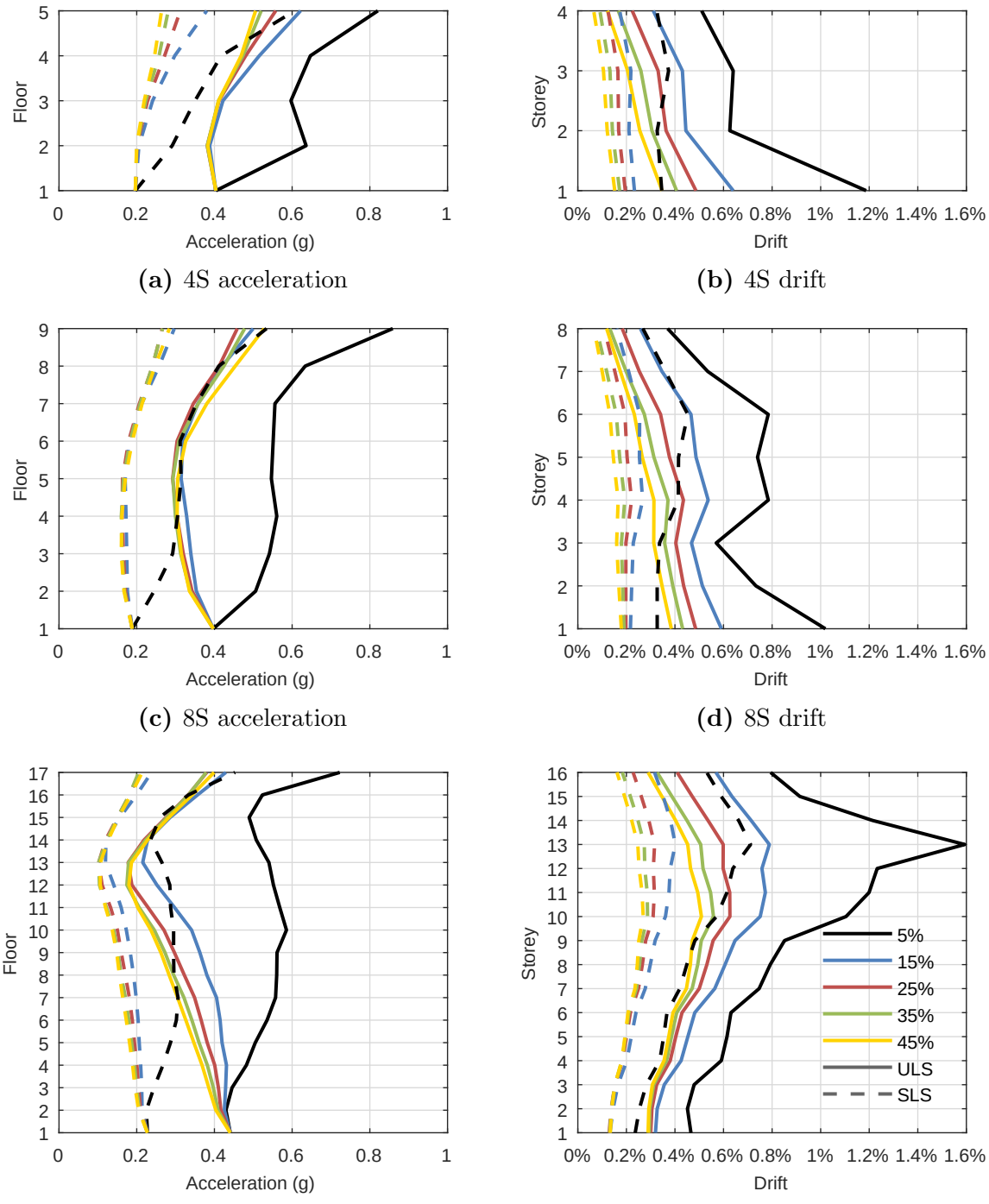

(a) 4S acceleration **(b)** 4S drift

(c) 8S acceleration **(d)** 8S drift

(e) 16S acceleration **(f)** 16S drift

Figure 5.5: Comparison of the mean peak engineering demand parameters (EDPs) considering several levels of damping for the standard buildings

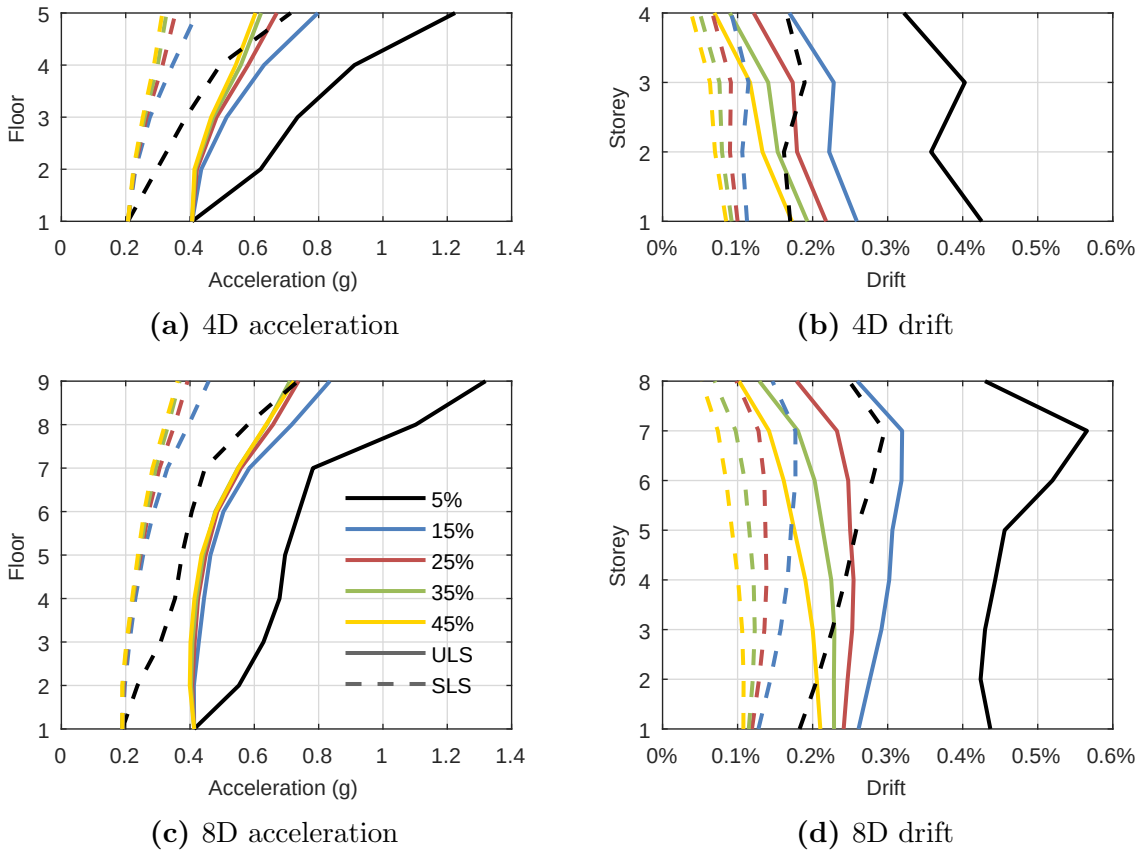

(a) 4D acceleration **(b)** 4D drift

(c) 8D acceleration **(d)** 8D drift

Figure 5.6: Comparison of the mean peak EDPs considering several levels of damping for the drift buildings

is increased. The peak accelerations of all buildings retrofitted with FVDs are generally similar irrespective of the amount of supplemental damping. However, the drift designs and structures 4S and 16S show minor decreases in the acceleration between 15% and 25% damping.

The IDRs noticeably reduce as supplemental damping is increased, however the drift reductions due to each subsequent 10% increase in damping have diminishing returns. This suggests that there is a limit at which further increases to supplement damping will no longer produce meaningful improvements.

5.5.2 Nonlinear Structural Response

The nonlinear behaviour of the structures retrofitted with FVDs was compared to the undamped benchmark results from Section 4.2.4. The standard designs were the subjects of focus, as the drift designs did not exhibit significant nonlinear structural behaviour.

5.5.2.1 Brace Behaviour

The nonlinear brace response of interest is classified as buckling or yielding (previously defined in Section 4.2.4). The percentages of all braces that yield or buckle are shown in Table 5.8 for the FVD retrofitted buildings. The results for the benchmark buildings with 5% Rayleigh damping are also reproduced for comparison. The SLS and drift designs are excluded, as reduced yielding and buckling occurred in both cases with 5% supplemental damping.

Table 5.8: Average ULS brace buckling and yielding for the FVD retrofitted standard designs

Damping	**4S**		**8S**		**16S**	
	Buckle	**Yield**	**Buckle**	**Yield**	**Buckle**	**Yield**
5%	74%	41%	56%	29%	79%	17%
10%	44%	18%	36%	11%	54%	4%
15%	26%	13%	22%	6%	33%	1%
20%	18%	8%	14%	4%	24%	0%
25%	15%	5%	13%	2%	20%	0%
30%	10%	4%	9%	2%	17%	0%
35%	7%	3%	7%	1%	15%	0%
40%	5%	2%	5%	1%	14%	0%
45%	5%	1%	4%	1%	13%	0%

A significant number of braces yield and buckle during the ULS analyses of the standard buildings. This structural damage would require costly and lengthy repairs. As expected, the addition of supplemental damping from FVDs decreases the amount of nonlinear brace behaviour. The energy introduced into the system by the earthquake can be dissipated by the FVDs, rather than only by the hysteretic behaviour of the concentric braced frames (CBFs) and Rayleigh damping. The FVD retrofitted designs successfully reduce brace damage even at low-to-moderate levels of damping. This suggests that structural damage would be minimised in the damped buildings following a ULS earthquake.

A visualisation of the mean brace nonlinear behaviour per storey is provided in Figure 5.7. Both the original and retrofitted standard building designs are included. The brace results for the FVD retrofitted buildings are shown for the lowest level of damping that

reduced the maximum concentration of drifts in a single storey to below 50%. Yielding results are excluded, as buckling governed the nonlinear behaviour of the braces.

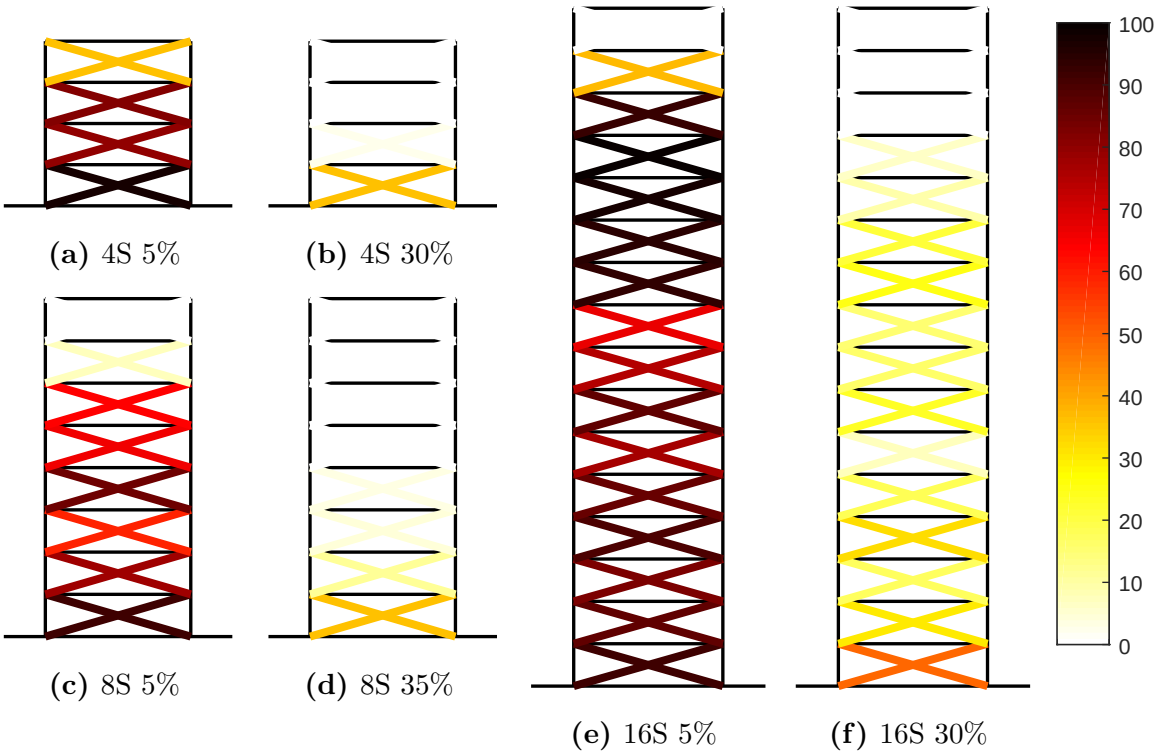

Figure 5.7: Percentage of ULS brace buckling per storey, original and FVD retrofitted standard buildings

For the original buildings, the majority of nonlinear brace behaviour relates to the concentration of interstorey drifts observed in the time history analysis results (4S – storey one, 8S – storeys one and four, 16S – storey 13). As the braces in a storey yield and buckle, the lateral stiffness of the storey will decrease. This will result in larger displacements. The use of FVDs prevents the concentration of brace damage from exceeding 50% in a single storey at levels of total damping between 30-35%. This is a desirable performance improvement, as the susceptibility to soft-storey formation is reduced with respect to the undamped buildings.

The nonlinear behaviour of braces will also have a significant effect on the behaviour of column members. The column forces due to braces, as well as FVDs, must be considered.

5.5.2.2 Column Behaviour

Retrofitting structures with FVDs can lead to column capacity problems. Several studies have shown that the addition of FVDs to a structure can significantly increase column axial forces (Uriz and Whittaker 2001; Martinez-Rodrigo and Romero 2003). If the maximum axial load in a column is increased, it must be accounted for in the retrofit design. This may require column or foundation strengthening.

The columns of the retrofitted structures were examined at each time-step of the time history analyses against failure using the design provisions of Eurocode 3 as described in Section 3.3. The time history analysis results of the FVD retrofitted buildings determined that column capacity failure did not occur. In comparison, Section 4.2.4 found that column buckling capacity in axial loading-bending was exceeded for the standard buildings in a small number of ULS analyses. The use of linear rather than nonlinear FVDs results in peak damper forces that are out-of-phase with the peak internal seismic forces.

It should be noted that the horizontal placement of dampers was not explored. The specifications of the damping coefficient within a storey, both in terms of the number of dampers and bay selection, will greatly influence the column axial forces.

5.5.3 Damping Ratio-Repair Cost Relationship

It has been shown that the seismic performance of structural members is improved even for low levels of supplemental damping. In order to establish the optimal amount of damping, nonstructural systems must also be considered. Measuring seismic performance using repair costs can take into consideration both drift- and acceleration-sensitive systems.

Seismic performance assessments using the FEMA P-58 procedure (2012b) were conducted for the FVD retrofitted buildings. Direct repair costs in 2011 US dollars resulting from damage to building assets are calculated, while indirect costs due to building downtime are out of scope. For a description of the parameters used in the FEMA P-58 procedure, refer to Section 3.6.

The damping ratio-repair cost relationship was represented using the mean and 90th percentile repair costs. The repair costs for each level of total damping are normalised

by the repair costs of the buildings without supplemental damping (i.e. 5% inherent damping). The damping ratio-repair cost relationship is shown in Figure 5.8 for three damping models: Rayleigh damping, FVDs with coefficients from the energy method, and FVDs with coefficients from the generalised modal method. The optimal level of damping for each building and limit state is indicated in the figure. Optimal damping is defined as the lowest level of damping that produces a cost within 2.5% of the minimum repair cost. The margin of 2.5% was selected to reflect the uncertainty in the assessment procedure. It is generally assumed that there is a positive relationship between the amount of damping and damper costs. As a result, the lowest level of damping producing the near-minimum cost is the most desirable.

Several trends regarding the damping ratio-repair cost relationship can be identified from Figure 5.8 for all damping methods:

1. Repair costs decrease as the total damping is increased. Diminishing returns are observed.

2. The reduction in repair costs due to damping increases as the flexibility of the building is increased. For example, consider the ULS repair costs presented in Figure 5.8e. The repair cost of 16S reduces to 40% of the undamped cost, while the repair cost of 4D plateaus at 60% of the undamped cost.

3. The SLS costs experience greater reductions at lower levels of damping than the ULS costs.

The results using only Rayleigh damping are shown in Figure 5.8a and 5.8b. It is observed that repair costs generally decrease as damping increases without limit. Only one case does not agree with this finding: the SLS 4D results between 40% and 45% total damping. Optimal damping with regards to mean costs is approximately 40-45%, while the optimal 90th repair costs are between 35-45%.

The damping-repair cost relationship using the energy method to approximate the damping ratio is shown in Figure 5.8c and 5.8d. Greater reductions in repair costs occur at lower levels of damping in comparison to the Rayleigh damping results. Optimal damping

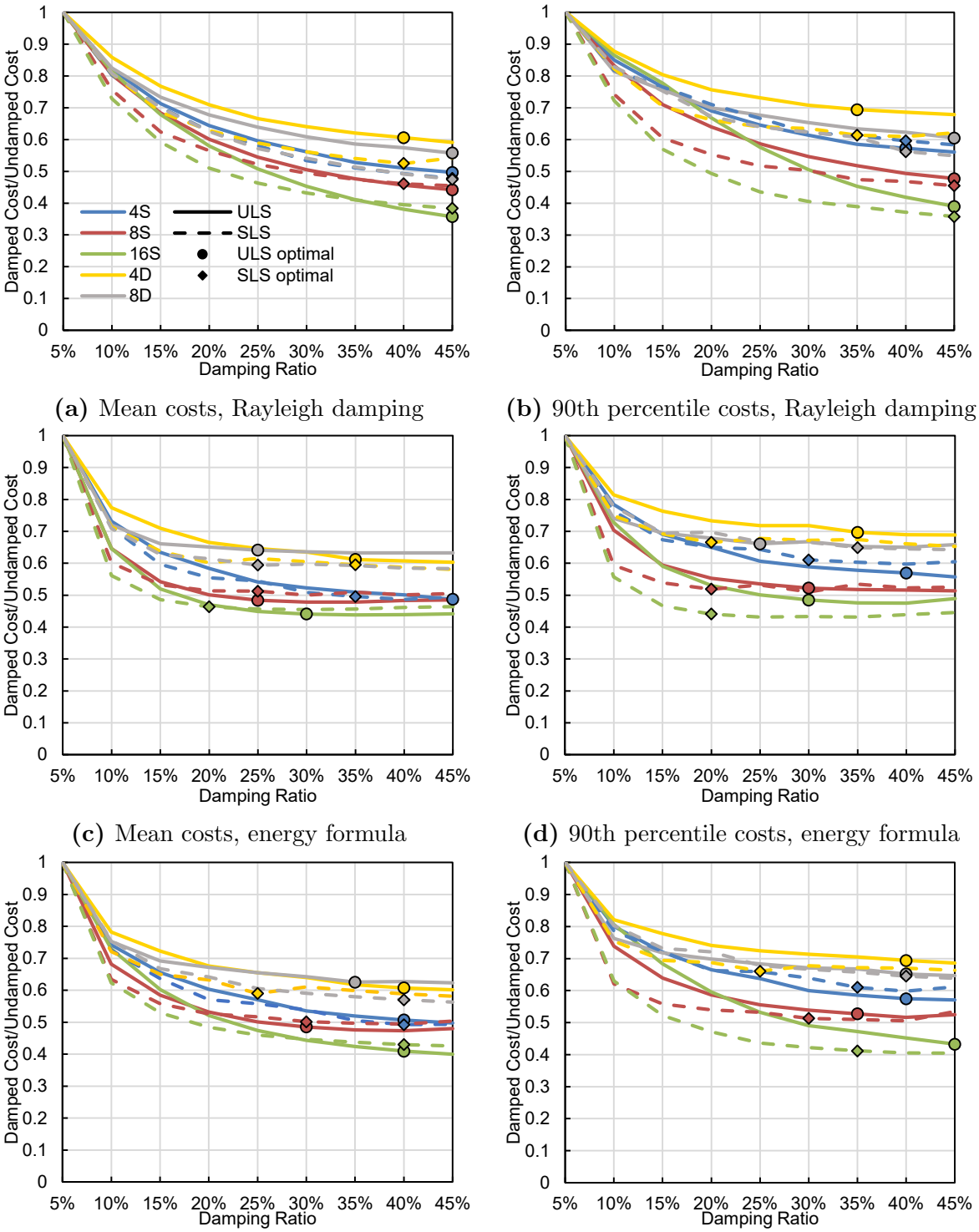

(a) Mean costs, Rayleigh damping

(b) 90th percentile costs, Rayleigh damping

(c) Mean costs, energy formula

(d) 90th percentile costs, energy formula

(e) Mean costs, non-classical damping

(f) 90th percentile costs, non-classical damping

Figure 5.8: Total damping ratio-repair cost relationship, with optimal damping values indicated

ranges from 20-45% for mean costs, and 20-40% for the 90th percentile costs. As the energy method is an approximation for the true damping ratio, the relationship may differ when considering the actual damping ratios achieved.

The damping-repair cost relationship considering non-classical damping when calculating the FVD coefficients is shown in Figure 5.8e and 5.8f. The minimum repair costs occur between 25-40% damping for the mean results, and between 25-45% for the 90th percentile results. The optimal damping level is greater than that from the energy method results. This can be attributed to the difference between the target damping of the energy formula and the actual damping achieved. The energy method results in values of damping that are higher than the target damping as previously shown in Table 5.4. This explains why the minimum costs are reached at "lower" levels of damping in the energy method results.

Retrofitting the standard buildings with FVDs can reduce repair costs to between 40% and 60% of the undamped repair costs. In comparison, the retrofitted drift designs reduce to between 57% and 70% of the undamped costs.

The optimal range of total damping is identified as 30-40% when considering only the standard designs and mean costs. This is in contrast to a previously suggested optimal damping of 20-25% based on EDPs (Occhiuzzi 2009). This highlights that retrofit methods may be improved by using repair costs, rather than structural parameters, when making decisions. However, it should be noted that the optimal amount of damping will be dependent on the building properties such as period of vibration and structural strength. The results presented in this section can serve as valuable guidance for selecting an initial damping target.

5.5.4 Repair Costs and Engineering Demand Parameters

In order to examine the damping ratio-repair cost relationship further, repair costs were disaggregated by EDP. The aim of this disaggregation is to identify the source of repair cost variations among different damping levels. The mean ULS and SLS repair costs sorted by EDP are displayed in Figure 5.9 and 5.10 for the standard and drift designs, respectively.

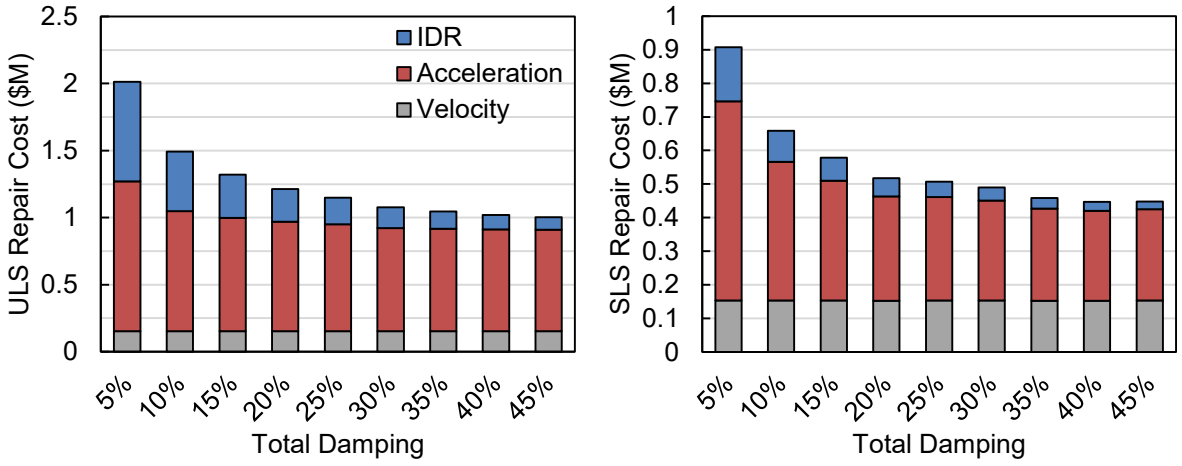

(a) 4S ULS **(b)** 4S SLS

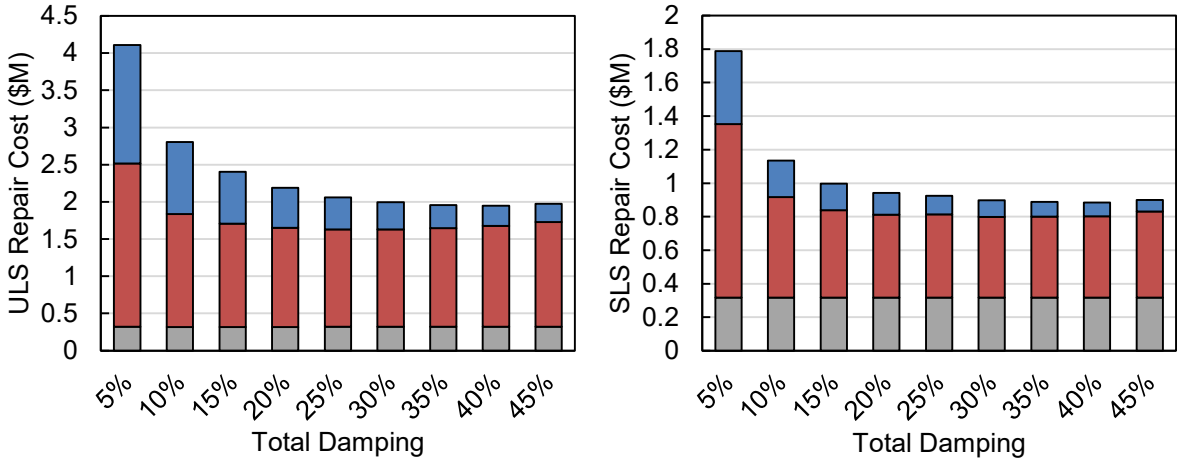

(c) 8S ULS **(d)** 8S SLS

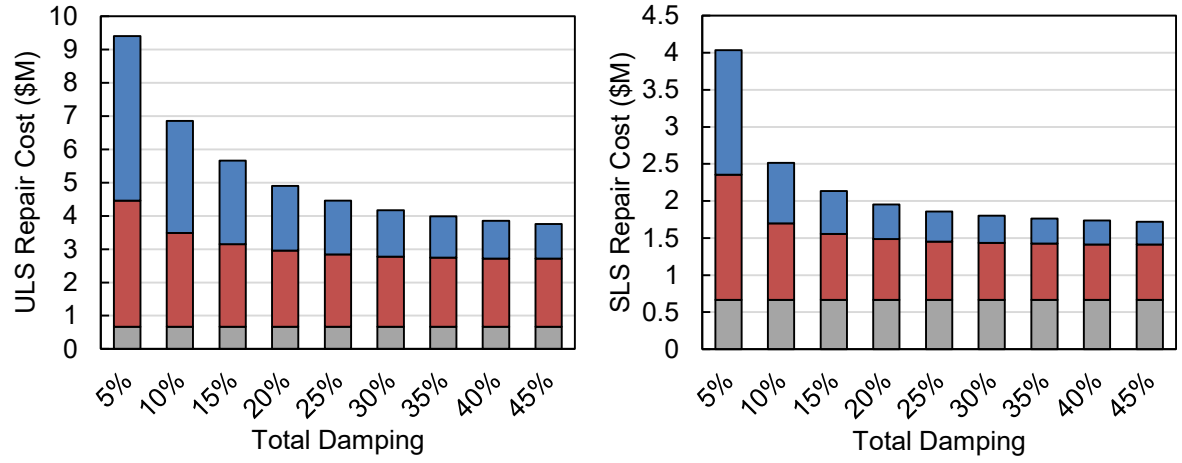

(e) 16S ULS **(f)** 16S SLS

Figure 5.9: Mean repair costs per engineering demand parameter of the FVD retrofitted standard buildings

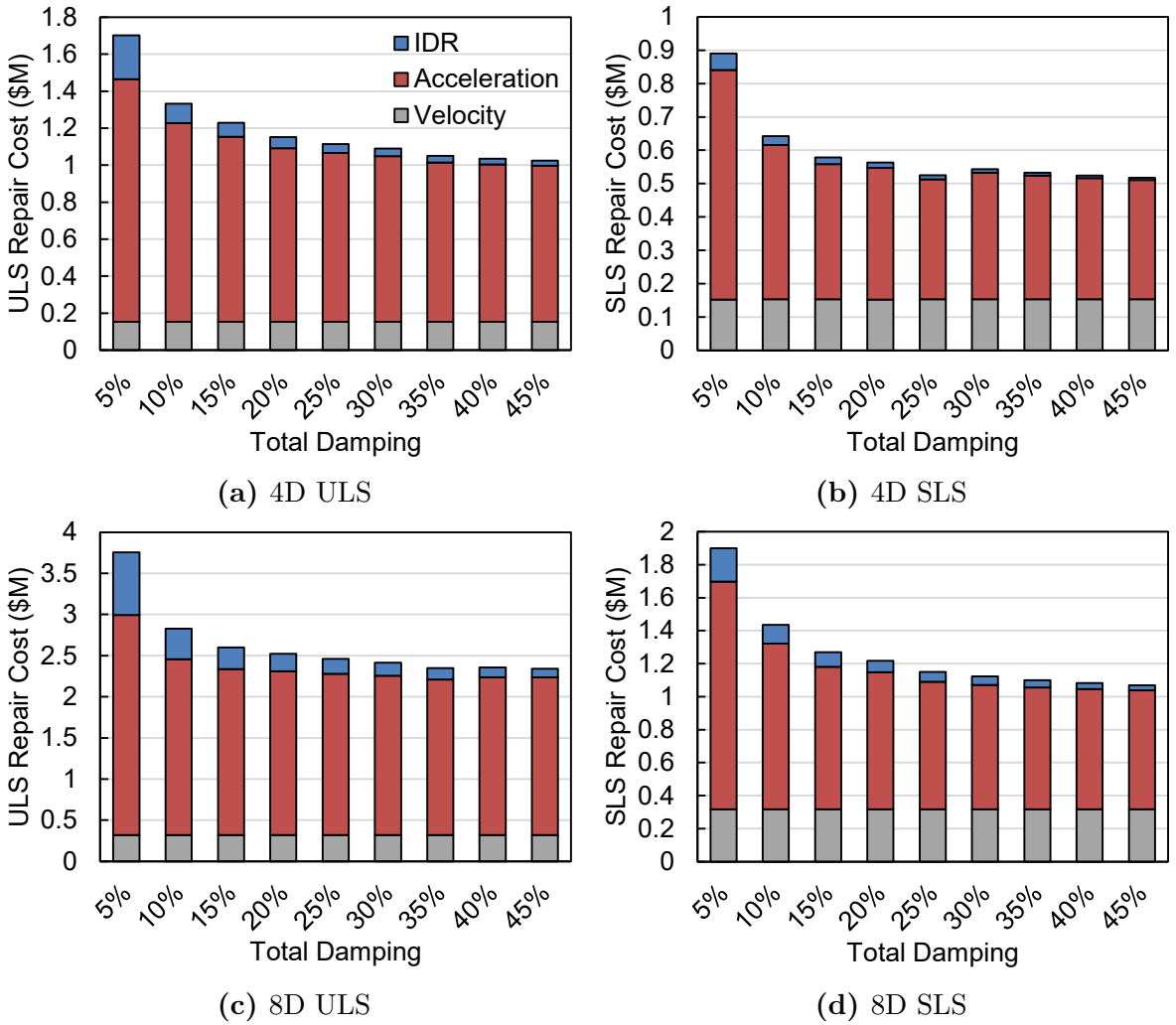

(a) 4D ULS **(b)** 4D SLS

(c) 8D ULS **(d)** 8D SLS

Figure 5.10: Mean repair costs per engineering demand parameter of the FVD retrofitted drift buildings

The incremental reduction in repair costs decreases as the damping is increased. There is a critical limit at which adding additional damping produces insignificant repair cost reductions, and therefore insignificant performance improvements. Other retrofit options such as equipment anchorage and isolation may be more effective at this limit.

Velocity damage is unchanged from the undamped results for all structures. It appears that FVDs cannot be used to reduce velocity-sensitive damage.

The ULS EDP results of the drift designs reveal a notable finding. The peak IDRs were shown to decrease as damping is increased in Figure 5.6. This observation is true even for larger amounts of damping, such as between 35% and 45% total damping. However, the IDR costs in Figure 5.10 exhibit minor-to-negligible reductions beyond 15% total damping. It appears that the drift designs achieve near-optimal IDRs for economic losses at low

levels of damping. Reducing IDRs past the near-optimal limit cannot further reduce costs, as drift-sensitive damage is already practically minimised. This demonstrates that repair costs should be evaluated in order to determine if the EDP reductions achieved by an alternative method of design have a meaningful impact on seismic performance. The near-optimal drift limit is estimated to be within the range of 0.15-0.25% based on the IDR values from Figure 5.6 that correspond to 25% damping.

5.5.4.1 Office Floor Fragility Functions

The observation of a near-optimal IDR limit prompted a further study on the relationship between IDR and drift-sensitive repair costs. All building assessments previously conducted were considered: the five conventional CBF buildings with total damping ranging from 5-45% at intervals of 5%. The mean FEMA P-58 repair costs of drift-sensitive fragility groups and the corresponding mean IDR were isolated for each storey. The performance assessment calculation tool (PACT) height factors, which reflect cost increases due to loss of repair works efficiency on upper levels, were removed to prevent the storey location from influencing the data points. One data point at 1.6% drift was excluded because it was an outlier in terms of IDR value. A simplified fragility function for an office storey was created, giving the IDR-repair cost relationship for all drift-sensitive systems. The relationship is displayed in Figure 5.11, with repair costs normalised by the floor area.

Figure 5.11 reveals that the drift-sensitive repair costs of an office storey will reach near-minimum values at approximately 0.2% drift. As previously discussed, reducing IDRs beyond this level will result in minimal seismic performance improvements.

Figure 5.11 also displays a trend-line function for the IDR-repair cost relationship, where x is the IDR value expressed as a percentage and y is the storey repair cost in $\$/m^2$. This simplified fragility function can be used to estimate drift-sensitive economic losses of an office storey. A limit of $x > 0.2\%$ is recommended. The formula could be used as an objective function for a damper placement method that aims to optimise seismic repair costs. However, this formula is limited to CBF buildings.

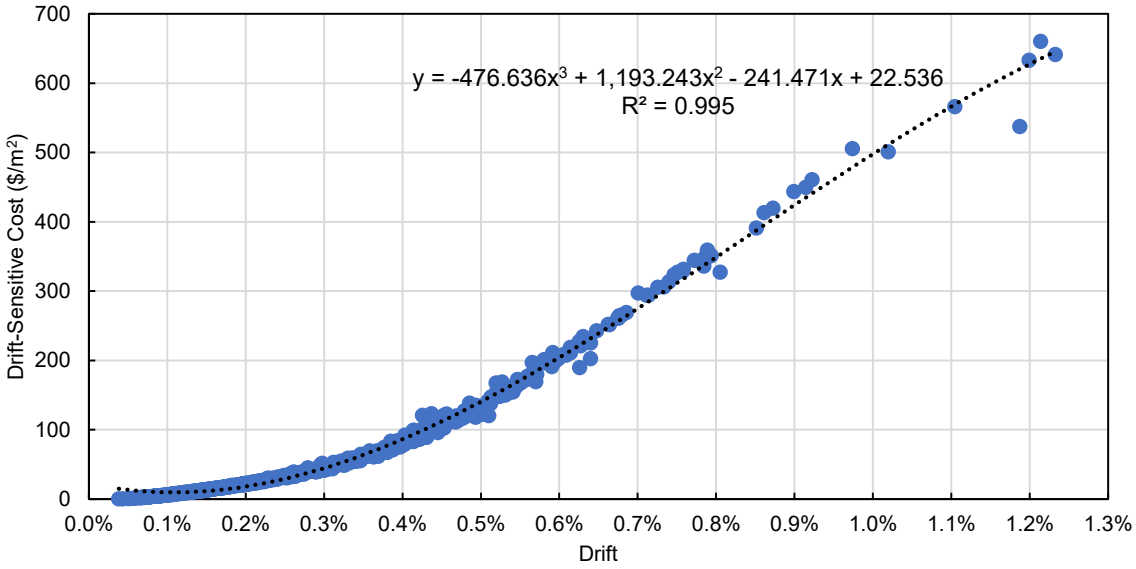

Figure 5.11: Simplified FEMA P-58 fragility function for an office storey, IDR-repair cost relationship for all drift-sensitive systems

The acceleration-repair cost relationship was also determined in the same manner. Figure 5.12 displays the relationship along with a trend-line function, where x is the peak absolute floor acceleration value expressed as in units of gravity and y is the storey repair cost in \$/m^2. A limit of $x > 0.115g$ is recommended. This simplified fragility function can be used to estimate acceleration-sensitive economic losses of an office storey. The formula could be used as an objective function for a damper placement method that aims to optimise seismic repair costs. However, this formula is limited to office floors. Roof repair costs can be considered negligible, while the formula is not valid for the ground level if additional acceleration-sensitive components such as HVAC systems are present.

5.6 Conclusions

Despite having the potential to be effective and economically viable solutions, research focusing on FVD applications for nonstructural enhancement has been limited. Previous research on the use of FVDs has focused on structural performance or EDPs. Repair costs are often not considered.

The supplemental damping ratio calculated by the energy method is an approximation. A comparison of the target damping ratio from the energy method and the actual damping ratio achieved was conducted. General modal analysis considering complex-valued modes

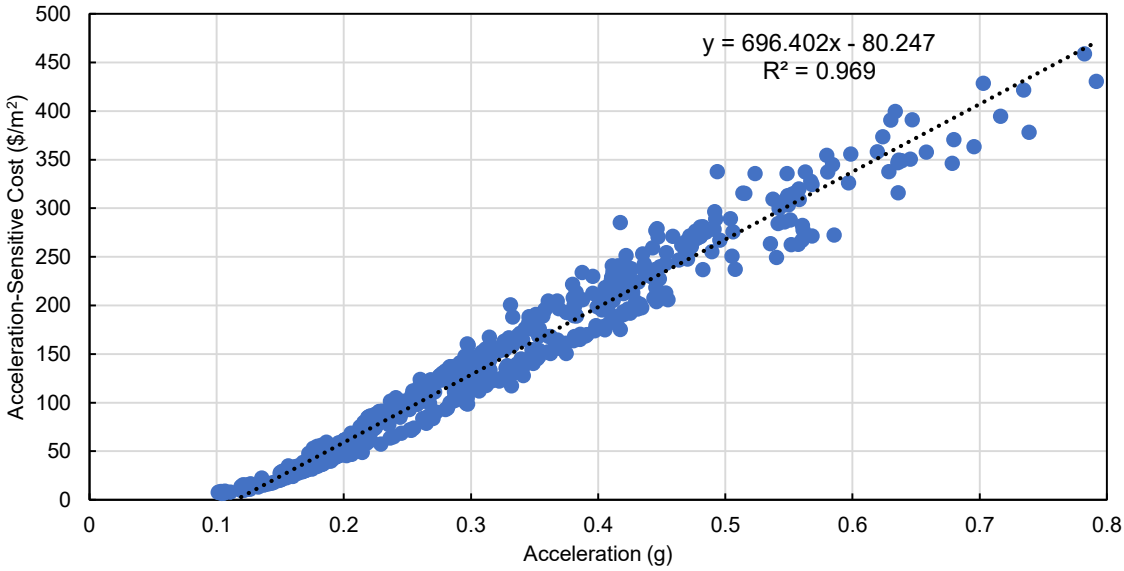

Figure 5.12: Simplified FEMA P-58 fragility function for an office floor, acceleration-repair cost relationship for all acceleration-sensitive systems

was performed to determine the damping ratios. It was found that the energy formula underestimated the achieved damping for uniform damping and linear FVDs.

The energy method formula was modified to improve the accuracy of the calculations by incorporating the modal mass participation factor. The improved energy formula can be used to rapidly select the linear damper coefficients for a desired level of total damping. The mean absolute relative error between the target and achieved damping ratio was reduced by the modified method in comparison to the original energy method. In particular, a substantial improvement was realised for the eight- and 16-storey structures. This suggests that the modified energy formula is an improvement on the original formula and should be considered in future studies.

Damping was included in the structures using Rayleigh damping and FVDs uniformly-distributed throughout the building height. Seismic performance assessments were conducted for total damping levels ranging from 5% to 45% in the first mode. The FVD retrofitted designs successfully reduce brace damage during the ULS even at low levels of damping.

Both IDRs and accelerations are significantly reduced by the use of FVDs. It is observed that IDRs continue to decrease as the damping increases, while accelerations are similar irrespective of the amount of supplemental damping. Identifying an optimal

amount of damping for both IDR and floor accelerations proved to be inconclusive. As a result, expected earthquake damage were examined in order to quantify the effects of increased damping in a conclusive manner.

The damping ratio-repair cost relationship was represented using the mean and 90th percentile repair costs. It was found that repair costs decrease as the total damping is increased, however, diminishing returns are observed. This suggests that there is a critical limit at which adding additional damping produces insignificant repair cost reductions, and therefore insignificant seismic performance improvements. Other retrofit options such as equipment anchorage and isolation may be more effective at this limit.

Considering the Eurocode-compliant standard CBF designs, the optimal range of damping to minimise mean economic losses is between 30-40%. The study was restricted to linear FVDs and uniform damper placement. The identified optimal range is in contrast to a previously suggested optimal damping of 20-25% based on EDPs (Occhiuzzi 2009). While practical considerations may sometimes prevent implementation of the highest levels of damping considered here, this highlights that retrofit decisions may be enhanced by using repair costs rather than structural parameters. The study on the damping-repair cost relationship provides insight when selecting levels of damping for structural design and retrofit.

The repair costs sorted by EDP were investigated. Velocity damage is unchanged from the undamped results, suggesting that FVDs cannot be used to significantly reduce velocity-sensitive damage. It was also revealed that there is a distinction between EDP reductions and meaningful seismic performance improvements. It was found that the drift designs achieve near-optimal IDRs at low levels of damping. Reducing IDRs past the near-optimal limit, estimated to be approximately 0.2%, cannot further reduce drift-sensitive economic losses.

Chapter 6

Improving Seismic Performance: Damper Retrofit or Drift Design?

6.1 Overview of Chapter

Evaluating the seismic performance of multi-storey buildings in Chapter 4 revealed that Eurocode-compliant structures are likely to experience extensive damage during both ultimate limit state (ULS) and serviceability limit state (SLS) earthquakes. The drift design structures were shown to have an improved ULS performance in comparison to the standard structures. It was also determined in Chapter 5 that retrofitting standard buildings with fluid viscous dampers (FVDs) can reduce repair costs to between 40% and 60% of the undamped building repair costs. Designing buildings to reach the advanced drift criteria and retrofitting buildings with FVDs are two methods with the same aim: to improve the seismic performance of standard buildings. This chapter investigates and compares the resulting performance of both methods.

The standard buildings were designed to reach a SLS interstorey drift ratio (IDR) limit of 0.5% and a ULS IDR limit of 1.0%. The drift design buildings were created by targeting a reduced ULS IDR limit of 0.5% (refer to Section 3.3 for building design). In this chapter, the standard designs are retrofitted with FVDs to reach the IDR performance of the drift designs. The required level of damping and corresponding damper coefficients are determined in Section 6.2. Section 6.3 examines the engineering demand parameter (EDP) results from the time history analyses, as well as the damper forces produced during the analyses. Sources of energy dissipation within the structural models are investigated

in Section 6.4. Section 6.5 examines the required investment in dampers. FEMA P-58 seismic performance assessments (FEMA 2012b) of the buildings are conducted in Section 6.6 to evaluate expected earthquake damage. Conclusions for this chapter are presented in Section 6.7.

6.2 Required Damping

The amount of supplemental damping required for the standard designs to attain the ULS IDR performance of the drift designs was determined. Although the 16-storey structure was unable to be designed feasibly following the drift design requirements, it was found that the advanced IDR performance level can be met using FVDs. The damping correction factor (η) required to realise the performance improvement was calculated using Eq. 5.1 and found to be $0.5\%/1\% = 0.5$. The level of supplemental damping corresponding to $\eta = 0.5$ was determined to be 35% using the Eurocode 8 (CEN 2013) method and 37% using the ASCE 7-10 (American Society of Civil Engineers 2013) method, as described in Section 5.2.1. Although both methods produce comparable levels of damping, the Eurocode 8 method is only valid for $\eta \geq 0.55$. As a result, a target overall damping ratio of 37% was selected in accordance with the ASCE method. This corresponds to a required supplemental damping of 32%, as 5% inherent damping is assumed.

Section 5.5 concluded that the optimal damping ratio is between 30-40%. The target of 37% total damping is therefore within the optimal range for the four-storey standard design (4S), eight-storey standard design (8S), and 16-storey standard design (16S) buildings. Elevation views of the standard designs with FVDs were previously show in Figure 5.2a.

In order to size and place the dampers, the desired supplemental damping was converted to viscous damping coefficients assuming uniform damper placement. The energy method from Whittaker *et al.* (2003), the modified energy formula developed in Section 5.4.2, and the general modal method considering complex-valued modes reviewed in Section 5.3.2 were used to calculate the damper coefficients at each storey j (c_j). Table 6.1 presents the resulting damper coefficients, along with the relative error (RE) with respect to the

general modal analysis calculated using

$$\text{RE} = \frac{c_{j,estimate} - c_{j,actual}}{c_{j,actual}} \times 100\%, \tag{6.1}$$

where $c_{j,actual}$ and $c_{j,estimate}$ are the actual and estimated damper coefficients, respectively.

Table 6.1: Damping coefficient per storey (c_j) required to produce 32% supplemental damping calculated using the energy, modified energy, and general modal analysis methods

Method	**c_j (N s/mm)**			**Relative Error**		
	4S	**8S**	**16S**	**4S**	**8S**	**16S**
Energy	10,019	19,420	23,578	18%	35%	80%
Modified Energy	8,086	14,565	15,373	-5%	1%	18%
General Modal	8,489	14,425	13,083	n/a	n/a	n/a

The modified energy method produces coefficients with a reduced error in comparison to the original energy method. The energy method results in significant error for the eight- and 16-storey structures in particular.

Damper coefficients calculated in accordance with the modified energy method were used in the following analysis unless noted. The drift designs were used as the benchmarks for the four- and eight-storey FVD retrofitted structures, while the 16S building was used as a benchmark for the 16-storey FVD retrofitted structure.

6.3 Time History Analyses

Time history analyses of the FVD retrofitted buildings were conducted using the ground motion suites compiled in Section 3.5. The OpenSees (McKenna 2017) models were created as detailed in Section 3.4 and Section 5.2.3. For the implementation of time history analysis in OpenSees, refer to Section 4.2.1.

6.3.1 Damped and Undamped Buildings

The EDPs of the standard designs retrofitted with FVDs (R) and the drift designs (D) are compared in Figure 6.1 for the four- and eight-storey structures. The mean peak results for all floors and storeys are displayed for the ULS and the SLS suites.

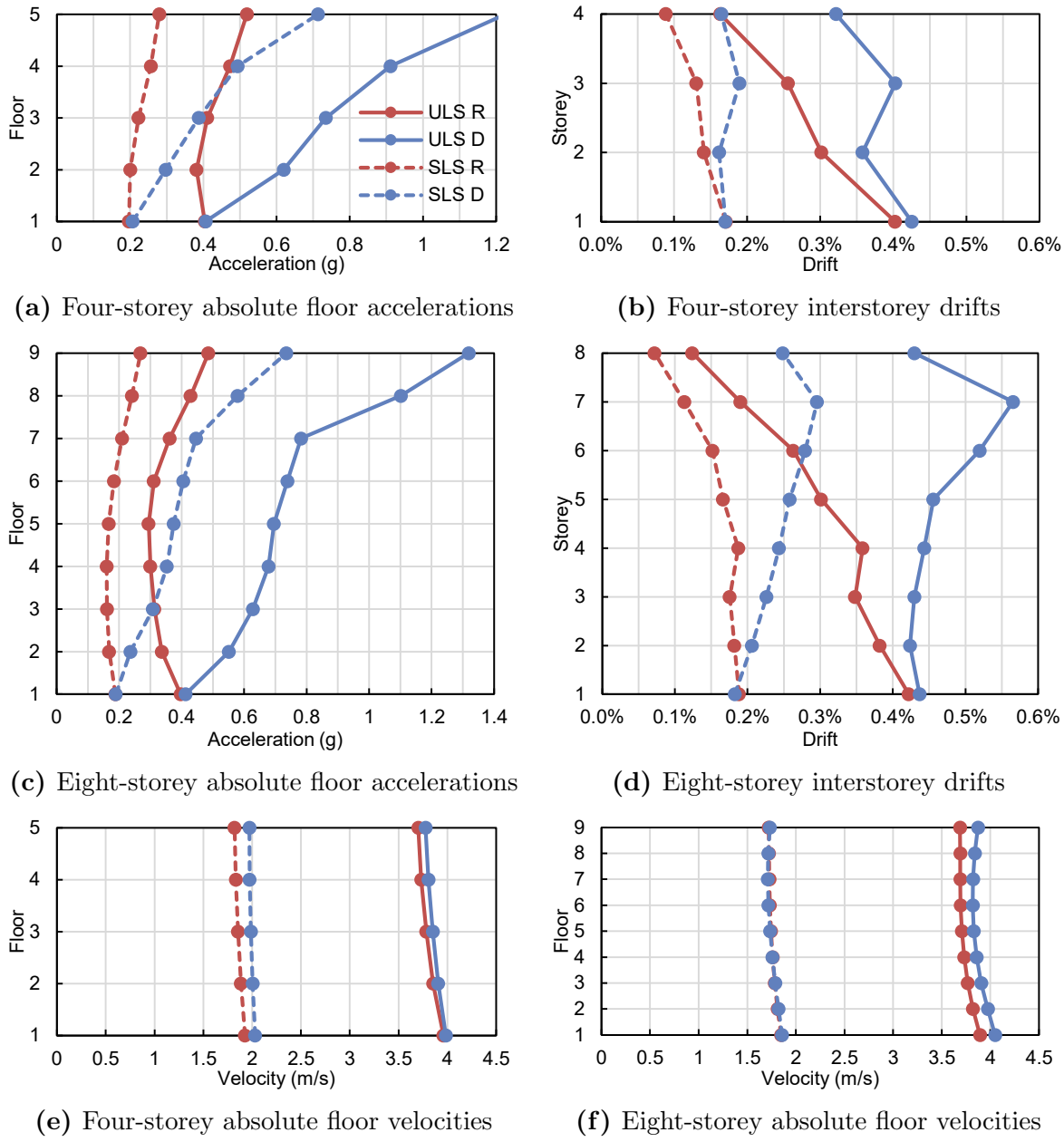

(a) Four-storey absolute floor accelerations

(b) Four-storey interstorey drifts

(c) Eight-storey absolute floor accelerations

(d) Eight-storey interstorey drifts

(e) Four-storey absolute floor velocities

(f) Eight-storey absolute floor velocities

Figure 6.1: Comparison of mean peak structural response parameters of the standard buildings with FVDs (R) and the drift designs (D)

The peak floor velocity values do not significantly vary between the FVD and drift designs. The velocity repair costs must be examined to determine if the minor velocity decreases achieved in the FVD buildings result in any seismic performance improvement.

Accelerations at the first floor remain unchanged between the two building sets. Ground acceleration is unaffected by the building design in analyses that do not consider ground-structure interaction. Another retrofit strategy must be incorporated to improve acceleration-sensitive performance at the ground level, such as equipment isolation.

Accelerations at all floors above the ground level exhibit significant reductions in the FVD retrofitted buildings. From floor three upwards, the FVD retrofitted buildings have ULS acceleration values that are comparable to the drift design SLS accelerations. The accelerations within the FVD buildings are also comparable at each floor. This is in contrast to the drift designs, which exhibit a concentration of maximum accelerations on the upper floors. Sensitive equipment would therefore not be limited to the lower floors in the FVD retrofitted buildings.

The interstorey drifts of the FVD retrofitted buildings show significant improvements with respect to the drift designs, excluding the first storey. The target ULS drift limit of 0.5% is achieved for both FVD structures. Several storeys of the FVD retrofitted structures experience ULS drifts equal to or less than the SLS drifts of the drift designs. The FVD retrofitted eight-storey building (8R) also does not exhibit the concentration of drift at the seventh storey experienced by the eight-storey drift design (8D). This desirable behaviour would prevent an uneven distribution of IDR demand, reducing the probability of a soft-storey mechanism.

The peak EDP results for the 16-storey standard design (S) and FVD retrofitted buildings are compared in Figure 6.2. The peak absolute floor accelerations are significantly improved by the FVD retrofit, excluding the ground floor as expected. The IDRs also are significantly improved. The ULS drifts of the retrofitted structure are comparable or improved with respect to the SLS drifts of the standard building. The target IDR limit of 0.5% during the ULS has been reached using FVDs. This IDR limit was unable to be met using the drift design approach. The drift concentration at storey 13 in the standard building is also prevented in the damped structure. However, the peak absolute floor velocities show little to no reductions.

6.3.2 Modified and Original Energy Methods

The modified energy method developed in Section 5.4.2 was used to calculate the FVD damper coefficients due to its improved accuracy compared to the original energy method. However, the original energy method from Whittaker *et al.* (2003) is frequently used. The

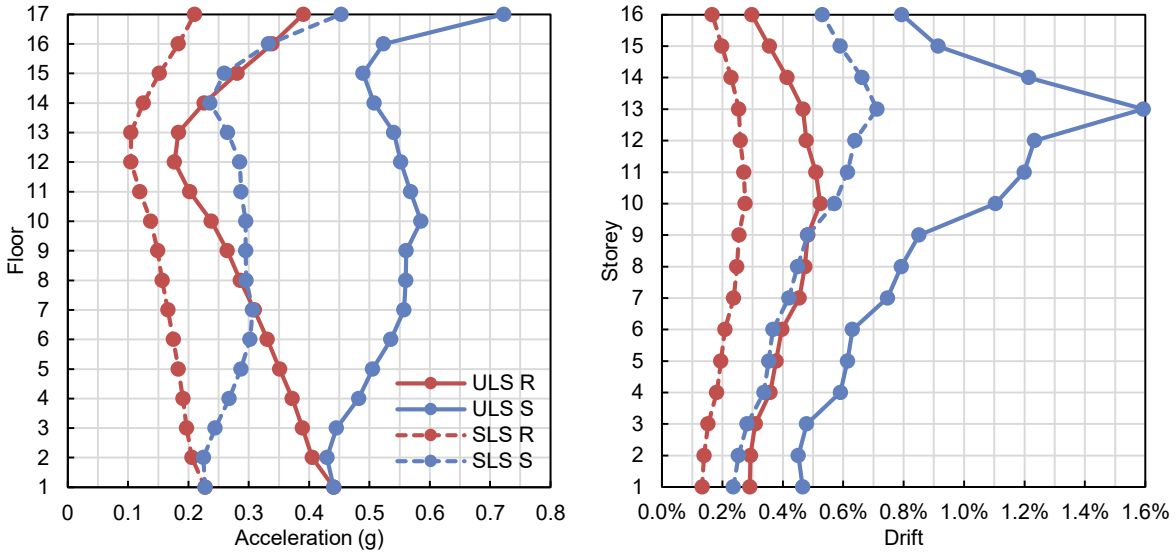

(a) Absolute floor accelerations

(b) Interstorey drifts

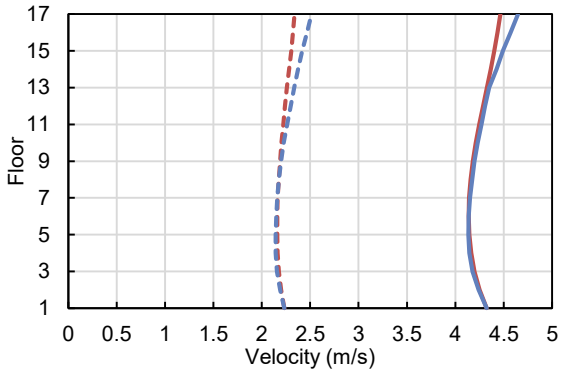

(c) Absolute floor velocities

Figure 6.2: Comparison of mean peak structural response parameters of building 16S with and without FVDs, referred to as R and S respectively

use of the original energy method may change the EDP results of the FVD retrofitted buildings. A second set of models were created to represent buildings retrofitted according to the original energy method. Figure 6.3 compares the mean of the peak absolute floor accelerations and IDRs per storey for both sets of models, where E refers to the buildings with damper coefficients calculated using the original energy method. The peak absolute floor velocities are omitted, as the mean values are not greatly influenced by the different sets of FVDs.

The energy method produces larger damping coefficients than the modified method. As a result, a greater amount of supplemental damping is introduced into the structure. Section 5.5.1 concluded that drifts decrease as damping is increased for large levels of

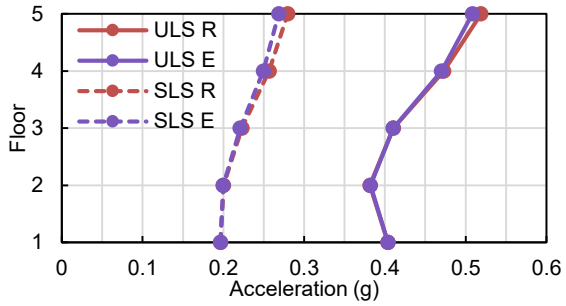

(a) Four-storey absolute floor accelerations

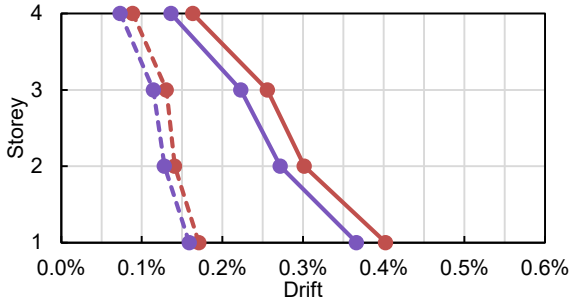

(b) Four-storey interstorey drifts

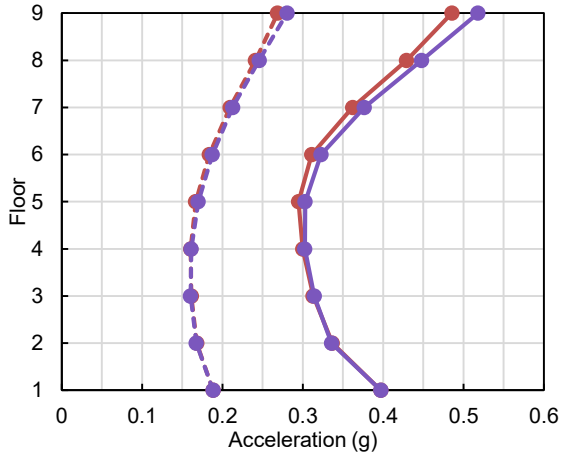

(c) Eight-storey absolute floor accelerations

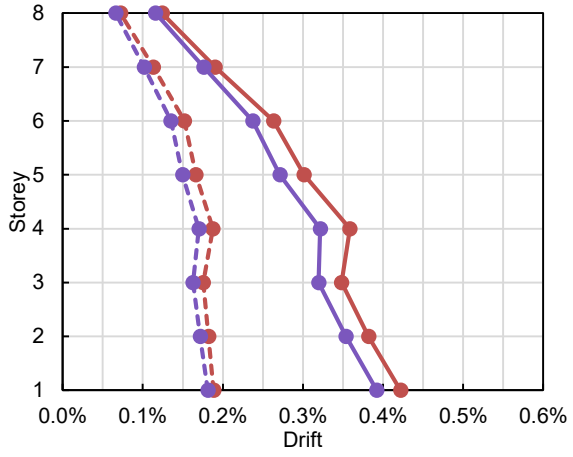

(d) Eight-storey interstorey drifts

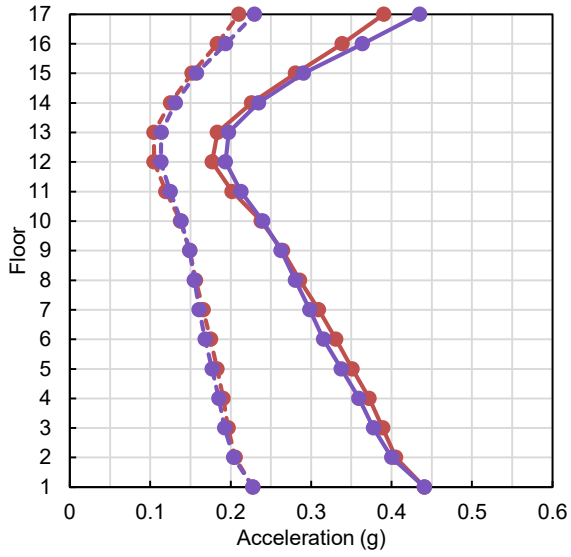

(e) 16-storey absolute floor accelerations

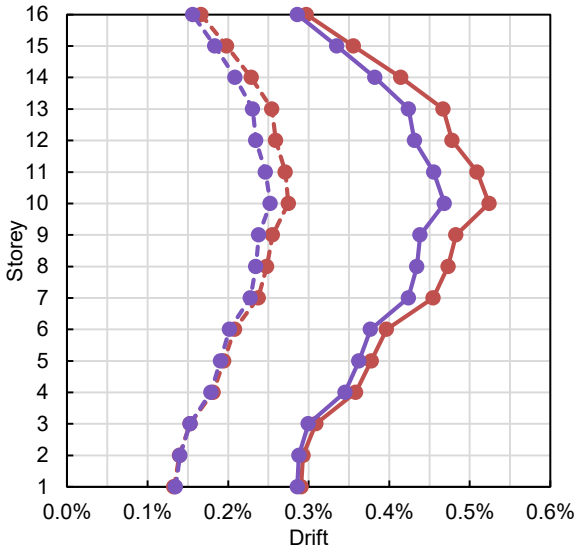

(f) 16-storey interstorey drifts

Figure 6.3: Comparison of mean peak absolute floor accelerations and interstorey drifts using the modified (R) and original (E) energy methods

damping; accelerations were found to remain similar. This finding agrees with the results of Figure 6.3. The drifts of the energy method structures are reduced in comparison to the modified method structures. The accelerations of the two sets of buildings do not vary significantly.

It can be assumed that the seismic performance of 4E will be equal to or more favourable than 4R, as drifts are improved and accelerations are approximately equal. However, the eight- and 16-storey buildings experience a trade-off between drifts and accelerations. Repair costs must be examined to determine which building set produces more favourable seismic performance.

The use of the modified or original energy method has been shown to influence EDPs. The different sets of damper coefficients will also influence the damper forces generated during an earthquake. These forces can affect the behaviour of structural elements.

6.3.3 Damper Forces

Damper forces were recorded during OpenSees analyses through the command *recorder Element* with the argument of *localForce*. Maximum damper forces are of interest, as this will govern effects on adjacent structural members and damper costs (Lavan and Avishur 2013; Gidaris and Taflanidis 2015; Landi *et al.* 2015). The maximum absolute force in each damper was determined for every ground motion analysis. The mean and maximum of these peak values per damper were identified. Figure 6.4 provides the resulting damper forces for both the modified and original energy methods.

The energy method produces larger damper forces than the modified method. This can be attributed to the larger damper coefficients of the original energy method. For both methods, damper forces near the base of the structures are several times larger than the forces near the roof level. This occurs despite the use of uniformly-distributed damper coefficients. Consistency between the distribution of maximum damper forces and damper coefficients over the building height can be used as a measure of damper placement efficiency when comparing alternative placement techniques (Hwang *et al.* 2013; Landi *et al.* 2015).

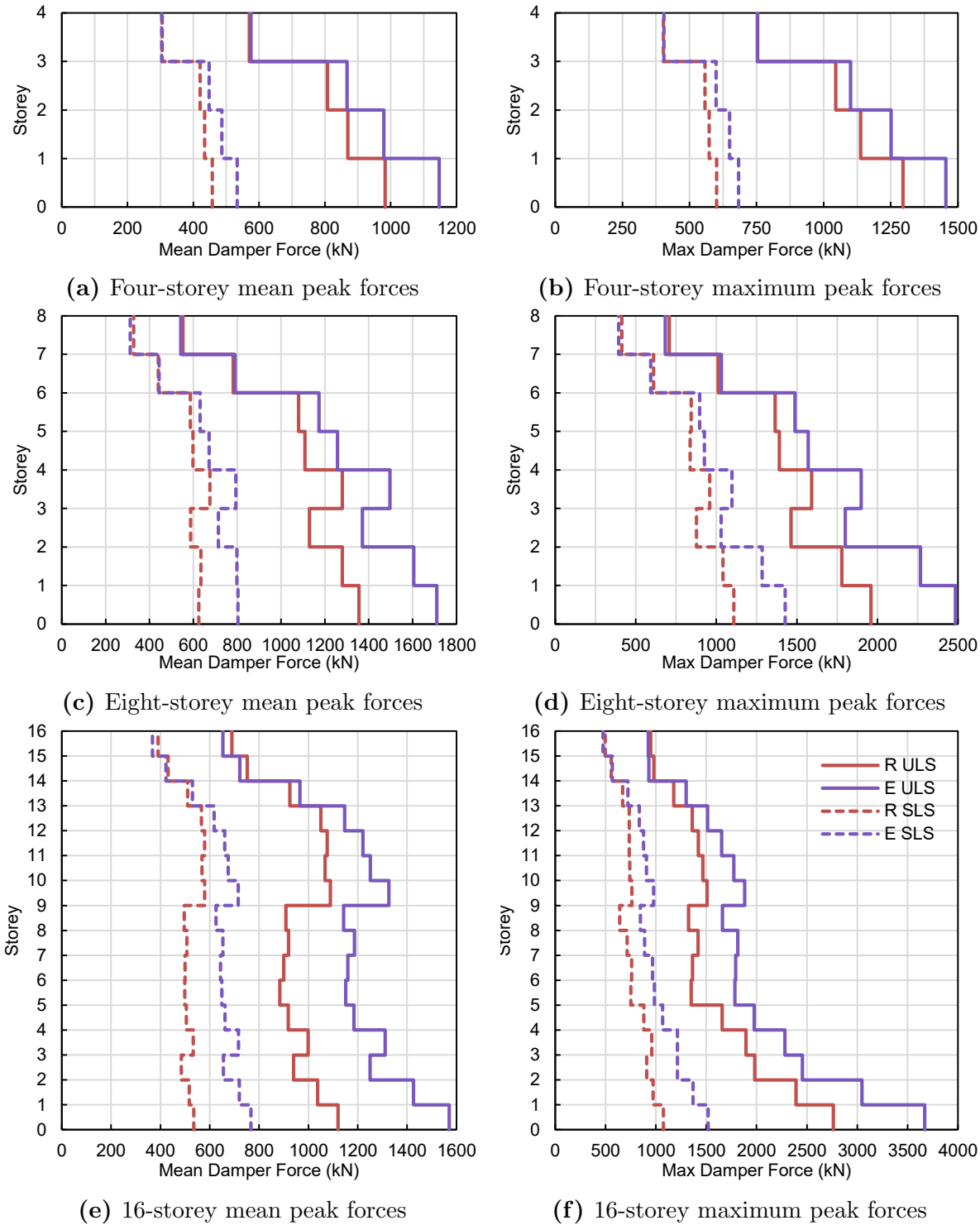

(a) Four-storey mean peak forces

(b) Four-storey maximum peak forces

(c) Eight-storey mean peak forces

(d) Eight-storey maximum peak forces

(e) 16-storey mean peak forces

(f) 16-storey maximum peak forces

Figure 6.4: Maximum and mean peak absolute damper forces per storey using the modified (R) and original (E) energy methods

The effect of damper forces on brace behaviour was investigated. Nonlinear brace behaviour did not occur during the SLS, while a minor amount occurred during the ULS. The small amount of brace buckling and yielding concurs with the results of Section 5.5.2.1, which determined that the use of FVDs would reduce brace damage even at low levels of damping. The percentage of all braces that yield or buckle during the ULS suite of time history analyses are shown in Table 6.2. In comparison, a significant number of braces yield and buckle during the ULS for the standard buildings (see Section 4.2.4). As supplemental damping is not provided in the standard buildings, the seismic energy must be dissipated through Rayleigh damping and the hysteretic behaviour of the braces. The use of FVDs would significantly reduce the need for structural repairs.

Table 6.2: Mean brace buckling and yielding for all ULS analyses of the FVD retrofitted buildings

Condition	**4R**	**8R**	**16R**
Yield	3%	2%	0%
Buckle	6%	6%	13%

The possible increase in column loading due to damper forces must be accounted for in the retrofit design. All column failure conditions were checked at each time-step of the time history analyses using Eurocode 3 (CEN 2010b) as described in Section 3.3. It was determined that column capacity failure did not occur. In comparison, column buckling capacity in axial loading-bending was exceeded in a small number of ULS analyses for the standard buildings (see Section 4.2.4).

6.4 Sources of Energy Dissipation

Examining the sources of energy dissipation in a structural model during a time history analysis can contribute to a greater understanding of the finite element model. Energy is introduced into the system due to the earthquake ground accelerations acting on the masses of the system. The model dissipates energy through the following means:

a. Energy dissipated by the hysteretic behaviour of brace members (W_B)

b. Energy dissipated by Rayleigh damping (W_R)

c. Energy dissipated by the FVDs (W_D)

To calculate the work done (W) by the forces of interest (F), and therefore the energy introduced or dissipated, the equation $W = \int F \cdot du = \int F\dot{u} \cdot dt$ was used. The work equations developed for the cases of interest are

$$\text{Dissipation} \begin{cases} W_D = \dfrac{1}{c_i} \displaystyle\int f_i^2 \cdot dt & (6.2) \\ W_R = \displaystyle\int f_R \cdot du & (6.3) \\ W_B = \displaystyle\int f_B \cdot de & (6.4) \end{cases}$$

$$\text{External work} \begin{cases} W_{eq} = -m \displaystyle\int \ddot{u}_g \cdot du, & (6.5) \end{cases}$$

where u refers to relative displacement, e refers to local brace elongation coordinates, $\ddot{u}_g$ refers to absolute ground acceleration and W_{eq} is the work done by the earthquake. The axial force in the braces (f_B) was readily available from the OpenSees models, while the Rayleigh damping forces (f_R) were recorded using the OpenSees command *recorder Node* with the argument *rayleighForces*.

The trapezoidal rule was used to perform the numerical integrations. The maximum absolute relative error (RE) between the energy input into the system through the earthquake (W_{ext}) and the energy dissipated (W_{dis}), calculated as $\text{RE} = \frac{W_{dis} - W_{ext}}{W_{ext}} \times 100\%$, was <1% for all structures. Figure 6.5 provides a sample of the cumulative integration for the FVD retrofitted four-storey structure undergoing a single ground motion. Table 6.3 provides the mean proportion of energy dissipation in all damped buildings.

Table 6.3: Mean proportions of energy dissipation considering all time history analyses

Building	**ULS**			**SLS**		
	FVDs	**Rayleigh**	**Braces**	**FVDs**	**Rayleigh**	**Braces**
Four-storey	84%	13%	3%	86%	14%	0%
Eight-storey	80%	17%	3%	83%	17%	0%
16-storey	79%	20%	1%	80%	20%	0%

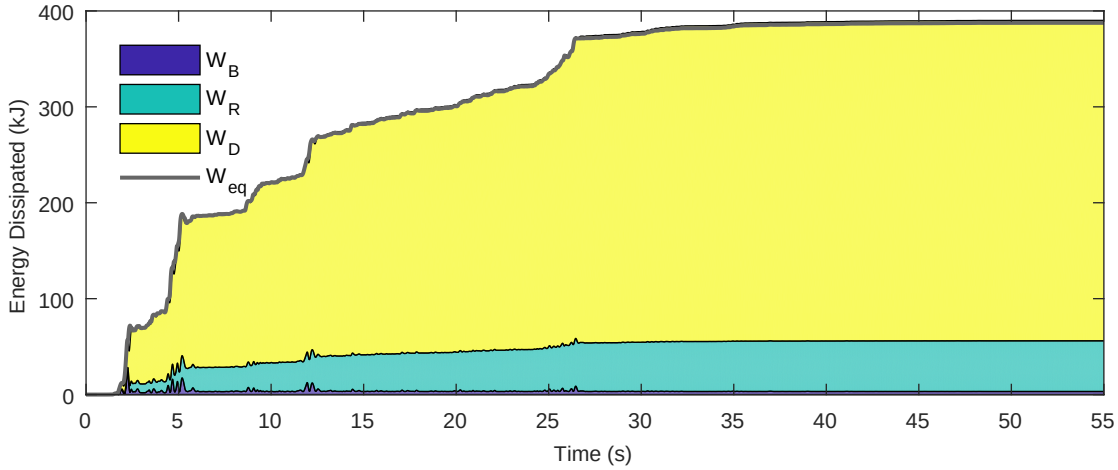

Figure 6.5: Cumulative energy dissipation over time for the damped four-storey structure, Imperial Valley-02 1940 with 1.34 scale

No energy dissipation is provided by the braces in the SLS, while a small amount of energy is dissipated by the braces during the ULS (<3%). These two results agree with the findings discussed in Section 6.3.3. Nonlinear structural behaviour was not observed in the damped buildings during the SLS, while a small proportion of the braces experienced nonlinear behaviour during the ULS.

The FVDs are responsible for the majority of energy dissipation, while the braces provide little to no dissipation. The FVD retrofits therefore successfully protect the brace members and minimise the amount of structural damage experienced. It has also been determined that Rayleigh damping provides significant energy dissipation even in the structures with FVDs. The application of Rayleigh damping should therefore be conducted with care.

With a target total damping of 37% in the first mode and 5% Rayleigh damping, the proportions of energy dissipation were expected to be approximately $100\% \times 32/37 = 86\%$ for the FVDs and 14% for Rayleigh damping. The calculated mean proportions of energy dissipation are comparable to the approximations.

It was previously found that damper forces near the base of the structures are several times larger than the forces near the roof level (Figure 6.4), despite the use of uniformly-distributed damper coefficients. The proportion of energy dissipated per FVD can be used as a measure of damper effectiveness. Figure 6.6 displays the mean percentage of

energy dissipation per storey (and therefore per FVD) for the FVD retrofitted standard structures.

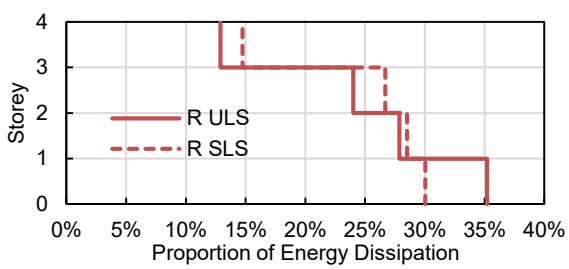

(a) 4R

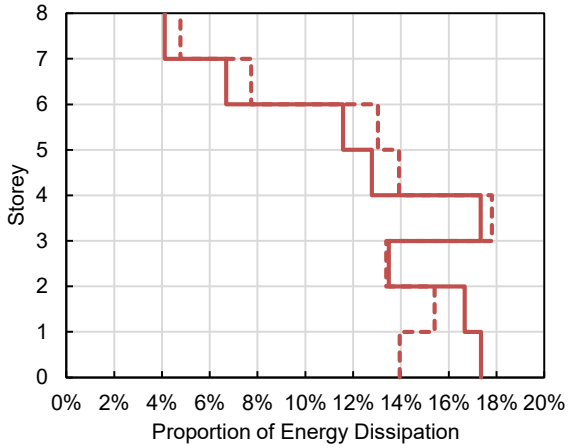

(b) 8R

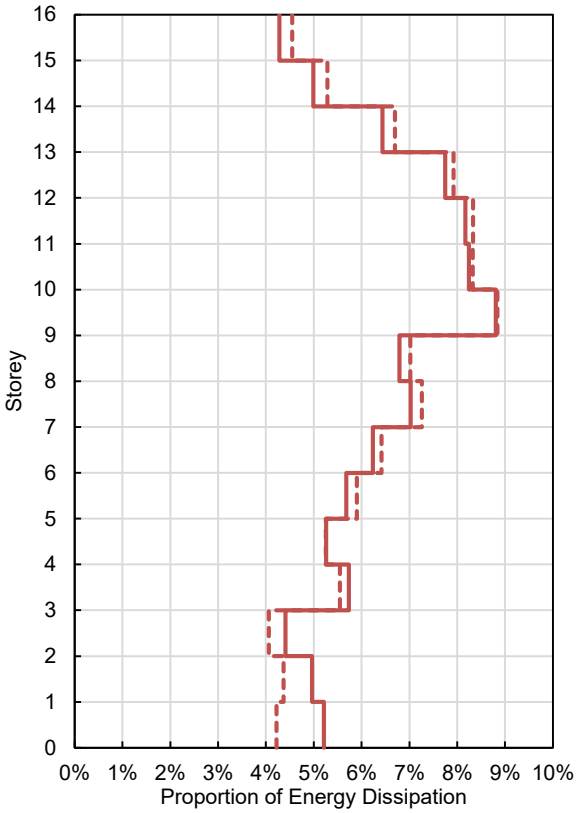

(c) 16R

Figure 6.6: Mean percentage of FVD energy dissipation per storey

The four- and eight-storey energy results display a similar pattern to the maximum damper forces. The majority of energy dissipation is contributed by FVDs located near the base of the structure. However, the 16-storey building does not follow this trend. The energy dissipation per storey is more evenly distributed throughout the building height. This result is influenced by the modal properties of the structures. The four- and eight-storey building responses are governed by the first mode, while the 16-storey building is subject to significant higher-mode responses.

6.5 Damper Costs

In addition to influencing energy dissipation, damper forces can also be related to the cost of a damper. The required damper investment should be considered when evaluating FVD

retrofit options. Gidaris and Taflanidis (2015) derived a cost equation for commercially available dampers. The equation is

$$\text{Cost}_i = 96.88(f_{max,i})^{0.607}, \tag{6.6}$$

where Cost_i is the cost of damper i in dollars and $f_{max,i}$ is the maximum force capacity of damper i in kN. It is recognised that this damper cost formula is an approximation and does not capture additional costs such as frame strengthening.

Total damper investment based on the maximum absolute ULS forces per FVD considering all time history analyses are shown in Table 6.4. The increase in structural cost due to the drift designs with respect to the standard designs, calculated in Section 4.3, are also reproduced for comparison.

Table 6.4: Comparison of the increases in building cost due to the FVD retrofit and the drift design approaches

Building	**FVD Retrofit**	**Drift Design**
Four-Storey	\$106,000	\$70,000
Eight-Storey	\$250,000	\$440,000

The FVD retrofits produce total building costs that are comparable to the use of drift designs. The total damper investment is less than 3% of the standard building cost for both the four- and eight-storey structures. Due to the relatively small increase in building investment, it is assumed that a risk-adverse client who is willing to improve seismic performance would consider these costs as negligible to minor. The increase in building value will be taken into account during the FEMA P-58 analyses of the FVD retrofitted structures.

The difference in damper investment resulting from the use of the modified and original energy methods was investigated. The required damper investment for both methods are provided in Table 6.5. As expected, the use of the original energy method produces a higher cost than the modified method. The cost savings due to the use of the modified method become more significant as the size of the structure increases (4%, 10%, and 12% difference in cost for the four-, eight- and 16-storey buildings, respectively).

Table 6.5: Comparison of damper investment using the modified and original energy methods

Building	Modified Method	Energy Method
Four-Storey	\$106,000	\$110,000
Eight-Storey	\$250,000	\$274,000
16-Storey	\$533,000	\$598,000

6.6 FEMA P-58 Results

Seismic performance assessments using the FEMA P-58 procedure (2012b) were conducted for the FVD retrofitted buildings. Direct repair costs in 2011 US dollars resulting from damage to building assets are calculated, while indirect costs due to building downtime are out of scope. Refer to Section 3.6 for a description of the FEMA P-58 procedure implemented in this thesis.

The performance of the undamped conventional buildings previously assessed in Section 4.4 serve as a benchmark on which to evaluate the performance of the FVD retrofitted structures. The seismic performance of the four- and eight-storey buildings with FVDs are assessed and contrasted with the results of the drift design structures in Section 6.6.1. The performance of the FVD retrofitted 16-storey structure is considered in Section 6.6.2 and the results are examined in relation to the undamped standard structure.

6.6.1 Damper Retrofit and Drift Design

6.6.1.1 Total Repair Costs

Cumulative distribution functions of the ULS and the SLS total repair costs normalised by the respective building cost are shown in Figure 6.7 for the four- and eight-storey buildings. The standard (S), drift (D), and FVD retrofitted (R) structures are included. The non-normalised cumulative distribution functions are shown in Figure 6.8 for the R and D sets.

It can be seen that the FVD retrofitted buildings significantly outperform the drift designs for both the ULS and the SLS. These results demonstrate that FVDs are a viable solution to improve the seismic resiliency of structures.

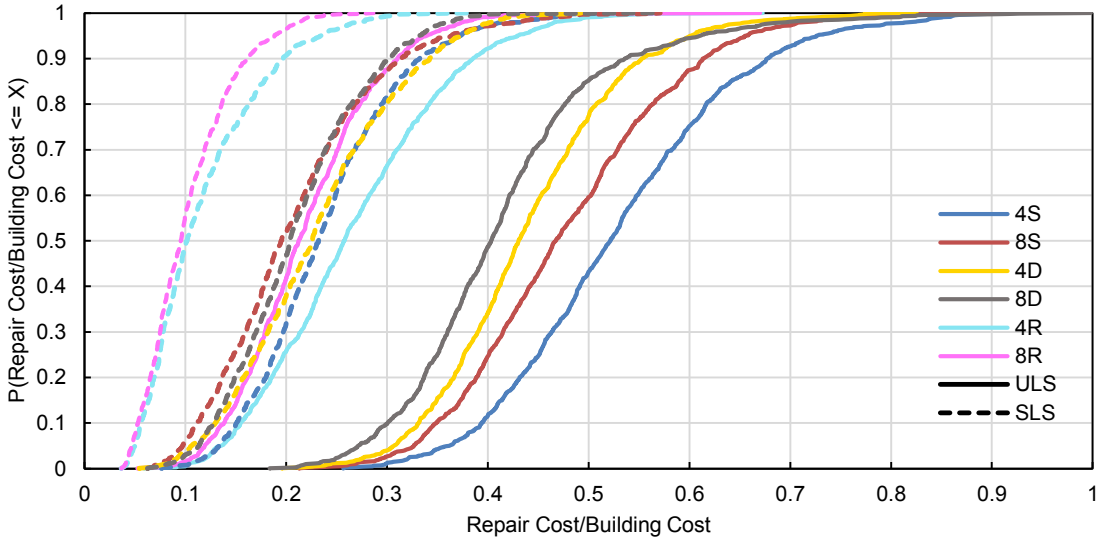

Figure 6.7: Cumulative distribution functions of total repair costs normalised by building value for the four- and eight-storey buildings. Standard (S), FVD retrofitted standard (R), and drift design (D) buildings

The ULS repair costs of the FVD retrofitted buildings are comparable to the SLS losses of the drift designs. Owners often elect to demolish and replace the existing building if repair costs exceed 40% of the building cost (FEMA 2012b). The median ULS repair costs of the drift designs exceed this guideline. In comparison, the median ULS repair costs of the FVD retrofitted buildings are well below the demolition threshold: 26% and 21% of the building values for 4R and 8R, respectively. The 90th percentile ULS repair costs of the R buildings are also below the demolition threshold. This represents a significant improvement in performance for the buildings with FVDs over the drift designs, as the need to demolish and replace the retrofitted buildings following a ULS earthquake is prevented in all but the most extreme cases.

The median SLS repair costs of the FVD retrofitted buildings are less than 10% of the building values. In comparison, the SLS median repair costs of the drift designs are greater than 20% of the building values. Building downtime is not determined in this project. However, it can be assumed that the significant reduction in total economic losses is closer towards achieving a level of damage that will minimise effects on building serviceability.

The damper coefficients of the R building set were calculated using the modified energy method. Another set of buildings, the E building set, was retrofitted with damper

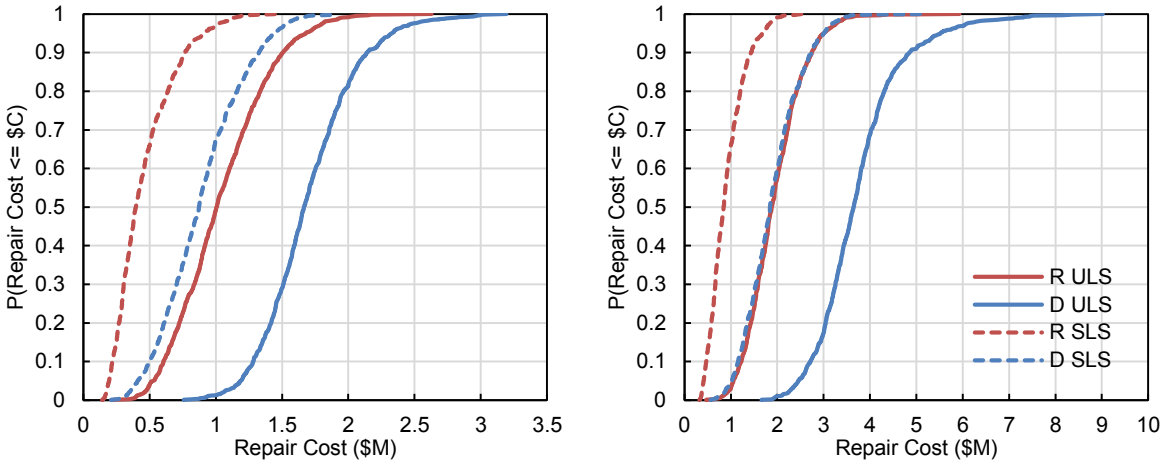

(a) Four-storey **(b)** Eight-storey

Figure 6.8: Comparison of the repair cost cumulative distributions for the FVD retrofitted standard buildings (R) and the drift design buildings (D)

coefficients calculated using the original energy method. The cumulative distribution functions of the R and E sets are compared in Figure 6.9.

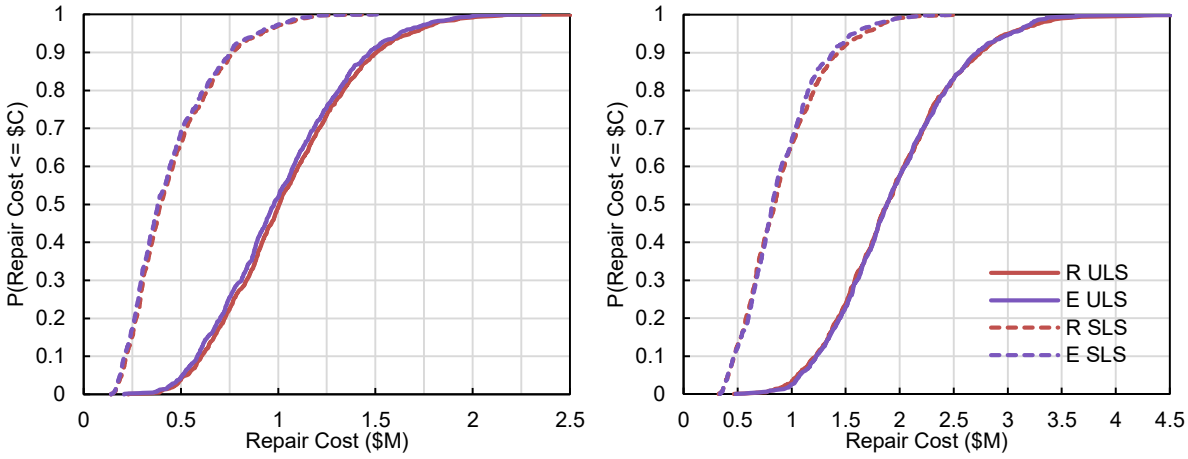

(a) Four-storey **(b)** Eight-storey

Figure 6.9: Cumulative distribution functions of repair costs considering the modified (R) and original (E) energy methods, four- and eight-storey buildings

Although the damping coefficients were significantly larger for the original energy method, the difference in repair costs is trivial for both the four- and eight-storey structures. The level of total damping targeted by the modified energy method was within the range of optimal damping identified in Chapter 5. It could therefore be expected that increasing the damping, as is effectively done by the original energy method, would produce trivial improvements to the expected economic losses. This result could not be determined by

examining the EDP results of Section 6.3.2. The drifts of the energy method structures were less than the modified method structures and the accelerations did not vary significantly. It can be concluded that the magnitude of the drift reductions achieved by the original energy method was therefore not sufficient to produce any meaningful changes in repair costs.

6.6.1.2 Repair Costs and Engineering Demand Parameters

Repair costs from the seismic performance assessments can be attributed to the EDP that generated the damage. This disaggregation can help to clarify variations in seismic performance between the different building design approaches. The mean repair costs associated with each EDP are shown in Figure 6.10 for the FVD retrofitted and drift design buildings. The results of the original energy method are excluded, as the disaggregation was nearly identical to the modified method results.

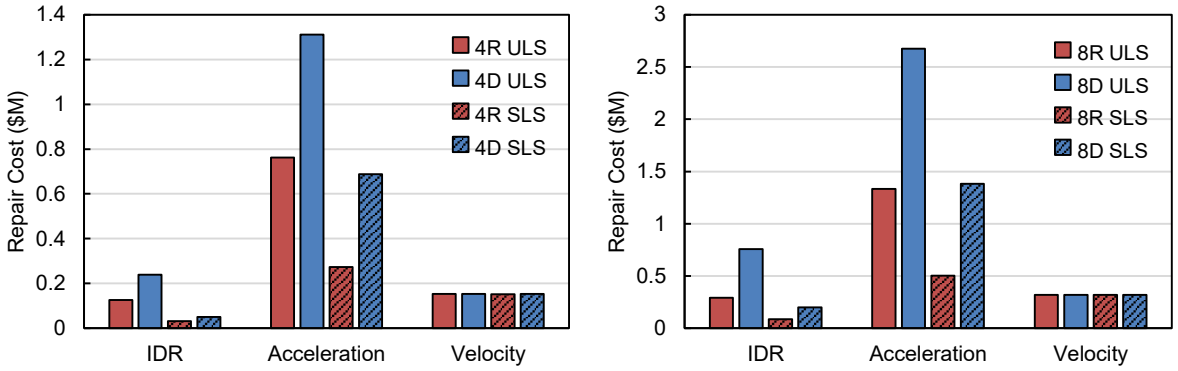

(a) Four-storey buildings **(b)** Eight-storey buildings

Figure 6.10: Mean repair costs grouped by EDP for the FVD retrofitted and drift design buildings

The FVD buildings significantly reduce both drift and acceleration damage when compared to the drift designs. The reduction in acceleration damage is greater than the reduction in drift damage. This can be rationalised by the drift design approach, which aims to minimise IDR at the expense of increased accelerations.

Minimal drift-sensitive damage is produced in the SLS for both building sets. Acceleration-sensitive damage accounts for the majority of damage in all cases. This reiterates the impact of acceleration on seismic performance.

To further investigate the relationship between EDPs and repair costs, mean EDP repair costs were organised based on floor level. It was found that both acceleration and drift damage was reduced for the standard designs retrofitted with FVDs at all floors with respect to the drift designs. This occurred for both the ULS and the SLS as expected based on the EDP results of the time history analyses. An example is shown in Figure 6.11 for the four-storey ULS repair costs.

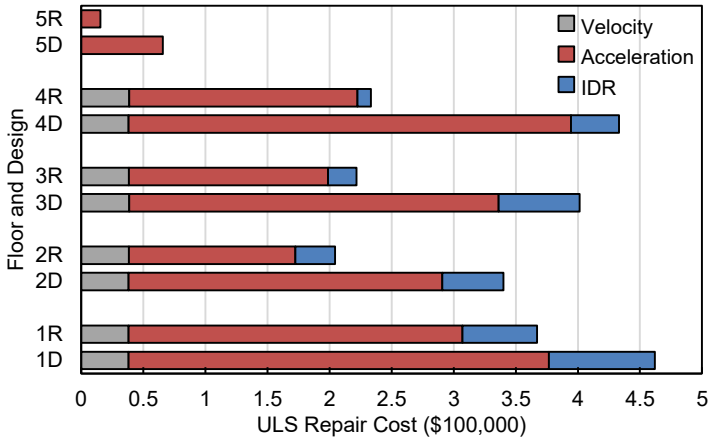

Figure 6.11: Mean ULS repair costs for each floor grouped by EDP, four-storey FVD and drift buildings

6.6.1.3 Repair Costs and Fragility Groups

The mean repair costs for each structural and nonstructural fragility group of the four- and eight-storey buildings were determined. The fragility-sorted repair costs are shown in Figure 6.12. As in the previous studies, the fragility groups that produce negligible repair costs in the standard designs are excluded.

Structural damage is negligible in the FVD retrofitted buildings. This concurs with the investigation on nonlinear structural behaviour conducted in Section 6.3.3 and gives confidence to the FEMA P-58 results. In comparison, the four- and eight-storey drift buildings experience ULS structural damage. This identifies a significant improvement in seismic performance for the FVD retrofitted buildings. Structural damage would introduce significant delays to re-occupancy following an earthquake. Preventing structural damage is a major step towards achieving building serviceability following a ULS level earthquake.

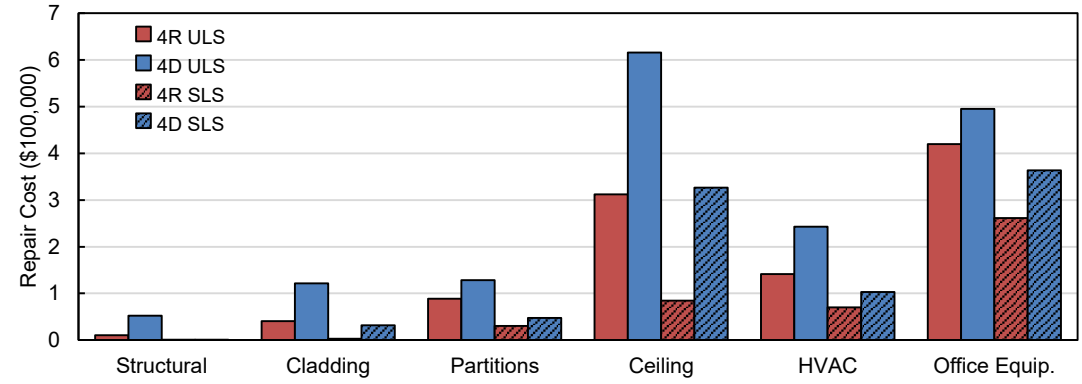

(a) Four-storey buildings

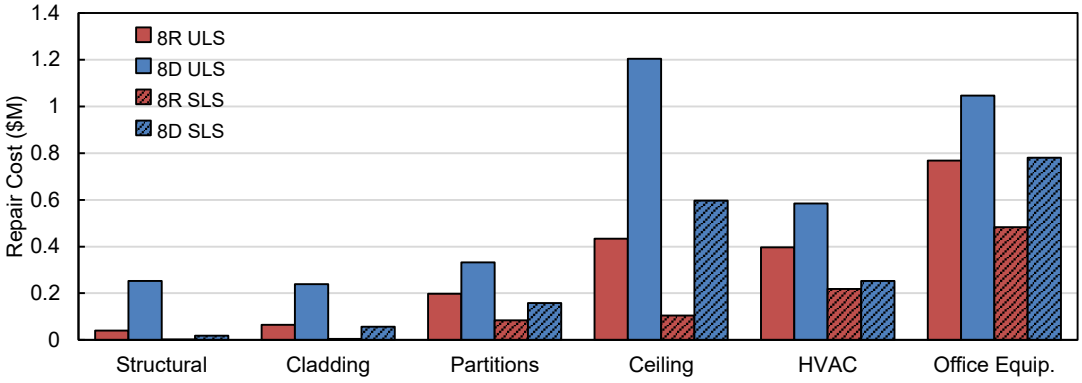

(b) Eight-storey buildings

Figure 6.12: Comparison of fragility-sorted repair costs for the FVD retrofitted standard buildings and the drift design buildings

Significant repair costs can be attributed to nonstructural systems. This is in agreement with previous findings of this thesis that stress the importance of considering nonstructural seismic performance when designing for a rapid return to building occupancy. Attaining a target level of seismic performance requires the harmonisation of structural and nonstructural performance. However, damage to nonstructural systems is not completely prevented in the FVD retrofitted buildings.

6.6.2 16-Storey Damper Retrofit and Standard Design

The FVD retrofitted four- and eight-storey standard structures have been shown to outperform the comparable drift design structures. Although the 16-storey structure was unable to be designed to meet the advanced IDR requirements using the drift design approach, the desired IDR performance was obtained using FVDs. The 16-storey standard design retrofitted with FVDs is explored in this section using the 16S benchmark.

6.6.2.1 Total Repair Costs

The expected total repair costs for the damped and undamped 16-storey structures are presented by cumulative distribution functions in Figure 6.13a. Both the ULS and the SLS repair cost distributions are provided.

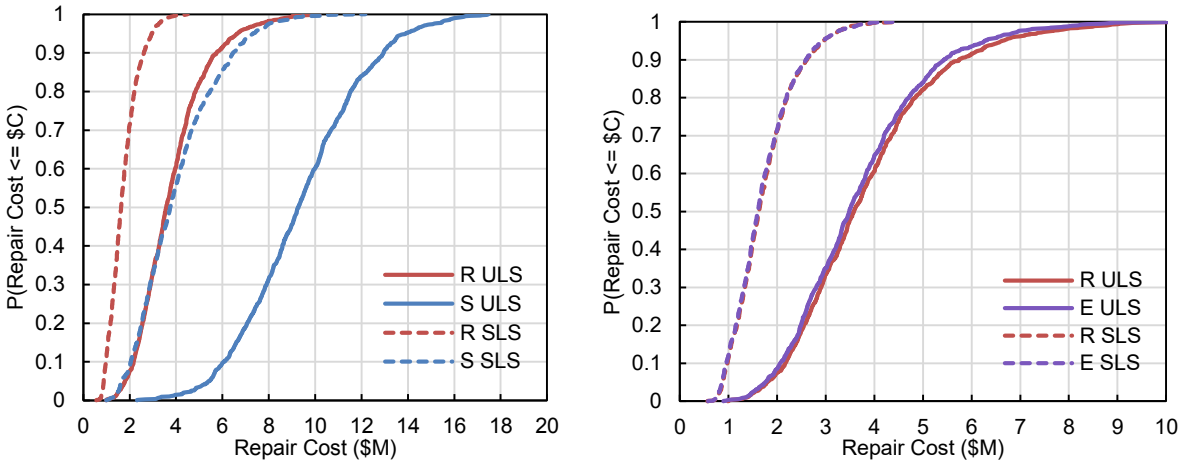

(a) FVD retrofitted (R) and unretrofitted (S) structures

(b) Modified (R) and original (E) energy methods

Figure 6.13: Cumulative distribution functions of repair costs for the 16-storey buildings

The ULS repair costs of the building with FVDs are less than or equal to the SLS costs of the standard design. Building 16S has median and 90th percentile ULS repair costs of approximately 50% and 69% of the building value, respectively. According to the FEMA (2012b) guideline, it is probable that this code-compliant building would be demolished and replaced following a ULS earthquake. In comparison, structure 16R has median and 90th percentile ULS repair costs of approximately 19% and 31% of the building value, respectively. These results are similar to those of the FVD retrofitted four- and eight-storey buildings. Structure 16R reaches the damage limit corresponding to building replacement, 40% of building value, at the 98th percentile. This represents a significant improvement in seismic performance for the buildings with FVDs.

The median SLS repair costs for the FVD building are 9% of the building value, while the standard building experienced damage of 20%. A total loss of under 10% is closer towards achieving a level of damage that will minimise effects on building serviceability.

The repair costs were also compared for the FVD retrofitted building using the original and modified energy methods in Figure 6.13b. Although the damping coefficient is significantly larger for the original energy method, the difference in repair costs is minor. This finding is identical to that of the four- and eight-storey buildings, and the same explanation applies.

6.6.2.2 Repair Costs and Engineering Demand Parameters

Repair costs from the seismic performance assessment of the 16-storey buildings were attributed to the EDP that generated the damage. The mean repair costs associated with each EDP for the 16-storey buildings are shown in Figure 6.14. The original energy method is excluded, as the disaggregation was nearly identical to the modified method results.

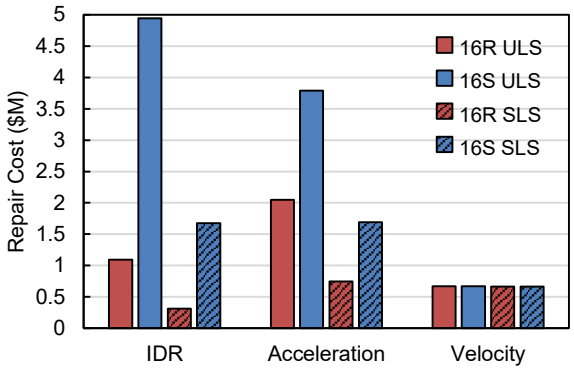

Figure 6.14: Mean repair costs grouped by associated EDP for the FVD retrofitted and undamped 16-storey standard buildings

The use of FVDs reduces drift-sensitive damage by 80% and acceleration-sensitive damage by approximately 50% with respect to the standard building costs. Velocity damage is unchanged, confirming that FVDs cannot meaningfully improve velocity-sensitive seismic performance. It was found in Section 5.5.1 that the changes in relative velocities were minor in comparison to the absolute velocities. Another technique such as anchorage may be used to prevent component toppling due to absolute floor velocities.

In order to further investigate the relationship between EDPs and repair costs, mean EDP repair costs were organised based on floor level. The ULS floor repair costs are shown in in Figure 6.15.

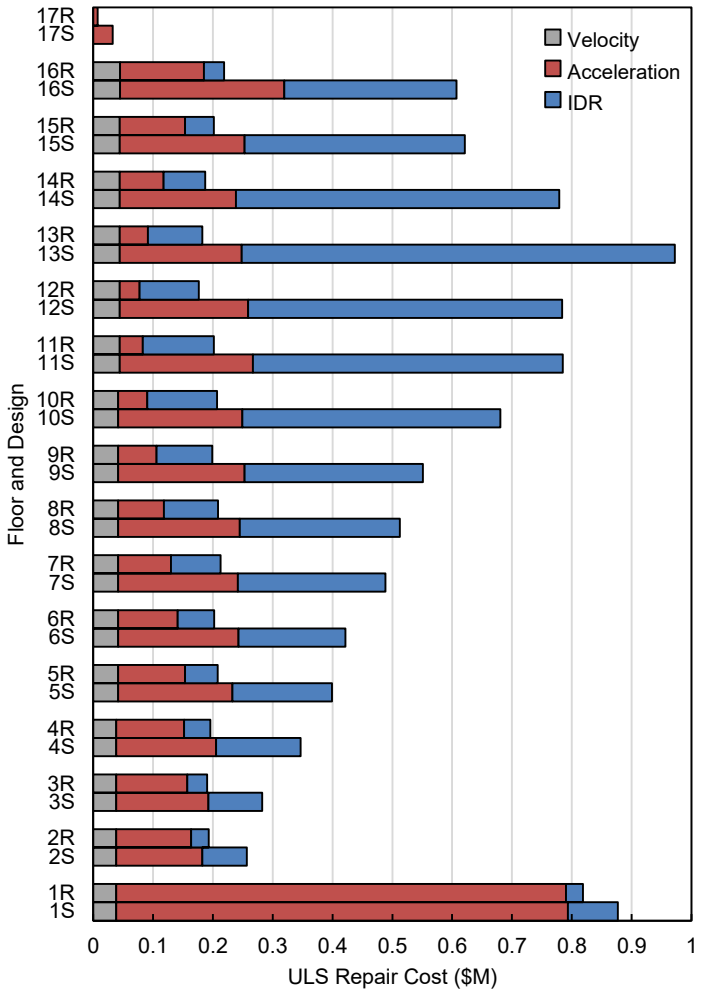

Figure 6.15: ULS mean EDP repair costs for each floor of the FVD retrofitted and undamped 16-storey standard buildings

Major reductions in drift-sensitive damage are achieved in the damped building at all floors. Significant reductions in acceleration-sensitive repair costs are realised for floors four to 16. Large acceleration repair costs are indicated on floor one due to a concentration of acceleration-sensitive nonstructural components such as HVAC equipment. Repair costs could be further decreased using equipment isolation or more robust components.

6.6.2.3 Repair Costs and Fragility Groups

The mean repair costs associated with each structural and nonstructural fragility group were calculated for the 16-storey damped and undamped buildings. The resulting fragility-sorted repair costs are shown in Figure 6.16.

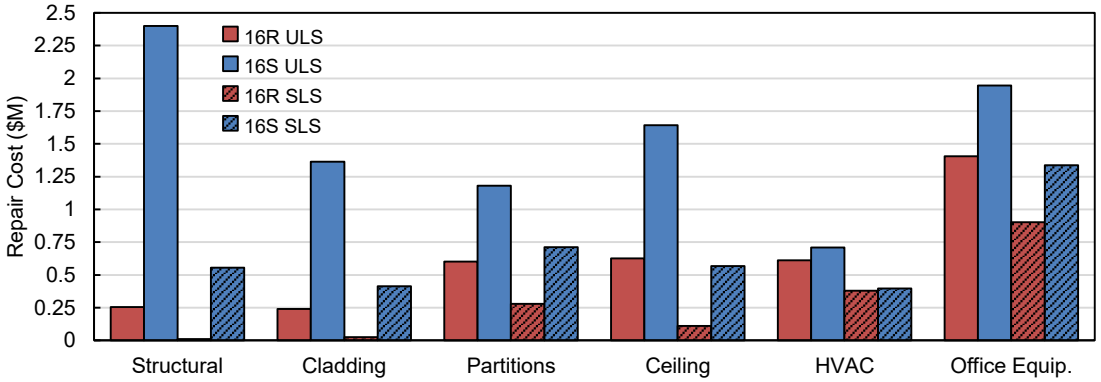

Figure 6.16: Comparison of fragility-sorted repair costs of the FVD retrofitted and undamped 16-storey standard buildings

Considering the undamped building, the largest portion of ULS repair costs results from structural damage. The standard building also experiences notable structural damage during the SLS. Damage to structural components should ideally be minimised in order to allow a rapid return to building occupancy. The FVD retrofitted building experiences minor structural damage during the ULS and negligible structure damage during the SLS. This demonstrates a significant seismic performance improvement achieved by the use of FVDs.

6.7 Conclusions

Designing structures to reach the advanced IDR criteria of the drift designs and retrofitting buildings with FVDs are two methods with the same aim: to improve the seismic performance of standard buildings. This chapter compared the resulting performance of both approaches. The standard designs were retrofitted with FVDs to allow the buildings to reach the IDR performance of the drift designs. Damper coefficients were calculated using the modified energy method. The resulting required total damping of 37% was within the optimal range of damping to minimise economic losses.

The 16-storey building was unable to reach the 0.5% IDR performance limit for the ULS using the drift design approach, however this limit was achieved using FVDs. Excluding the ground level, peak floor accelerations and IDRs of the FVD retrofitted buildings were significantly improved with respect to the drift designs.

A second set of FVD retrofitted buildings was created with damper coefficients calculated using the original energy method. The difference between the structural parameter results of the modified and original energy methods was inconclusive, in terms of variations between different parameters and between values at different building heights for the same parameter. This reinforced the benefits of using repair costs rather than structural parameters to evaluate the seismic performance of structural designs. The repair costs were compared for both sets of FVD retrofitted buildings. Although the damping coefficients were significantly larger for the original energy method, the difference in repair costs was trivial. The level of total damping targeted by the modified energy method was within the range of optimal damping. It could therefore be expected that increasing the damping, as is effectively done by the original energy method, would produce trivial improvements to the expected economic losses.

The maximum ULS damper forces allowed the total damper investment to be estimated. It was found that the use of FVDs would increase the building cost by less than 3% for all structures. This investment is comparable to the cost increase due to the drift designs.

Examining the expected repair costs revealed that the FVD retrofitted buildings significantly outperform the drift designs for both the ULS and the SLS. Although the ULS repair costs of the drift designs decrease with respect to the undamped standard buildings, the median repairs are still above the guideline for building demolition according to FEMA (2012b). In comparison, the 90th percentile ULS repair costs of the FVD retrofitted buildings are below this limit. This represents a significant advantage of using FVDs to retrofit buildings over the drift designs. The median SLS repair costs for the FVD buildings are approximately half of the SLS median values for the drift designs.

Limitations of FVD retrofit include velocity-sensitive damage, and acceleration-sensitive damage at the ground level. Another retrofit strategy must be incorporated to improve performance related to these parameters, such as equipment anchorage to prevent toppling due to high velocities, or isolating acceleration-sensitive nonstructural systems that are on the ground level.

Structural damage can be expected to introduce significant delays to building re-occupancy following an earthquake. It was found that damage to structural components is negligible in the FVD retrofitted buildings for the ULS. This represents a significant improvement in seismic performance for the FVD retrofitted buildings. Preventing structural damage is a major step towards achieving building serviceability following a ULS level earthquake.

The performance assessment of the FVD and drift structures demonstrate that FVDs are a viable solution to improve the seismic resiliency of structures. Seismic performance improvements were realised using uniform damper placement. A large number of damper placement methods have been proposed in literature that claim to improve performance. Some of these advanced placement techniques may be able to further increase seismic performance and is the subject of the following chapter.

Chapter 7

Optimal Damper Placement

7.1 Overview of Chapter

The previous chapters have demonstrated that the use of fluid viscous dampers (FVDs) is a viable solution to reduce earthquake-induced damage to multi-storey buildings. Seismic performance improvements were realised using uniform damper placement. Advanced damper placement strategies may be able to further improve performance. The distribution of dampers within a building is a critical decision, as damper placement affects structural response and the required damper investment. Despite this, building codes do not prescribe a damper placement method.

While a large number of FVD placement methods have been proposed, the review of literature presented in Section 2.5 revealed that only limited comparisons of methods have been conducted. Research comparing FVD placement methods has evaluated structural parameters rather than repair costs. As a result, an optimal placement technique is often not conclusively identified due to performance variations between storeys and between structural parameters. Other common limitations include the use of simplified shear building models, the use of a limited set of ground motions, the selection of only a small number of different placement techniques, and the omission of serviceability limit state (SLS) performance.

This chapter evaluates and compares the effectiveness of several damper placement methods considering structural and nonstructural performance in repair costs. The placement methods that are considered in this chapter are listed and described in Section 7.2. The total damping coefficient is allocated according to the different methods and the

resulting distributions are compared in Section 7.3. Section 7.4 evaluates results of time history analyses conducted using the FVD retrofitted building models. Repair costs of the buildings are assessed using the FEMA P-58 procedure (FEMA 2012b) in Section 7.5. Conclusions of the chapter are presented in Section 7.6.

7.2 Selected Damper Placement Methods

In addition to producing an efficient damper distribution, it is desirable that damper placement methods are practical enough to be used routinely by practising engineers. The scope of this thesis excludes placement methods that require extensive problem-specific tailoring or rely on complex tools and techniques not familiar to practising engineers. These characteristics inhibit the common uptake of a method in practice, as the method cannot be easily incorporated into the design process.

Six damper placement methods were selected for study in this chapter. They include iterative methods as well as simple methods. Each of these methods were chosen based on prevalence in literature and level of practicality. The damper placement methods considered are:

1. Uniform damping
2. Stiffness proportional damping
3. The storey shear strain energy method (SEM)
4. The efficient storey shear strain energy method (ESEM)
5. The simplified sequential search algorithm (SSSA)
6. The fully stressed design algorithm (FSDA)

A brief description of each method follows. These damper placement methods and the respective strengths and weaknesses of each method are reviewed in detail in Section 2.5.

Uniform damping evenly distributes the total viscous damping coefficient between each storey. This simple technique is one of the most commonly used placement methods

in research and often serves as a benchmark (Lopez Garcia and Soong 2002; Pavlou and Constantinou 2006; Hwang *et al.* 2013; Palermo *et al.* 2013; Landi *et al.* 2015; Dall'Asta *et al.* 2016). The damping coefficient at storey j (c_j) is calculated using the equation

$$c_j = \frac{C_{total}}{n}, \tag{7.1}$$

where C_{total} is the total viscous damper coefficient added to the structure and n is the number of storeys.

Stiffness proportional damping distributes the damping coefficient in proportion to the relative storey stiffness. This placement method typically results in damper coefficients concentrated in the lower storeys. Stiffness proportional damping serves as a preliminary measure of advanced placement techniques implemented in regular structures, as many proposed methods have minimal damping in the upper storeys and concentrate dampers near the bottom of the structure (Whittle *et al.* 2012). The method is presented by the equation

$$c_j = \frac{K_j}{\sum_i K_i} C_{total}, \tag{7.2}$$

where K_j is the stiffness of storey j and i is each storey.

The SEM (Hwang *et al.* 2013) distributes the damping coefficient along the building height in proportion to the storey shear strain energy corresponding to the first mode of vibration of the structure. The damping coefficient at storey j is calculated using

$$c_j = \frac{S_j \phi_{rj}}{\sum_i S_i \phi_{ri}} C_{total}, \tag{7.3}$$

where ϕ_{rj} is the relative modal displacement of storey j and S_j is a storey parameter proportional to the shear force. The storey parameter is calculated using $S_j = \sum_{i=j}^{roof} m_i \phi_i$, where m_i is the mass of the ith storey and ϕ_i is the modal displacement.

The ESEM (Hwang *et al.* 2013) is a modification of the SEM. The damping coefficient is allocated only to the storeys with a shear strain energy greater than the average storey shear strain energy, i.e. $S_j \phi_{rj} > \frac{1}{n} \sum_i S_i \phi_{ri}$. The damping coefficient is distributed to the "efficient" storeys using

$$c_j = \frac{S_j \phi_{rj}}{\sum_{z=1}^{k} S_z \phi_{rz}} C_{total}, \tag{7.4}$$

where k is the number of storeys whose shear strain energy is greater than the average storey shear strain energy and z refers to all storeys meeting that condition.

Two iterative techniques are studied: the SSSA (Lopez-Garcia 2001) and the FSDA (Levy and Lavan 2006). The SSSA places an incremental damping coefficient sequentially in the storey with a maximum location index. For linear FVDs the location index is peak interstorey velocity. The FSDA is an analysis and redesign procedure that uses a recurrence relationship to allocate damping coefficients to each storey based on a performance index. The recurrence relationship is a function of interstorey drift for linear cases.

The considered placement methods use linear structural response to optimise damper placement. However, the structural models in this thesis capture nonlinear response. The performance of each FVD retrofitted structure can therefore be expected to deviate from the linear behaviour assumed by the placement methods.

This chapter is limited to the placement of linear FVDs. Horizontal damper placement within each storey of the building is not considered, as the majority of damper placement methods produce a vertical distribution of dampers within a structure.

7.3 Distributing the Damping Coefficient

The total damping coefficient was allocated to several structures using the identified damper placement methods. Three Eurocode-compliant concentric braced frame (CBF) buildings were included in this study: the four-storey standard design (4S), the eight-storey standard design (8S), and the 16-storey standard design (16S). Specifications of the buildings are provided in Chapter 3.

7.3.1 Comparison Constraint

In order to compare the different damper placement techniques, the total viscous damping coefficient added to the structure is constrained to be the same value for each method. The total viscous damping coefficient is widely used in literature to compare damper placement methods. An alternative basis for comparison, such as total retrofit cost, could

also be considered. However, only approximations for damper costs are currently available and were considered too unreliable to be used in a robust comparison of damper placement methods.

As the placement of damping coefficients along the structure's height can affect the achieved damping ratio, the ratios will be investigated in Section 7.3.5. It has been noted that the cost of a FVD is dependent on several parameters in addition to the damping coefficient, such as the maximum absolute damper force. However, taking the sum of damping coefficients as an objective is similar to taking the sum of peak damping forces in simple cases (Lavan and Avishur 2013). The cost of the dampers will be investigated in Section 7.4.2.

Two levels of total damping were selected for this investigation: 15% and 30%. Section 5.5 identified 30% as the lower bound of optimal damping for the Eurocode standard structures. The second selected level of damping, 15%, was chosen to represent a smaller and more frequently targeted level of damping.

The C_{total} corresponding to each level of total damping was calculated using the modified energy formula presented in Section 5.4.2 and a uniform damping distribution. The total damping coefficient for each building model and level of damping are provided in Table 7.1, where values are halved due to the use of 2D structural models.

Table 7.1: Total damping coefficient (C_{total}) used in the comparison of damper placement methods

Total Damping	$\boldsymbol{C_{total}}$ **(N s/mm)**		
	4S	**8S**	**16S**
15%	10,107	36,412	76,865
30%	25,267	91,030	192,163

The buildings were modelled in OpenSees (McKenna 2017), as detailed in Section 3.4. The values of C_{total} were allocated to the models without any further analyses using the one-step placement methods (uniform damping, stiffness proportional damping, the SEM, and the ESEM). The two iterative methods (the SSSA and the FSDA) require further analyses and are discussed below.

7.3.2 Simplified Sequential Search Algorithm Iterations

The SSSA attempts to place dampers sequentially where their effect will be maximised. The algorithm is subject to the assumption that the optimal storey to allocate a damper is the one that undergoes a maximum structural response during the ground motion. Location indices are calculated for each storey at the end of a time history analysis using one ground motion. As linear FVDs are velocity-dependent dampers, the location indices are given by peak interstorey velocity. The response of the bare frame is determined and the first damper is allocated to the storey with the greatest location index. The damper properties are incorporated into the model and the process is repeated until all dampers have been placed.

Time history analyses of the OpenSees models were conducted as described in Chapter 3. All steel materials in the models were assigned elastic behaviour for the iterations in accordance with the SSSA. The relative velocity of each floor was recorded in OpenSees using the node recorder (*recorder Node ... vel*). Interstorey velocity values could then be calculated and the absolute peak values identified.

The number of dampers (n_d), and therefore the number of iterations conducted, determine the value of the incremental damping coefficient ($c_{incr} = C_{total}/n_d$). The number of dampers was selected to be equal to two times the number of storeys ($n_d = 2n_{storey}$); this number was proposed by Lopez Garcia and Soong (2002) as the optimal number of dampers for the SSSA.

An example of the iterative process of the SSSA is shown in Figure 7.1 for the eight-storey building with 30% total damping, where the peak interstorey velocities are shown for each iteration. The ground motion record used is Taiwan SMART1 (45) 1986. The dampers were placed in the following order of storeys: 6, 7, 6, 5, 4, 5, 4, 4, 7, 5, 3, 6, 3, 1, 2, 1. The final design reduces the peak interstorey velocity of all storeys and produces comparable peak values for all storeys.

One limitation of the SSSA is that the resulting damper distribution is dependent on the ground motion record used to conduct the procedure. If multiple ground motion records are considered, it was found that the resulting damper distributions differed for

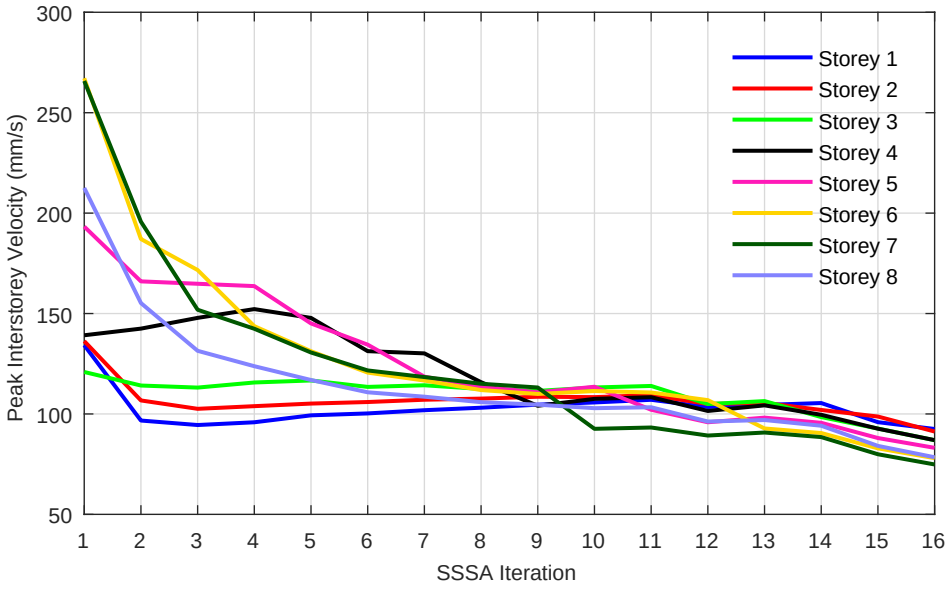

Figure 7.1: Peak interstorey velocity-SSSA iteration number results for the eight-storey building with 30% total damping. Taiwan SMART1 (45) 1986 ground motion

each record (Lopez Garcia and Soong 2002). The SSSA requires engineering judgement to select a final damper distribution.

To address this limitation, seven ground motion records with the smallest mean squared error (MSE) with respect to the Eurocode 8 target spectrum were used to conduct the SSSA. The ground motion suites for each building were created in Section 3.5. The number of records was chosen according to Eurocode 8 recommendations for time history analyses (CEN 2013). The median damper coefficient values of each storey were then selected as the final SSSA distribution. Figure 7.2 – 7.4 display the SSSA results for each of the seven ground motion records and all building models. The record sequence numbers (RSN) and the corresponding earthquake and station are listed in Appendix A.

Figure 7.4b reveals a concentration of dampers in one storey of the 16-storey structure when the SSSA is conducted using ground motion RSN 4207 (Niigata Japan 2004). The SSSA iteration process for the outlier is displayed in Figure 7.5. This outlier demonstrates the possible variation in results when conducting the SSSA, as well as the importance of using several ground motion records with engineering judgement. The use of median c_j values is less sensitive to outliers than the mean.

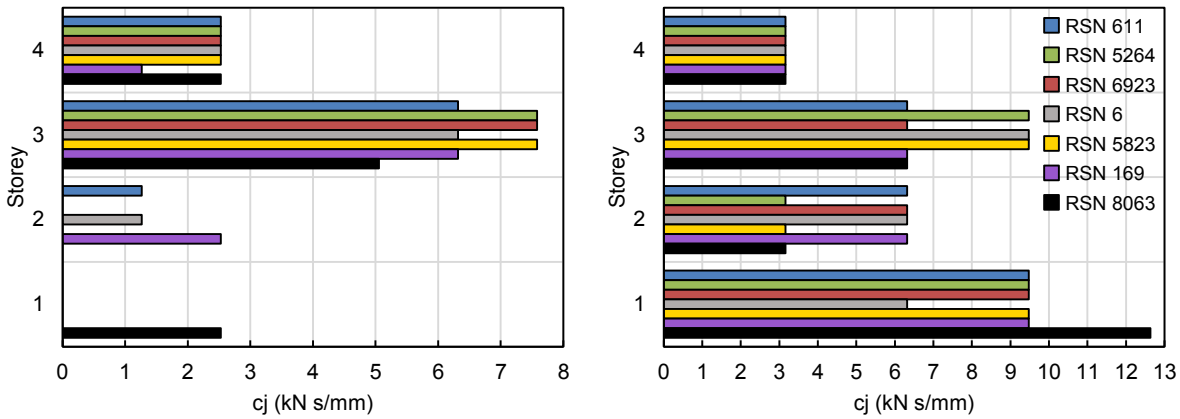

(a) 15% total damping **(b)** 30% total damping

Figure 7.2: SSSA distributions for the four-storey building. RSN = record sequence number

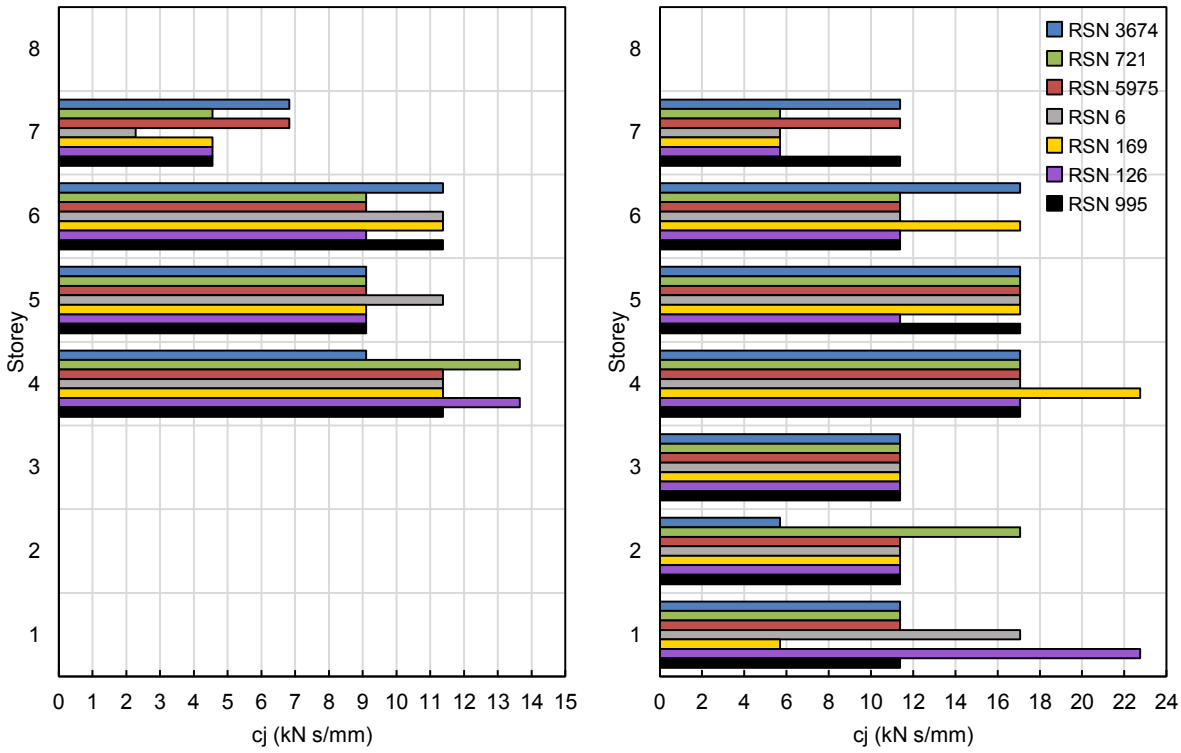

(a) 15% total damping **(b)** 30% total damping

Figure 7.3: SSSA distributions for the eight-storey building. RSN = record sequence number

7.3.3 Fully Stressed Design Algorithm Iterations

The FSDA is the second iterative damper placement method considered in this chapter. The modified algorithm (Lavan and Levy 2009) was used, which minimises the maximum mean squared interstorey drift ratio (IDR) for a constrained amount of total added

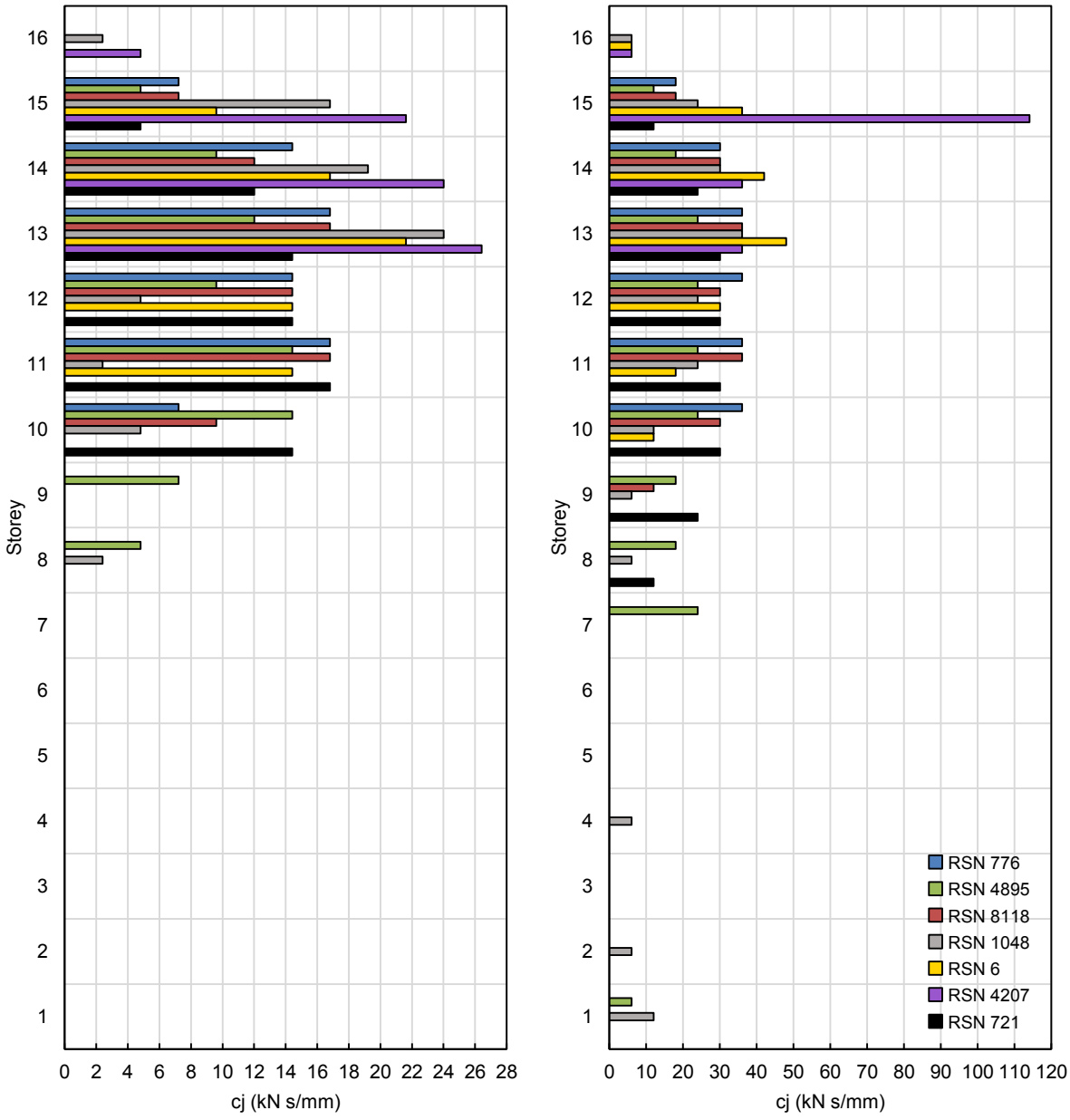

(a) 15% total damping **(b)** 30% total damping

Figure 7.4: SSSA distributions for the 16-storey building. RSN = record sequence number

damping. The recurrence relationship

$$c_j^{k+1} = c_j^k \left(pi_j^k\right)^{\frac{1}{q}} \frac{C_{total}}{\sum_i c_i^k \left(pi_i^k\right)^{\frac{1}{q}}} \tag{7.5}$$

is used to allocate damping coefficients to each storey based on a performance index, where c_j^k is the damping coefficient of the jth-storey at iteration k, pi_j^k is the performance index, and q is a convergence parameter.

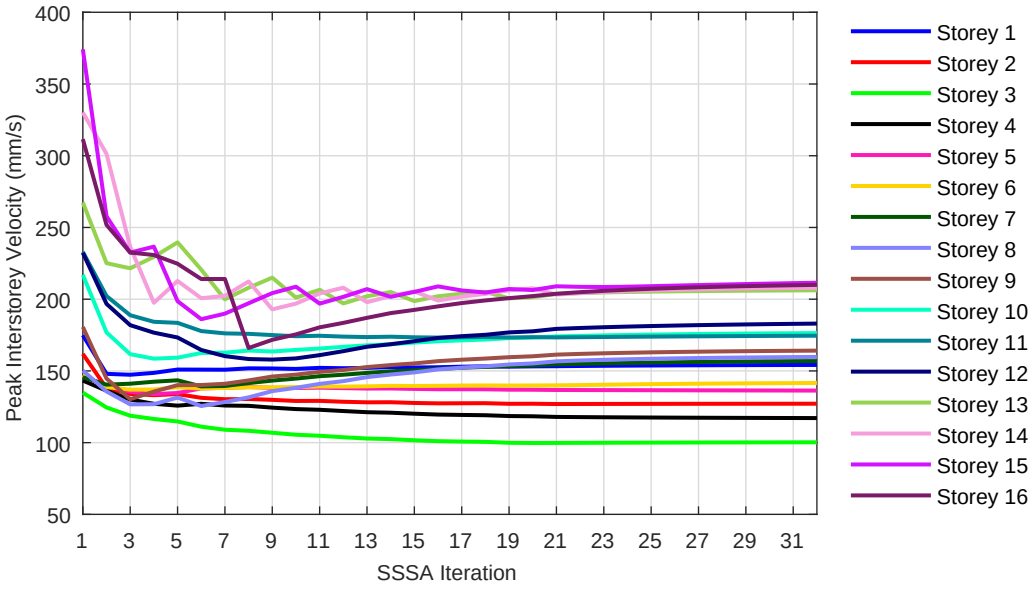

Figure 7.5: Peak interstorey velocity-SSSA iteration number results for the 16-storey building with 30% total damping, RSN 4207

The maximum IDR (d_j) normalised by the allowable IDR (d_a) is the performance index for 2D linear models: $pi_j = \frac{d_j}{d_a}$, where $d_j = \max_t(\text{idr}_j(t))$. However, the modified algorithm is defined such that the allowable drift limit does not affect the final damper distribution as long as the value is equal for all storeys. In this case, the recurrence relationship of the modified algorithm (Eq. 7.5) reduces to a form where d_a is no longer present:

$$c_j^{k+1} = c_j^k \left(d_j\right)^{k\frac{1}{q}} \frac{C_{total}}{\sum_i c_i^k \left(d_i^k\right)^{\frac{1}{q}}}. \tag{7.6}$$

The algorithm terminates once the changes in all c_j values for two subsequent iterations are sufficiently small. This was defined to be <5%. A value of $q = 0.5$ was used as suggested for linear problems by Levy and Lavan (2006).

The starting c_j values were initialised using a uniform damping distribution (Levy and Lavan 2006). The design procedure is started with one "active" ground motion. The active ground motion is chosen for the linear problem based on the maximum spectral displacement at the first period of the structure for all records in the ground motion suite. The analysis and redesign procedure is carried out until the stopping criterion is reached. This is referred to as one run of the FSDA in this chapter.

The design determined using the first run of the FSDA is then assessed by conducting time history analyses using all other ground motions in the suite of interest. If any ground motion in the inactive set produces a $\max_j (pi_j)$ that exceeds that of the active set, the inactive record with the largest pi_j is added to the active set. A second run of the FSDA is performed, where the envelope of the active set pi_j is used to determine the new c_j values. The algorithm is complete once the stopping criterion of a run is reached and no additional records are added to the active set.

Seven ground motion records with the smallest MSE with respect to the Eurocode 8 target spectrum were used to conduct the FSDA. These are the same suites of ground motions used for the SSSA.

It was found that a maximum of one run was necessary for the four-storey building, while the eight- and 16-storey buildings required two runs. An example of the FSDA iterative process is provided in Figure 7.6 for the four-storey building with 30% total damping. The interstorey drift and damping coefficient values per storey at each iteration are provided. The stopping criterion of c_j convergence was reached at 19 iterations. As all other ground motions in the suite of seven records did not exceed the performance index of the active set, only one run was required.

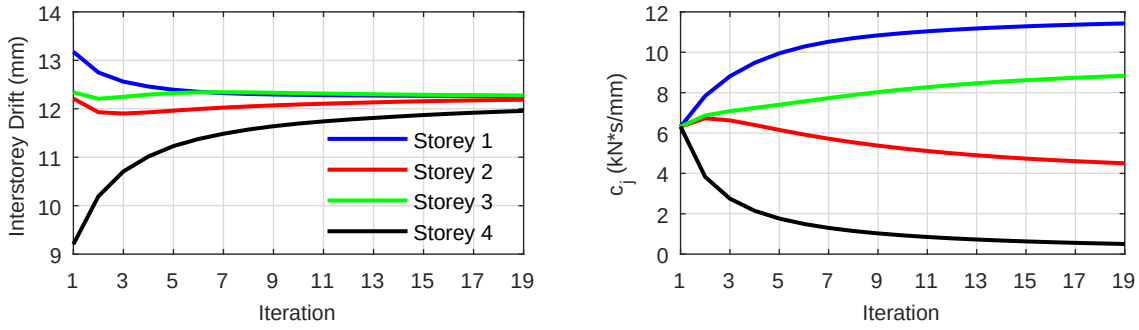

(a) Interstorey drift **(b)** c_j

Figure 7.6: Iterations of the FSDA for the four-storey building with 30% total damping

An example of the FSDA iterative process when two runs are required is provided in Figure 7.7 for the eight-storey building with 30% total damping. The interstorey drift and damping coefficient values per storey at each iteration are shown. The stopping criterion of c_j convergence was reached after only five iterations in the second run.

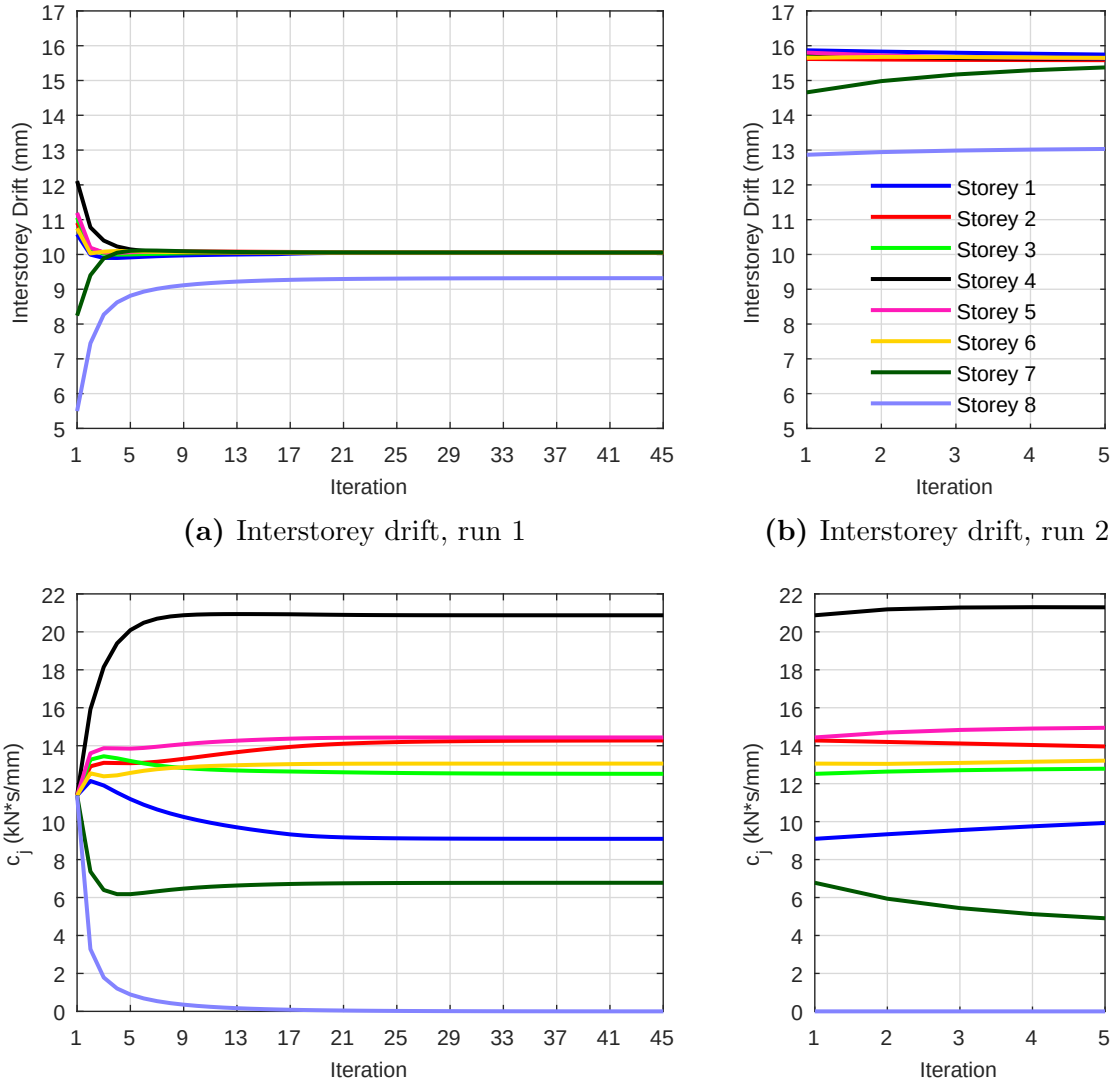

(a) Interstorey drift, run 1

(b) Interstorey drift, run 2

(c) c_j, run 1

(d) c_j, run 2

Figure 7.7: Iterations of the FSDA for the eight-storey building with 30% total damping

7.3.4 Analysis Time Required for the Iterative Methods

A limitation of both the FSDA and the SSSA is that they are iterative procedures. The methods can be time consuming and computationally expensive if many iterations must be performed or if complex models are used. The analysis time required to perform the iterative damper placement methods is listed in Table 7.2. The average time for the 15% and 30% total damping models is included. Analysis was carried out on a Windows 7 desktop with an Intel Core i7-4770 CPU, 16GB RAM, and a 7200RPM hard drive. Both methods require a reasonable amount computational time and could be implemented in

practice. The FSDA outperforms the SSSA for the eight- and 16-storey models with regards to the required analysis time, however the differences are minor.

Table 7.2: Average time required to implement the iterative damper placement methods

Method	Four-Storey	Eight-Storey	16-Storey
SSSA	6 min	27 min	105 min
FSDA	5 min	12 min	61 min

7.3.5 Comparison of Damping Coefficient Distributions

The damping coefficient distributions resulting from each considered damper placement method were compared to one another. The resulting damper distributions are presented in Figure 7.8 – 7.10, where K refers to stiffness proportional damping and *Uni* refers to uniform damping.

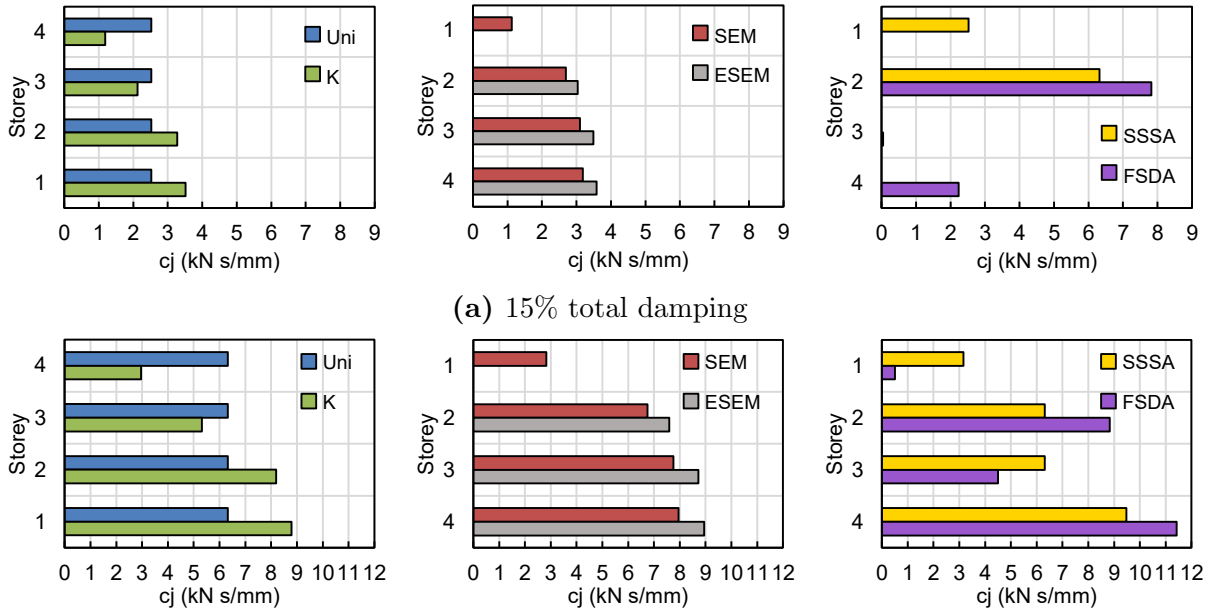

(a) 15% total damping

(b) 30% total damping

Figure 7.8: Damping coefficient distributions for the four-storey building resulting from several damper placement methods

The damper distributions exhibit similar results for the four- and eight-storey structures. The non-iterative methods generally produce an even distribution of dampers, excluding the top storeys which are allocated minimal damping. The SSSA and the FSDA concentrate dampers in the middle storeys, although this concentration is significantly more pronounced

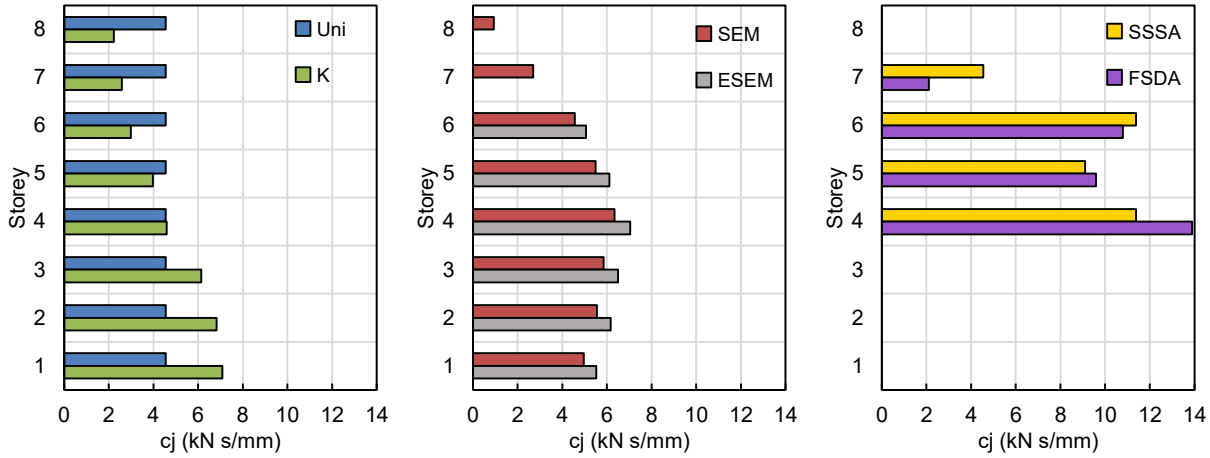

(a) 15% total damping

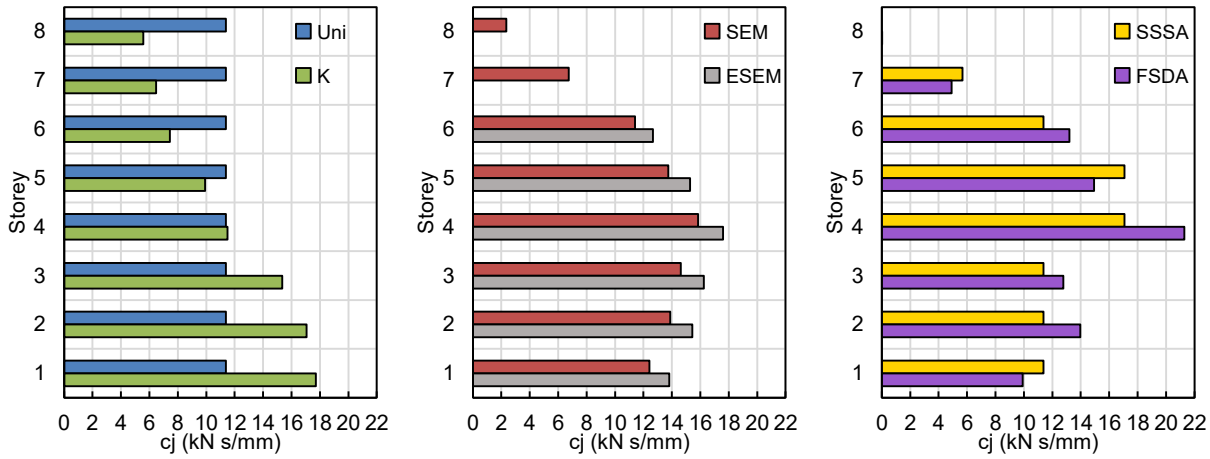

(b) 30% total damping

Figure 7.9: Damping coefficient distributions for the eight-storey building resulting from several damper placement methods

for 15% than 30% total damping. The concentration of dampers is reduced for the 30% case as enough supplemental damping is provided to sufficiently improve the iterative performance indices of the "weak" storeys. Dampers can then be allocated to additional storeys.

The damping distributions of the 16-storey building have some variation with respect to the patterns of the four- and eight-storey buildings. The SEM and the ESEM place dampers in the middle storeys, with reduced values of damping in the lower and upper storeys. The SSSA and the FSDA concentrate dampers in the middle to upper storeys, and this concentration is pronounced for both considered levels of damping.

It has been noted that the vertical position of damping coefficients can affect the damping ratio of a structure for a given amount of C_{total}. The achieved total damping

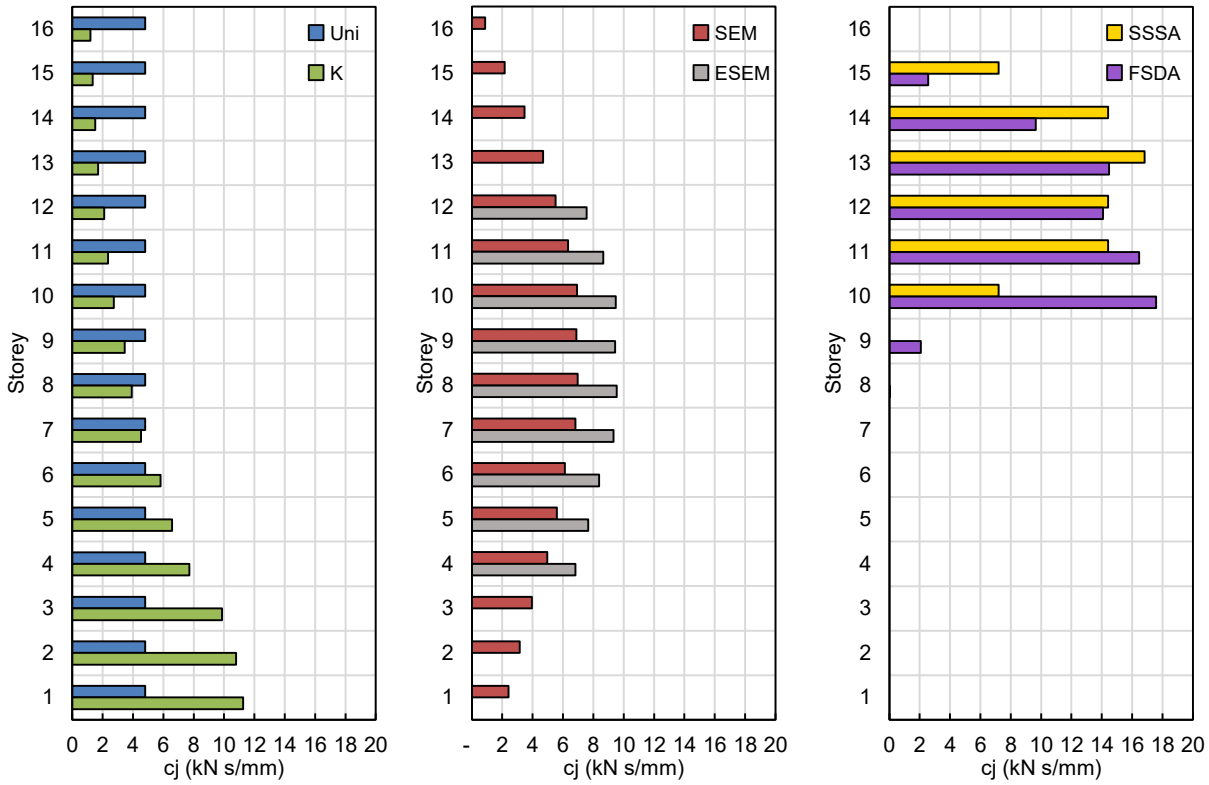

(a) 15% total damping

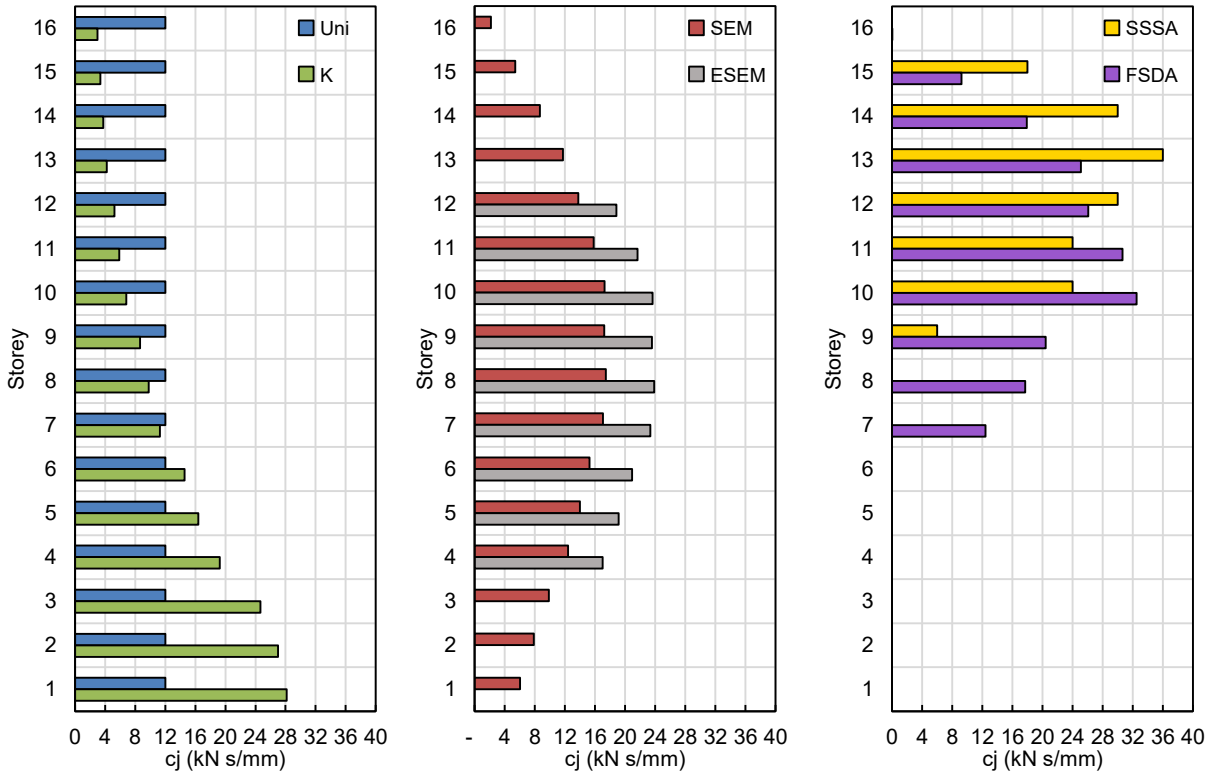

(b) 30% total damping

Figure 7.10: Damping coefficient distributions for the 16-storey building resulting from several damper placement methods

ratios resulting from the different damper placement methods were calculated according to the general modal analysis method considering complex-valued modes described in Section 5.3.2. The achieved damping ratios are listed in Table 7.3.

Table 7.3: Achieved damping ratios (%) from the different damper placement methods

Method	**Four-Storey**		**Eight-Storey**		**16-Storey**	
Target	15	30	15	30	15	30
Uniform	15	30	16	31	17	35
Stiffness	14	29	14	30	12	23
SEM	14	29	16	33	17	36
ESEM	14	29	15	32	17	37
SSSA	15	29	20	32	23	31
FSDA	16	28	20	34	23	47

The achieved damping ratios are approximately equal to the target levels for the four-storey building. The iterative methods of the eight- and 16-storey buildings significantly exceed the target damping level for 15% total damping. For the 16-storey building and 30% target damping, all damper placement methods excluding stiffness proportional damping considerably surpass the target level. Stiffness proportional damping of the 16-storey building notably underachieves the target level for both 15% and 30% damping. The four-storey building is the simplest of the three considered structures, while the 16-storey building is the most complex due to the building height and greater range in storey stiffness.

7.4 Time History Analyses

Time history analyses of each structural model and damper placement distribution were performed in OpenSees using the ultimate limit state (ULS) and the SLS ground motion suites. Each suite contains 25 records as described in Section 3.5.

7.4.1 Engineering Demand Parameters

The effect of the damper placement methods on seismic response can be observed by comparing the engineering demand parameter (EDP) results of the FVD designs. The peak EDPs are also used as inputs for the FEMA P-58 seismic performance assessment

(FEMA 2012b). The mean peak absolute floor accelerations and IDRs per building level are shown in Figure 7.11 and 7.12 for the buildings with 15% and 30% total damping, respectively. The peak absolute velocity results are omitted, as it was previously shown that the impact on absolute velocities is modest (refer to Section 5.5). It was found that no placement method produced optimal results for both IDR and acceleration.

The EDPs for 15% total damping are shown in Figure 7.11. The differences in the SLS results for all placement methods are minimal. The ULS accelerations display a similar pattern for all three building heights: the SSSA and the FSDA, referred to in this thesis as the iterative methods, have larger acceleration values at the floors below the concentration of FVDs with respect to the non-iterative methods. The iterative methods have poor ULS drift control at the lower storeys when compared to the non-iterative methods; the iterative methods do not allocate significant damping coefficient to these lower storeys. Improved drift control is achieved by the iterative methods at the upper storeys where FVDs are concentrated.

Stiffness proportional damping and the ESEM exhibit a large ULS drift concentration at storey 13 of the 16-storey building. This reveals a limitation of the damper placement methods, as stiffness discontinuities, weak storeys or other structural shortcomings may not be addressed.

The EDPs for 30% total damping are shown in Figure 7.12. The difference in the acceleration results between all placement methods are negligible for the four- and eight-storey structures. The drifts of the four- and eight-storey buildings do not display any large differences or meaningful patterns.

The accelerations of the 16-storey building vary greatly among the damper placement methods. As in the case of 15% damping, the methods that concentrate dampers in only a few storeys (the SSSA, the FSDA and the ESEM) exhibit large accelerations with respect to uniform damping at the storeys below the concentration of dampers.

The ULS drifts of the 16-storey building with 30% damping generally exhibit the same trends as in the 15% case. The iterative methods have poor drift control at the lower storeys without FVDs.

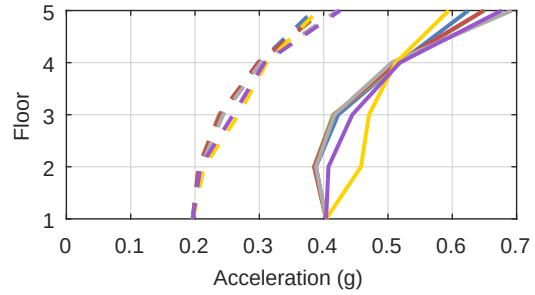

(a) Four-storey absolute acceleration

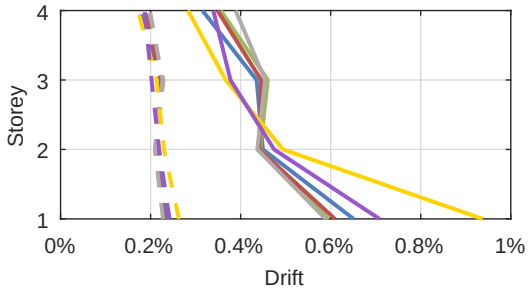

(b) Four-storey interstorey drift

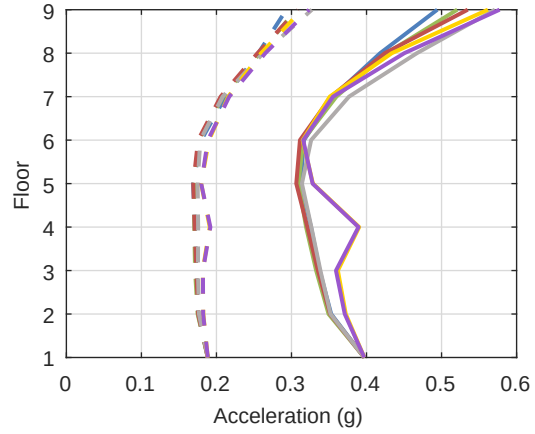

(c) Eight-storey absolute acceleration

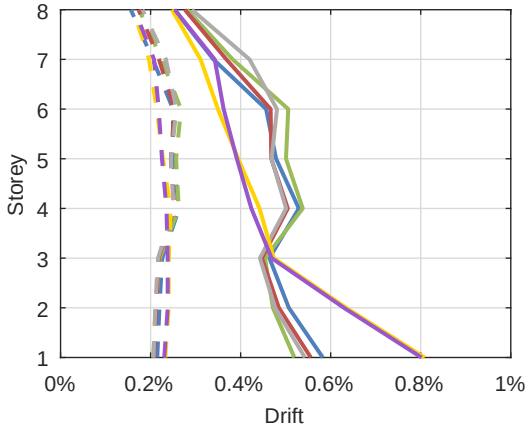

(d) Eight-storey interstorey drift

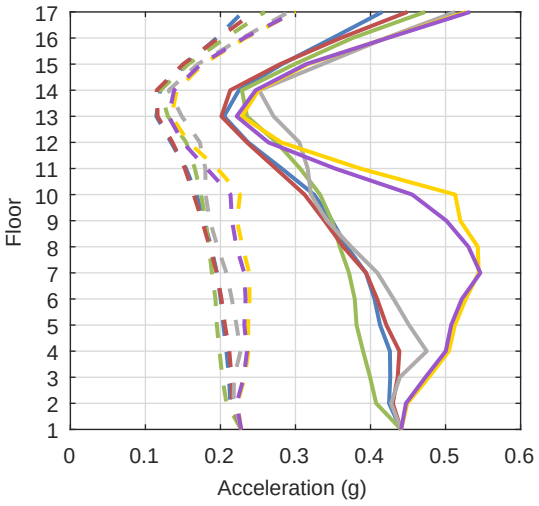

(e) 16-storey absolute acceleration

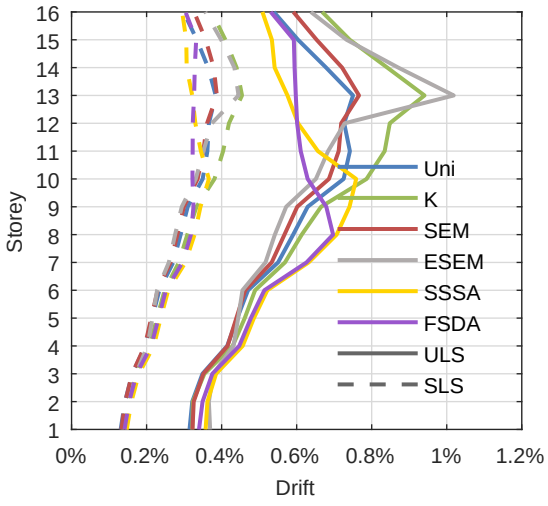

(f) 16-storey interstorey drift

Figure 7.11: Comparison of the mean peak EDPs from the different damper placement methods, 15% total damping

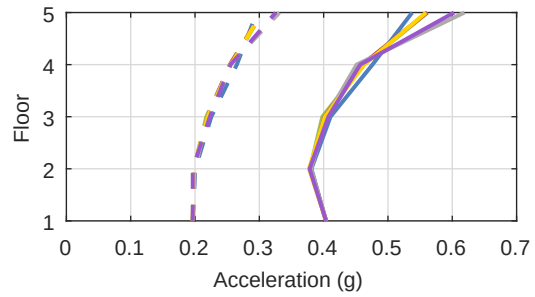

(a) Four-storey absolute acceleration

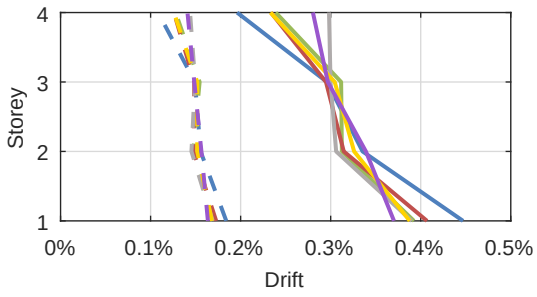

(b) Four-storey interstorey drift

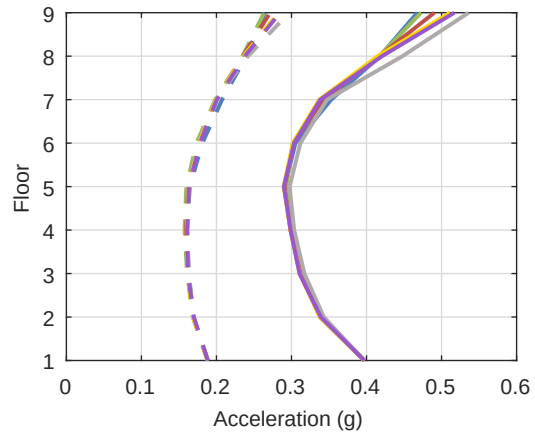

(c) Eight-storey absolute acceleration

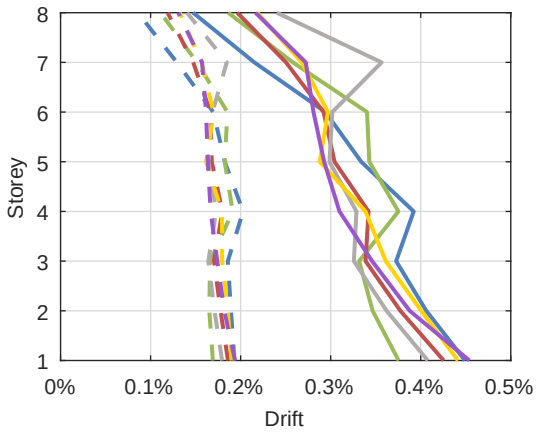

(d) Eight-storey interstorey drift

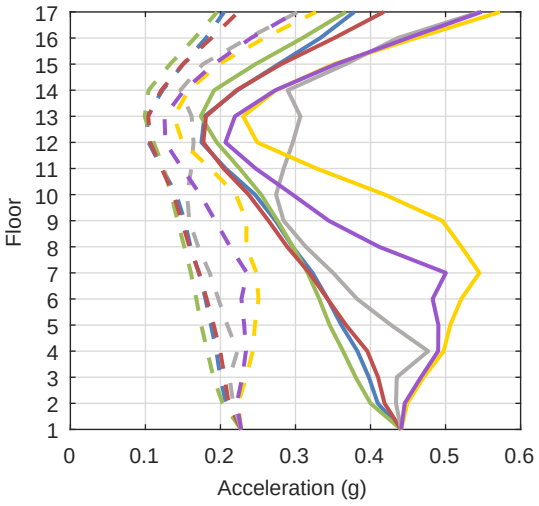

(e) 16-storey absolute acceleration

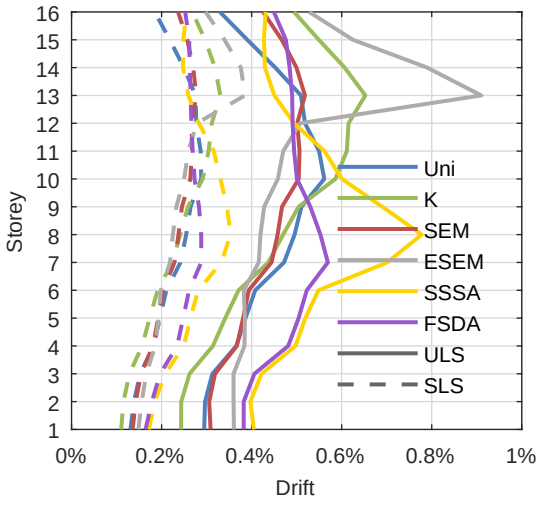

(f) 16-storey interstorey drift

Figure 7.12: Comparison of the mean peak EDPs from the different damper placement methods, 30% total damping

7.4.2 Damper Force

Examining damper forces generated by the different damper distributions can also help to distinguish between the placement methods. Damper forces can be used to measure the efficiency of damper placement and estimate the required damper investment. The damper forces generated during the time history analyses were recorded in OpenSees using the command *recorder Element* with the argument of *localForce*. The maximum absolute ULS damper forces are of interest, as they will govern the effects on adjacent structural members as well as the required damper investment (Lavan and Avishur 2013; Gidaris and Taflanidis 2015; Landi *et al.* 2015).

The maximum absolute force in each damper was determined for every ground motion analysis. The mean of these peak values per damper were then calculated. Figure 7.13 provides the resulting mean peak forces for both considered levels of total damping.

The FSDA, the SSSA and the ESEM have concentrations of damper forces, as these methods concentrate dampers in a small number of storeys. The stiffness proportional distribution also produces large damper forces in the first several storeys of the 16-storey building. These large forces must be considered during structural retrofit and local strengthening of structural members may be required.

7.4.2.1 Efficiency Ratio

Consistency between the distribution of maximum absolute damper forces and damper coefficients over the building height was proposed by Hwang *et al.* (2013) as a measure of damper placement efficiency. If the distribution of the maximum damper forces is consistent with the distribution of damping coefficients, the damping coefficients can be thought to efficiently engage in energy dissipation (Hwang *et al.* 2013; Landi *et al.* 2015). This measure of damper efficiency was examined due to its frequency in relevant literature, however the measure was not presented with robust justification by the original proposers.

As linear FVDs are used in this study, the ratio of maximum damper force to damping coefficient is the peak interstorey velocity (assuming vertical movements are minor in comparison to the horizontal motion). The SSSA should therefore produce approximately

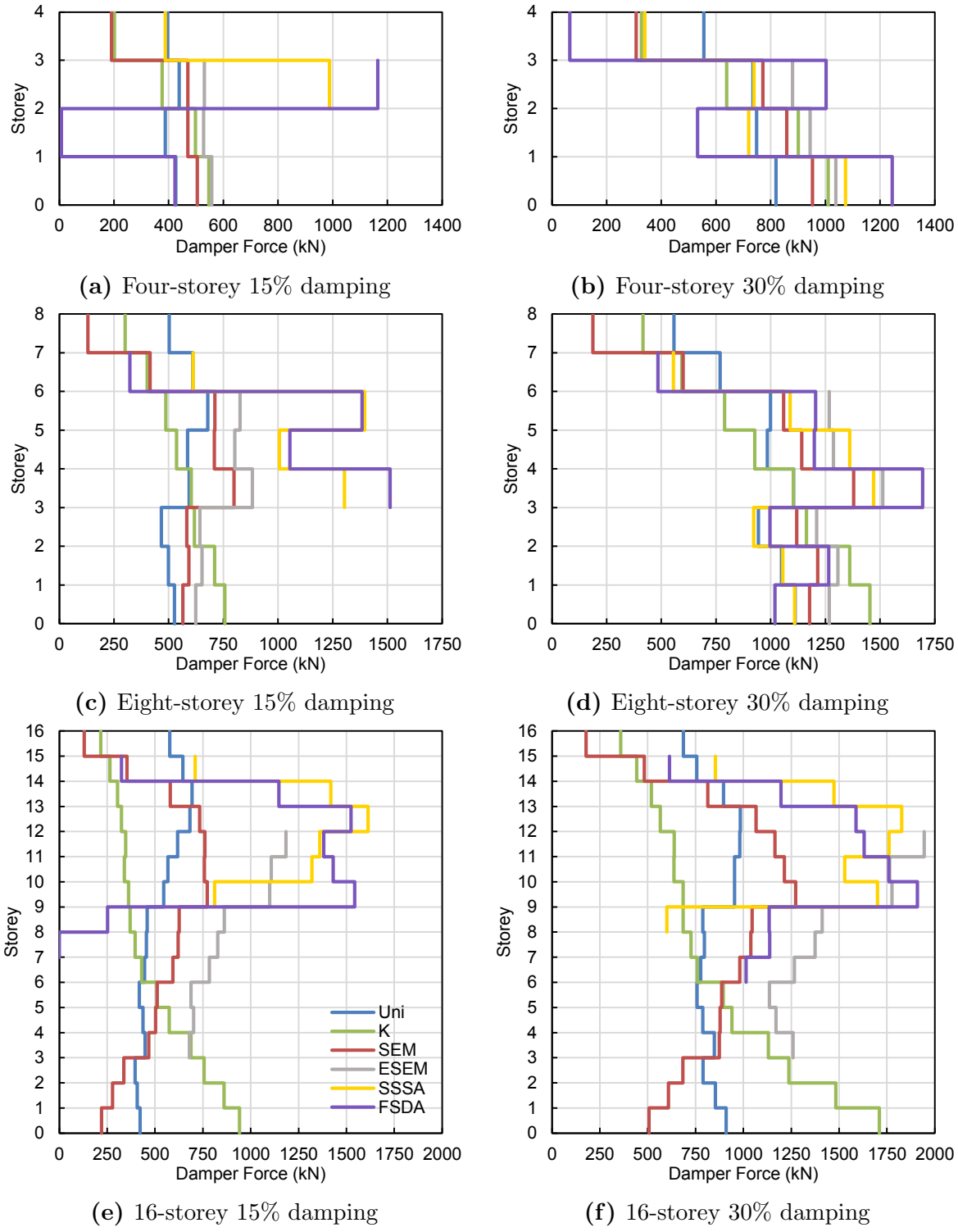

(a) Four-storey 15% damping

(b) Four-storey 30% damping

(c) Eight-storey 15% damping

(d) Eight-storey 30% damping

(e) 16-storey 15% damping

(f) 16-storey 30% damping

Figure 7.13: Mean peak damper forces per damper for the different placement methods

uniform efficiency ratios. Figure 7.14 displays the ratio of the maximum damper forces and damper coefficient (F/C ratio) per storey for each damper placement method and level of total damping considered.

The difference between the maximum and minimum F/C_j ratio increases as the total building height increases. Uniform damping produces ratios less than, and therefore less efficient than, those of stiffness proportional damping and the SEM at higher storeys as expected. The SEM and the ESEM generally produce the most favourable F/C ratios considering both levels of damping and all three building heights. However, the difference in F/C ratios between the various placement methods is minor and should not be overstated.

Damper energy dissipated per storey was investigated in Section 6.4 for uniform damping. It was found that dampers at the lower storeys dissipated the most energy for the four- and eight-storey buildings, while the middle storeys (six – 14) were the most efficient for the 16-storey building. The SEM and the ESEM generally allocated dampers to these identified storeys. This observation aligns with the favourable ratios produced by the SEM and the ESEM considering all cases with respect to the other damper placement methods.

7.4.2.2 Damper Cost

The required damper investment should be considered when evaluating FVD placement methods. Damper costs for each placement method were determined using the Gidaris and Taflanidis (2015) cost equation for commercially available dampers,

$$\text{Cost}_i = 96.88(f_{max,i})^{0.607}, \tag{7.7}$$

where Cost_i is the cost of damper i in dollars and $f_{max,i}$ is the maximum absolute force capacity of damper i in kN. As previously noted, it is recognised that this damper cost formula is an approximation and does not capture additional costs such as frame strengthening.

The total damper investment for each damper placement method was determined based on the maximum absolute ULS forces of each damper considering all time history

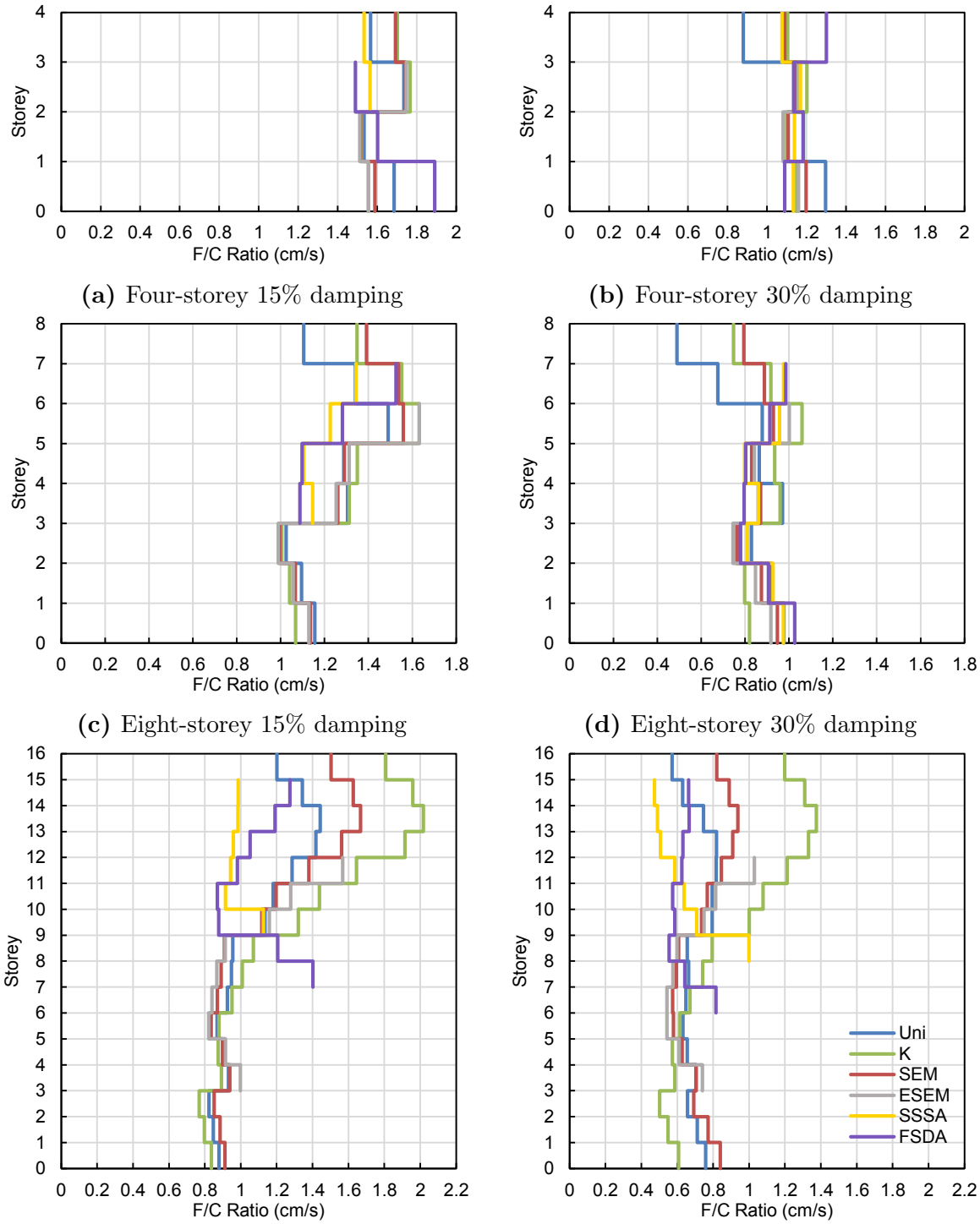

(a) Four-storey 15% damping

(b) Four-storey 30% damping

(c) Eight-storey 15% damping

(d) Eight-storey 30% damping

(e) 16-storey 15% damping

(f) 16-storey 30% damping

Figure 7.14: Ratio of the maximum damper forces and damper coefficient per storey for different placement methods

analyses. The damper investments for each method normalised by the maximum damper investment of the given building model and level of damping are shown in Figure 7.15. The maximum damper cost for each case is also indicated.

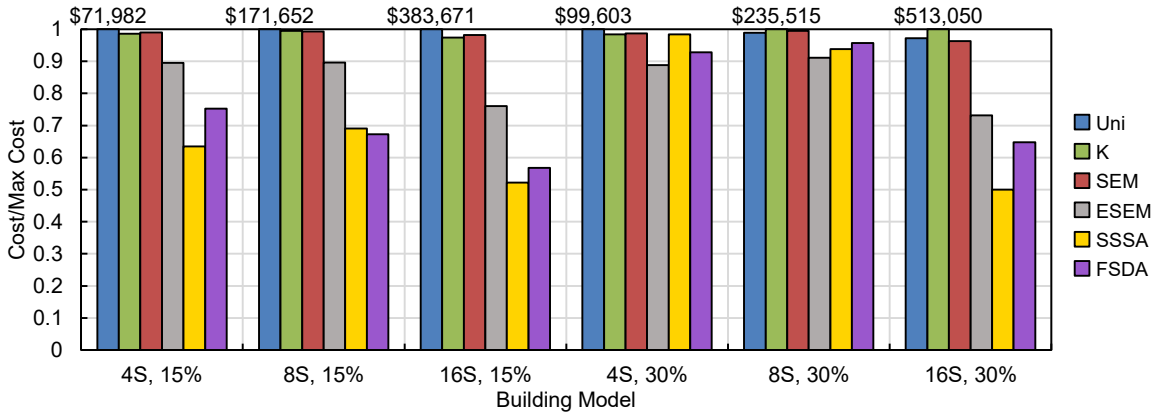

Figure 7.15: Comparison of damper costs for each placement method and building model

The iterative methods (the FSDA and the SSSA) generally produce the minimum required damper cost. The damper investment decreases by as much as 48% with respect to the maximum value. The ESEM also produces a reduction in cost to a lesser extent when considering the other non-iterative damper placement methods. The range in damper cost is greater for the lower level of damping and the larger buildings.

While the relative damper costs demonstrate significant variations, the actual dollar values must be considered to evaluate the magnitude of the damper cost range with respect to the total building cost. The damper costs for each case are listed in Table 7.4, where $\Delta_{cost,max}$ is the range in investment. All damper costs are less than 3% of the total building costs that were established in Section 4.3

Values of $\Delta_{cost,max}$ are sufficiently small to be considered generally negligible for the four- and eight-storey structures. The 16-storey structure is associated with more substantial ranges of required damper investment. The variation in damper costs for the different 16-storey placement methods may be significant depending on the corresponding changes in earthquake repair costs.

Table 7.4: Damper investment for each placement method ($1,000)

Method	15% Damping			30% Damping		
	4S	**8S**	**16S**	**4S**	**8S**	**16S**
Uniform	72	172	384	100	233	499
Stiffness	71	171	374	98	236	513
SEM	71	170	377	98	234	494
ESEM	64	154	292	89	215	375
SSSA	46	119	200	98	221	256
FSDA	54	115	218	92	225	332
$\Delta_{cost,max}$	26	56	184	11	21	257

7.5 FEMA P-58 Assessments

The EDPs from time history analyses allow seismic performance to be evaluated in repair costs using the FEMA P-58 procedure (2012b) described in Section 3.6. This evaluation enables the various damper placement methods to be compared considering total-building seismic performance. Direct repair costs in 2011 US dollars resulting from damage to building assets are calculated, while indirect costs due to building downtime are out of scope.

7.5.1 Total Repair Costs

Cumulative distribution functions of the ULS and SLS total repair costs are shown in Figure 7.16 and Figure 7.17 for 15% and 30% total damping, respectively. The effect of increasing the total level of damping from 15% to 30% on estimated repair costs was examined, as damage reductions may be offset to some extent by the additional upfront FVD expenditure. The range of median and 90th percentile ULS repair costs for each building are provided in Table 7.5, along with the maximum damper investment for comparison. It was found that the additional reductions in repair costs from increasing the damping to 30% offset the increases in the maximum damper costs.

The SLS total cost distributions for the buildings with 15% total damping (shown in Figure 7.16) do not significantly vary between the different damper placement methods. In contrast to the SLS results, the ULS total costs for 15% damping differ among the various placement methods. The SEM and uniform damper placement generally produce

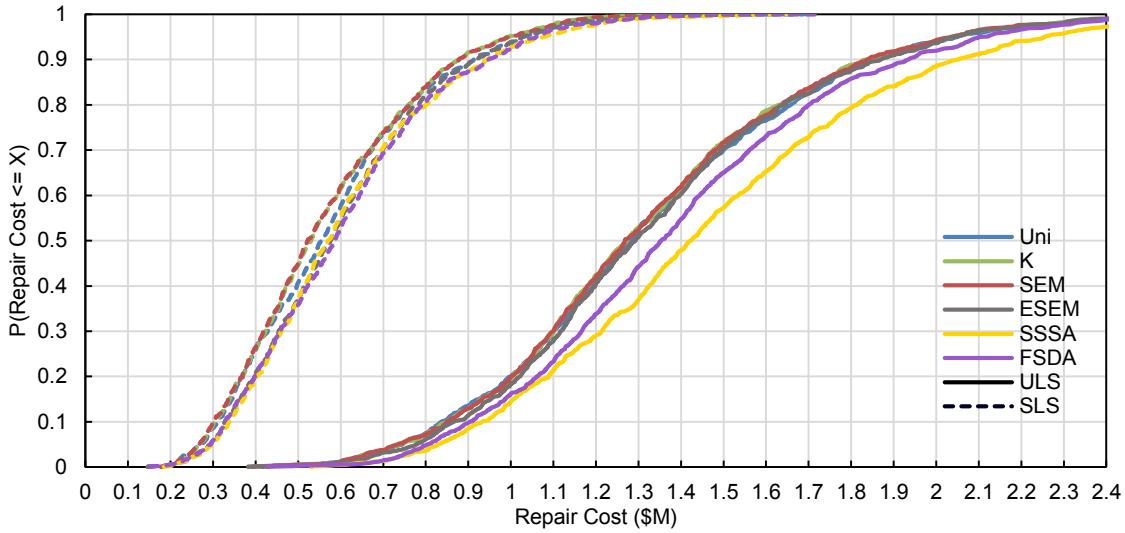

(a) Four-storey

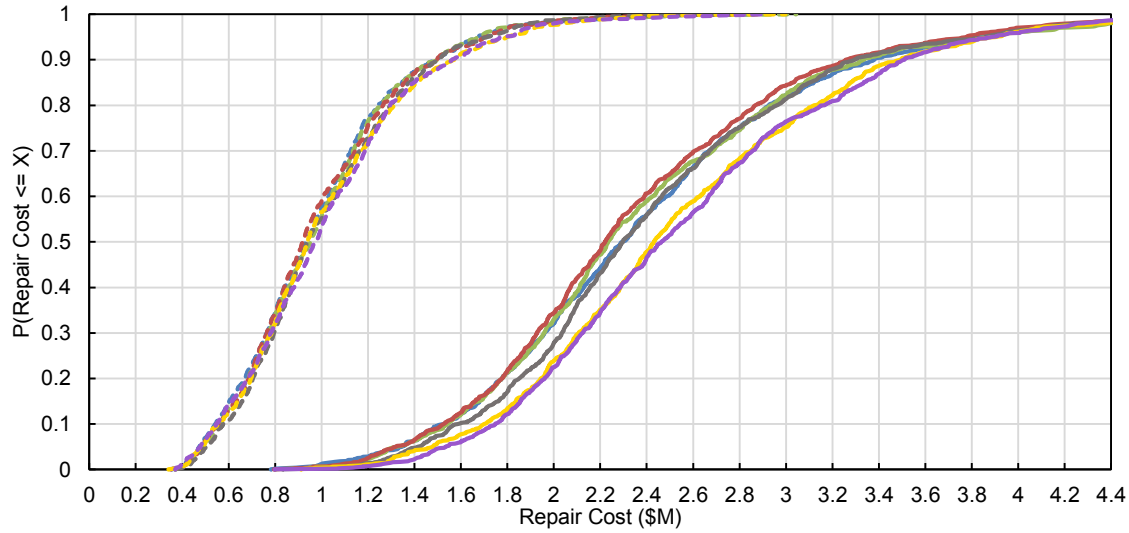

(b) Eight-storey

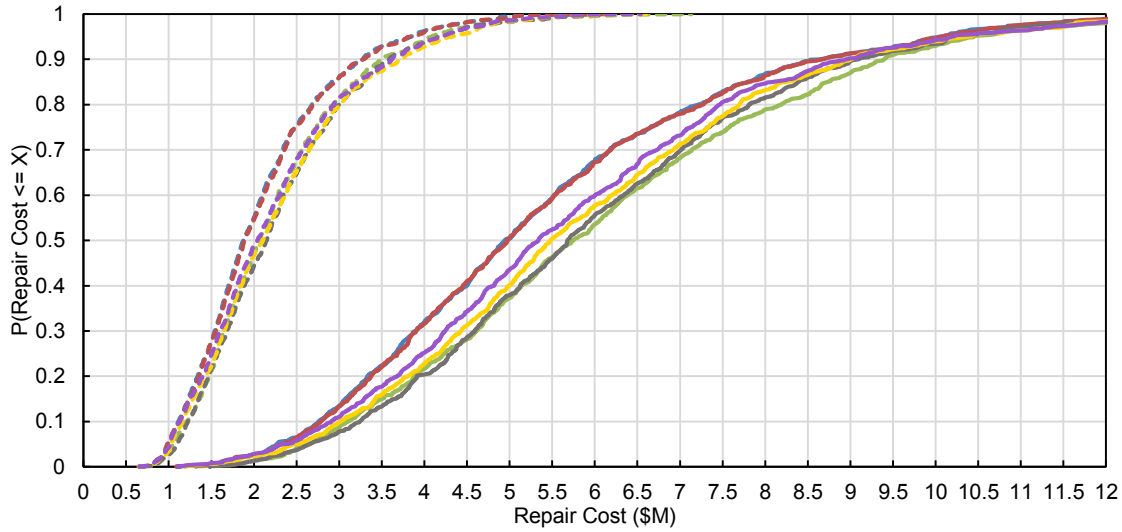

(c) 16-storey

Figure 7.16: Cumulative distribution functions of total repair costs with 15% total damping

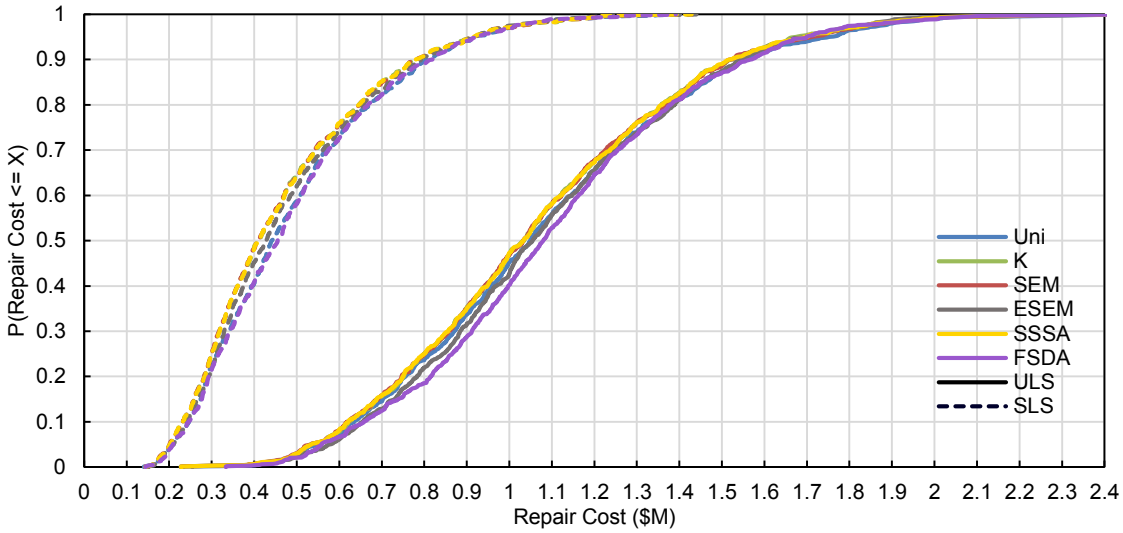

(a) Four-storey

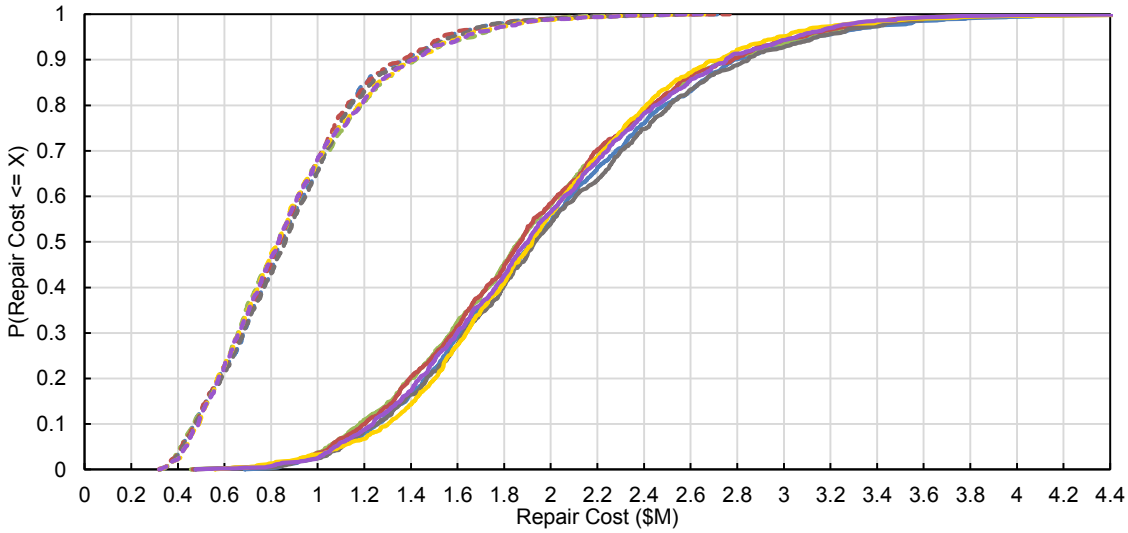

(b) Eight-storey

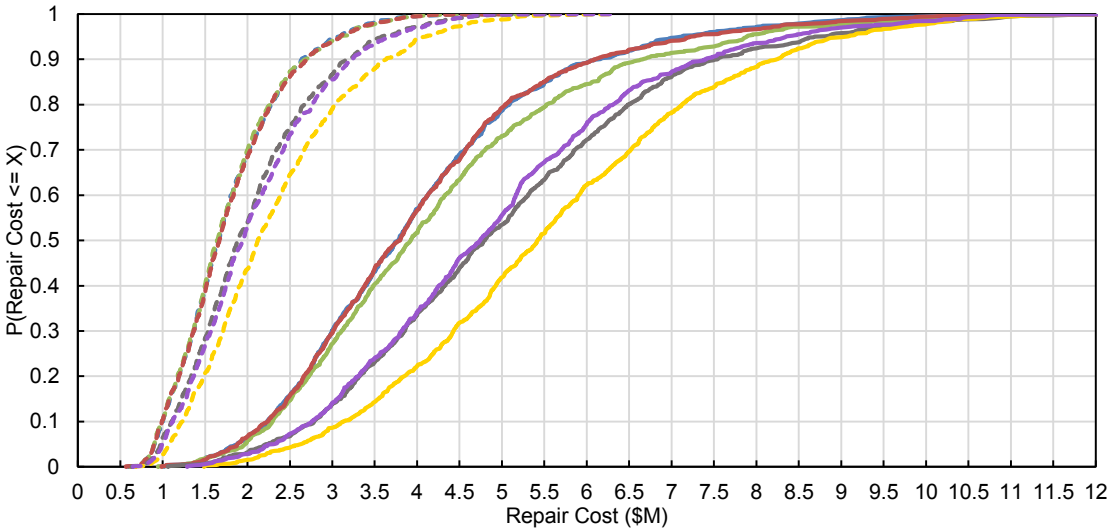

(c) 16-storey

Figure 7.17: Cumulative distribution functions of total repair costs with 30% total damping

Table 7.5: Total ULS repair costs ($M) for the different damper placement methods

Building	Damping	Median	90th Percentile	Max FVD Cost
4-Storey	15%	1.3 – 1.4	1.8 – 2.1	0.1
	30%	1.0 – 1.1	1.5 – 1.6	0.1
8-Storey	15%	2.2 – 2.5	3.3 – 3.5	0.2
	30%	1.9	2.7 – 2.8	0.2
16-Storey	15%	4.9 – 5.7	8.7 – 9.4	0.4
	30%	3.8 – 5.4	6.1 – 8.2	0.5

smaller repair costs than the other methods, while the iterative approaches (the SSSA and the FSDA) generally result in larger repair costs (the least favourable costs for the four- and eight-storey buildings).

For 30% total damping, the total repair cost distributions of the four- and eight-storey buildings do not differ for each damper placement method (refer to Figure 7.17). This holds true for both the ULS and the SLS results. For the 16-storey buildings, the earthquake damage of each placement method exhibits the same relative performance for both the ULS and the SLS. The SSSA results in significantly larger repair costs than any other method. The cost distributions for the FSDA and the ESEM are between those of the SSSA and the remaining non-iterative methods. It appears that the concentration of dampers in a small number of storeys encouraged by the SSSA, the FSDA, and the ESEM has an overall negative effect on total-building seismic performance. The SEM and uniform damping produce the smallest, and therefore most favourable, total repair costs.

Reviewing the cumulative distribution functions of the total repair costs and the relative performance of each damper placement method reveals interesting results. The findings are summarised below and are limited to linear FVDs:

1. The SEM, and notably the simplest method of uniform damping, generally produce repair costs that are more favourable than, or equal to, the other damper placement methods.

The SEM and uniform damping produce the smallest ULS repair costs for the three structures with 15% total damping and the 16-storey building with 30% damping. The

SLS repair costs for 15% damping and the repair costs of the four- and eight-storey building with 30% damping for both limit states do not vary according to the different placement approaches.

2. The iterative methods do not improve seismic performance.

Although the iterative methods attempt to optimise seismic performance, the resulting total repair costs are not reduced with respect to the other damper placement methods. The iterative methods are superficially appealing, as the required investment in dampers is less than other methods. They also purport to optimise a representative measure of seismic performance. However, the iterative methods often produced the least favourable repair cost distributions. This is a result of the iterative methods optimising parameters other than repair costs. These methods that purport to optimise seismic performance do not achieve that objective for total-building performance. Optimising for a single parameter such as drift may worsen another parameter such a floor acceleration that also has a significant impact on earthquake damage and repair cost. The methods also optimise a local parameter (drift or velocity of each storey) assuming that the performance of each local parameter is independent. In contrast, the placement of a FVD in one storey will change the performance of additional storeys. Further complexities are introduced by the total repair cost being dependent on each individual building level. The concentration of dampers in a small number of storeys encouraged by the SSSA, the FSDA, and the ESEM has an overall negative effect on total-building seismic performance.

3. It appears unlikely that large shifts in total repair cost cumulative distribution functions can be achieved using an "optimal" damper placement method. Repair cost functions are more sensitive to the level of total damping than to the damper placement method used. Damper placement optimisation may be more fruitful for taller buildings.

The results of this study revealed that the costs functions are more sensitive to the level of total damping than to the damper placement method used. Variations in the total repair

cost functions between the different methods should not be overstated, as the achieved changes in cost are comparable to the FEMA P-58 sensitivity to modelling assumptions as determined in Section 4.6. At the higher level of damping, the four- and eight-storey ULS costs did not vary among the different damper distributions. However, the repair cost distributions of the 16-storey building displayed significant variations among the different damper distributions. It is possible that damper placement optimisation may be more effective for high-rise or irregular structures.

7.5.2 Repair Costs and Engineering Demand Parameters

In order to further understand the variation in seismic performance among the different damper placement methods, repair costs from the seismic performance assessment were disaggregated using EDPs. The mean repair costs considering the associated EDP are shown in Figure 7.18 and 7.19 for 15% and 30% total damping, respectively. The eight-storey building results are excluded, as the distribution of damage considering each EDP is similar to the four-storey results. Among the considering cases, no damper placement method produces optimal costs for both IDR and acceleration.

Mean EDP repair costs for each building floor are displayed in Figure 7.20 and Figure 7.21 for 15% and 30% total damping, respectively. Results are provided for the ULS, as the SLS distributions generally did not differ significantly among the various placement methods. Floor one indicates the ground level.

For both levels of damping, the IDR costs of each storey are proportional to the peak interstorey drift recorded during the time history analyses. The most interesting result is the relative proportions of acceleration damage at the ground floor compared to all other levels. The ground floor acceleration damage is several times larger than the costs of all other levels for the eight- and 16-storey buildings. This large variation in damage is due to: (1) the concentration of expensive acceleration-sensitive nonstructural components on the ground floor that are not present on other levels such as HVAC equipment; (2) the fact that FVDs cannot reduce the peak ground floor acceleration. In order to reduce this

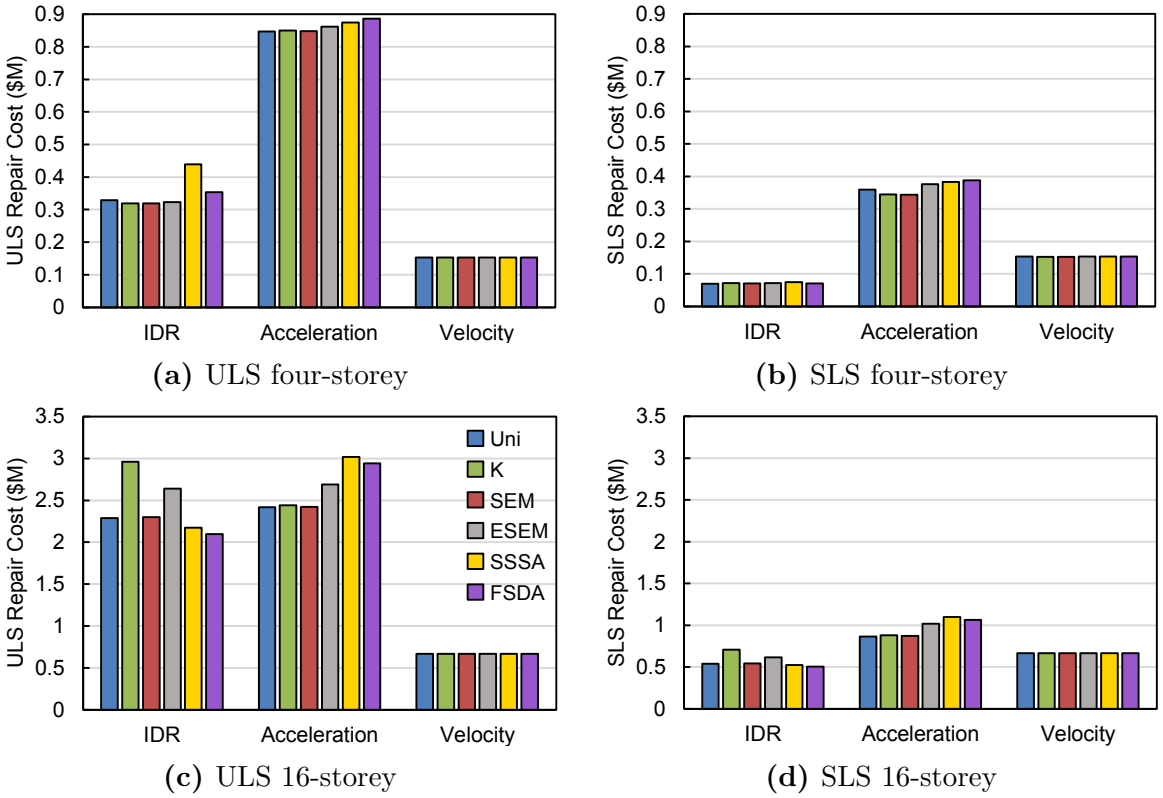

(a) ULS four-storey **(b)** SLS four-storey

(c) ULS 16-storey **(d)** SLS 16-storey

Figure 7.18: Mean repair costs grouped by associated EDP for different damper placement methods, 15% total damping

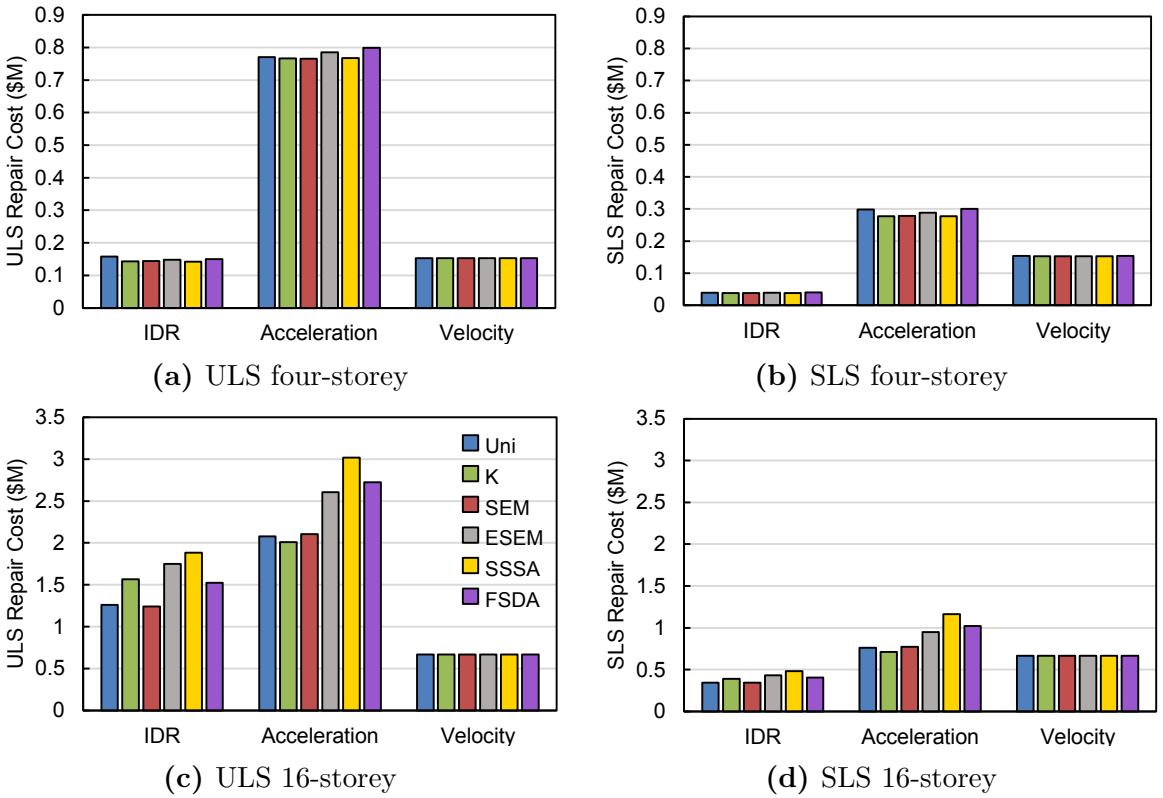

(a) ULS four-storey **(b)** SLS four-storey

(c) ULS 16-storey **(d)** SLS 16-storey

Figure 7.19: Mean repair costs grouped by associated EDP for the different damper placement methods, 30% total damping

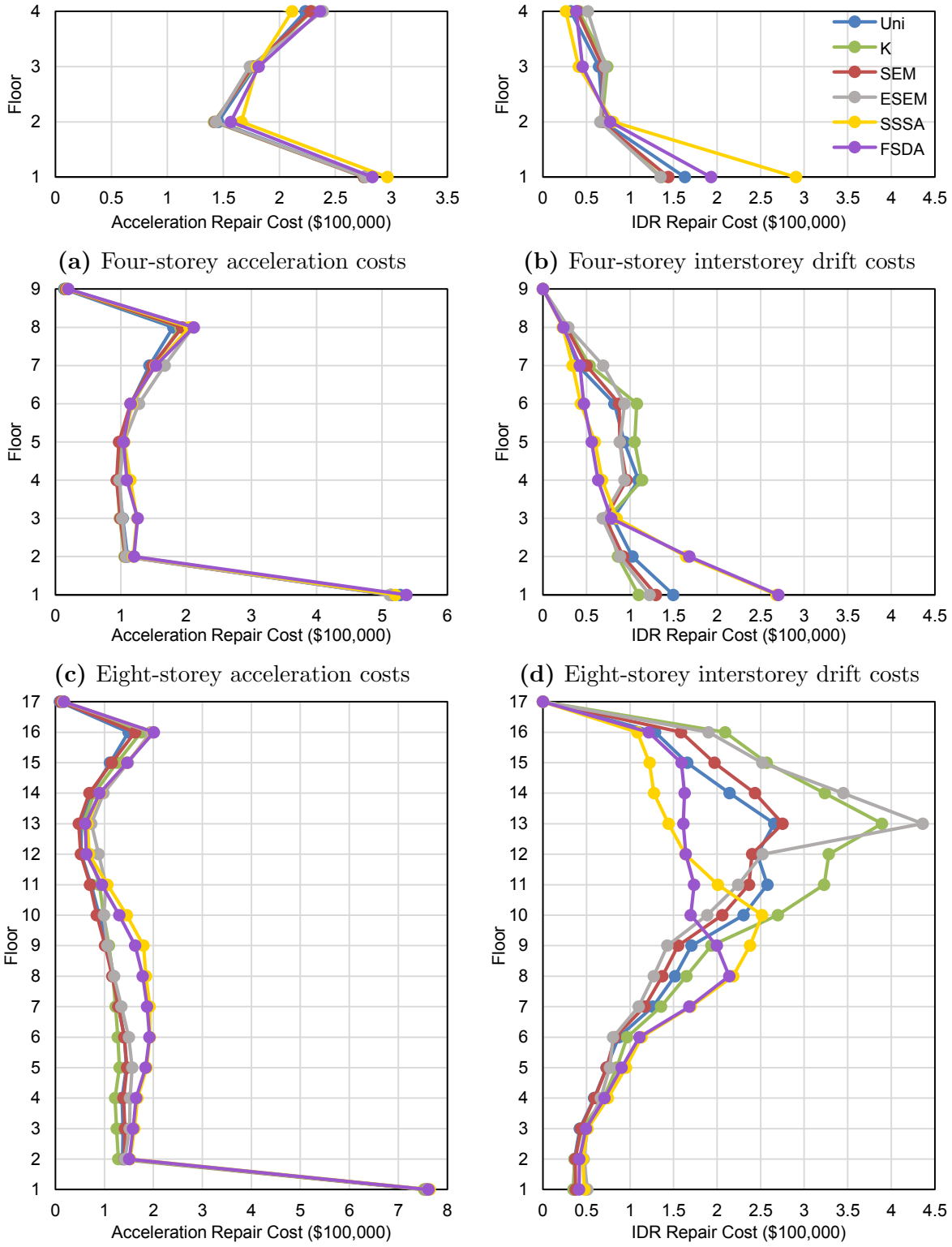

(a) Four-storey acceleration costs

(b) Four-storey interstorey drift costs

(c) Eight-storey acceleration costs

(d) Eight-storey interstorey drift costs

(e) 16-storey acceleration costs

(f) 16-storey interstorey drift costs

Figure 7.20: Comparison of the mean ULS acceleration and drift repair costs at each floor for the different damper placement methods, 15% total damping

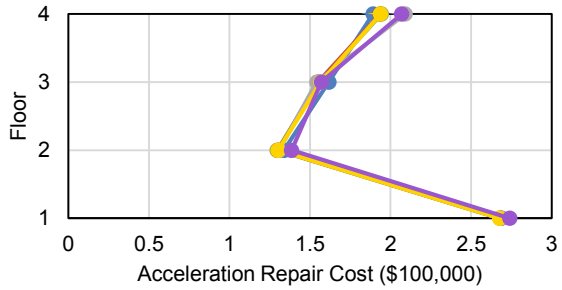

(a) Four-storey acceleration costs

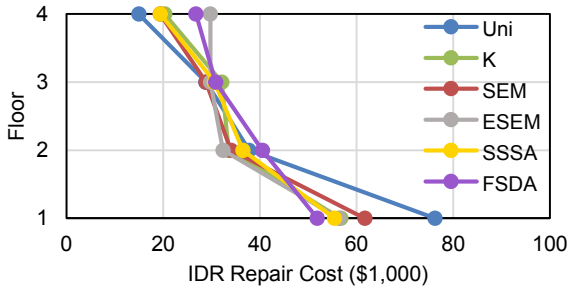

(b) Four-storey interstorey drift costs

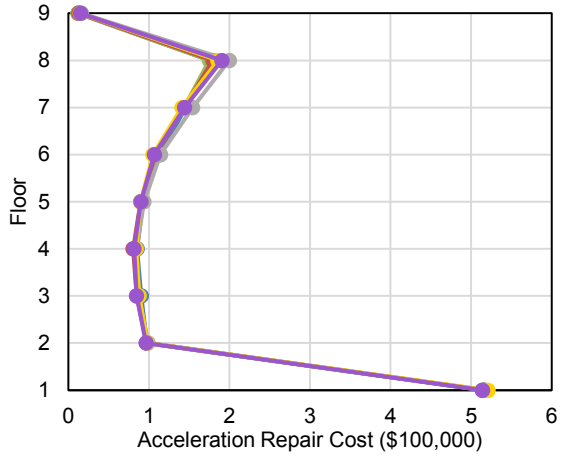

(c) Eight-storey acceleration costs

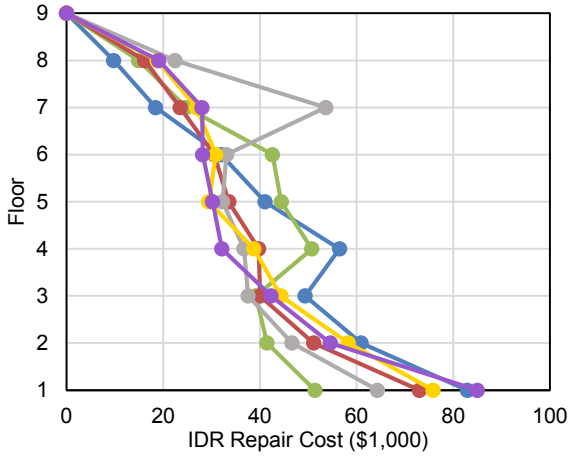

(d) Eight-storey interstorey drift costs

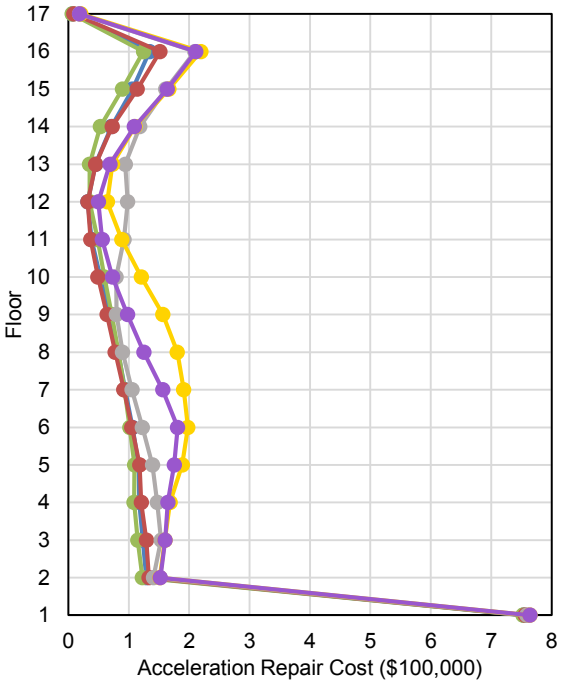

(e) 16-storey acceleration costs

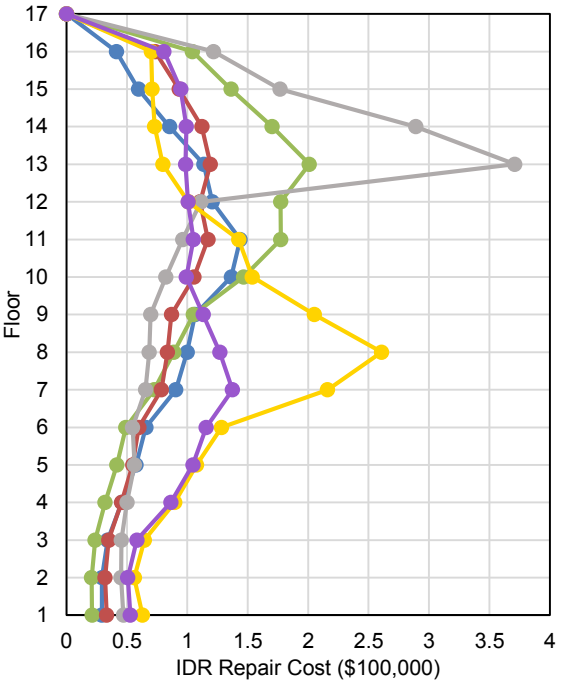

(f) 16-storey interstorey drift costs

Figure 7.21: Comparison of the mean ULS acceleration and drift repair costs at each floor for the different damper placement methods, 30% total damping

damage, another damage mitigation strategy such as individual equipment isolation of acceleration-sensitive systems on the ground level can be used.

7.6 Conclusions

The distribution of dampers within a building is a critical decision, as damper placement affects structural response and the required damper investment. While a large number of FVD placement methods have been proposed, only limited comparisons of methods have been conducted. This chapter evaluated and compared the effectiveness of several major damper placement methods considering structural and nonstructural performance in repair costs.

Six damper placement methods were selected for study. Each of these methods were chosen based on prevalence in literature and level of practicality. In order to compare the different placement techniques, the total viscous damping coefficient added to the structure was constrained to be the same value for each method. Two levels of total damping were selected: 30% as it is the lower bound of optimal damping for the standard structures, and 15% chosen to represent a smaller, more common level of damping.

Damper placement distributions are similar for the four- and eight-storey structures. At 15% damping, the SSSA and the FSDA concentrate dampers in the middle storeys. The non-iterative methods generally exhibit an even distribution of dampers excluding the top storeys. For 30% damping, all methods excluding uniform damping concentrate dampers in the lower and middle storeys. For the 16-storey building, the SEM and the ESEM allocate dampers to the middle storeys, while the iterative methods concentrate dampers in the middle to upper storeys.

Time history analyses of each structural model and damper placement method were performed in OpenSees using ground motion suites representing the ULS and the SLS. The peak absolute floor accelerations and IDRs were investigated. Differences in the SLS acceleration and drift results for all placement methods are minimal.

The iterative methods generally have poor ULS drift control at the lower storeys without FVDs and improved drift control where FVDs are concentrated with respect

to uniform damping. Stiffness proportional damping and the ESEM exhibit a large drift concentration at storey 13 for the 16-storey building. This reveals a limitation of the placement methods, as stiffness discontinuities, weak storeys or other structural shortcomings may not be addressed.

For 15% damping, the ULS accelerations display a similar pattern for all three building heights; the iterative methods have larger acceleration values at the floors below the concentration of FVDs with respect to the non-iterative methods. For 30% damping, the FVDs are more evenly distributed for the four- and eight-storey structures. As a result, the difference in the acceleration results (both ULS and SLS) between all placement methods are negligible. For the 16-storey building, the SSSA, the FSDA and the ESEM continue to concentrate dampers in only a few storeys. As a result, these methods exhibit large accelerations with respect to uniform damping at the storeys below the concentration of dampers.

No damper placement method produced optimal results when considering both IDR and acceleration. The expected earthquake damage was examined in order to clarify the effects of the various damper placement methods on seismic performance. Findings are summarised below:

1. The SEM, and notably the simplest method of uniform damping, generally produce repair costs that are more favourable than, or equal to, the other damper placement methods.

2. The iterative methods do not improve seismic performance.

The iterative methods that purport to optimise seismic performance do not achieve this objective for total-building performance. Optimising for a single parameter may worsen another parameter that also has a significant impact on earthquake damage (e.g. IDR and floor acceleration). The methods optimise a local parameter, such as interstorey drift or velocity of each storey, assuming that the performance of each local parameter is independent. In contrast, the placement of a FVD in one storey will affect the performance of additional storeys. Optimising global parameters would be more

effective. The concentration of dampers in a small number of storeys encouraged by the SSSA, the FSDA, and the ESEM has an overall negative effect on total-building seismic performance.

3. It appears unlikely that large shifts in total repair cost cumulative distribution functions can be achieved using an "optimal" damper placement method. Repair cost functions are more sensitive to the level of total damping than to the damper placement method used. Damper placement optimisation may be more fruitful for taller buildings.

The results of this study revealed that the repair cost functions are more sensitive to the level of total damping than to the damper placement method used. It appears that pursuing optimised linear FVD placement is unlikely to produce significant improvement in total earthquake repair costs for low- and mid-rise structures. To improve the total-building seismic performance of low- and mid-rise structures using linear FVDs, the SEM or uniform damping should be used with a target total damping ratio within the optimal range of 30-40%. However, the repair cost distributions of the 16-storey building displayed significant variations among the different damper distributions. This suggests that damper placement optimisation may be more successful for high-rise or irregular structures. Both absolute floor accelerations and IDRs should to be considered in any optimisation methods.

Chapter 8

Conclusions and Future Work

8.1 Overview of Chapter

Five research objectives were defined for this thesis following a literature review on the topics of nonstructural seismic performance and the use of fluid viscous dampers (FVDs) to improve total-building performance. Conclusions for each objective are summarised in Section 8.2 – 8.6. Section 8.7 explores areas for future research.

8.2 Benchmark of Code-Compliant Building Performance

Objective 1: Benchmark the total-building seismic performance of code-compliant buildings designed for seismic regions in terms of repair costs

Five concentric braced frame (CBF) building designs for seismic regions were created in accordance with the Eurocode standards (CEN 2010c). Two sets of designs were created to meet different interstorey drift ratio (IDR) limits. The seismic performance of the Eurocode-compliant buildings was benchmarked. Large repair costs were generated for both the ULS and the SLS. Median repair costs corresponding to the ULS were above the FEMA P-58 demolish limit (FEMA 2012b), suggesting that modern Eurocode structures may be demolished following a ULS earthquake. Structural damage during the SLS was predicted for the eight- and 16-storey standard designs.

Conventional building codes control drifts but do not place limitations on floor accelerations. It was observed that acceleration-sensitive damage is comparable to, or of

greater consequence than, drift-sensitive damage. The influence of acceleration on seismic performance should be more appropriately reflected in the design procedure of structures.

Nonstructural systems are treated in a simplified manner during structural design. It was found that the majority of repair costs can be attributed to these systems. Storeys satisfying the Eurocode drift limit for nonstructural protection nevertheless experienced drift- and acceleration-sensitive damage. The studied nonstructural systems are of the highest seismic design category — significant amplification of repair costs was found to occur if more vulnerable nonstructural seismic design categories or increased nonstructural quantities were considered. These results draw attention to the need for structural design procedures that enhance nonstructural seismic performance. There is a need for building-level solutions such as the use of FVDs.

8.3 Optimal Level of Damping for Total-Building Performance

Objective 2: Investigate the optimal amount of damping for structural and nonstructural seismic performance considering expected repair costs

Linear FVDs with a uniform distribution were added to the Eurocode-compliant structures. The total damping ranged from 5% to 45% in the first mode. Seismic performance assessments were conducted for the SLS and the ULS. The damping ratio-repair cost relationship was identified using the mean and 90th percentile costs. The optimal damping to minimise repair costs is between 30-40%. This is in contrast to a previously suggested optimal damping of 20-25% based on engineering demand parameters (EDPs) (Occhiuzzi 2009). This highlights that retrofit methods may be enhanced by using repair costs rather than structural parameters. It was found that decreasing IDRs past the near-optimal limit, estimated to be approximately 0.2%, cannot further reduce drift-sensitive economic losses in Eurocode-compliant CBF office buildings. This study provides insight when selecting target damping levels for structural design and retrofit.

8.4 Damping Ratio Calculation for Buildings with Fluid Viscous Dampers

Objective 3: Evaluate the energy method frequently used to approximate the supplemental damping ratio produced by FVDs

General modal analysis considering complex-valued modes was performed to determine damping ratios for structures with linear FVDs. It was found that the energy formula from Whittaker *et al.* (2003) underestimated the achieved damping ratio for the considered cases. The energy method formula was modified to improve its accuracy by incorporating the modal mass participation factor. The mean absolute relative error between the target and the achieved damping ratio was improved in comparison to the original energy method. In particular, a substantial improvement is realised for the eight- and 16-storey structures. This suggests that the modified energy formula is an improvement on the original formula and should be considered in future studies. The modified energy formula is limited to linear FVDs.

8.5 Advantages and Limitations of Fluid Viscous Dampers

Objective 4: Identify the advantages and limitations of using FVDs to improve total-building seismic performance

The standard Eurocode designs were retrofitted with linear FVDs to reach the IDR performance of the drift designs. Uniform damper placement was used. The required total damping of 37% is within the optimal range that was previously identified. The 16-storey building was unable to meet the 0.5% IDR limit during the ULS using the drift design approach. However, this limit was achieved using FVDs.

Examining the expected repair costs revealed that the FVD retrofitted buildings significantly outperform the drift designs for both the ULS and the SLS. The median ULS repair costs of the undamped buildings exceed the FEMA P-58 demolish limit (FEMA 2012b). In comparison, the 90th percentile ULS repair costs of the FVD retrofitted

buildings are below this limit. The median SLS repair costs of the FVD buildings are approximately half of the repair costs of the undamped designs. It was found that structural damage is negligible in the FVD retrofitted buildings for the ULS. Preventing structural damage is a major step towards achieving building serviceability following a ULS level earthquake. Limitations of FVD retrofit include velocity-sensitive damage and damage to acceleration-sensitive systems on the ground level. Other retrofit strategies must be incorporated to improve performance related to these parameters, such as equipment anchorage to prevent toppling due to high velocities, or isolation of acceleration-sensitive nonstructural systems on the ground level.

8.6 Optimal Damper Placement

Objective 5: Evaluate and compare the effectiveness of several major damper placement methods considering structural and nonstructural economic losses, using realistic building models, large ground motion suites and multiple earthquake intensities

The simplified sequential search algorithm (SSSA), the fully stressed design algorithm (FSDA), the storey shear strain energy method (SEM), and the efficient storey shear strain energy method (ESEM) were found to be practical damper placement methods. The simple methods of uniform and stiffness proportional damping were also considered. In order to compare the different placement techniques, the total viscous damping coefficient added to each structure was held constant for all methods. Two levels of total damping were selected: 30% as it is the lower bound of optimal damping for the standard structures, and 15% to represent a smaller, more common level of damping. It was found that the SSSA and the FSDA (iterative methods) can concentrate dampers in a limited number of storeys near the middle of the building.

Differences in SLS structural parameter results among the various placement methods were minimal. The iterative methods generally produced the least favourable ULS drifts at the lower storeys without FVDs, and improved drift control at the middle storeys where FVDs were concentrated. A limit of stiffness proportional damping and the ESEM was

identified, as stiffness discontinuities or other structural shortcomings are not addressed by these placement methods. The iterative methods have larger acceleration values at the floors below the concentration of FVDs with respect to the non-iterative methods.

No damper placement method produced optimal results when considering both IDR and acceleration. The expected earthquake damage was examined in order to clarify the effects of the various damper placement methods on seismic performance. Findings are summarised below:

1. The SEM, and notably the simplest method of uniform damping, generally produce repair costs that are more favourable than, or equal to, the other damper placement methods.

2. The iterative methods do not improve seismic performance.

The iterative methods purport to optimise seismic performance, however this objective is not achieved for total-building performance. Optimising for a single parameter may worsen another parameter that also has a significant impact on earthquake damage (e.g. interstorey drift and floor acceleration). The methods optimise a local parameter (drift or velocity of each storey) rather than a global parameter. The concentration of dampers in a small number of storeys often encouraged by the iterative methods has an overall negative effect on total-building seismic performance.

3. It appears unlikely that large shifts in total repair cost cumulative distribution functions can be achieved using an "optimal" damper placement method. Repair cost functions are more sensitive to the level of total damping than to the damper placement method used. Damper placement optimisation may be more fruitful for taller buildings.

The results of this study revealed that the repair cost functions are more sensitive to the level of total damping than to the damper placement method used. It appears that pursuing optimised FVD placement is unlikely to produce significant improvement in total earthquake repair costs for low- and mid-rise structures. To improve the total-building

seismic performance of low- and mid-rise structures using linear FVDs, the SEM or uniform damping should be used with a target total damping ratio within the optimal range of 30-40%. Damper placement optimisation may be more successful for high-rise or irregular structures. Both absolute floor accelerations and interstorey drifts should to be considered in any optimisation methods.

8.7 Future Work

Following the completion of this thesis, there are several avenues worth exploring for future research work.

The scope of the thesis was limited to Eurocode-compliant steel CBF structures. The investigated buildings could be expanded to include moment resisting and concrete structures, as well as structures designed using North American building standards. It would be valuable to determine if the optimal range of total damping deviates from that identified for the steel CBF structures, and if so, if any trends can be identified.

This thesis was one of the first studies to investigate optimal damping using repair costs and the FEMA P-58 procedure. As a result, the scope was limited to linear FVDs. It is recognized that nonlinear FVDs are often used in practice, and an obvious extension would be to consider nonlinear dampers. Investigating the effect of nonlinear dampers on the optimal damping ratio and damper placement method would be an important research contribution.

It was indicated that damper placement optimisation may be more successful for high-rise or irregular structures. It would be valuable to pursue this area of research. Both absolute floor accelerations and interstorey drifts should be considered. One promising research thrust is to explore a new damper placement method that uses simplified fragility functions defined for a typical building floor. Fragility functions that estimate total repair costs for a building floor based on the IDR and acceleration could be created using FEMA P-58, similar to the work presented in Section 5.5.4.1. These simplified fragility curves could be used as objective functions for damper placement optimisation. The developed

placement method should avoid extensive problem-specific tailoring or rely on complex techniques not familiar to practising engineers.

There is an opportunity to expand this research in the area of consequence modelling. The thesis has focused on repair costs as a basis for comparison between different damper placement options. Downtime was out of scope, as it was decided that downtime estimates were not yet sufficiently well-evolved to be reliable. However, consequence modelling is an active field of research. It is probable that new developments will enable accurate downtime estimates to be included in a future study of this type.

The focus of this thesis is on the relative performance results of different building designs and damper placement methods. Two earthquake levels defined by the Eurocode 8 uniform hazard spectrum were considered. The earthquake scenario modelling could be expanded in future research to investigate economic losses over the lifetime of the buildings. A site-specific seismic hazard curve would allow expected annual losses to be evaluated for structures with and without damper retrofit. The issue of building site selection would need to be addressed. It should also be noted that although annual costs and net present values are useful for investment decisions, the seismic performance of buildings cannot be viewed as an annuity problem in isolation. The consequences of earthquake damage are more than simply cash flows to be considered.

The total viscous damping coefficient was used to compare damper placement methods. An alternative basis for comparison, such as total retrofit cost, could also be considered. However, only approximations for damper costs are currently widely available and were considered too unreliable to be used in a robust comparison of damper placement methods. Determining more accurate cost formulas for FVDs including installation costs and using them to compare damper placement methods would be a valuable area of research.

Appendix A

Ground Motion Suites

Section 3.5 describes the selection and scaling of ground motion records. Records were obtained from the PEER ground motion database (PEER 2013). Table A.1 – A.10 provide the ground motion suites used in the performance assessments for each building. RSN refers to the record sequence number of the ground motion, Mag. refers to the magnitude of the ground motion, scale refers to the linear scale factor applied to the ground motion, and MSE is the mean squared error of the ground motion spectrum with respect to the Eurocode 8 spectrum calculated using Eq. 3.8.

Table A.1: The four-storey standard design (4S) ultimate limit state (ULS) ground motion suite

Earthquake	**Station**	**RSN**	**Mag.**	**Scale**	**MSE**
Imperial Valley-02, 1940	El Centro Array #9	6	6.95	1.2069	0.0255
Managua Nicaragua-01, 1972	Managua ESSO	95	6.24	1.1149	0.0645
Gazli USSR, 1976	Karakyr	126	6.8	0.6893	0.05
Imperial Valley-06, 1979	Delta	169	6.53	1.4044	0.0278
Westmorland, 1981	Westmorland Fire Sta	319	5.9	0.9871	0.0519
Coalinga-01, 1983	Cantua Creek School	322	6.36	1.622	0.0369
Chalfant Valley-02, 1986	Zack Brothers Ranch	558	6.19	0.7751	0.0404
Whittier Narrows-01, 1987	Compton - Castlegate St	611	5.99	1.2323	0.0161
Superstition Hills-02, 1987	El Centro Imp. Co. Cent	721	6.54	1.2138	0.0415
Loma Prieta, 1989	Palo Alto - 1900 Embarc.	786	6.93	1.4673	0.0427
Erzican Turkey, 1992	Erzincan	821	6.69	1.0932	0.0459
Big Bear-01, 1992	Desert Hot Springs	902	6.46	1.7779	0.0451
Northridge-01, 1994	Arleta - Nordhoff Fire Sta	949	6.69	1.1602	0.033
Kobe Japan, 1995	Shin-Osaka	1116	6.9	1.5623	0.0552
Dinar Turkey, 1995	Dinar	1141	6.4	1.1007	0.0701
Kocaeli Turkey, 1999	Duzce	1158	7.51	1.2637	0.0397
Chi-Chi Taiwan, 1999	TCU055	1495	7.62	1.4795	0.0574
Chi-Chi Taiwan-03, 1999	TCU065	2618	6.2	1.8828	0.0787
Parkfield-02 CA, 2004	PARKFIELD - UPSAR 10	4146	6	1.5421	0.0337
Friuli (aftershock 9) Italy, 1976	Buia	4276	5.5	1.8704	0.0502
Chuetsu-oki Japan, 2007	NIG018	5264	6.8	0.7829	0.0193
Iwate Japan, 2008	Nakashinden Town	5774	6.9	1.8091	0.0447
El Mayor-Cucapah Mexico, 2010	Chihuahua	5823	7.2	1.5505	0.0265
Darfield New Zealand, 2010	Kaiapoi North School	6923	7	1.2294	0.0253
Christchurch New Zealand, 2011	Christchurch Botanical Gardens	8063	6.2	0.8172	0.0294

Table A.2: The 4S serviceability limit state (SLS) ground motion suite

Earthquake	**Station**	**RSN**	**Mag.**	**Scale**	**MSE**
Imperial Valley-02, 1940	El Centro Array #9	6	6.95	0.6069	0.0255
Northern Calif-03, 1954	Ferndale City Hall	20	6.5	1.1649	0.0329
Point Mugu, 1973	Port Hueneme	97	5.65	1.8583	0.0315
Imperial Valley-06, 1979	Delta	169	6.53	0.7062	0.0278
Victoria Mexico, 1980	Chihuahua	266	6.33	1.2	0.0305
Coalinga-01, 1983	Cantua Creek School	322	6.36	0.8156	0.0369
Morgan Hill, 1984	Halls Valley	461	6.19	1.0438	0.0356
Taiwan SMART1(45), 1986	SMART1 O08	582	7.3	1.3726	0.0341
Whittier Narrows-01, 1987	Compton - Castlegate St	611	5.99	0.6197	0.0161
Loma Prieta, 1989	Fremont - Emerson Court	761	6.93	1.3331	0.0138
Northridge-01, 1994	Manhattan Beach - Manhattan	1035	6.69	1.2179	0.0188
Kobe Japan, 1995	Sakai	1115	6.9	1.1217	0.0379
Kocaeli Turkey, 1999	Zeytinburnu	1177	7.51	1.9258	0.0293
Chi-Chi Taiwan, 1999	TCU098	1526	7.62	1.5554	0.0125
Manjil Iran, 1990	Abhar	1634	7.37	1.2154	0.0345
Northridge-06, 1994	Sylmar - Converter Sta	1736	5.28	1.036	0.036
Chi-Chi Taiwan-03, 1999	CHY101	2507	6.2	1.5489	0.0376
Whittier Narrows-02, 1987	Bell Gardens - Jaboneria	3687	5.27	1.7242	0.0379
Chi-Chi Taiwan-06, 1999	CHY004	3864	6.3	1.9193	0.0275
Parkfield-02 CA, 2004	Parkfield - Fault Zone 15	4117	6	1.255	0.0275
Niigata Japan, 2004	FKS028	4159	6.63	1.4788	0.0386
Chuetsu-oki Japan, 2007	Hinodecho Yoshida Tsubame City	4880	6.8	1.489	0.0361
El Mayor-Cucapah Mexico, 2010	Chihuahua	5823	7.2	0.7797	0.0265
Darfield New Zealand, 2010	Kaiapoi North School	6923	7	0.6182	0.0253
Christchurch New Zealand, 2011	LINC	8102	6.2	1.791	0.0309

Table A.3: The eight-storey standard design (8S) ULS ground motion suite

Earthquake	**Station**	**RSN**	**Mag.**	**Scale**	**MSE**
Imperial Valley-02, 1940	El Centro Array #9	6	6.95	1.3217	0.0312
Managua Nicaragua-01, 1972	Managua ESSO	95	6.24	1.3233	0.0844
Gazli USSR, 1976	Karakyr	126	6.8	0.7409	0.0344
Imperial Valley-06, 1979	Delta	169	6.53	1.5527	0.0331
Westmorland, 1981	Westmorland Fire Sta	319	5.9	0.994	0.0535
Coalinga-01, 1983	Pleasant Valley P.P. - bldg	367	6.36	1.1072	0.0444
N. Palm Springs, 1986	North Palm Springs	529	6.06	0.8586	0.0567
Chalfant Valley-02, 1986	Zack Brothers Ranch	558	6.19	0.8604	0.0784
Superstition Hills-02, 1987	El Centro Imp. Co. Cent	721	6.54	1.2911	0.0264
Loma Prieta, 1989	Hollister Differential Array	778	6.93	1.341	0.0533
Big Bear-01, 1992	Desert Hot Springs	902	6.46	1.9301	0.0902
Northridge-01, 1994	LA - Hollywood Stor FF	995	6.69	1.8409	0.0353
Kobe Japan, 1995	Kakogawa	1107	6.9	1.8314	0.0654
Dinar Turkey, 1995	Dinar	1141	6.4	0.9597	0.084
Kocaeli Turkey, 1999	Duzce	1158	7.51	1.2304	0.0372
Chi-Chi Taiwan, 1999	TCU055	1495	7.62	1.3825	0.0431
Duzce Turkey, 1999	Duzce	1605	7.14	0.8506	0.0988
Taiwan SMART1(45), 1986	SMART1 M04	3674	7.3	1.9297	0.0229
Parkfield-02 CA, 2004	Parkfield - Fault Zone 7	4111	6	1.7026	0.0641
Umbria Marche (foreshock) Italy, 1997	Colfiorito	4337	5.7	1.5799	0.1008
Chuetsu-oki Japan, 2007	Sanjo Shinbori	4860	6.8	1.1128	0.0483
Iwate Japan, 2008	Nakashinden Town	5774	6.9	1.9307	0.0418
El Mayor-Cucapah Mexico, 2010	Calexico Fire Station	5975	7.2	1.6381	0.0265
Darfield New Zealand, 2010	Christchurch Cashmere High School	6890	7	1.4672	0.037
Christchurch New Zealand, 2011	Christchurch Hospital	8066	6.2	0.8965	0.0497

Table A.4: The 8S SLS ground motion suite

Earthquake	**Station**	**RSN**	**Mag.**	**Scale**	**MSE**
Imperial Valley-02, 1940	El Centro Array #9	6	6.95	0.6652	0.0312
Point Mugu, 1973	Port Hueneme	97	5.65	1.769	0.04
Tabas Iran, 1978	Boshrooyeh	138	7.35	1.796	0.0525
Imperial Valley-06, 1979	Delta	169	6.53	0.7814	0.0331
Victoria Mexico, 1980	Chihuahua	266	6.33	1.096	0.0531
Coalinga-01, 1983	Pleasant Valley P.P. - bldg	367	6.36	0.5572	0.0444
N. Palm Springs, 1986	Palm Springs Airport	530	6.06	1.6566	0.0535
Superstition Hills-02, 1987	El Centro Imp. Co. Cent	721	6.54	0.6498	0.0264
Loma Prieta, 1989	Sunnyvale - Colton Ave.	806	6.93	1.0393	0.0531
Landers, 1992	Indio - Coachella Canal	862	7.28	1.7294	0.0414
Big Bear-01, 1992	San Bernardino - 2nd & Arrowhead	930	6.46	1.8387	0.0485
Northridge-01, 1994	LA - Pico & Sentous	1000	6.69	1.8434	0.0348
Kobe Japan, 1995	Sakai	1115	6.9	1.164	0.0418
Kocaeli Turkey, 1999	Duzce	1158	7.51	0.6192	0.0372
Chi-Chi Taiwan, 1999	TCU098	1526	7.62	1.4854	0.0223
Manjil Iran, 1990	Rudsar	1637	7.37	1.8744	0.0368
Chi-Chi Taiwan-04, 1999	CHY088	2744	6.2	1.8106	0.0494
Chi-Chi Taiwan-06, 1999	CHY039	3277	6.3	1.648	0.019
Taiwan SMART1(40), 1986	SMART1 O02	3653	6.32	1.3647	0.0526
Taiwan SMART1(45), 1986	SMART1 M04	3674	7.3	0.9712	0.0229
Parkfield-02 CA, 2004	PARKFIELD - VINEYARD CANYON	4074	6	1.0739	0.027
Chuetsu-oki Japan, 2007	Hinodecho Yoshida Tsubame City	4880	6.8	1.5608	0.0326
Iwate Japan, 2008	Nakashinden Town	5774	6.9	0.9717	0.0418
El Mayor-Cucapah Mexico, 2010	Calexico Fire Station	5975	7.2	0.8244	0.0265
Darfield New Zealand, 2010	Christchurch Cashmere High School	6890	7	0.7384	0.037

Table A.5: The 16-storey standard design (16S) ULS ground motion suite

Earthquake	**Station**	**RSN**	**Mag.**	**Scale**	**MSE**
Imperial Valley-02, 1940	El Centro Array #9	6	6.95	1.3436	0.0385
Managua Nicaragua-01, 1972	Managua ESSO	95	6.24	1.7129	0.1068
Imperial Valley-06, 1979	Chihuahua	165	6.53	1.6993	0.0597
Victoria Mexico, 1980	Chihuahua	266	6.33	1.6965	0.1277
Coalinga-01, 1983	Cantua Creek School	322	6.36	1.5789	0.0867
Coalinga-05, 1983	Pleasant Valley P.P. - yard	412	5.77	1.8945	0.108
N. Palm Springs, 1986	North Palm Springs	529	6.06	0.9807	0.0695
Chalfant Valley-02, 1986	Zack Brothers Ranch	558	6.19	1.3714	0.1368
Taiwan SMART1(45), 1986	SMART1 O07	581	7.3	1.7406	0.0543
Superstition Hills-02, 1987	El Centro Imp. Co. Cent	721	6.54	1.1342	0.0476
Loma Prieta, 1989	Hollister - South & Pine	776	6.93	0.6616	0.0135
Northridge-01, 1994	Northridge - 17645 Saticoy St	1048	6.69	1.2503	0.0367
Kobe Japan, 1995	Shin-Osaka	1116	6.9	1.319	0.0541
Dinar Turkey, 1995	Dinar	1141	6.4	0.9108	0.0863
Chi-Chi Taiwan, 1999	ILA013	1317	7.62	1.5504	0.0584
Hector Mine, 1999	Mecca - CVWD Yard	1810	7.13	1.9196	0.1076
Taiwan SMART1(40), 1986	SMART1 O03	3654	6.32	1.896	0.0577
Landers, 1992	Indio - Jackson Road	3754	7.28	1.2324	0.0844
Parkfield-02 CA, 2004	PARKFIELD - 1-STORY SCHOOL BLDG	4084	6	1.4336	0.1006
Niigata Japan, 2004	NIG017	4207	6.63	1.2771	0.0472
Chuetsu-oki Japan, 2007	Kashiwazaki NPP Unit 5: ground surface	4895	6.8	0.6536	0.0162
Iwate Japan, 2008	Misato Miyagi Kitaura - A	5781	6.9	1.8352	0.1556
El Mayor-Cucapah Mexico, 2010	El Centro Array #11	5992	7.2	1.0131	0.0905
Darfield New Zealand, 2010	Kaiapoi North School	6923	7	1.1757	0.105
Christchurch New Zealand, 2011	Papanui High School	8118	6.2	1.2438	0.0358

Table A.6: The 16S SLS ground motion suite

Earthquake	**Station**	**RSN**	**Mag.**	**Scale**	**MSE**
Imperial Valley-02, 1940	El Centro Array #9	6	6.95	0.6812	0.0385
Parkfield, 1966	Cholame - Shandon Array #5	30	6.19	1.1859	0.0623
Managua Nicaragua-02, 1972	Managua ESSO	96	5.2	1.0238	0.0333
Imperial Valley-06, 1979	Chihuahua	165	6.53	0.8616	0.0597
Westmorland, 1981	Salton Sea Wildlife Refuge	317	5.9	1.4957	0.0347
Coalinga-01, 1983	Parkfield - Fault Zone 7	345	6.36	1.0477	0.044
Morgan Hill, 1984	Gilroy Array #3	457	6.19	1.8027	0.0517
N. Palm Springs, 1986	Desert Hot Springs	517	6.06	0.9851	0.0369
Taiwan SMART1(45), 1986	SMART1 O07	581	7.3	0.8825	0.0543
Superstition Hills-02, 1987	El Centro Imp. Co. Cent	721	6.54	0.575	0.0476
Loma Prieta, 1989	Coyote Lake Dam (Downst)	754	6.93	1.7465	0.0295
Landers, 1992	North Palm Springs	882	7.28	1.4777	0.0354
Big Bear-01, 1992	San Bernardino - E & Hospitality	931	6.46	1.4056	0.051
Northridge-01, 1994	Camarillo	958	6.69	1.1836	0.0296
Kobe Japan, 1995	Kakogawa	1107	6.9	1.0177	0.062
Chi-Chi Taiwan, 1999	TAP095	1456	7.62	1.1896	0.0286
Manjil Iran, 1990	Rudsar	1637	7.37	1.8992	0.0432
Chi-Chi Taiwan-06, 1999	CHY037	3276	6.3	1.1374	0.068
Taiwan SMART1(40), 1986	SMART1 O02	3653	6.32	1.2528	0.0219
Parkfield-02 CA, 2004	Parkfield - Vineyard Cany 3W	4134	6	1.3402	0.0427
Niigata Japan, 2004	NIG017	4207	6.63	0.6475	0.0472
Chuetsu-oki Japan, 2007	NIG022	5268	6.8	1.8104	0.0291
Iwate Japan, 2008	Yoneyamacho Tome City	5785	6.9	0.9853	0.077
Darfield New Zealand, 2010	LRSC	6930	7	1.7693	0.0311
Christchurch New Zealand, 2011	Papanui High School	8118	6.2	0.6306	0.0358

Table A.7: The four-storey drift design (4D) ULS ground motion suite

Earthquake	**Station**	**RSN**	**Mag.**	**Scale**	**MSE**
Imperial Valley-02, 1940	El Centro Array #9	6	6.95	1.215	0.0243
Managua Nicaragua-01, 1972	Managua ESSO	95	6.24	1.0805	0.052
Imperial Valley-06, 1979	Delta	169	6.53	1.3982	0.027
Westmorland, 1981	Westmorland Fire Sta	319	5.9	1.0142	0.0443
Coalinga-01, 1983	Cantua Creek School	322	6.36	1.7321	0.036
Coalinga-05, 1983	Burnett Construction	405	5.77	1.4346	0.0317
Morgan Hill, 1984	Halls Valley	461	6.19	1.9666	0.0217
Chalfant Valley-02, 1986	Zack Brothers Ranch	558	6.19	0.7454	0.0184
Whittier Narrows-01, 1987	Santa Fe Springs - E.Joslin	692	5.99	0.861	0.0235
Superstition Hills-02, 1987	El Centro Imp. Co. Cent	721	6.54	1.226	0.04
Loma Prieta, 1989	Oakland - Outer Harbor Wharf	783	6.93	1.5169	0.0239
Erzican Turkey, 1992	Erzincan	821	6.69	1.189	0.009
Big Bear-01, 1992	Desert Hot Springs	902	6.46	1.8219	0.0424
Northridge-01, 1994	Canyon Country - W Lost Cany	960	6.69	0.9214	0.0267
Kocaeli Turkey, 1999	Duzce	1158	7.51	1.3036	0.0445
Chi-Chi Taiwan, 1999	CHY036	1203	7.62	1.503	0.0541
Northwest China-03, 1997	Jiashi	1752	6.1	1.442	0.0471
Chi-Chi Taiwan-06, 1999	CHY082	3306	6.3	1.9544	0.0217
Parkfield-02 CA, 2004	PARKFIELD - UPSAR 10	4146	6	1.5226	0.0294
Friuli (aftershock 9) Italy, 1976	Buia	4276	5.5	1.9422	0.0493
Chuetsu-oki Japan, 2007	NIG018	5264	6.8	0.7921	0.0142
Iwate Japan, 2008	Furukawa Osaki City	5814	6.9	1.6951	0.0339
El Mayor-Cucapah Mexico, 2010	Chihuahua	5823	7.2	1.6009	0.0185
Darfield New Zealand, 2010	Kaiapoi North School	6923	7	1.2379	0.0175
Christchurch New Zealand, 2011	Christchurch Botanical Gardens	8063	6.2	0.8137	0.022

Table A.8: The 4D SLS ground motion suite

Earthquake	**Station**	**RSN**	**Mag.**	**Scale**	**MSE**
Imperial Valley-02, 1940	El Centro Array #9	6	6.95	0.6103	0.0243
Northern Calif-03, 1954	Ferndale City Hall	20	6.5	1.2305	0.0231
Imperial Valley-06, 1979	Delta	169	6.53	0.7024	0.027
Imperial Valley-07, 1979	El Centro Array #2	200	5.01	1.4421	0.0268
Victoria Mexico, 1980	Chihuahua	266	6.33	1.1843	0.0292
Coalinga-02, 1983	TRA (temp)	388	5.09	1.6795	0.0306
Coalinga-05, 1983	Burnett Construction	405	5.77	0.7207	0.0317
Morgan Hill, 1984	Halls Valley	461	6.19	0.9879	0.0217
Taiwan SMART1(45), 1986	SMART1 O08	582	7.3	1.455	0.018
Whittier Narrows-01, 1987	Downey - Co Maint Bldg	615	5.99	0.8958	0.0245
Loma Prieta, 1989	Fremont - Emerson Court	761	6.93	1.3128	0.0136
Erzican Turkey, 1992	Erzincan	821	6.69	0.5973	0.009
Northridge-01, 1994	Manhattan Beach - Manhattan	1035	6.69	1.2251	0.0145
Chi-Chi Taiwan, 1999	TCU098	1526	7.62	1.5974	0.0177
Northridge-06, 1994	Sylmar - Converter Sta	1736	5.28	1.0238	0.0312
Hector Mine, 1999	Baker Fire Station	1766	7.13	1.3799	0.0237
Taiwan SMART1(40), 1986	SMART1 O08	3658	6.32	1.7456	0.0162
Whittier Narrows-02, 1987	Bell Gardens - Jaboneria	3687	5.27	1.6057	0.0195
Chi-Chi Taiwan-06, 1999	CHY002	3863	6.3	1.0203	0.0129
Parkfield-02 CA, 2004	PARKFIELD - 1-STORY SCHOOL BLDG	4084	6	0.999	0.0179
Iwate Japan, 2008	Minamikatamachi Tore City	5786	6.9	1.2355	0.0223
El Mayor-Cucapah Mexico, 2010	Chihuahua	5823	7.2	0.8042	0.0185
Tottori Japan, 2000	HRS014	6207	6.61	1.9636	0.0311
Darfield New Zealand, 2010	Kaiapoi North School	6923	7	0.6218	0.0175
Christchurch New Zealand, 2011	LINC	8102	6.2	1.8155	0.0229

Table A.9: The eight-storey drift design (8D) ULS ground motion suite

Earthquake	**Station**	**RSN**	**Mag.**	**Scale**	**MSE**
Imperial Valley-02, 1940	El Centro Array #9	6	6.95	1.2383	0.0186
Managua Nicaragua-01, 1972	Managua ESSO	95	6.24	1.1713	0.08
Gazli USSR, 1976	Karakyr	126	6.8	0.7137	0.0363
Coalinga-01, 1983	Cantua Creek School	322	6.36	1.5345	0.0312
Coalinga-05, 1983	Burnett Construction	405	5.77	1.6134	0.1098
Morgan Hill, 1984	Gilroy Array #4	458	6.19	1.7154	0.1165
N. Palm Springs, 1986	North Palm Springs	529	6.06	0.7979	0.0993
Chalfant Valley-02, 1986	Zack Brothers Ranch	558	6.19	0.8053	0.0559
Whittier Narrows-01, 1987	Compton - Castlegate St	611	5.99	1.2781	0.0211
Superstition Hills-02, 1987	El Centro Imp. Co. Cent	721	6.54	1.219	0.0388
Loma Prieta, 1989	Palo Alto - 1900 Embarc.	786	6.93	1.3582	0.0554
Erzican Turkey, 1992	Erzincan	821	6.69	1.0137	0.0755
Big Bear-01, 1992	Desert Hot Springs	902	6.46	1.7695	0.0469
Northridge-01, 1994	Arleta - Nordhoff Fire Sta	949	6.69	1.1646	0.0325
Dinar Turkey, 1995	Dinar	1141	6.4	1.0289	0.078
Kocaeli Turkey, 1999	Duzce	1158	7.51	1.2435	0.0384
Chi-Chi Taiwan-03, 1999	TCU065	2618	6.2	1.8394	0.0966
Parkfield-02 CA, 2004	Parkfield - Fault Zone 7	4111	6	1.5491	0.0397
Friuli (aftershock 9) Italy, 1976	Buia	4276	5.5	1.9068	0.0713
Umbria Marche (foreshock) Italy, 1997	Colfiorito	4337	5.7	1.5663	0.0961
Chuetsu-oki Japan, 2007	NIG018	5264	6.8	0.7507	0.0376
Iwate Japan, 2008	Nakashinden Town	5774	6.9	1.8491	0.0497
El Mayor-Cucapah Mexico, 2010	Calexico Fire Station	5975	7.2	1.5748	0.0254
Darfield New Zealand, 2010	Christchurch Cashmere High School	6890	7	1.5213	0.0283
Christchurch New Zealand, 2011	Christchurch Botanical Gardens	8063	6.2	0.783	0.0337

Table A.10: The 8D SLS ground motion suite

Earthquake	**Station**	**RSN**	**Mag.**	**Scale**	**MSE**
Imperial Valley-02, 1940	El Centro Array #9	6	6.95	0.6256	0.0186
Point Mugu, 1973	Port Hueneme	97	5.65	1.7875	0.0401
Tabas Iran, 1978	Boshrooyeh	138	7.35	1.8216	0.0455
Imperial Valley-06, 1979	Delta	169	6.53	0.7534	0.0365
Victoria Mexico, 1980	Chihuahua	266	6.33	1.1792	0.0387
Coalinga-01, 1983	Cantua Creek School	322	6.36	0.7753	0.0312
Whittier Narrows-01, 1987	Compton - Castlegate St	611	5.99	0.6457	0.0211
Superstition Hills-02, 1987	El Centro Imp. Co. Cent	721	6.54	0.6159	0.0388
Loma Prieta, 1989	Fremont - Emerson Court	761	6.93	1.3878	0.0351
Landers, 1992	Indio - Coachella Canal	862	7.28	1.7487	0.0403
Northridge-01, 1994	LA - Pico & Sentous	1000	6.69	1.841	0.0314
Kobe Japan, 1995	Sakai	1115	6.9	1.1468	0.0437
Kocaeli Turkey, 1999	Zeytinburnu	1177	7.51	1.8932	0.0285
Chi-Chi Taiwan, 1999	TCU098	1526	7.62	1.5123	0.0197
Manjil Iran, 1990	Abhar	1634	7.37	1.2127	0.0356
Chi-Chi Taiwan-03, 1999	CHY101	2507	6.2	1.5163	0.0397
Chi-Chi Taiwan-04, 1999	CHY088	2744	6.2	1.9127	0.0396
Chi-Chi Taiwan-06, 1999	CHY039	3277	6.3	1.746	0.028
Taiwan SMART1(45), 1986	SMART1 M04	3674	7.3	1.0488	0.0298
Whittier Narrows-02, 1987	LA - W 70th St	3717	5.27	1.3924	0.0442
Parkfield-02 CA, 2004	PARKFIELD - VINEYARD CANYON	4074	6	1.0396	0.0221
Chuetsu-oki Japan, 2007	Hinodecho Yoshida Tsubame City	4880	6.8	1.5103	0.0377
Iwate Japan, 2008	Takanashi Daisen	5798	6.9	1.4511	0.0447
El Mayor-Cucapah Mexico, 2010	Calexico Fire Station	5975	7.2	0.7956	0.0254
Darfield New Zealand, 2010	Christchurch Cashmere High School	6890	7	0.7686	0.0283

Appendix B

FEMA P-58 Information

B.1 Overview of Appendix

Section 3.6 describes the implementation of the FEMA P-58 procedure in this thesis. This appendix lists the fragility groups used in the project and the quantities associated with each group. All data for each fragility group is available in FEMA P-58 (2012b). Section B.2 provides information on the structural fragility quantities used in the Building Performance Model. The nonstructural fragility quantities used in the Building Performance Model are listed in Section B.3.

B.2 Structural Component Quantities

Each building design has different structural members. As a result, the structural component fragilities used in Building Performance Models are different for each building. Table B.1 – B.5 provide information on the structural fragility classification numbers (FCN) and the quantities (QTY). The engineering demand parameter (EDP) for all structural fragilities is interstorey drift ratio (IDR). W refers to the linear weight of the steel member in pounds per linear foot (plf).

Table B.1: Structural quantities of the four-storey standard design (4S)

Floor	FCN	Description	QTY
1–4	B1031.001	Bolted shear tab gravity connections	78
	B1033.053a	Ordinary Concentric Braced Frame (OCBF) with compact X braces, W<40 plf	4
3	B1031.021a	Welded column splices, W<150 plf	20

Table B.2: Structural quantities of the eight-storey standard design (8S)

Floor	FCN	Description	QTY
1–8	B1031.001	Bolted shear tab gravity connections	70
	B1033.053a	OCBF with compact X braces, W <40 plf	8
3	B1031.021a	Welded column splices, W <150 plf	6
	B1031.021b	Welded column splices, 150 plf <W <300 plf	14
5,7	B1031.021a	Welded column splices, W <150 plf	20

Table B.3: Structural quantities of the 16-storey standard design (16S)

Floor	FCN	Description	QTY
1–16	B1031.001	Bolted shear tab gravity connections	70
	B1033.053a	OCBF with compact X braces, W<40 plf	8
3	B1031.021b	Welded column splices, 150 plf<W<300 plf	16
	B1031.021c	Welded column splices, W>300 plf	4
5,7,9	B1031.021a	Welded column splices, W<150 plf	8
	B1031.021b	Welded column splices, 150 plf<W<300 plf	12
11,13,15	B1031.021a	Welded column splices, W<150 plf	20

Table B.4: Structural quantities of the four-storey drift design (4D)

Floor	FCN	Description	QTY
1–4	B1031.001	Bolted shear tab gravity connections	70
	B1033.053a	OCBF with compact X braces, W<40 plf	8
3	B1031.021a	Welded column splices, W<150 plf	20

Table B.5: Structural quantities of the eight-storey drift design (8D)

Floor	FCN	Description	QTY
1–8	B1031.001	Bolted shear tab gravity connections	70
1–6	B1033.053b	OCBF with compact X braces, 41 plf<W<99 plf	8
3	B1031.021a	Welded column splices, W<150 plf	6
	B1031.021b	Welded column splices, 150 plf<W<300 plf	10
	B1031.021c	Welded column splices, W>300 plf	4
5	B1031.021a	Welded column splices, W<150 plf	6
	B1031.021b	Welded column splices, 150 plf<W<300 plf	14
7	B1031.021a	Welded column splices, Column W<150 plf	20
7–8	B1033.053a	OCBF with compact X braces, W<40 plf	8

B.3 Nonstructural Component Quantities

This section provides information on the nonstructural fragility groups. As the individual floor areas are unchanged among the building designs, each building has identical roof and office floor nonstructural fragilities. This data is presented in Table B.6, where quantities with the superscript d refer to directional quantities and SDC refers to the seismic design category. The unit value refers to the assumed value used in the FEMA P-58 repair cost consequence functions. The actually quantity of each nonstructural component is the quantity value multiplied by the PACT unit value. The PACT unit abbreviations are square foot (SF), linear foot (LF), individual unit (EA), amp (AP), ton (TN), and cubic feet per minute (CF). The 90th percentile nonstructural quantities used in the sensitivity study of Section 4.6.2 are referred to as 90th QTY.

Nonstructural components unique to the ground floor are based on a building's total floor area. As a result, these nonstructural groups will vary for the buildings with a different number of storeys. Information on the nonstructural fragility groups unique to the ground floor is provided in Table B.7 – B.9. The EDP for a fragility group can be one of IDR, peak absolute floor acceleration (PFA) or peak absolute floor velocity (PFV) and is indicated in the tables.

Table B.6: Roof and office floor nonstructural quantities

Floor	FCN	Description	EDP	Unit	QTY	90th QTY
Roof	B3011.011	Concrete tile roof, tiles secured and compliant with UBC	IDR	100 SF	64[d]	83[d]
Office	B2022.002	Curtain walls - generic midrise, insulating glass	IDR	30 SF	124[d]	127[d]
	C1011.001a	Full height wall partition, gypsum with metal studs, fixed ends	IDR	100 LF	7[d]	8[d]
	C2011.011b	Precast concrete stair assembly	IDR	1 EA	1[d]	1[d]
	C3011.002a	Full height wall partition, gypsum and ceramic tile, fixed ends	IDR	100 LF	1[d]	2[d]
	C3027.001	Raised access floor, non seismically rated	PFA	100 SF	48	57
	C3032.003d	Suspended ceiling A>2500 sf, SDC D,E, vertical\lateral support	PFA	2500 SF	3	3
	C3034.002	Independent pendant lighting - seismically rated	PFA	1 EA	95	127
	D2021.013a	Cold water piping (D>2.5 in), SDC D,E,F	PFA	1000 LF	0.10	0.13
	D2021.013b	Cold water pipe bracing (D>2.5 in), SDC D,E,F	PFA	1000 LF	0.10	0.13
	D2022.013a	Hot water piping - small diameter, SDC D,E,F	PFA	1000 LF	0.57	1.38
	D2022.013b	Hot water pipe bracing - small diameter, SDC D,E,F	PFA	1000 LF	0.57	1.38
	D2022.023a	Hot water piping - large diameter, SDC D,E,F	PFA	1000 LF	0.23	0.32
	D2022.023b	Hot water pipe bracing - large diameter, SDC D,E,F	PFA	1000 LF	0.23	0.32
	D2031.013b	Sanitary waste pipe bracing, SDC D,E,F	PFA	1000 LF	0.36	0.78
	D3041.011c	HVAC ducting A<6 ft, SDC D,E,F	PFA	1000 LF	1	1
	D3041.012c	HVAC ducting A>6 ft, SDC D,E,F	PFA	1000 LF	1	1
	D3041.031b	HVAC drops in suspended ceilings, SDC C	PFA	10 EA	6	13
	D3041.041b	Variable air volume box, SDC C	PFA	10 EA	5	7
	D4011.023a	Fire sprinkler water piping, SDC D,E,F	PFA	1000 LF	2	2
	D4011.063a	Fire sprinkler drop - hard ceiling, SDC D,E,F	PFA	100 EA	1	1
	D5012.021a	Low voltage switchgear - 100 to 350 AP	PFA	225 AP	1	1
	E2022.001	Modular office work stations	PFA	1 EA	45	51
	E2022.023	Desktop electronics on smooth surface	PFA	1 EA	45	51
	E2022.106a	Bookcase, 6 shelves, unanchored	PFV	1 EA	13	26
	E2022.114a	Filing cabinet, 4 drawer, unanchored	PFV	1 EA	6	13

Table B.7: Ground nonstructural quantities of the four-storey buildings

Floor	FCN	Description	EDP	Unit	QTY	90th QTY
Ground	D1014.011	Traction elevator, U.S. installations 1998 or later	PFA	1 EA	1	3
	D3031.011a	Chiller <100 TN - equipment fragility	PFA	75 TN	1	2
	D3031.021a	Cooling tower <100 TN - equipment fragility	PFA	75 TN	1	2
	D3052.011c	Air handling unit, 10000 to 25000 CFM - equipment fragility	PFA	20000 CF	1	2
	D5012.013a	Motor control centre - equipment fragility	PFA	1 EA	2	2

Table B.8: Ground nonstructural quantities of the eight-storey buildings

Floor	FCN	Description	EDP	Unit	QTY	90th QTY
Ground	D1014.011	Traction elevator, U.S. installations 1998 or later	PFA	1 EA	2	5
	D3031.011b	Chiller, 100 to 350 TN - equipment fragility	PFA	250 TN	1	1
	D3031.021b	Cooling tower, 100 to 350 TN - equipment fragility	PFA	250 TN	1	1
	D3052.011d	Air handling unit, 25000 to 40000 CFM - equipment fragility	PFA	30000 CF	2	2
	D5012.013a	Motor control centre - equipment fragility	PFA	1 EA	3	4

Table B.9: Ground nonstructural quantities of the 16-storey buildings

Floor	FCN	Description	EDP	Unit	QTY	90th QTY
Ground	D1014.011	Traction elevator, U.S. installations 1998 or later	PFA	1 EA	3	9
	D3031.011c	Chiller, 350 to 750 TN - equipment fragility	PFA	500 TN	1	1
	D3031.021c	Cooling tower, 350 to 750 TN - equipment fragility	PFA	500 TN	1	1
	D3052.011d	Air handling unit, 25000 to 40000 CFM - equipment fragility	PFA	30000 CF	3	4
	D5012.013a	Motor control centre - equipment fragility	PFA	1 EA	5	8

References

Achour, Nebil, Masakatsu Miyajima, Masaru Kitaura, and Andrew Price (2011). "Earthquake-induced structural and nonstructural damage in hospitals". EN. In: *Earthquake Spectra* 27.3, pp. 617–634.

Ahmadizadeh, M (2007). "On equivalent passive structural control systems for semi-active control using viscous fluid dampers". In: *Structural Control and Health Monitoring* 14.6, pp. 858–875.

Almufti, Ibbi (2014). *Resilience-based earthquake design initiative (REDi) rating system for the next generation of buildings*. London, UK.

Almufti, Ibrahim and Michael Willford (2013). *The resilience-based earthquake design initiative (REDi) rating system*. Tech. rep. October. Arup.

American Society of Civil Engineers (2013). *Minimum design loads for building and other structures, ASCE/SEI 7-10*. Tech. rep.

Antonucci, R, F Balducci, F Bartera, M G Castellano, K Fuller, and R Giacchetti (2004). "Shaking table testing of an RC frame with dissipative bracings". In: *13th World Conference on Earthquake Engineering*. 1967. Vancouver, Canada.

Astrella, Michael J and Andrew S Whittaker (2005). *The performance-based design paradigm*. Tech. rep. Buffalo, USA: Multidisciplinary Center for Earthquake Engineering Research (MCEER).

ATC (2010). *Modeling and acceptance criteria for seismic design and analysis of tall buildings*. Tech. rep. PEER.

Baird, Andrew, Ali Sahin Tasligedik, Alessandro Palermo, and Stefano Pampanin (2014). "Seismic performance of vertical nonstructural components in the 22 February 2011 Christchurch earthquake". In: *Earthquake Spectra* 30.1, pp. 401–425.

Banihashemi, M.R., A.R. Mirzagoltabar, and H.R. Tavakoli (2015). "Performance-based plastic design method for steel concentric braced frames". In: *International Journal of Advanced Structural Engineering* 7.3, pp. 281–293.

Black, R. G., W. A. Wenger, and E. P. Popov (1980). *Inelastic Buckling of Steel Struts Under Cyclic Load Reversal*.

Booth, Edmund and David Key (2006). *Earthquake Design Practice for Buildings*. 2nd. London, UK: Thomas Telford Publishing.

Brandonisio, G., M. Toreno, E. Grande, E. Mele, and a. De Luca (2012). "Seismic design of concentric braced frames". In: *Journal of Constructional Steel Research* 78, pp. 22–37.

Bruno, S. and C. Valente (2002). "Comparative response analysis of conventional and innovative seismic protection strategies". In: *Earthquake Engineering & Structural Dynamics* 31.5, pp. 1067–1092.

CEN (2010a). *Eurocode 1: Actions on structures*. Brussels, Belgium.

— (2010b). *Eurocode 3: Design of steel structures*. Brussels, Belgium.

— (2010c). *Eurocode: Basis of structural design*. Brussels, Belgium.

CEN (2013). *Eurocode 8: Design of structures for earthquake resistance - Part 1: General rules, seismic actions and rules for buildings*. Brussels, Belgium.

Charney, Finley A. (2008). "Unintended consequences of modeling damping in structures". In: *Journal of structural engineering* 134.4, pp. 581–592.

Chaudhuri, Samit Ray and Tara C Hutchinson (2005). *Performance characterization of bench- and shelf-mounted equipment*. Tech. rep. August. Berkeley, USA: Pacific Earthquake Engineering Research Center (PEER).

Chen, Chui-hsin and Stephen A Mahin (2012). *Performance-based seismic demand assessment of concentrically braced steel frame buildings*. Tech. rep. December. Berkeley, USA: Pacific Earthquake Engineering Research Center (PEER).

Chidiac, S. (2013). *Plane Frame*. Hamilton, Canada.

Chopra, Anil K. (2012). *Dynamics of Structures*. 4th. New Jersey: Prentice Hall.

Christopoulos, Constantin and A Filiatrault (2006). *Principles of Passive Supplemental Damping and Seismic Isolation*. Pavia, Italy: IUSS Press.

Cimellaro, Gian Paolo and Rodrigo Retamales (2007). "Optimal softening and damping design for buildings". In: *Structural Control and Health Monitoring* 14, pp. 831–857.

Comerio, Mary C. (2005). *PEER testbed study on a laboratory building: exercising seismic performance assessment*. Tech. rep. Berkeley, USA: Pacific Earthquake Engineering Research Center (PEER).

Comerio, Mary C. and William T. Holmes (2003). "Seismic protection of building contents at U.C. Berkeley". In: *ATC-29-2 Proceedings of Seminar on Seismic Design, Performance, and Retrofit of Nonstructural Components in Critical Facilities*. Newport Beach, USA, pp. 77–90.

Comerio, Mary C., John C. Stallmeyer, William Holmes, Peter Morris, and Sophia Lau (2001). *Nonstructural loss estimation: The UC Berkeley case study*. Tech. rep. PEER Report 2002/01. Berkeley, USA: Pacific Earthquake Engineering Research Center (PEER).

Computers and Structures Inc. (2013). *SAP2000*.

Connor, J.J. (2003). *Introduction to Structural Motion Control*. Upper Saddle River, USA: Pearson Education.

Constantinou, M.C., T.T. Soong, and G.F. Dargush (1998). *Passive energy dissipation systems for structural design and retrofit*. Tech. rep. Buffalo, USA: Multidisciplinary Center for Earthquake Engineering Research (MCEER).

Craig, J.I., B.J. Goodno, P. Towashiraporn, and J. Park (2002). *Response modification applications for essential facilities*. Tech. rep. March. Atlanta, USA: Mid-America Earthquake Center (MAE).

Crosby, Patrick, James Kelly, and J. P. Singh (1994). "Utilizing visco-elastic dampers in the seismic retrofit of a thirteen story steel framed building". eng. In: *Structures Congress XII*. Atlanta, USA: American Society of Civil Engineers (ASCE), pp. 1286–1291.

Cutfield, M. and K. Ryan (2016). "Comparative Life Cycle Analysis of Conventional and Base Isolated Buildings". In: *Earthquake Spectra* 32.1, pp. 323–343.

Dall'Asta, Andrea, Enrico Tubaldi, and Laura Ragni (2016). "Influence of the nonlinear behavior of viscous dampers on the seismic demand hazard of building frames". In: *Earthquake Engineering & Structural Dynamics* 45, pp. 149–169.

D'Aniello, M., G. La Manna Ambrosino, F. Portioli, and R. Landolfo (2013). "Modelling aspects of the seismic response of steel concentric braced frames". In: *Steel and Composite Structures* 15.5, pp. 539–566.

D'Aniello, M., G. La Manna Ambrosino, F. Portioli, and R. Landolfo (2015). "The influence of out-of-straightness imperfection in physical theory models of bracing members on seismic performance assessment of concentric braced structures". In: *The Structural Design of Tall and Special Buildings* 24.3, pp. 176–197.

Dhakal, Rajesh P (2010). "Damage to non-structural components and contents in 2010 Darfield earthquake". In: *Bulletin of the New Zealand Society for Earthquake Engineering* 43.4, pp. 404–411.

Dicleli, Murat and Anshu Mehta (2007). "Seismic performance of chevron braced steel frames with and without viscous fluid dampers as a function of ground motion and damper characteristics". In: *Journal of Constructional Steel Research* 63.8, pp. 1102–1115.

Elghazouli, A. Y. (2010). "Assessment of European seismic design procedures for steel framed structures". In: *Bulletin of Earthquake Engineering* 8.1, pp. 65–89.

Elsesser, E. (1984). "Life hazards created by nonstructural elements". In: *Nonstructural Issues of Seismic Design and Construction*, pp. 27–36.

Erduran, Emrah, N.D. Dao, and K.L. Ryan (2012). "Comparative response assessment of minimally compliant low-rise conventional and base-isolated steel frames". In: *Earthquake Engineering & Structural Dynamics* 40.10, pp. 1123–1141.

Fan, Fa-Gung and Goodarz Ahmadi (1992). "Seismic responses of secondary systems in base-isolated structures". In: *Engineering Structures* 14.1, pp. 35–48.

Fathali, Saeed and André Filiatrault (2007a). *Evaluation of isolation/restraint systems for mechanical equipment part 1: Heavy equipment study*. Tech. rep. 1323. Buffalo, USA: Multidisciplinary Center for Earthquake Engineering Research (MCEER).

— (2007b). *Evaluation of isolation/restraint systems for mechanical equipment part 2: Light equipment study*. Tech. rep. 1323. Buffalo, USA: Multidisciplinary Center for Earthquake Engineering Research (MCEER).

FEMA (2012a). *FEMA E-74 reducing the risks of nonstructural earthquake damage - a practical guide*. Tech. rep. Federal Emergency Management Agency (FEMA).

— (2012b). *FEMA P-58, Seismic Performance Assessment of Buildings, Methodology and Implementation*. Tech. rep. Washington, D.C.: Federal Emergency Management Agency.

— (2012c). *FEMA P-58, Seismic Performance Assessment of Buildings, Volume 1 - Methodology*. Tech. rep. Washington, D.C.: Federal Emergency Management Agency.

— (2012d). *FEMA P-58, Seismic Performance Assessment of Buildings, Volume 2 - Implementation Guide*. Tech. rep. Washington, D.C.: Federal Emergency Management Agency.

Fierro, Eduardo A., Eduardo Miranda, and Cynthia L. Perry (2011). "Behavior of nonstructural components in recent earthquakes". en. In: *Architectural Engineering Conference (AEI) 2011*. Oakland, California, United States: American Society of Civil Engineers (ASCE), pp. 369–377.

Filiatrault, A, C. Uang, B. Folz, C. Christopoulos, and K. Gatto (2001a). *Reconnaissance report of the February 28, 2001 Nisqually (Seattle-Olympia) earthquake*. Tech. rep. San Diego, USA: Pacific Earthquake Engineering Research (PEER) Center and the Consortium of Universities for Earthquake Engineering (CUREE).

Filiatrault, André, Constantin Christopoulos, and Christopher Stearns (2001b). *Guidelines, specifications, and seismic performance characterization of nonstructural building domponents and equipment*. Tech. rep. September 2001. Berkeley, USA: Pacific Earthquake Engineering Research Center (PEER).

Filiatrault, Andre and Imothy Sullivan (2014). "Performance-based Seismic Design of Nonstructural Building Components : The Next Frontier of Earthquake Engineering". In: *Earthquake Engineering and Engineering Vibration* 13, pp. 17–46.

Flood Precast (n.d.). *Safe load table for Hollowcore*.

Gidaris, Ioannis and Alexandros A. Taflanidis (2015). "Performance assessment and optimization of fluid viscous dampers through life-cycle cost criteria and comparison to alternative design approaches". In: *Bulletin of Earthquake Engineering* 13.4, pp. 1003–1028.

Gioncu, Victor and Federico M. Mazzolani (2011). *Earthquake Engineering for Structural Design*. London, UK: Spon Press, p. 584.

Goggins, J and S Salawdeh (2013). "Validation of nonlinear time history analysis models for single-storey concentrically braced frames using full-scale shake table tests". In: *Earthquake Engineering & Structural Dynamics* 42.10, pp. 1151–1170.

Gould, NC and MJ Griffin (2003). "The value of seismically installing and strengthening non-structural equipment and systems to significantly reduce business interruption losses". In: *ATC-29-2 Proceedings of Seminar on Seismic Design, Performance, and Retrofit of Nonstructural Components in Critical Facilities*. Newport Beach, USA, pp. 215–226.

Goulet, Christine A, Curt B Haselton, Judith Mitrani-Reiser, James L Beck, Gregory G Deierlein, Keith A Porter, and Jonathan P Stewart (2007). "Evaluation of the seismic performance of a code-conforming reinforced-concrete frame building - from seismic hazard to collapse safety and economic losses". In: *Earthquake Engineering & Structural Dynamics* 36.13, pp. 1973–1997.

Guerrero, Héctor, Amador Terán-Gilmore, Tianjian Ji, and José A. Escobar (2017). "Evaluation of the economic benefits of using Buckling-Restrained Braces in hospital structures located in very soft soils". In: *Engineering Structures* 136, pp. 406–419.

Hanson, Robert D. and T T Soong (2001). *Seismic Design with Supplemental Energy Dissipation Devices*. Oakland, USA: Earthquake Engineering Research Institute (EERI).

Hsiao, Po-Chien, Dawn E. Lehman, and Charles W. Roeder (2012). "Improved analytical model for special concentrically braced frames". In: *Journal of Constructional Steel Research* 73, pp. 80–94.

Hunt, Jeffrey P. and Bozidar Stojadinovic (2010). *Seismic performance assessment and probabilistic repair cost analysis of precast concrete cladding systems for multistory buildings*. Tech. rep. Berkeley, USA: Pacific Earthquake Engineering Research Center (PEER).

Hwang, Jenn-Shin, Wang-Chuen Lin, and Nian-Juan Wu (2013). "Comparison of distribution methods for viscous damping coefficients to buildings". In: *Structure and Infrastructure Engineering* 9.1, pp. 28–41.

Jarrett, Jordan a., Johnn P. Judd, and Finley a. Charney (2015). "Comparative evaluation of innovative and traditional seismic-resisting systems using the FEMA P-58 procedure". In: *Journal of Constructional Steel Research* 105, pp. 107–118.

Ji, Xiaodong, Mikiko Kato, Tao Wang, Toko Hitaka, and Masayoshi Nakashima (2009). "Effect of gravity columns on mitigation of drift concentration for braced frames". In: *Journal of Constructional Steel Research* 65.12, pp. 2148–2156.

Jin, Jun and Sherif El-Tawil (2003). "Inelastic Cyclic Model for Steel Braces". In: *Journal of Engineering Mechanics* 129.5, pp. 548–557.

Kam, Weng Y. and Stefano Pampanin (2012). "Revisiting performance-based seismic design in the aftermath of the Christchurch 2010-2011: Raising the bar to meet

societal expectations". In: *15th World Conference on Earthquake Engineering*. Lisbon, Portugal.

Kam, Weng Y., Stefano Pampanin, Rajesh Dhakal, Henri P. Gavin, and Charles Roeder (2010). "Seismic performance of reinforced concrete buildings in the September 2010 Darfield (Canterbury) earthquake". In: *Bulletin of the New Zealand Society for Earthquake Engineering* 43.4, pp. 340–350.

Karamanci, Emre and Dg Lignos (2014). "Computational Approach for Collapse Assessment of Concentrically Braced Frames in Seismic Regions". In: *Journal of Structural Engineering* 140.8.

Kasai, Kazuhiko, Yaomin Fu, and Atsushi Watanabe (1998). "Passive control systems for seismic damage mitigation". In: *Journal of Structural Engineering* 124.5, pp. 501–512.

Kasai, Kazuhiko, Hiroshi Ito, Yoji Ooki, Tsuyoshi Hikino, Koichi Kajiwara, Shojiro Motoyui, Hitoshi Ozaki, and Masato Ishii (2010). "Full-scale shake table tests of 5-story steel building with various dampers". In: *7th International Conference on Urban Earthquake Engineering (7CUEE) & 5th International Conference on Earthquake Engineering (5ICEE)*. Tokyo, Japan, pp. 11–22.

Kircher, C. A. (2003). "It makes dollars and sense to improve nonstructural system performance". In: *ATC-29-2 Proceedings of Seminar on Seismic Design, Performance, and Retrofit of Nonstructural Components in Critical Facilities*. Newport Beach, USA, pp. 109–119.

Konstantinidis, Dimitrios and Nicos Makris (2005). *Experimental and analytical studies on the seismic response of freestanding and anchored laboratory equipment*. Tech. rep. January. Berkeley, USA: Pacific Earthquake Engineering Research Center (PEER).

Kostic, S.M. and F.C. Filippou (2012). "Section Discretization of Fiber Beam-Column Elements for Cyclic Inelastic Response". In: *Journal of Structural Engineering* 138.5, pp. 592–601.

Landi, Luca, Filippo Conti, and Pier Paolo Diotallevi (2015). "Effectiveness of different distributions of viscous damping coefficients for the seismic retrofit of regular and irregular RC frames". In: *Engineering Structures* 100.1, pp. 79–93.

Lavan, O. and M. Avishur (2013). "Seismic behavior of viscously damped yielding frames under structural and damping uncertainties". In: *Bulletin of Earthquake Engineering* 11.6, pp. 2309–2332.

Lavan, Oren and Gary F. Dargush (2009). "Multi-Objective Evolutionary Seismic Design with Passive Energy Dissipation Systems". In: *Journal of Earthquake Engineering* 13.6, pp. 758–790.

Lavan, Oren and Robert Levy (2009). "Simple iterative use of Lyapunov's solution for the linear optimal seismic design of passive devices in framed buildings". In: *Journal of Earthquake Engineering* 13.December 2013, pp. 650–666.

Lee, D. and D. P. Taylor (2001). "Viscous damper development and future trends". In: *The Structural Design of Tall and Special Buildings Buildings* 10.5, pp. 311–320.

Levy, R. and O. Lavan (2006). "Fully stressed design of passive controllers in framed structures for seismic loadings". In: *Structural and Multidisciplinary Optimization* 32.6, pp. 485–498.

Levy, R and O Lavan (2009). "Quantitative Comparison of Optimization Approaches for the Design of Supplemental Damping in Earthquake Engineering Practice". In: *Journal of Structural Engineering* 135.3, pp. 321–325.

Lin, Wen-Hsiung and Anil K. Chopra (2003). "Asymmetric one-storey elastic systems with non-linear viscous and viscoelastic dampers: Earthquake response". In: *Earthquake Engineering & Structural Dynamics* 32.4, pp. 555–577.

Lloyd, R.J. (2003). "Case studies of anchorage failures". In: *ATC-29-2 Proceedings of Seminar on Seismic Design, Performance, and Retrofit of Nonstructural Components in Critical Facilities*. Newport Beach, USA, pp. 189–200.

Lopez Garcia, D. and T. T. Soong (2002). "Efficiency of a simple approach to damper allocation in MDOF structures". In: *Journal of Structural Control* 9.1, pp. 19–30.

Lopez-Garcia, Diego (2001). "A simple method for the design of optimal damper configurations in MDOF structures". In: *Earthquake Spectra* 17.3, pp. 387–398.

MacRae, G. A., Y. Kimura, and C. Roeder (2004). "Effect of Column Stiffness on Braced Frame Seismic Behavior". In: *Journal of Structural Engineering* 130.3, pp. 381–391.

Mahjoubi, S. and S. Maleki (2015). "Seismic performance assessment of steel frames equipped with a novel passive damper using a new damper performance index". In: *Structural Control and Health Monitoring* 22.4, pp. 774–797.

Martinez-Rodrigo, M. and M. L. Romero (2003). "An optimum retrofit strategy for moment resisting frames with nonlinear viscous dampers for seismic applications". In: *Engineering Structures* 25.7, pp. 913–925.

Mayes, Ronald L, Craig Goings, Wassim Naguib, Stephen Harris, Jennifer Lovejoy, Jerome P Fanucci, Pavel Bystricky, and John R Hayes (2004). "Comparative performance of buckling-restrained braces and moment frames". In: *13th World Conference on Earthquake Engineering*. 2887. Vancouver, Canada.

Mayes, Ronald, Nicholas Wetzel, Ben Weaver, Ken Tam, Will Parker, Andrew Brown, and Dario Pietra (2013). "Performance Based Design of Buildings to Assess and Minimize Damage and Downtime". In: *Bulletin of New Zealand Society for Earthquake Engineering* 46.1, pp. 40–55.

McCrum, Daniel P. and B. M. Broderick (2013). "An experimental and numerical investigation into the seismic performance of a multi-storey concentrically braced plan irregular structure". In: *Bulletin of Earthquake Engineering* 11.6, pp. 2363–2385.

McKenna, Frank (2017). *OpenSees*.

McKevitt, W. E., P. A. M. Timler, and K. K. Lo (1995). "Nonstructural damage from the Northridge earthquake". en. In: *Canadian Journal of Civil Engineering* 22.2, pp. 428–437.

Merczel, D. B., J. M. Aribert, H. Somja, and M. Hjiaj (2016). "Plastic analysis-based seismic design method to control the weak storey behaviour of concentrically braced steel frames". In: *Journal of Constructional Steel Research* 125, pp. 142–163.

Merczel, Dániel B., Hugues Somja, Jean-Marie Aribert, and János Lógó (2013). "On the behaviour of concentrically braced frames subjected to seismic loading". In: *Periodica Polytechnica Civil Engineering* 57.2, pp. 113–122.

Miranda, Eduardo, Gilberto Mosqueda, Rodrigo Retamales, and Gokhan Pekcan (2012). "Performance of nonstructural components during the 27 February 2010 Chile earthquake". EN. In: *Earthquake Spectra* 28.S1, S453–S471.

Morgan, Troy A and Stephen A Mahin (2011). *The use of base isolation systems to achieve complex seismic performance objectives*. Tech. rep. Berkeley, USA: Pacific Earthquake Engineering Research Center (PEER).

Motahari, S.a., M. Ghassemieh, and S.a. Abolmaali (2007). "Implementation of shape memory alloy dampers for passive control of structures subjected to seismic excitations". In: *Journal of Constructional Steel Research* 63.12, pp. 1570–1579.

National Office Furniture (2011). *National Office Furniture - Casegoods*. Jasper, Indiana.

Occhiuzzi, Antonio (2009). "Additional viscous dampers for civil structures: Analysis of design methods based on effective evaluation of modal damping ratios". In: *Engineering Structures* 31.5, pp. 1093–1101.

Palermo, Michele, Saverio Muscio, Stefano Silvestri, Luca Landi, and Tomaso Trombetti (2013). "On the dimensioning of viscous dampers for the mitigation of the earthquake-induced effects in moment-resisting frame structures". In: *Bulletin of Earthquake Engineering* 11.6, pp. 2429–2446.

Pavlou, Eleni and Michael C. Constantinou (2006). "Response of nonstructural components in structures with damping systems". en. In: *Journal of Structural Engineering* 132.7, pp. 1108–1117.

PEER (2013). *PEER NGA-WEST 2 Ground Motion Database*.

— (2017). *OpenSees command manual*.

Porter, KA and AS Kiremidjian (2001). *Assembly-based vulnerability of buildings and its uses in seismic performance evaluation and risk-management decision-making*. Tech. rep. Stanford, USA: The John A. Blume Earthquake Engineering Center.

Puthanpurayil, Arun M. and Paul Reynolds (2008). "Development of optimal viscous dampers for RC structures in near field ground motions". In: *2008 Seismic Engineering Conference Commemorating the 1908 Messina and Reggio Calabria Earthquake*. Vol. 1020. 2008. Reggio Calabria, Italy: AIP Publishing, pp. 1459–1466.

Retamales, Rodrigo, Gilberto Mosqueda, Andre Filiatrault, and Andrei Reinhorn (2008). *New experimental capabilities and loading protocols for seismic qualification and fragility assessment of nonstructural systems*. Tech. rep. Buffalo, USA: Multidisciplinary Center for Earthquake Engineering Research (MCEER).

Roeder, Charles W, Dawn E Lehman, and Eric Lumpkin (2009). *Fragility Curves for Concentrically Braced Steel Frames with Buckling Braces*. Tech. rep. FEMA.

RSMeans Online (2017). *Square Foot Estimator*.

Saatcioglu, Murat, Robert Tremblay, Denis Mitchell, Ahmed Ghobarah, Dan Palermo, Rob Simpson, Perry Adebar, Carlos Ventura, and Hanping Hong (2013). "Performance of steel buildings and nonstructural elements during the 27 February 2010 Maule (Chile) earthquake". en. In: *Canadian Journal of Civil Engineering* 40.8, pp. 722–734.

Salawdeh, Suhaib and Jamie Goggins (2013). "Numerical simulation for steel brace members incorporating a fatigue model". In: *Engineering Structures* 46, pp. 332–349.

Solomos, G, A Pinto, and S Dimova (2008). "A review of the seismic hazard zonation in national building codes in the context of Eurocode 8". In: *JRC Scientific and Technical Reports*.

Soong, T. T. and G F Dargush (1997). *Passive Energy Dissipation Systems in Structural Engineering*. Wiley.

Soong, T.T. and B.F. Spencer Jr (2002). "Supplemental energy dissipation: State-of-the-art and state-of-the-practice". In: *Engineering Structures* 24.3, pp. 243–259.

Soós, M and LG Vigh (2012). "On the Eurocode 8 limited damage criteria for non-structural elements - Analysis and requirements". In: *15th World Conference on Earthquake Engineering*. Lisbon, Portugal.

Starosielec, Sebastian and Daniel Hagele (2014). "Discrete-time windows with minimal RMS bandwidth for given RMS temporal width". In: *Signal Processing* 102, pp. 240–246.

Sullivan, Timothy J., Paolo M. Calvi, and Roberto Nascimbene (2013). "Towards improved floor spectra estimates for seismic design". In: *Earthquakes and Structures* 4.1, pp. 109–132.

Symans, M. D., F. A. Charney, A. S. Whittaker, M. C. Constantinou, C. A. Kircher, M. W. Johnson, and R. J. McNamara (2008). "Energy dissipation systems for seismic applications: Current practice and recent developments". In: *Journal of Structural Engineering* 134.1, pp. 3–21.

Taghavi, Shahram and Eduardo Miranda (2003). *Response assessment of nonstructural building elements*. Tech. rep. Berkeley, USA: Pacific Earthquake Engineering Research Center (PEER).

Tajirian, F.F. (2009). "Seismic vulnerability of data centers". In: *2009 ATC & SEI Conference on Improving the Seismic Performance of Buildings and Other Structures*. San Francisco, USA, pp. 686–695.

Takewaki, Izuru (1997). "Optimal damper placement for minimum transfer functions". In: *Earthquake Engineering and Structural Dynamics* 26.February, pp. 1113–1124.

Taly, N. (1988). "The Whittier Narrows, California earthquake of October 1, 1987 - Performance of buildings at California State University, Los Angeles". In: *Earthquake Spectra* 4.2, pp. 277–317.

Tata Steel Europe Limited (2014). *Tata Steel Sections Blue Book*. Berkshire, UK.

Terzic, V, S A Mahin, and M Comerio (2014). "Comparative life-cycle cost and performance analysis of structural systems for buildings". In: *10th U.S. National Conference on Earthquake Engineering: Frontiers of Earthquake Engineering, NCEE 2014* March.

The MathWorks Inc. (2017). *MATLAB and Statistics Toolbox*. Natick, Massachusetts.

Tian, Yuan, Andre Filiatrault, and Gilberto Mosqueda (2013). *Experimental seismic study of pressurized fire sprinkler piping subsystems*. Tech. rep. Cmmi. Buffalo, USA: Multidisciplinary Center for Earthquake Engineering Research (MCEER).

Towashiraporn, P., J. Park, B.J. Goodno, and J.I. Craig (2002). "Passive control methods for seismic response modification". In: *Progress in Structural Engineering and Materials* 4.1, pp. 74–86.

Tremblay, Robert (2002). "Inelastic seismic response of steel bracing members". In: *Journal of Constructional Steel Research* 58.5-8, pp. 665–701.

— (2003). "Achieving a Stable Inelastic Seismic Response for Multi-Story Concentrically Braced Steel Frames". In: *Engineering Journal* 40.2, pp. 111–129.

Tremblay, Robert, Denis Mitchell, and René Tinawi (2013). "Damage to industrial structures due to the 27 February 2010 Chile earthquake". en. In: *Canadian Journal of Civil Engineering* 40.8, pp. 735–749.

Uriz, P. and A. S. Whittaker (2001). "Retrofit of pre-northridge steel moment-resisting frames using fluid viscous dampers". In: *The Structural Design of Tall Buildings* 10.5, pp. 371–390.

Uriz, Patxi, Filip C. Filippou, and Stephen A. Mahin (2008). "Model for Cyclic Inelastic Buckling of Steel Braces". In: *Journal of Structural Engineering* 134.4, pp. 619–628.

Uriz, Patxi and Stephen Mahin (2008). *Toward earthquake-resistant design of concentrically braced steel-frame structures*. Tech. rep. Berkeley, USA: Pacific Earthquake Engineering Research Center (PEER).

Vargas, Ramiro E. and Michel Bruneau (2006). *Analytical investigation of the structural fuse concept*. Tech. rep. Buffalo, USA: Multidisciplinary Center for Earthquake Engineering Research (MCEER).

Vargas, Ramiro and Michel Bruneau (2007). "Effect of supplemental viscous damping on the seismic response of structural systems with metallic dampers". en. In: *Journal of Structural Engineering* 133.10, pp. 1434–1444.

Veletsos, Anestis S. and Carlos E. Ventura (1986). "Modal analysis of non-classically damped linear systems". In: *Earthquake Engineering & Structural Dynamics* 14.2, pp. 217–243.

Villaverde, Roberto (1997). "Seismic design of secondary structures: State of the art". In: *Journal of Structural Engineering* 123.8, pp. 1011–1019.

Vulcano, Alfonso and Fabio Mazza (2000). "Comparative study of the seismic performance of frames using different dissipative braces". In: *Proceedings of the 12th World Conference on Earthquake Engineering*. Auckland, New Zealand.

Wang, Mickw (2008). "Seismic risk assessment of operational and functional components for new and existing buildings". In: *14th World Conference on Earthquake Engineering*. Beijing, China.

Wanitkorkul, Assawin and André Filiatrault (2008). "Influence of passive supplemental damping systems on structural and nonstructural seismic fragilities of a steel building". In: *Engineering Structures* 30.3, pp. 675–682.

Whittaker, Andrew S, Michael C Constantinou, Oscar M Ramirez, Martin W Johnson, and Christis Z Chrysostomou (2003). "Equivalent Lateral Force and Modal Analysis Procedures of the 2000 NEHRP Provisions for Buildings with Damping Systems". In: *Earthquake Spectra* 19.4, pp. 959–980.

Whittle, J. K., M. S. Williams, T. L. Karavasilis, and A. Blakeborough (2012). "A comparison of viscous damper placement methods for improving seismic building design". In: *Journal of Earthquake Engineering* 16.4, pp. 540–560.

Wieser, Joseph D, Gokhan Pekcan, Arash E Zaghi, Ahmad M Itani, and Emmanuel Maragakis (2012). *Assessment of floor accelerations in yielding buildings*. Tech. rep. 716. Buffalo, USA: Multidisciplinary Center for Earthquake Engineering Research (MCEER).

Wijesundara, K.K., R. Nascimbene, and G.a. Rassati (2014). "Modeling of different bracing configurations in multi-storey concentrically braced frames using a fiber-beam based approach". In: *Journal of Constructional Steel Research* 101, pp. 426–436.

Wolff, ED and MC Constantinou (2004). *Experimental study of seismic isolation systems with emphasis on secondary system response and verification of accuracy of dynamic response history analysis methods*. Tech. rep. Buffalo, USA: Multidisciplinary Center for Earthquake Engineering Research (MCEER).